



3 4456 0266667 5

ORNL/TM-10506

ornl

**OAK RIDGE
NATIONAL
LABORATORY**

MARTIN MARIETTA

Detection of Vapors of Flammable Liquids in Air by Atmospheric Sampling Mass Spectrometry/Mass Spectrometry Progress Report: March 31, 1987

S. A. McLuckey
G. L. Glish
K. G. Asano
E. H. McBay

OAK RIDGE NATIONAL LABORATORY
CENTRAL RESEARCH LIBRARY
CIRCULATION SECTION
DO NOT REMOVE
LIBRARY LOAN COPY
DO NOT TRANSFER TO ANOTHER PERSON
If you wish someone else to see this
report, send it along with report card
the library will arrange a loan.

OPERATED BY
MARTIN MARIETTA ENERGY SYSTEMS, INC.
FOR THE UNITED STATES
DEPARTMENT OF ENERGY

Printed in the United States of America Available from
National Technical Information Service
U.S. Department of Commerce
5285 Port Royal Road, Springfield, Virginia 22161
NTIS price codes—Printed Copy: A08 Microfiche A01

This report was prepared as an account of work sponsored by an agency of the United States Government. Neither the United States Government nor any agency thereof, nor any of their employees, makes any warranty, express or implied, or assumes any legal liability or responsibility for the accuracy, completeness, or usefulness of any information, apparatus, product, or process disclosed, or represents that its use would not infringe privately owned rights. Reference herein to any specific commercial product, process, or service by trade name, trademark, manufacturer, or otherwise, does not necessarily constitute or imply its endorsement, recommendation, or favoring by the United States Government or any agency thereof. The views and opinions of authors expressed herein do not necessarily state or reflect those of the United States Government or any agency thereof.

ORNL/TM-10506

Contract No. DE-AC05-84OR21400

Analytical Chemistry Division

**Detection of Vapors of Flammable Liquids in Air by
Atmospheric Sampling Mass Spectrometry/Mass Spectrometry
Progress Report: March 31, 1987**

by

S. A. McLuckey, G. L. Glish, K. G. Asano, and E. H. McBay
Analytical Chemistry Division
Oak Ridge National Laboratory
Oak Ridge, TN 37831

Date Published: August 1987

OAK RIDGE NATIONAL LABORATORY
Oak Ridge, Tennessee 37831
operated by
Martin Marietta Energy Systems, Inc.
for the
Department of Energy

MARTIN MARIETTA ENERGY SYSTEMS LIBRARIES



3 4456 0266667 5

TABLE OF CONTENTS

	<u>Page</u>
I. Introduction	3
II. Instrumentation.....	5
A. Atmospheric Sampling Ion Source.....	5
B. MS/MS Instrument.....	9
III. Characterization of Fuel Mixtures.....	17
IV. Vapors of Flammable Liquids and Atmospheric Sampling Glow Discharge Ionization: Mass Spectra and MS/MS Spectra.....	33
A. Pure Samples.....	34
1. Heptanes.....	34
2. Benzene.....	39
3. Toluene.....	39
4. n-Propylbenzene.....	43
5. n-Butylbenzene.....	43
6. Methanol.....	47
7. Ethanol.....	49
8. Isopropanol.....	49
9. Water.....	50
10. Acetone.....	53
B. Mixtures.....	55
1. Gasolines.....	55
2. Kerosene.....	60
3. Jet fuel.....	64
4. Lighter fluid.....	64
5. Perfumes and rum.....	66
C. Detection Limits.....	66
V. Conclusions and Future Work.....	69
Appendix I.....	71
Appendix II.....	83
Appendix III.....	105
Appendix IV.....	113
Appendix V.....	121
Appendix VI.....	141

LIST OF FIGURES

	<u>Page</u>
1. Conceptual schematic of the atmospheric sampling ionization MS/MS approach to detecting organics in ambient air	4
2. Schematic diagram of the atmospheric sampling glow discharge ionization source.....	6
3. Mass spectra of n-butylbenzene at a) low discharge voltage, b) intermediate voltage, and c) high voltage.....	8
4. Schematic diagram of the quadrupole/time-of-flight mass spectrometer.....	12
5. Data acquisition schematic for the quadrupole/time-of-flight mass spectrometers.....	14
6. 70 eV electron impact mass spectrum of gasoline.....	18
7. Gas chromatograph of gasoline.....	20
8. First 20 minutes of gasoline GC run.....	21
9. Scan #17 of GC run.....	22
10. Gas chromatograph of kerosene.....	23
11. 70 eV electron impact mass spectrum of kerosene.....	26
12. Gas chromatograph of jet fuel.....	27
13. 70 eV electron impact mass spectrum of jet fuel.....	31
14. 70 eV electron impact mass spectrum of lighter fuel.....	32
15. Glow discharge mass spectrum of heptanes.....	35
16. Daughter ions MS/MS spectrum of the m/z 100 ion in the glow discharge mass spectrum of heptanes.....	37
17. Same spectrum as shown in Figure 16 except that the electric sector plate voltages are reduced by about 10 volts each.....	40

List of Figures - Contd.

	<u>Page</u>
18. Daughter ion MS/MS spectrum of the benzene molecular ion (m/z 78).....	41
19. Daughter ion MS/MS spectrum of the toluene molecular ion (m/z 92).....	42
20. Daughter ion MS/MS spectrum of the m/z ion in the glow discharge mass spectrum of toluene.....	44
21. Daughter ion MS/MS spectrum of the n-propylbenzene molecular ion (m/z 120).....	45
22. Daughter ion MS/MS spectrum of the n-butylbenzene molecular ion (m/z 134).....	46
23. Glow discharge mass spectrum of methanol.....	48
24. Glow discharge mass spectrum of water.....	51
25. Daughter ion MS/MS spectrum of the m/z 91 ion in the glow discharge mass spectrum of water.....	52
26. Glow discharge mass spectrum of acetone.....	54
27. Glow discharge mass spectra of gasoline from a) m/z 10-200 and b) m/z 50-200.....	56
28. Glow discharge mass spectrum of viscous gasoline sample.....	58
29. Daughter ion MS/MS spectrum of the m/z 134 ion in the glow discharge mass spectrum of gasoline.....	59
30. Glow discharge mass spectrum of kerosene-low discharge voltage.....	61
31. Glow discharge mass spectrum of kerosene-high discharge voltage.....	62
32. Comparison of MS/MS spectra of m/z 128 from a) kerosene and b) naphthalene.....	63
33. Glow discharge mass spectra of lighter fluid acquired at a) low and b) high discharge voltages.....	65

LIST OF TABLES

	<u>Page</u>
1. Unleaded Gasoline.....	24
2. Kerosene 1K.....	28
3. 1A Jet Fuel.....	29

DETECTION OF VAPORS OF FLAMMABLE LIQUIDS IN AIR BY
ATMOSPHERIC SAMPLING MASS SPECTROMETRY/MASS SPECTROMETRY
PROGRESS REPORT: MARCH 31, 1987

S. A. McLuckey, G. L. Glish, K. G. Asano, and E. H. McBay

ABSTRACT

The detection of vapors of flammable liquids by atmospheric sampling glow discharge ionization coupled with mass spectrometry/mass spectrometry (MS/MS) is described. An atmospheric sampling ionization source based on a glow discharge has been developed for ionizing trace organic molecules in ambient air. This ion source has been coupled with a tandem mass spectrometer consisting of a quadrupole mass filter and a time-of-flight analyzer. This ion source/spectrometer combination has been evaluated for detecting vapors of flammable liquids in the positive ion mode. The flammable liquids tested include inter alia alcohols, hydrocarbon solvents, and several hydrocarbon fuel mixtures. The hydrocarbon fuel mixtures were first characterized by gas chromatography/mass spectrometry using 70 eV electron impact ionization. Mass spectra using a glow discharge ionization source were acquired for all samples. MS/MS spectra were acquired for all of the major ions observed in the mass spectra. The mass spectra are described as are some of the MS/MS spectra. Both mass spectra and MS/MS spectra are included in appendices. The approach has been found to provide both high sensitivity and high specificity for the detection of vapors of flammable liquids in ambient air. The limits of detection for most of the compounds studied is expected to be on the order of parts per billion or less.

I. Introduction

The development and evaluation of methods for the detection of vapors of flammable liquids using an atmospheric sampling ion source and mass spectrometry/mass spectrometry (MS/MS) have been undertaken in our laboratory. Conceptually, the approach consists of preferentially ionizing organic vapors in ambient air, analyzing the mass/charge (m/z) ratios of the ions formed, and, if needed, dissociating the ions prior to a second stage of mass analysis for greater structural information. The procedure is indicated in Figure 1 which shows a schematic diagram of an MS/MS instrument. Ions formed in the ion source and mass analyzed by a first stage mass spectrometer are injected into a collision region where they can undergo inelastic collisions with a target gas. Many of the parent ions that undergo collision fragment to give daughter ions in a process referred to as collision-induced dissociation (CID). The daughter ions are then mass analyzed by a second stage of mass spectrometry. The MS/MS daughter ion spectrum, in addition to the m/z ratio of the parent ion, serves to identify the parent molecule. A second important feature of MS/MS is that it can overcome interferences that occur in single stage mass spectrometry from two or more compounds that form parent ions at the same nominal mass. If the MS/MS spectra are distinct, as is usually the case, a compound can be detected even in the presence of a large excess of another compound that gives a parent ion of the same nominal m/z . The combination of an atmospheric sampling ion source with MS/MS, therefore, promises to provide both high sensitivity and high specificity for the detection of organic compounds in air.

This report summarizes the work to date in the application of MS/MS to the detection of vapors of flammable liquids. Efforts have been directed in three major areas. These include the development of an atmospheric sampling ion source and MS/MS instrument, the characterization of several gasolines and other fuel mixtures by gas chromatography/mass spectrometry (GC/MS), and the acquisition of mass spectra and MS/MS daughter ion spectra derived from the fuel mixtures and other flammable liquids using the atmospheric sampling MS/MS instrument. Each of these areas is described, in turn, below.

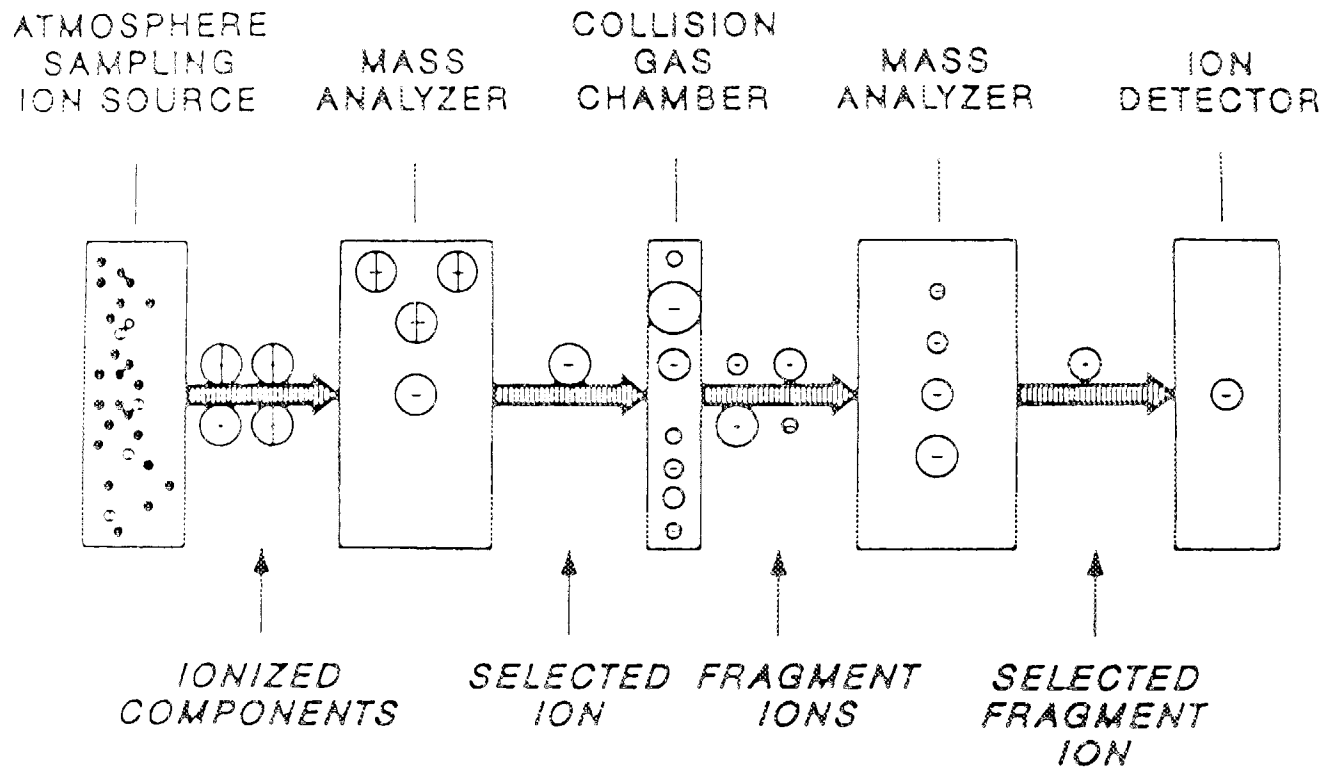


Figure 1. Conceptual schematic of the atmospheric sampling ionization MS/MS approach to detecting organics in ambient air.

II. Instrumentation

This section is divided into two subsections. The first describes an atmospheric sampling ion source, and the second describes the MS/MS instrument. Both devices were designed and constructed in our laboratory.

A. Atmospheric sampling ion source

A new type of atmospheric sampling ion source has been developed in our laboratory (patent pending). It has proven to provide a simple and sensitive means for ionizing organic compounds in ambient air for subsequent analysis by mass spectrometry and MS/MS. The ion source is shown schematically in Figure 2. Ionization is based on the establishment of a glow discharge between two electrodes in a region of reduced pressure (in the range of 0.1-1 torr). The ion source consists of a plate containing an atmospheric sampling aperture (A1), a pair of parallel plates (P1,P2) in the ionization region separated by a distance of about 1 cm, and a plate containing an ion exit aperture (A2). The distance between A1 and A2 is about 1.5 cm. The diameter of the atmospheric sampling aperture is typically 0.2 mm, which allows about 6 ml of air per second to enter the ionization region when the ionization region is being pumped by a 15 l/s roughing pump. The ion exit aperture is typically 0.8 mm in diameter. Under the conditions described above, a 1000 l/s vacuum pump in the mass spectrometer chamber maintains a pressure of about 5×10^{-5} torr. The ionization volume is situated in a six inch Conflat flange. Plates that contain A1 and A2 attach to the atmosphere and vacuum sides of the flange, respectively, and are each sealed by an O-ring. The O-rings also serve to electrically isolate these plates from the flange. The ionization region is pumped through four ports that enter from the circular side of the flange.

There are two general modes of operation of the ion source. In one mode, a glow discharge is established coaxially with the ion-beam flight direction in the air between the plates containing A1 and A2. In the other mode, a glow discharge is established perpendicular to the ion-beam flight direction between plates P1 and P2. In both cases, a glow discharge occurs spontaneously when the voltage difference between

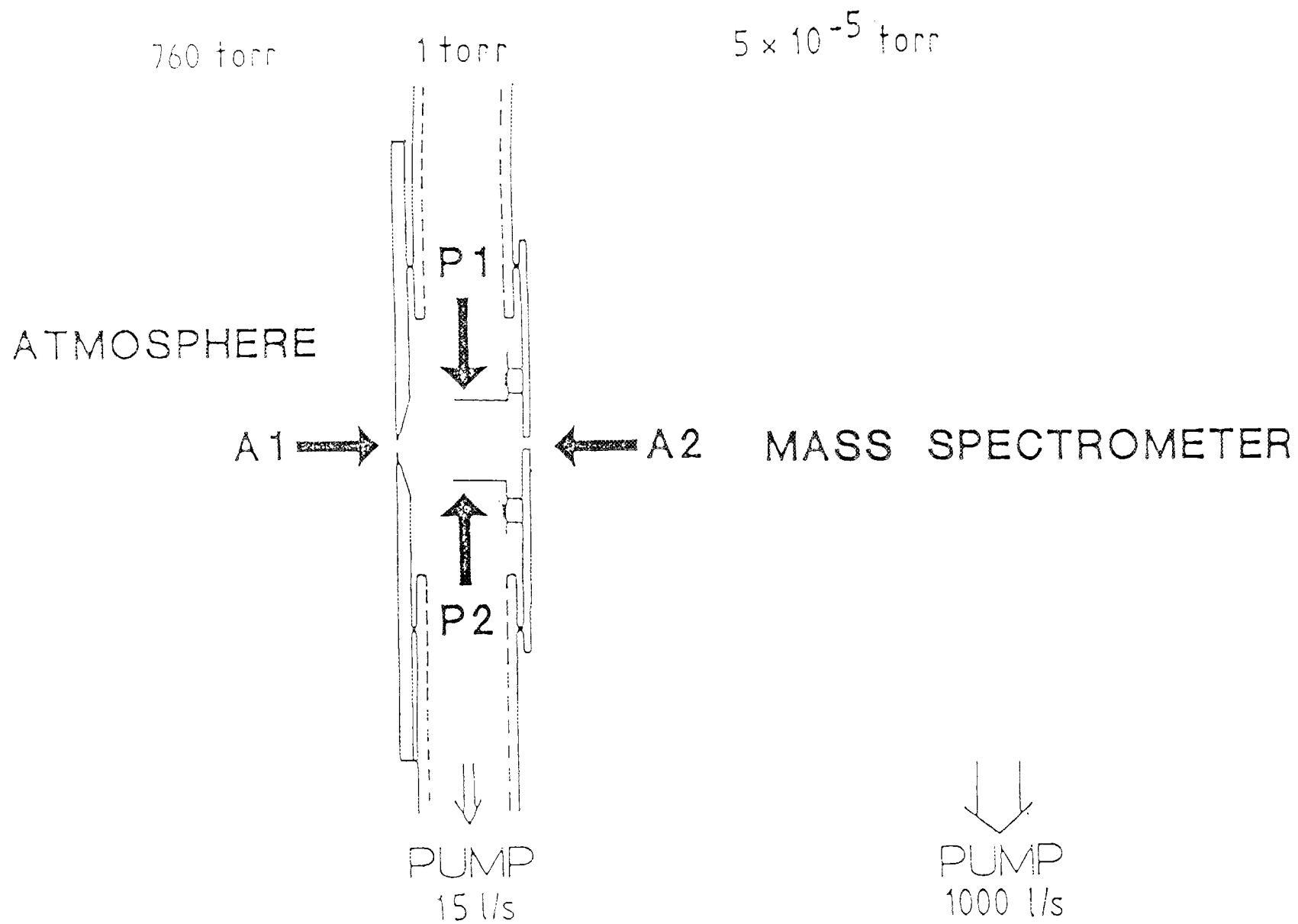


Figure 2. Schematic diagram of the atmospheric sampling glow discharge ionization source.

the opposite electrodes is about 400 V with a discharge current of 3-10 mA. The former mode is used when negative ions are sampled by the mass spectrometer. In this case, the plate containing A1 is held at about -400 V and the plate containing A2 is held at about -10 V. The latter mode is better suited to studying positive ions. P1 and P2 are typically held at about +200 V and -200 V, respectively, and the plate containing A2 is varied to optimize extraction of the ions into the mass spectrometer.

The detection of vapors of flammable liquids in air is best accomplished by sampling positive ions. Most of the compounds of interest, e.g. hydrocarbons, do not form stable negative ions and therefore are not detected in the negative ion mode. For this reason, efforts relevant to the detection of vapors of flammable liquids have exclusively employed the second method of operating the glow discharge ionization source, viz. establishing the discharge between plates P1 and P2. Ions are formed by a variety of mechanisms in the glow discharge. Molecules present in trace quantities, however, are predominantly ionized from proton transfer or electron transfer with ions present in excess. The ions present in excess are derived from ambient air and are mostly O_2^+ , H_3O^+ , and water clusters of the formula $(H_2O)_nH^+$ where $n \leq 5$. In this regard, the mass spectra observed are often similar to those obtained with chemical ionization (CI) ion sources, where similar pressures are employed. The ions identified above serve as the "reagent ions" in the positive ion mode. The mass spectra obtained in the positive ion mode are often sensitive to the discharge voltage (or current). This is illustrated in Figure 3 which compares mass spectra obtained for n-butylbenzene (molecular weight=134 daltons) using three different discharge voltages. The n-butylbenzene molecular ion is a much studied ion in mass spectrometry and its fragmentation behavior is well characterized. It has been repeatedly observed that the ratio of the daughter ions m/z 91 ($C_7H_7^+$)/ m/z 92 ($C_7H_8^+$) increases with the internal energy of the molecular ion. This ratio has therefore been used to characterize different methods of ionization and excitation with respect to the energy deposited into the molecular ion. Referring to Figure 3, at low

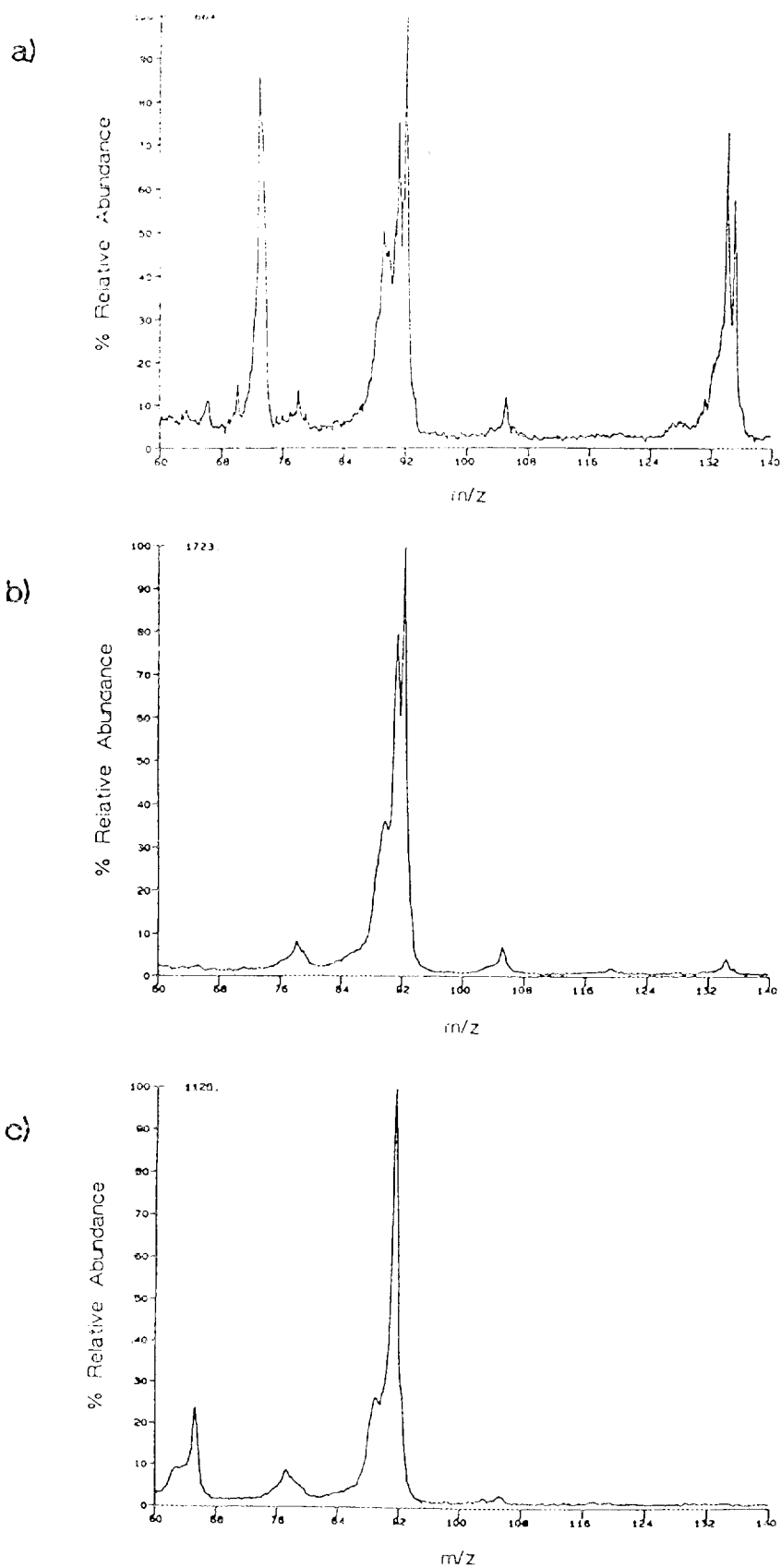


Figure 3. Mass spectra of *n*-butylbenzene at a) low discharge voltage, b) intermediate voltage, and c) high voltage.

discharge voltage (376 V), a voltage just above that required to sustain the discharge, the molecular ion is observed at m/z 134 and the protonated molecule appears at m/z 135. Daughter ions appear at m/z 89, 91, 92, and 105. A large peak is observed at m/z 73 which is due to the protonated tetramer of water, $(H_2O)_4H^+$. The protonated pentamer of water is also present and contributes to the signal at m/z 91. (This is not obvious from the mass spectrum but is clearly shown in the MS/MS spectrum. See section III.) Even with a significant contribution to m/z 91 from $(H_2O)_5H^+$, the ion at m/z 92 is the base peak in the spectrum. At the intermediate discharge voltage of 392 V, the molecular ion and protonated molecule signals are much diminished relative to the daughter ions. The water cluster ions drop out of the spectrum and the ion at m/z 91 is made up almost entirely of $C_7H_7^+$. Greater energy deposition into the molecular ion upon formation is indicated both by its diminished intensity and by the increase in abundance of $C_7H_7^+$ relative to $C_7H_8^+$. This trend is further demonstrated in the spectrum acquired using a discharge voltage of 409 V. The molecular ion is no longer observed, m/z 91 dominates the spectrum, and daughter ions that require greater energies for formation appear at m/z 78 and 65. This example is given to demonstrate that the ion source provides a degree of flexibility in ionization. At low discharge voltages ions are formed with low internal energies, whereas at high discharge voltages greater energies are imparted upon ionization resulting in more extensive fragmentation.

B. MS/MS Instrument

The atmospheric sampling ion source has been mated to a tandem mass spectrometer that consists of a quadrupole mass filter and a time-of-flight mass spectrometer. The quadrupole/time-of-flight combination was chosen to provide both high transmission and fast data acquisition to allow for fast measurements on low level signals. A quadrupole mass filter was chosen as the first stage mass analyzer since the ion transmission is relatively high (2-15%) and the voltages applied to the rods can be quickly and reproducibly changed to hop from one peak of interest to the next. Furthermore, quadrupoles are compatible with ion sources held near ground potential. It is desirable to avoid use of an

ion source that must be held at kilovolt potentials in order to avoid sparking, a problem often observed at the pressures used by the atmospheric sampling ion source. A magnetic analyzer is much less suitable for the present application. Time-of-flight was chosen as the second mass analyzer due to its inherently high transmission (>90%) and its capability to obtain the complete MS/MS daughter ion spectrum in a single pulse.

The triple quadrupole instrument is perhaps the beam-type MS/MS geometry that comes closest to the quadrupole/time-of-flight in terms of sensitivity and speed and therefore serves as a benchmark for comparison. The overall efficiency of an instrument in the MS/MS mode is determined by the transmission of the various analyzers and the efficiency of CID. Both the triple quadrupole and quadrupole/time-of-flight instruments employ low energy collisions so the CID efficiency should be the same. The product of the collection efficiency and the transmission of the last quadrupole in a triple quadrupole instrument is typically about 2% at high collision gas pressures and up to about 9% at low collision gas pressures. For a variety of positively charged ions and negatively charged ions studied with the quadrupole instrument, the product of the collection efficiency and transmission of the time-of-flight analyzer is from 25% at high collision gas pressures to 95% at low collision gas pressures. The MS/MS efficiency of the quadrupole/time-of-flight geometry is therefore roughly an order of magnitude greater than that of the triple quadrupole instrument. A further advantage is realized from the ability to obtain the complete MS/MS spectrum in a single pulse using time-of-flight analysis. For a hypothetical example of unit mass resolution with a parent ion of m/z 200, the maximum duty cycle of the time-of-flight analyzer is 0.5% ($1/\text{resolution}$), whereas the last quadrupole in a triple quadrupole system must scan over an absolute minimum of 400 points (equivalent to a duty cycle of 0.25%) and in practice will probably scan over 1000 to 2000 points (0.1 to 0.05% duty cycle). Thus, the time-of-flight analyzer will have at least a factor of 2 increase in sensitivity and more likely a factor of 5-10 over the quadrupole analyzer as a result of its "simultaneous" detection capabilities. In principle, therefore,

the quadrupole/time-of-flight geometry has between one and two orders of magnitude greater sensitivity (or speed) than a triple quadrupole system for acquiring a complete MS/MS spectrum.

Figure 4 shows a schematic diagram of the quadrupole/time-of-flight instrument constructed at ORNL. Ions that issue from the ion source are focussed into a standard Extrel quadrupole mass filter (pole diameter = 1.6 cm). This mass filter is controlled by Extrel C50 electronics and is operated at 1.2 MHz with a 200 watt rf supply. The mass range of the quadrupole operated under these conditions is about 500 daltons. Ions that exit the quadrupole are focussed by an einzel lens into a 1 cm long collision cell. Ions that exit the collision cell are then accelerated into the time-of-flight portion of the instrument.

The time-of-flight portion of the instrument originally consisted of a linear drift region of approximately one meter in length. Since then, a 180° electric sector has been incorporated into the time-of-flight measurement making the flight length about 1.3 meters. The electric sector was added to allow for future studies with high collision energy MS/MS. For the experiments to date, however, it serves to dramatically reduce the background noise previously observed with the former line-of-sight geometry of the instrument by reducing the number of neutral species and photons that reach the detector. No slits are used with the electric sector minimizing its energy discrimination. Since all ions are accelerated into the time-of-flight region, the energy spread of the ions is relatively small (a few percent). This allows the voltages applied to the electric sector plates to remain fixed during the experiment while transmitting both parent and daughter ions. The ions are gated into the time-of-flight region by a set of deflection plates mounted on the last plate of the acceleration lens assembly. After transit through the time-of-flight drift region, the ions are detected by a modified Galileo model 4873 channeltron electron multiplier. This detector was modified by changing the angle of the conversion dynode from approximately 60° to the plane normal to the ion beam to about 85°. This modification improved the ion detection and further reduced background noise. Ion

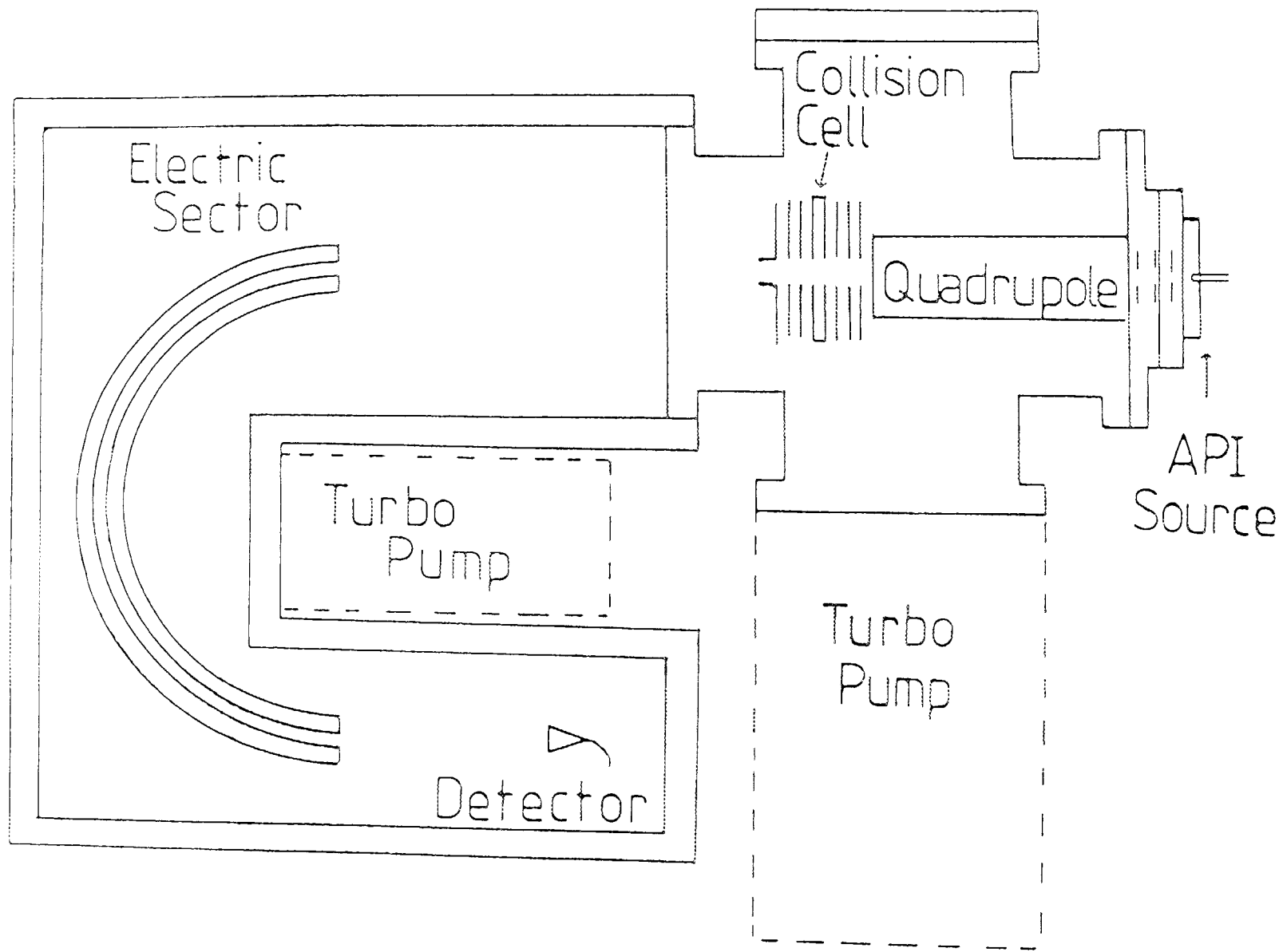


Figure 4. Schematic diagram of the quadrupole/time-of-flight mass spectrometer.

kinetic energies are on the order of tens of electron volts as they pass through the quadrupole mass filter and enter the collision cell. For time-of-flight analysis, all ions that exit the collision cell must be accelerated to several kiloelectron volts to reduce their relative energy spread. This is accomplished by accelerating the ions by approximately 3000 V and floating the time-of-flight drift region at the accelerating potential. The electric sector plate voltages are therefore adjusted so that the central trajectory of the ions through the electric sector is at the accelerating potential and field-free regions of the time-of-flight region are surrounded by screens that are maintained at the accelerating potential.

The quadrupole mass filter, collision cell and lens system of the instrument are housed in a six-way cross with ten-inch conflat flanges. This region is pumped by a 1000 l/s turbomolecular pump. The base pressure of the instrument when the atmospheric sampling ion source is attached is about 5×10^{-5} torr. When gas is admitted into the collision cell to a pressure of about 1×10^{-3} torr, the pressure in the six-way cross rises to about 9×10^{-5} torr. The time-of-flight region is housed by a flight tube connected on one end to the ten-inch six-way cross and on the other to a box that contains the electric sector. A four and one-half inch six-way cross is attached to the electric sector box at the exit side of the electric sector. This cross houses the detector and is pumped by a 110 l/s turbomolecular pump.

In order to realize the potential of time-of-flight in MS/MS, a high speed data acquisition system was constructed. The system is shown schematically in Figure 5. The system is controlled by an IBM-XT and is based on an 8-hit time-to-digital converter (TDC) (LeCroy model 4208) and a CAMAC crate controller (LeCroy model 4802). The 8-hit TDC will accept up to eight stop signals for every start pulse. The flight times of up to eight ions can therefore be recorded for every time-of-flight pulse. The time-of-flight gate is pulsed through a dual gate timer (LeCroy model 2323A) to start the TDC and the stop pulses come from the detection of ions by the channeltron, which is operated in the

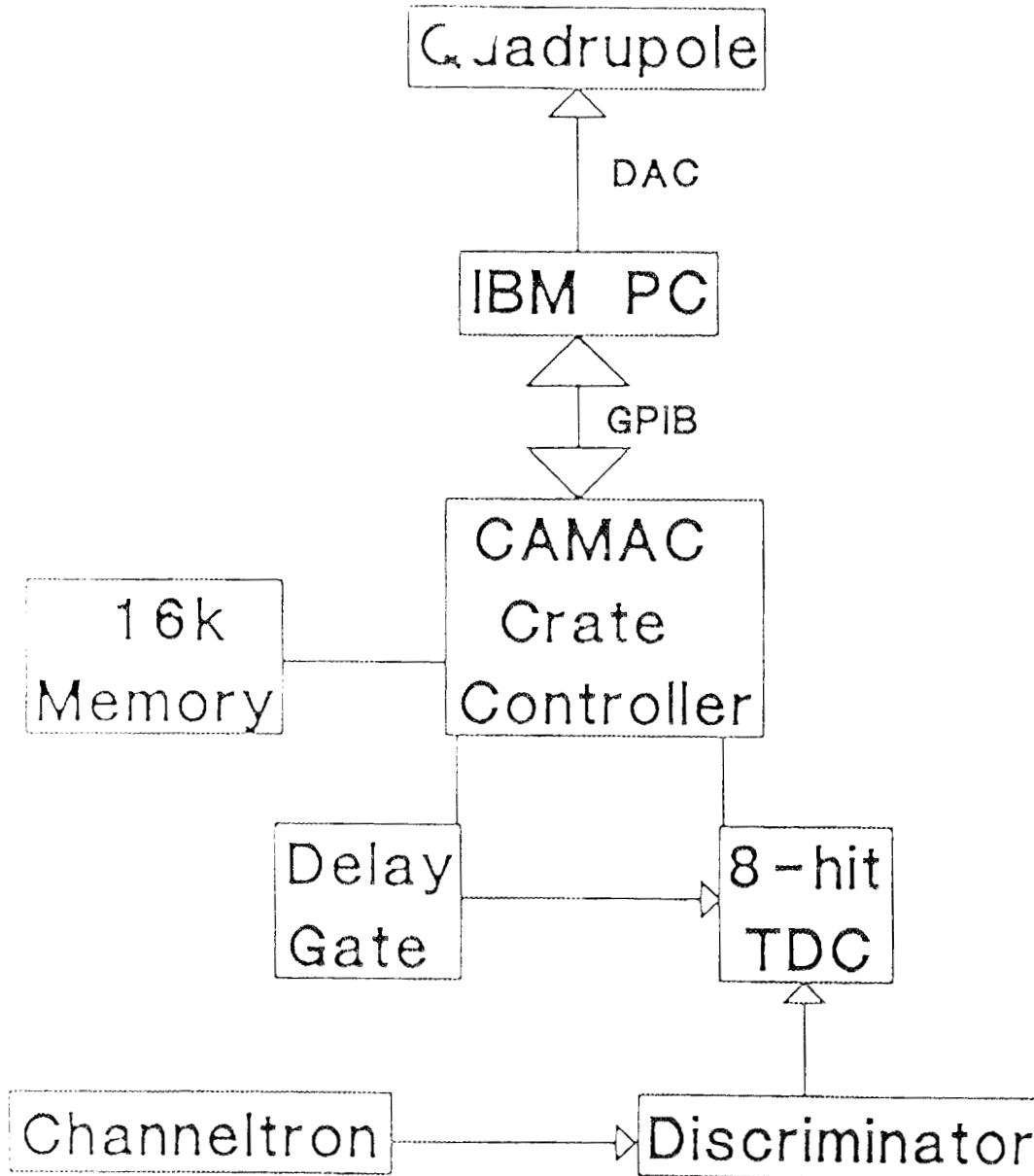


Figure 5. Data acquisition schematic for the quadrupole/time-of-flight mass spectrometer.

pulse counting mode. The TDC is shut off either by the eighth stop pulse or by a delay pulse, whichever comes first, and the data are then transferred from the TDC to the CAMAC crate controller. When the data transfer is complete, the TDC is cleared and ready for the next time-of-flight pulse. While data are being acquired for the subsequent time-of-flight pulse, the data in the CAMAC crate controller from the previous pulse are being histogrammed and stored in memory in the CAMAC crate. For the experiments described here, this sequence is repeated at a frequency of 20 kHz.

The CAMAC crate controller communicates with the host IBM-XT via a GPIB interface. The program for the CAMAC crate controller is downloaded from the IBM and, when a time-of-flight experiment is completed, the data are transferred from the CAMAC crate controller to the IBM. A time or intensity limit, entered by the operator via the IBM keyboard, determines when data acquisition is to be stopped. The CAMAC crate controller is also capable of controlling the time period of the delay gate and various voltages used in the system such as the deflection plate voltage. The IBM-XT controls the quadrupole mass filter directly and is currently being programmed to control other parameters such as lens, ion source, and detector voltages.

III. Characterization of Fuel Mixtures

Several types of hydrocarbon fuel mixtures were obtained for testing with the atmospheric sampling MS/MS instrument. These included six gasoline samples obtained from local distributors, kerosene, jet fuel, and lighter fluid. Prior to testing these complex mixtures with the tandem mass spectrometer, they were studied using gas chromatography/mass spectrometry (GC/MS) with electron impact ionization in order to identify the major mixture components. Electron impact ionization, unlike atmospheric sampling glow discharge ionization, is a more or less universal ionization method. The cross-sections for ionization of most organic molecules by electron impact using 70 eV energy electrons do not vary by orders of magnitude, as they can with selective ionization methods such as chemical ionization. The GC/MS results therefore provide us with a basis for interpreting the results obtained with glow discharge ionization.

All GC/MS for the gasoline samples were acquired using a Kratos MS25 GC/MS instrument. A 25 m x 0.2 mm fused silica column, deactivated with Carbowax 20M, with a methyl silicone stationary phase was used for the chromatography with helium carrier gas at a flow rate of 2 ml/min. The injector, interface and transfer lines were maintained at 240° C and the re-entrant was held at 175° C. The temperature program consisted of holding the sample at -30° C for 5 minutes and then ramping the temperature at a rate of 4° C/min. up to 240° C and holding at this temperature for 20 min. In each case, 0.05 µl of sample was injected directly onto the column. Mass spectra were obtained at an accelerating voltage of 2 kV using 70 eV electron impact ionization and an ion source temperature of 200° C. The mass spectrum was scanned at a rate of 1 s/decade with a mass resolution ($M/\delta M$ at half height) of about 600.

The gas chromatograms for all of the gasoline samples were very similar. Likewise, the mass spectra obtained for any given GC peak varied little with the sample. Therefore, data for one gasoline sample is discussed in detail here. Figure 6 shows the 70 eV electron impact mass spectrum from a 0.15 µl sample of gasoline, obtained at the Oak

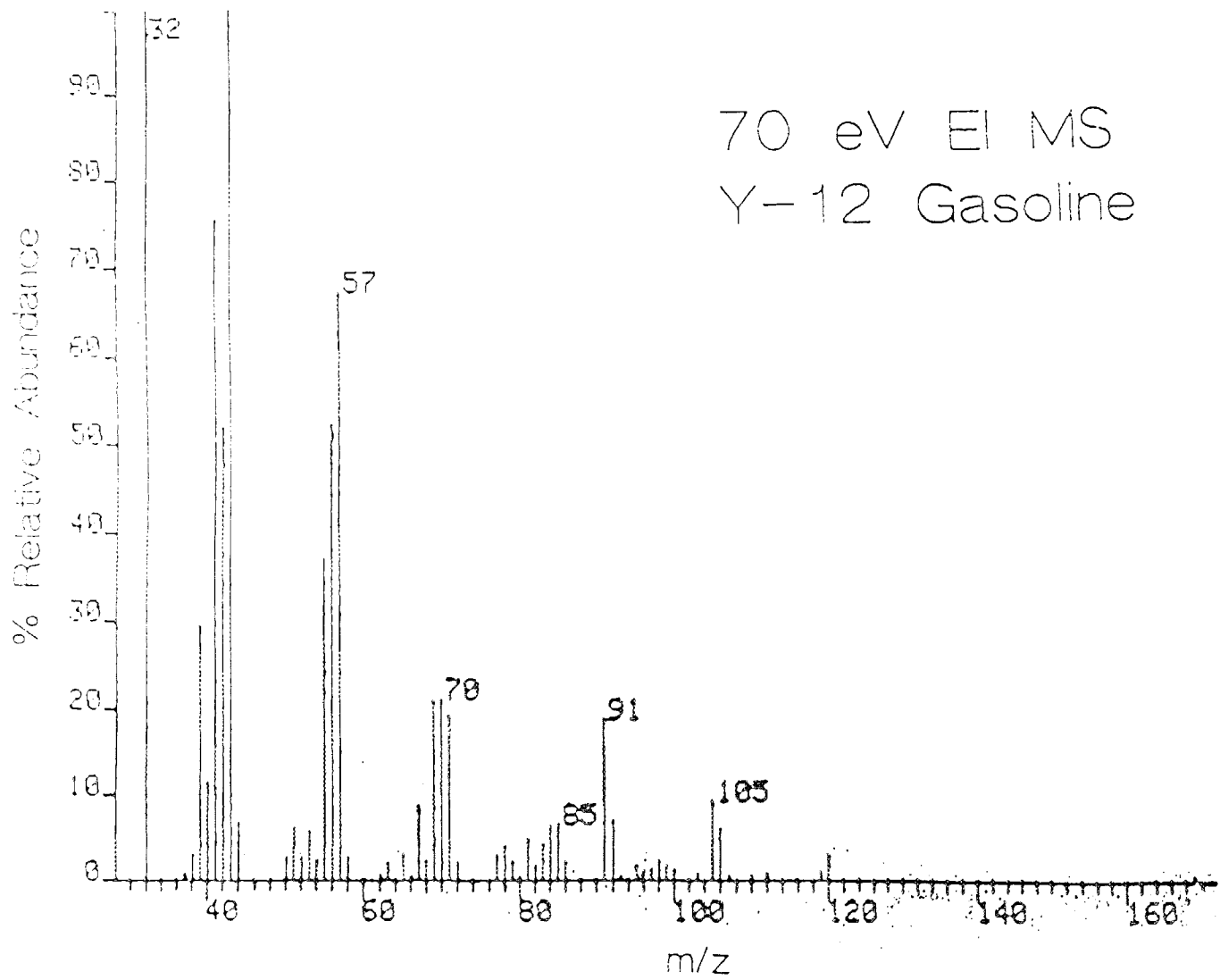


Figure 6. 70 eV electron impact mass spectrum of gasoline.

Ridge Y-12 plant, admitted directly into the ion source (no chromatography) via a direct insertion probe. The mass spectrum shows primarily low mass fragments that are commonly observed from hydrocarbons. The groups of ions with m/z values in the low forties, mid to upper fifties, low seventies, and mid eighties are typical of alkanes and alkenes. The ions at or near m/z 120, 105, 91, 78, 65, 51, and 39 are typical of aromatic hydrocarbons, alkylbenzenes in particular. Figure 7 shows the full gas chromatogram for this sample. The ordinate at the top of the figure is time and the ordinate at the bottom of the figure indicates the mass spectrum number. In many cases, a GC peak was comprised of several co-eluting mixture components so that the mass spectrum reflected contributions from each of these mixture components. Figure 8 shows the chromatogram obtained during the first 20 minutes of data collection. At scan number 17 the mass spectrum shown in Figure 9 was obtained. This spectrum matches that of n-butane. Similarly, the mass spectrum obtained for the peak observed at scan number 30 matched that of 3-methylbutane. Broad peaks reflecting poor separation are seen throughout the chromatogram. For example, mass spectra obtained from the broad signal observed in the scan numbers of 80 to 90 indicate a mixture of primarily C_6H_{14} hydrocarbons. Assignments of the compounds that are likely to give rise to the peaks in Figure 7 have been made based on the mass spectra. The assignments are listed in Table I. Several general trends are noted in the data. For example, the samples are made up primarily of C_4 - C_8 alkanes and alkenes and C_0 - C_4 alkylbenzenes. The alkanes and alkenes pass through the chromatograph before the alkylbenzenes and, within a compound class, compounds elute from the column in the order of low mass to high mass. These observations are consistent with the general trends in vapor pressures.

A sample of 1K low sulfur grade kerosene was analyzed by GC/MS. The GC conditions are the same as those used for the gasoline samples except that the kerosene was held at $0^\circ C$ for 5 minutes before the $4^\circ C/min.$ temperature ramp rather than at $-30^\circ C$. Figure 10 shows the full gas chromatograph obtained for kerosene. A large unresolved

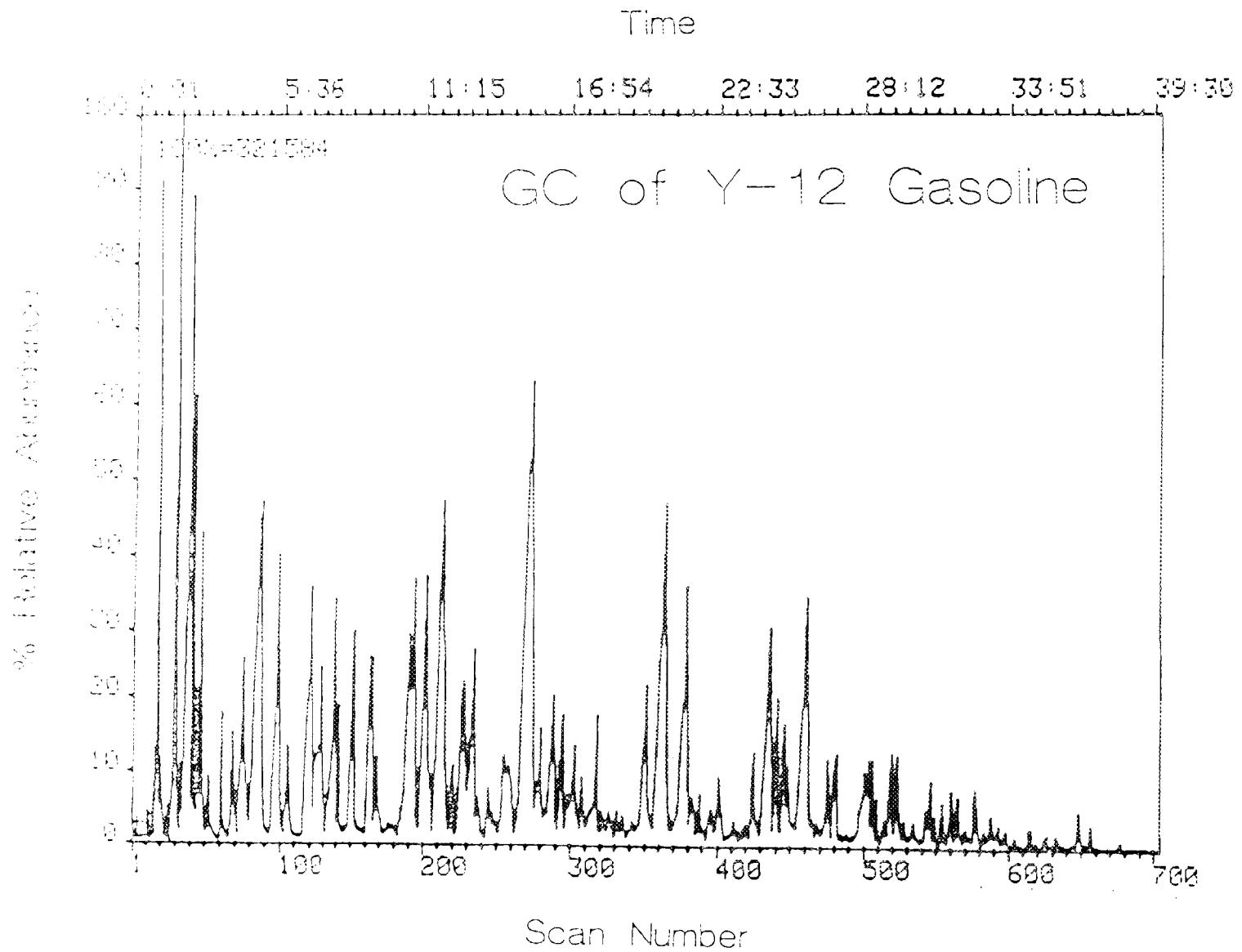


Figure 7. Gas chromatograph of gasoline.

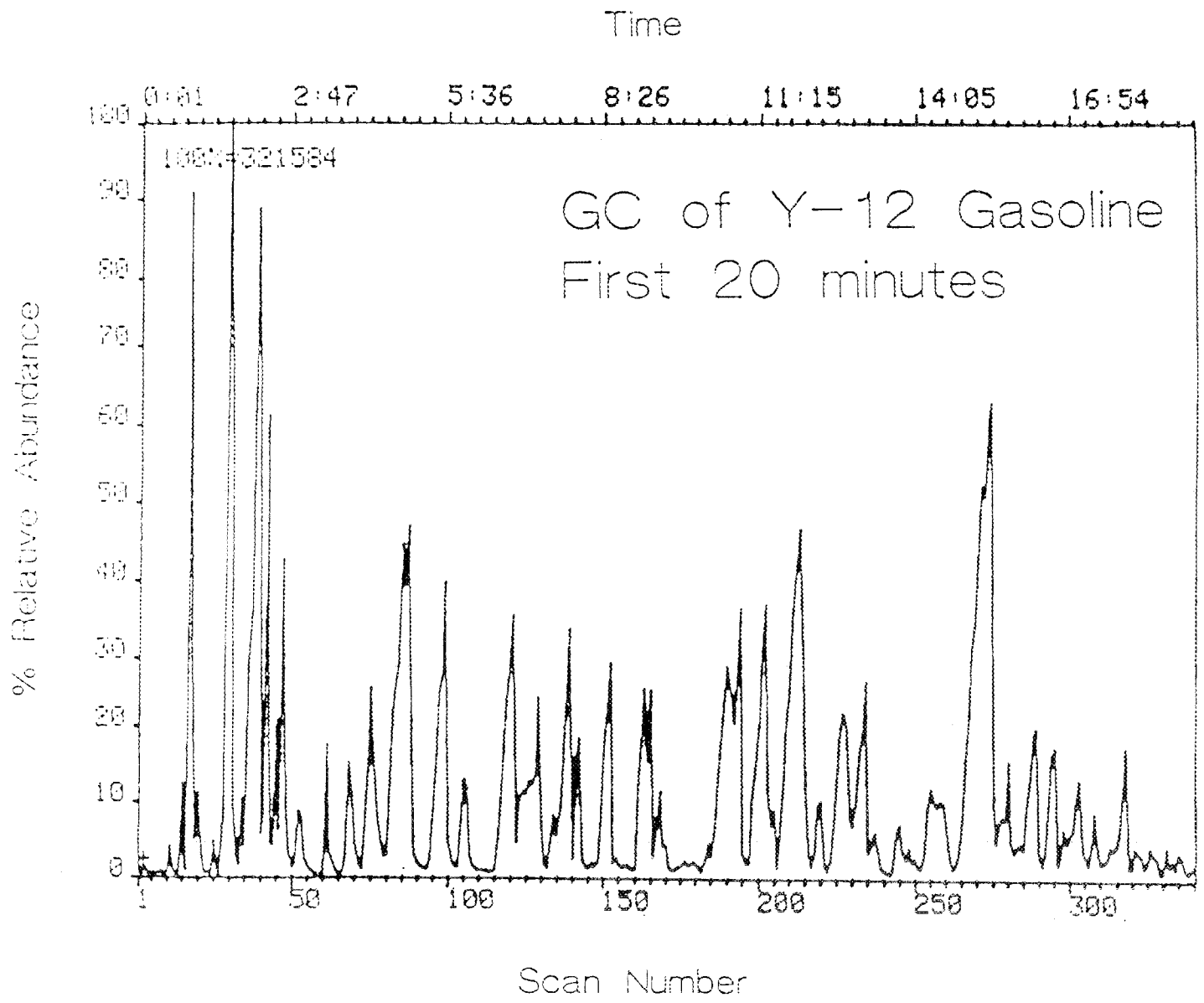


Figure 8. First 20 minutes of gasoline GC run.

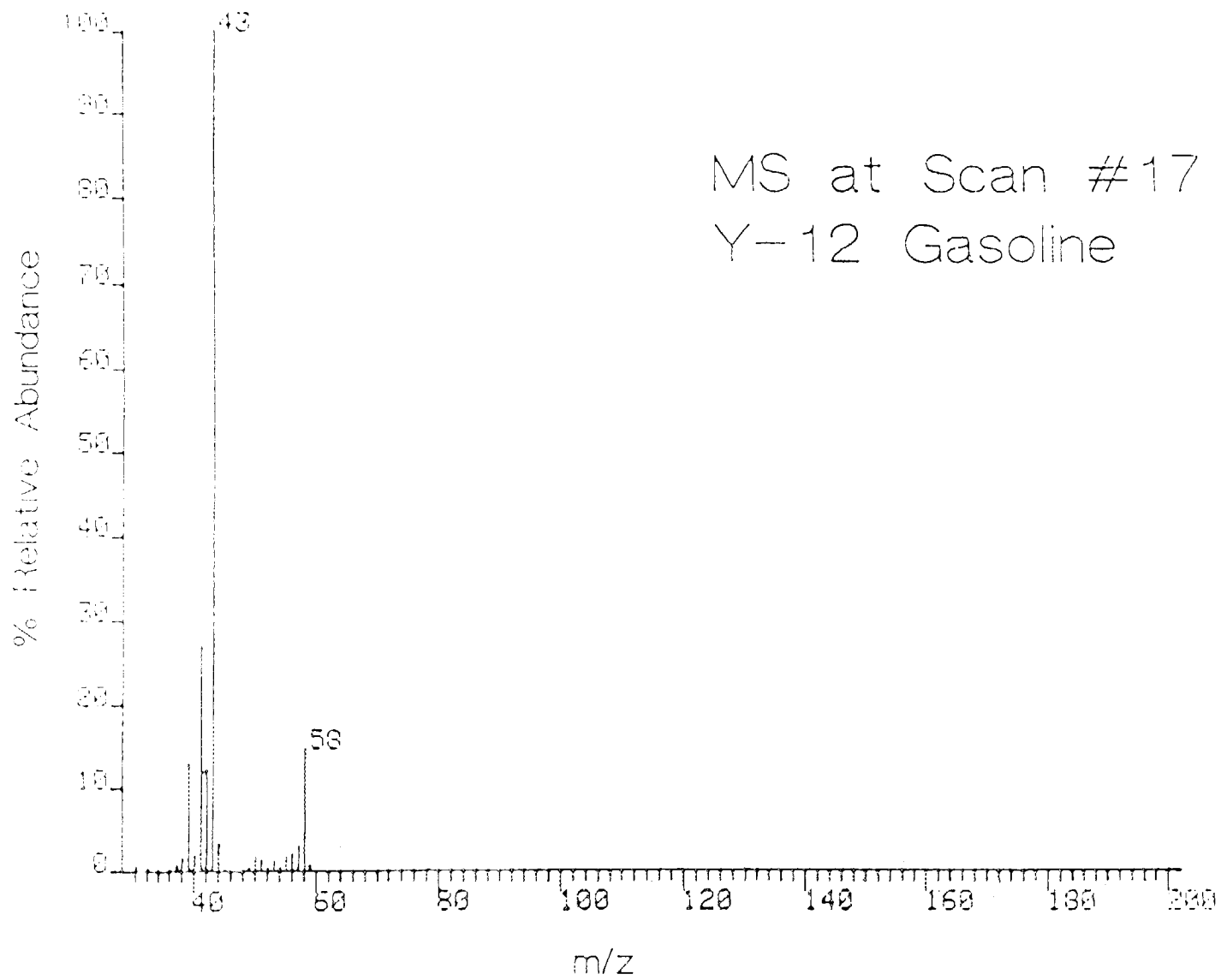


Figure 9. Scan #17 of GC run.

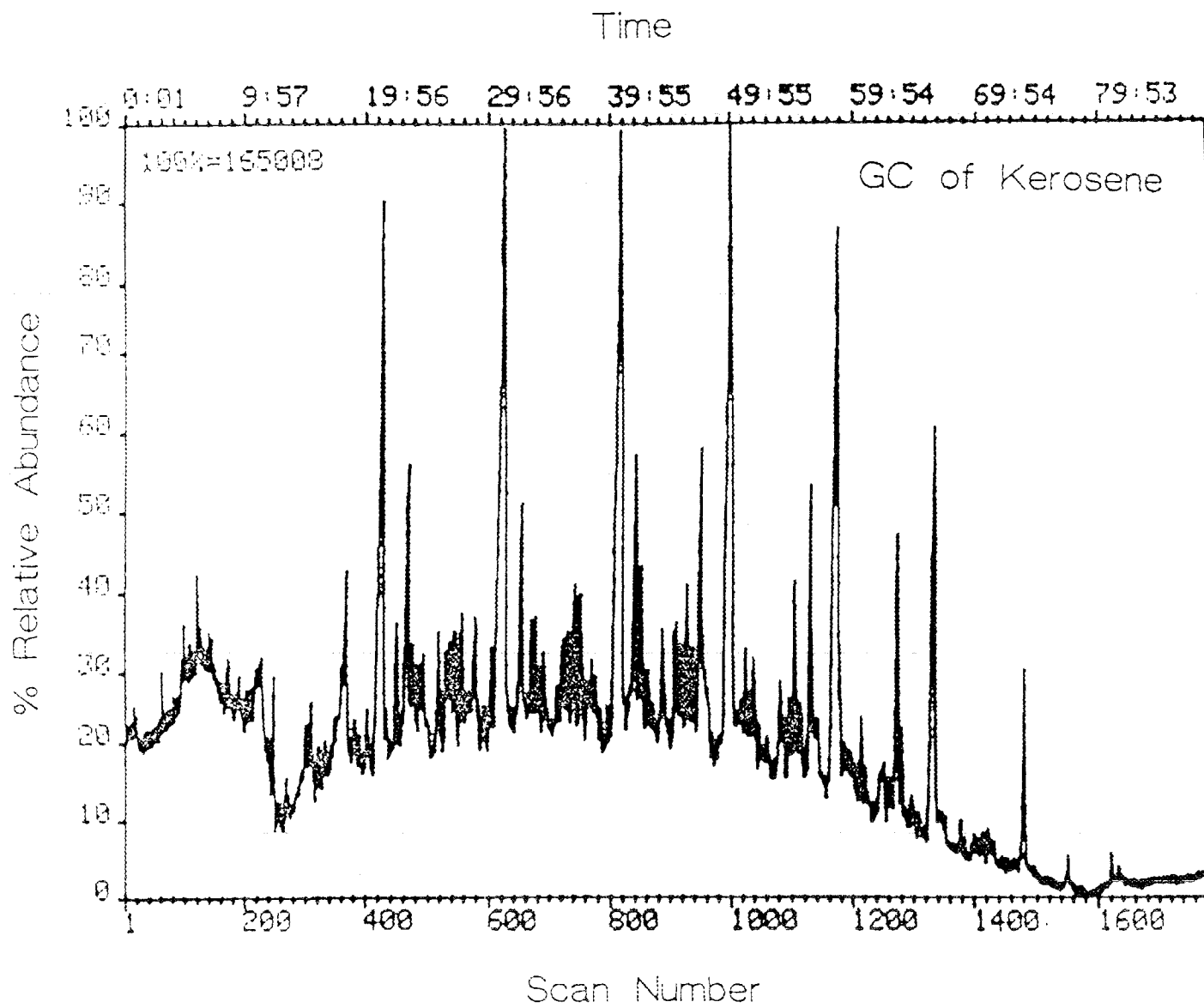


Figure 10. Gas chromatograph of kerosene.

Table I
Unleaded Gasoline

Scan #	Probable compound(s)	Scan #	Probable Compound(s)
15	iso-butane C_4H_{10}	219	methylhexadiene C_7H_{12}
17	n-butane C_4H_{10}	224	heptadiene C_7H_{14}
20	butenes C_4H_8	227	C_7H_{16} , C_7H_{14} , C_7H_{12}
25	2 or 3-methylbutene	232	C_7H_{14}
30	2-methylbutane C_5H_{12}	234	"
34	1-pentene C_5H_{10}	237	dimethylcyclopentane
36	dimethylcyclopropane	255	dimethylhexane C_8H_{18}
39	n-pentane C_5H_{12}	266	toluene and C_8H_{18}
42	2-pentene C_5H_{10}	271	toluene
45	2-pentene C_5H_{10}	274	"
47	2-methyl-2-butene	280	2,3-dimethylhexane
49	pentadiene C_5H_8	286	dimethylcyclohexane
61	cyclopentene C_5H_8	289	dimethylhexane
69	C_6H_{12} and C_5H_{10}	293	methylheptane
74	2,3-dimethylbutane	295	dimethylhexane
75	" "	303	tetramethylhexane
78	C_6H_{12} and C_6H_{14}	308	C_8H_{14} and C_8H_{16}
81	2-methylpentane	318	C_8H_{14} , C_8H_{16} , C_8H_{18}
85	" "	348	a xylene
87	" "	351	"
95	3-methylpentene	358	"
97	" "	364	"
99	" "	366	" and C_9H_{16}
104	2-methyl-1-pentene	376	"
106	3-hexene C_6H_{12}	381	" and C_9H_{18}
117	C_6H_{14} and C_6H_{12}	384	trimethylheptane
121	n-hexane C_6H_{14}	401	propylbenzene, C_9H_{20}
124	C_6H_{12} and C_6H_{10}	403	" , C_9H_{18}
126	2-hexene C_6H_{12}	432	methylethylbenzene
129	methylpentene(s)	436	" "
134	2-hexene (cis)	441	trimethylbenzene
137	methylcyclopentane	445	methylethylbenzene
139	" "	448	C_9H_{20}
142	methylpentene(s)	455	trimethylbenzene
149	C_6H_8 and C_7H_{16}	475	methylethylbenzene
152	C_7H_{16}	480	$C_{10}H_{14}$
163	benzene C_6H_6	497	diethylbenzene $C_{10}H_{14}$
165	2,4-hexadiene C_6H_{10}	500	methylpropylbenzene
168	cyclohexane C_6H_{12}	506	dimethylethylbenzene
186	C_7H_{14}	509	methylpropylbenzene
189	C_7H_{14}	519	3-propyltoluene
194	2-methylhexane C_7H_{14}	521	$C_{10}H_{14}$
198	a dimethylcyclopentane	543	dimethylethylbenzene
202	C_7H_{14} and C_7H_{16}	549	$C_{11}H_{24}$
205	dimethylpentene(s)	554	allyltoluene $C_{10}H_{12}$
209	trimethylpentane	565	$C_{10}H_{14}$, $C_{11}H_{16}$
213	" "	577	naphthalene, azulene
216	" " and C_7H_{14}	588	dimethylindan

background is observed throughout most of the chromatograph. Virtually all mass spectra obtained throughout the experiment showed intense peaks at m/z values of 41, 43, 55, 57, 69, 71, and 85 indicating that the background is composed largely of aliphatic and olefinic hydrocarbons. Mass spectra were obtained for the compounds that make up the major peaks observed in gas chromatograph. Assignments of the likely compound type(s) that gives rise to the major peaks in the gas chromatograph, based on the 70 eV electron impact mass spectra, are listed in Table II. The results show that kerosene is a complex mixture composed primarily of C_9 - C_{16} alkanes and alkenes with smaller amounts of C_4 -alkylbenzenes and C_0 - C_2 naphthalenes. The overall mixture is more highly concentrated in saturated hydrocarbons than the gasoline samples. Figure 11 shows the 70 eV electron impact mass spectrum obtained from 0.1 μ l of kerosene admitted directly into the ion source (no chromatography). Like the gasoline mass spectrum, low mass ions indicative of aliphatic hydrocarbons are dominant. This spectrum indicates, however, the presence of higher mass hydrocarbons as reflected by the signals at masses greater than m/z 85. The presence of alkyl aromatic hydrocarbons is indicated by the peaks at m/z 119 and m/z 105. These ions are in greater relative abundance than m/z 91, in contrast to the gasoline samples. This is, of course, consistent with the fact that primarily C_4 -alkylbenzenes are present in kerosene whereas C_0 - C_3 -alkylbenzenes are present in gasoline. Finally, only small peaks are observed at m/z 128, m/z 142, and m/z 154 that may reflect the presence of the C_0 - C_2 naphthalenes.

Jet fuel (1A) was analyzed by GC/MS using the same conditions as used for kerosene. Figure 12 shows the chromatograph obtained for jet fuel and Table III lists the compound types assigned to the major GC peaks based on the mass spectra. The data show that jet fuel is a complex mixture very similar to kerosene. The distribution of carbon numbers appears to be slightly narrower in the jet fuel than in the kerosene. The distribution is peaked at C_{12} with smaller relative contributions from C_{10} and C_{16} compounds than in the kerosene sample. Like the kerosene sample, the jet fuel sample is comprised of at most a few percent of alkylbenzenes and naphthalenes. The 70 eV electron

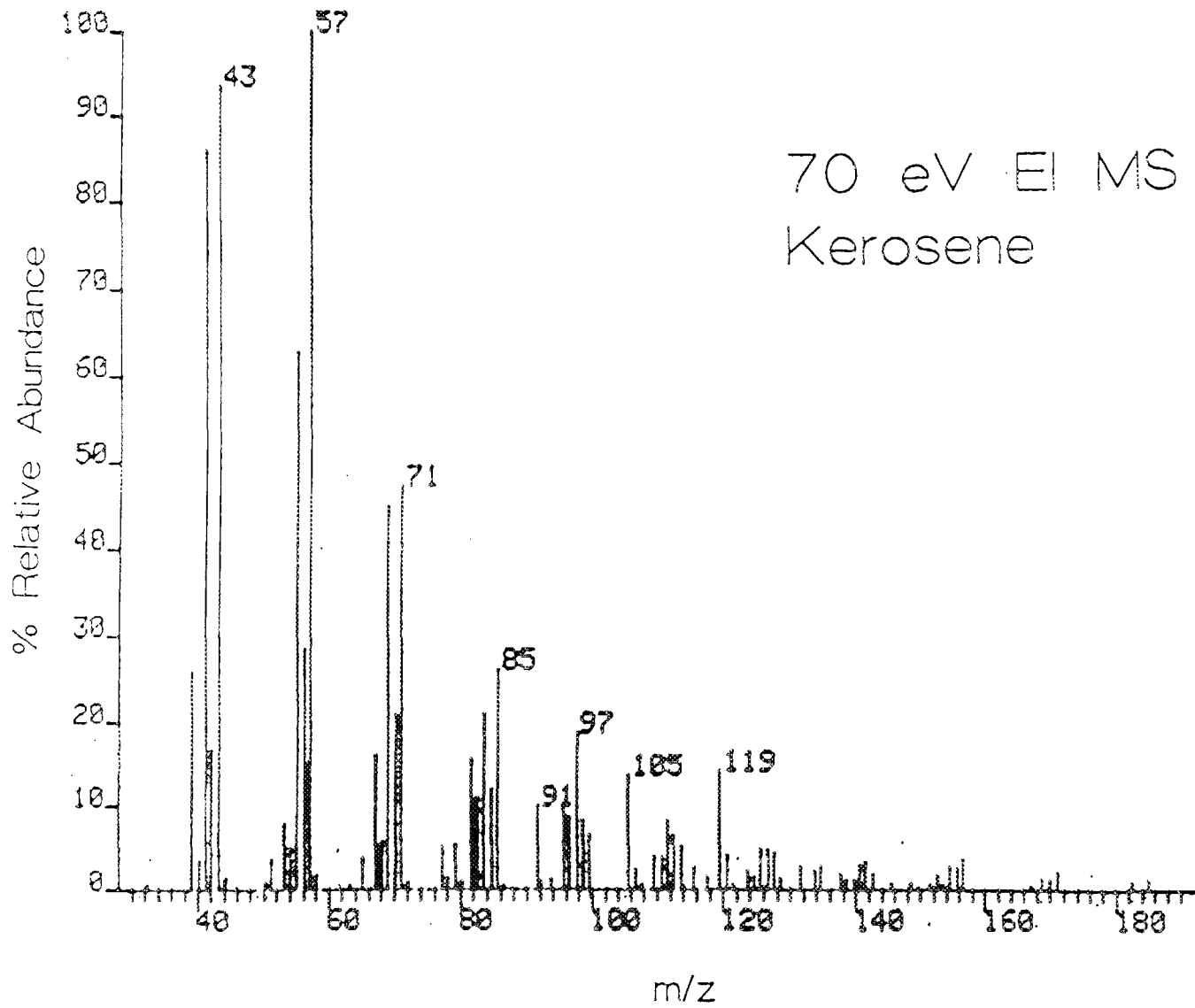


Figure 11. 70 eV electron impact mass spectrum of kerosene.

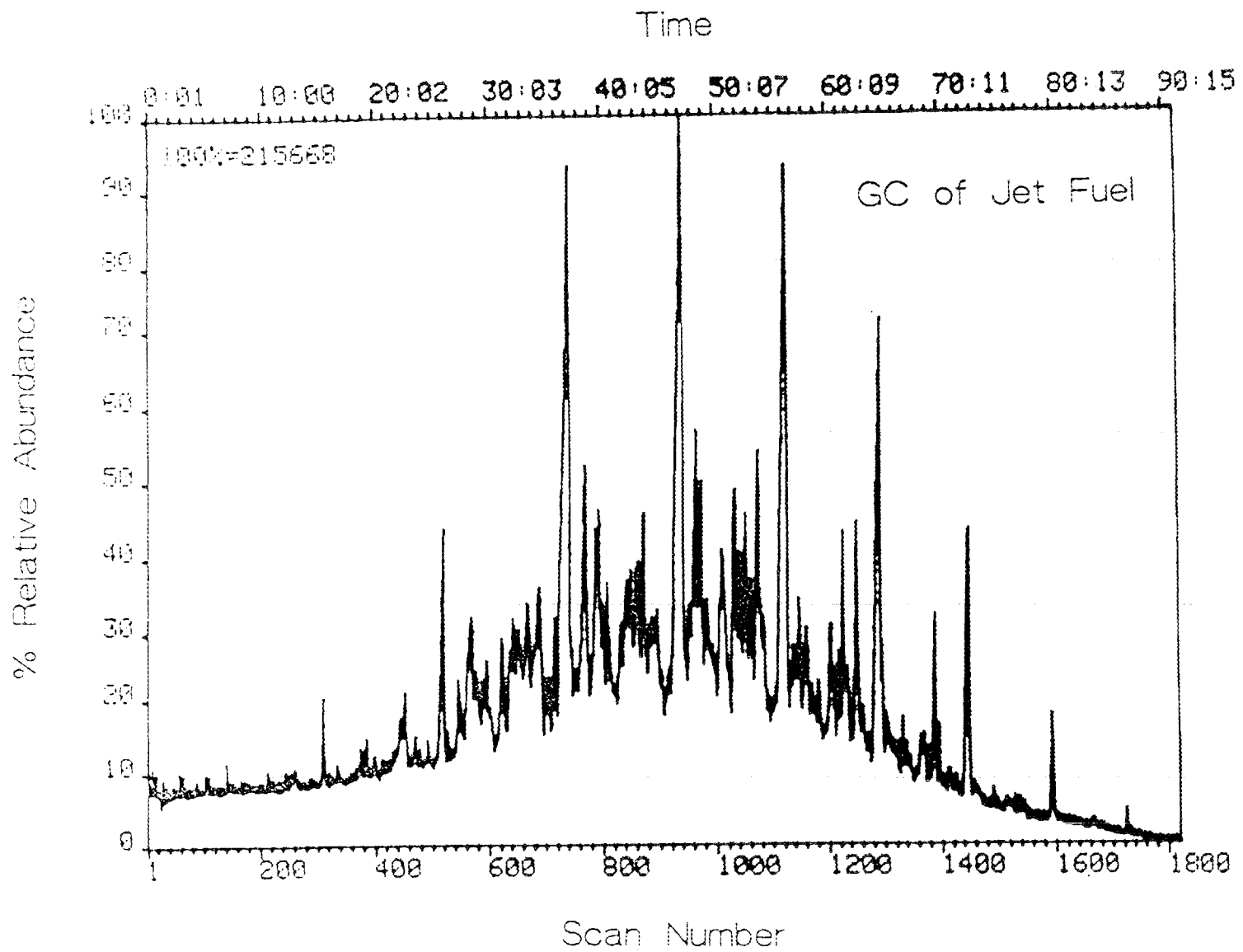


Figure 12. Gas chromatograph of jet fuel.

Table II
Kerosene 1K

<u>Scan #</u>	<u>Possible Compound(s)</u>
250	C_9H_{20} branched hexane or pentane; alkylbenzene
367	$C_{10}H_{20}$ 1-decene
428	$C_{10}H_{22}$ methylnonane or other branched hydrocarbon
452	$C_{10}H_{20}$ butylcyclohexane
470	$C_{11}H_{24}$ methyldecane isomer
518	$C_{10}H_{14}$ C_4 -alkylbenzene
557	$C_{11}H_{22}$ undecane
625	$C_{11}H_{24}$ methyldecane isomer
657	$C_{11}H_{16}$ dimethylpropylbenzene; diene
668	an alkylbenzene
677	$C_{10}H_8$ naphthalene
817	$C_{12}H_{26}$ methylundecane
843	$C_{13}H_{28}$ dimethylundecane
851	$C_{12}H_{24}$ dodecene or cyclododecane
886	$C_{11}H_{10}$ methylnaphthalene
950	$C_{14}H_{30}$
1001	$C_{13}H_{28}$ dimethylundecane
1105	$C_{12}H_{12}$ dimethylnaphthalene
1132	$C_{12}H_{12}$ " "
1175	$C_{14}H_{30}$ dimethyldodecane
1334	$C_{15}H_{32}$
1481	$C_{16}H_{34}$

Table III
1A Jet Fuel

<u>Scan #</u>	<u>Possible Compound(s)</u>
310	C_9H_{20} branched hexane or pentane
453	$C_{10}H_{20}$ decene
522	$C_{10}H_{22}$ methylnonane
546	$C_{10}H_{20}$ butylcyclohexane
570	$C_{10}H_{14}$ C_4 -alkylbenzene
625	$C_{10}H_{14}$ C_4 -alkylbenzene
668	$C_{11}H_{22}$ undecene
690	$C_{11}H_{20}$ undecadiene
740	$C_{11}H_{24}$ undecane
770	$C_{11}H_{22}$ undecene; C_4 -alkylbenzene
940	$C_{12}H_{26}$ methylundecane
965	$C_{13}H_{28}$ dimethylundecane
1010	$C_{11}H_{10}$ methylnaphthalene isomer
1032	$C_{11}H_{10}$ " "
1053	$C_{11}H_{10}$ " "
1074	$C_{14}H_{30}$ dimethyldodecane
1125	$C_{13}H_{28}$ dimethylundecane
1226	$C_{12}H_{12}$ dimethylnaphthalene
1292	$C_{14}H_{30}$ dimethyldodecane
1390	$C_{16}H_{34}$
1449	$C_{15}H_{32}$
1595	$C_{16}H_{34}$

impact mass spectrum of 0.1 μl of the jet fuel is virtually indistinguishable from that of kerosene (see Figure 13).

A 70 eV electron impact mass spectrum of a 0.5 μl sample of ZippoTM lighter fluid was acquired and is shown in Figure 14. The container lists the contents to be "naptha", a low boiling fraction of petroleum. The principle components of naptha are pentanes and hexanes. The intense peaks at m/z 43, m/z 57, m/z 71, m/z 85, m/z 97, and m/z 112 in the mass spectrum of Figure 14 indicates a high aliphatic hydrocarbon content. The presence of alkylbenzenes is also indicated by peaks at m/z 91 and m/z 106. Fewer high mass peaks are observed for lighter fluid than for kerosene which probably reflects the lower carbon number fraction of petroleum that constitutes naptha.

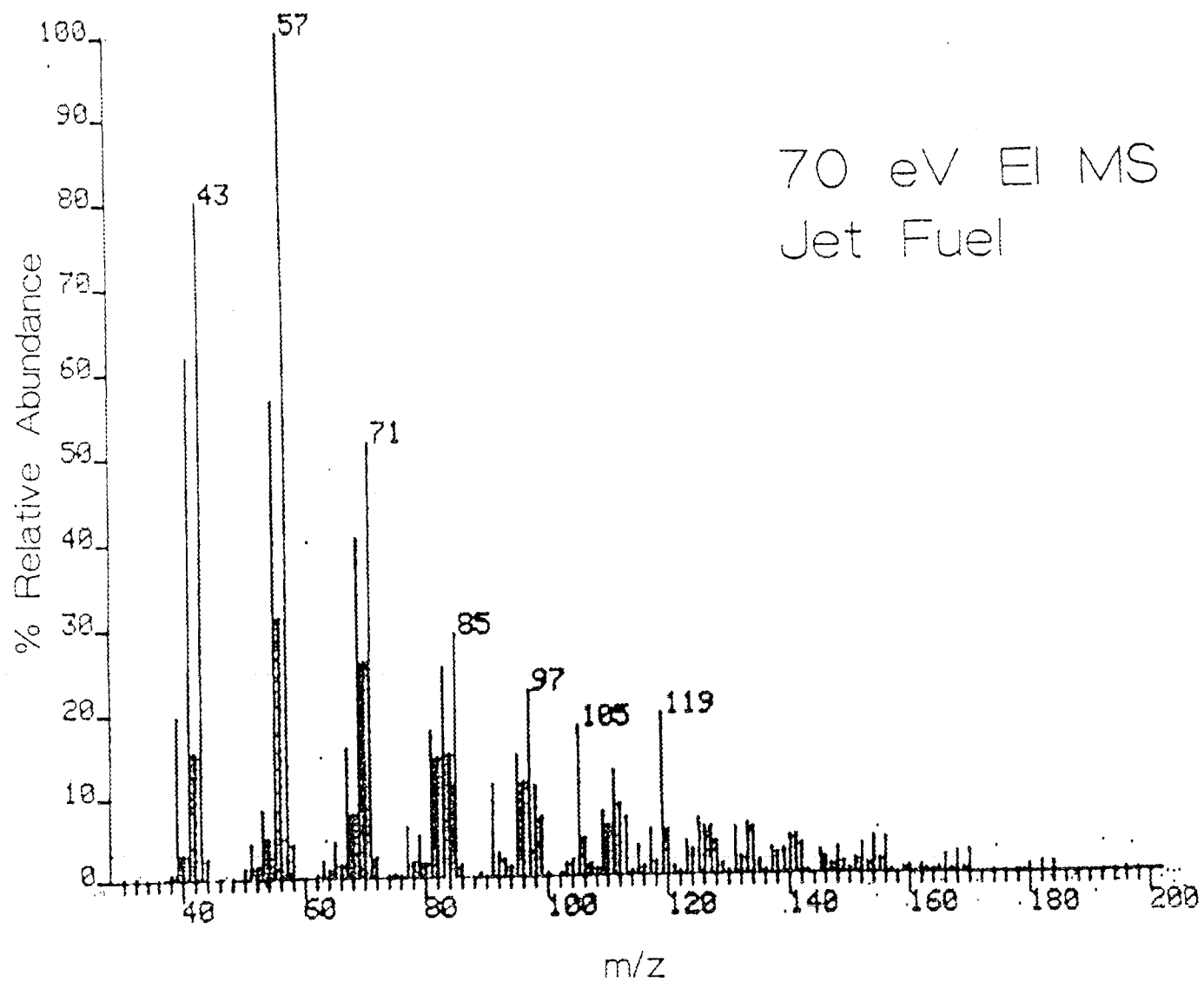


Figure 13. 70 eV electron impact mass spectrum of jet fuel.

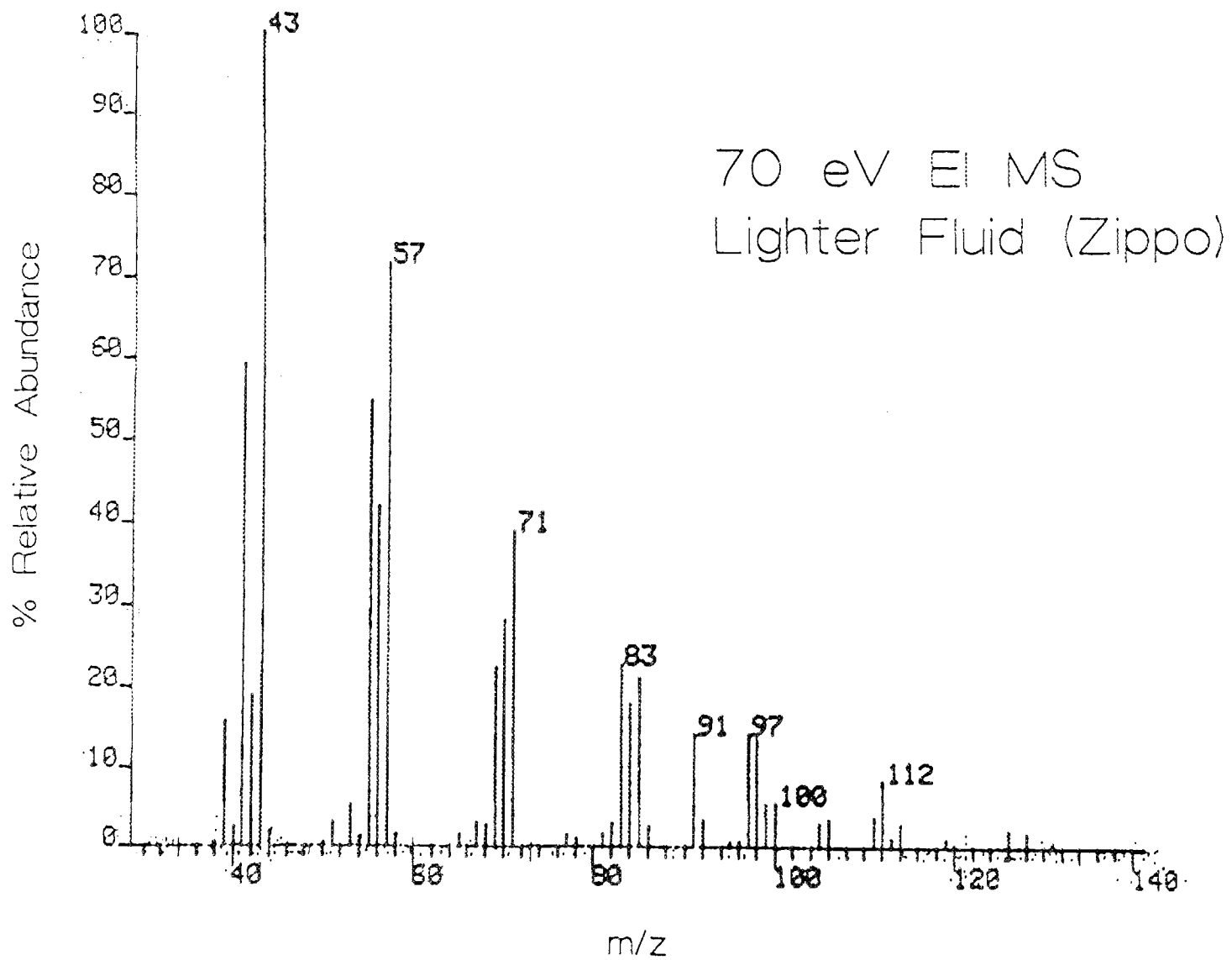


Figure 14. 70 eV electron impact mass spectrum of lighter fluid.

IV. Vapors of Flammable Liquids and Atmospheric Sampling Glow Discharge Ionization: Mass Spectra and MS/MS Spectra

Mass spectra have been obtained for a number of flammable liquids including pure liquids and complex mixtures. MS/MS daughter ion spectra have been acquired for the major ions observed in the mass spectra. All data reported in this section were obtained using the atmospheric sampling glow discharge ionization source and the MS/MS instrument described in Section II. In each case the instrument was operated in the positive ion mode. Samples include benzene, toluene, n-propylbenzene, n-butylbenzene, heptanes, methanol, ethanol, i-propanol, acetone, six gasoline samples, jet fuel, kerosene, and lighter fluid. Two perfume samples and a sample of rum were also tested as was the air over warm water. Water was sampled to evaluate the possible effects of relative humidity on the glow discharge mass spectra.

As indicated in Section II, the discharge voltage can have a significant effect on the appearance of the mass spectrum. In most cases, the mass spectra shown here were obtained under discharge conditions that optimize signal due to the samples of interest. In some cases, spectra at several sets of conditions are shown. Samples were admitted by placing a small vial in a plastic box with a glass tube extending from inside the box to the atmosphere aperture of the glow discharge ionization source and allowing the vapors to be drawn into the source along with lab air. In most cases, the vials were only loosely capped in order to obtain data quickly. Mass spectra were acquired by scanning the quadrupole mass filter. When mass spectra are acquired, both deflection plates are held at the accelerating potential so that the entire beam can pass through the electric sector and flight tube undeflected. MS/MS daughter ion spectra were acquired by setting the quadrupole to pass only the m/z ratio of interest, admitting air into the collision cell to a pressure of a few millitorr, and decreasing the voltage on one of the deflection plates by 150 V. The data acquisition system then controls the timing of a 150 V pulse added back to the deflection plate which deflects the ions for a short period of time (typically 300-500 ns) back into the flight path to the

detector. The masses of the ions are then determined by their flight times to the detector. Time-of-flight spectra were obtained at a rate of 20 kHz.

A. Pure Samples

Several flammable liquids consisting primarily of a single component were tested. Some of these are readily available in the pure form, e.g. i-propanol, while others constitute major components of flammable mixtures or serve as solvents in many commercial products, e.g. toluene in nail polish. These data, in addition to being useful in their own right, serve as guidelines for approaches to analyzing mixtures of flammable liquids.

1. Heptanes

Figure 15 shows the mass spectrum obtained for a mixture of heptanes from m/z 40 to m/z 120 using the atmospheric sampling glow discharge ion source operated at a discharge voltage of 385 V. This moderately low voltage maximizes the signals at higher masses, e.g. the molecular ion at m/z 100. At discharge voltages greater than 400 V, ions at m/z 100 and m/z 99 are no longer observed and the peaks at and near m/z 55 and m/z 43 become the dominant ions in the spectrum. Greater fragmentation is generally observed with greater discharge voltage, as discussed in Section II. Several observations are noteworthy from the spectrum. First, the ions typically observed in the electron impact mass spectrum of various heptanes are observed at masses m/z 100, m/z 71, m/z 55, and m/z 43. A peak is also observed at m/z 99, which is not observed in the electron impact mass spectrum. This peak presumably arises from hydride abstraction to form $C_7H_{15}^+$. Such a mechanism is operative in isobutane chemical ionization where a hydride abstraction reaction occurs to give the reagent ion $C_4H_9^+$. Finally, the mass resolution in the lower mass region (see, for example, the m/z 55 region) is poorer than at higher masses. This is unusual for a quadrupole mass filter which can either be operated in a constant resolution mode, as in this case, or in a constant transmission mode where mass resolution decreases with m/z . Poor mass resolution, particularly at low m/z values, is often observed, however, for samples that contain high concentrations of aliphatic hydrocarbons.

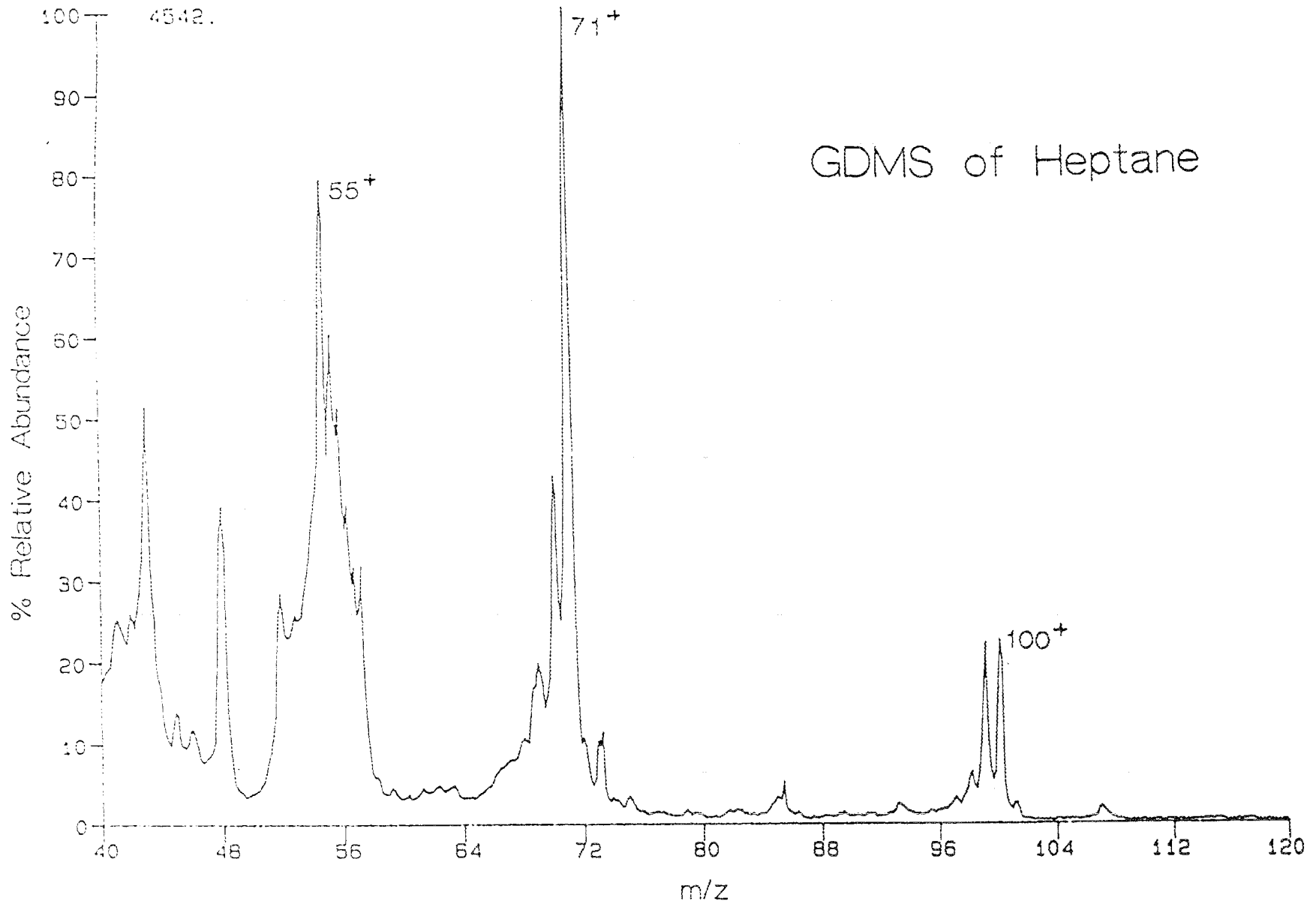


Figure 15. Glow discharge mass spectrum of heptanes.

The reason for this observation is not clear, but a possible cause is fragmentation occurring after ions exit from the ion source but before they pass through the quadrupole. The pressure in this region is high due to gas streaming from the exit aperture and electric fields from the ion lenses accelerate the ions so that they can undergo collision-induced dissociation (CID). This is particularly likely for hydrocarbon ions since they readily fragment. CID can occur throughout the region after the exit aperture up to the quadrupole entrance and the angular and energy spread of the ions formed by CID are much wider than those formed in the ion source. These factors may cause a decrease in mass resolution. The peak width of m/z 100 in the time-of-flight spectrum is roughly one half that of m/z 55 mass-selected by the quadrupole. This indicates that the latter ion has a wider energy spread which is consistent with the interpretation discussed here.

Figure 16 shows the MS/MS daughter ion spectrum obtained by time-of-flight for the ions at m/z 100. The spectrum shows the ions expected from the various $C_7H_{16}^+$ isomers, viz. m/z 71, m/z 55, m/z 43, m/z 41, m/z 29, and m/z 27. Note that m/z 99 is not observed in this spectrum. This supports the interpretation that the ion at m/z 99 in the mass spectrum arises from hydride abstraction rather than fragmentation of $C_7H_{16}^+$. The mass resolution in the time-of-flight spectra is relatively poor (typically $M/\delta M$ at 50% valley is from 30 to 70). This is due to several factors that spread out the arrival times of a particular mass ion. The most important limitation to mass resolution is the kinetic energy spread of the ions that exit the collision cell. The spread in energies arises from several sources, the major ones being a spread in energy of the parent ion entering the quadrupole, a spread due to kinetic energy losses experienced by the parent ions that undergo collision, and an energy spread resulting from kinetic energy released in the dissociation of the parent ion. Mass resolution can also be affected by the duration of the time-of-flight pulse but the energy spread is large enough in this experiment that mass resolution is insensitive to the pulse duration at pulse times less than a few hundred nanoseconds.

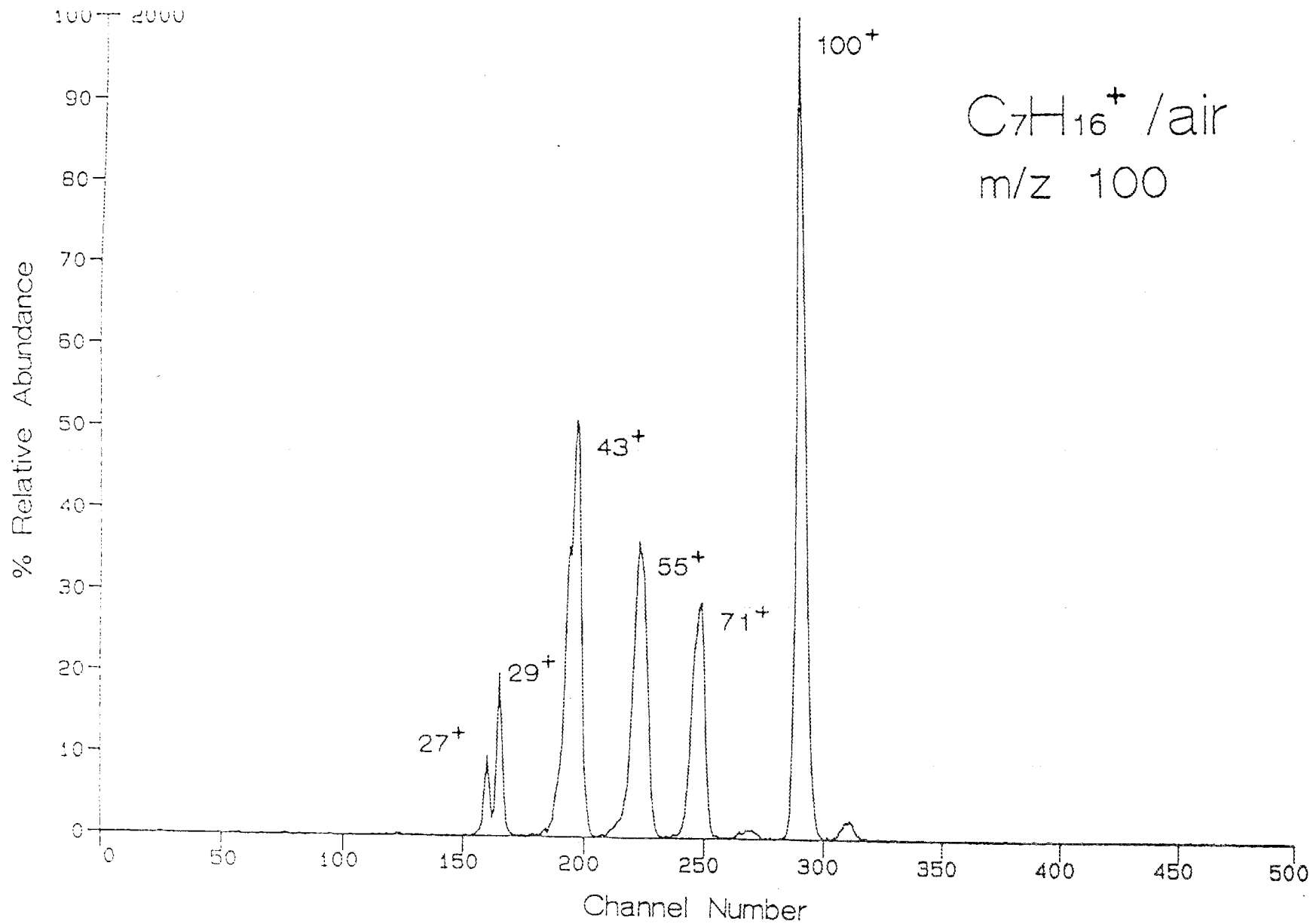


Figure 16. Daughter ion MS/MS spectrum of the m/z 100 ion in the glow discharge mass spectrum of heptanes.

The time-of-flight experiment performed here is somewhat different than the conventional situation in which all ions are formed at the same kinetic energy. In this experiment, the ions that enter the collision cell already have a kinetic energy of up to 100 eV. When the parent ion fragments, the kinetic energy is partitioned between the fragments according to their masses. For example, if a 100 eV parent ion splits into two fragments of equal mass, both fragments will have a kinetic energy centered at 50 eV. The range of kinetic energies that the ions can have as they exit the collision cell can be from a few eV up to the kinetic energy of the parent ion. All of the ions are then accelerated by several kilovolts which reduces the relative range of kinetic energies. Nevertheless, daughter ions formed in the collision cell have kinetic energies of up to tens of electron volts less than that of the parent ion. In the quadrupole/time-of-flight apparatus with the electric sector incorporated into the time-of-flight, the range of kinetic energies resulting from CID can effect the data in two ways. First, the flight time of an ion formed as a daughter ion in the collision cell will be slightly longer than the flight time of the same ion formed in the ion source. This has no effect on the resolution but changes the position of the daughter ion peak in the time-of-flight spectrum relative to that of the same ion mass-selected from the ion source. This effect is most pronounced at low accelerating voltages and with low mass fragment ions. In any case, however, the effect is small. For example, ions of m/z 43 with kinetic energies of 3100 eV and 3010 eV, respectively, differ in their flight times over a distance of 1.3 m by 1.7×10^{-7} s. This corresponds to about one half of a mass unit, in this case. The second effect arises from use of the electric sector to bend the ions through 180° . No slits are used for the electric sector so that the energy resolution is very low. The kinetic energy band pass of the sector is on the order of 100 eV. The transmission across this band pass is not constant, however, so that ions with kinetic energies that fall near the edges of the band pass of the electric sector are discriminated against. The settings of the electric sector can therefore have a significant effect on the relative abundances of the ions in the MS/MS spectrum. This can be seen in

comparing Figure 16 with Figure 17. The latter figure also shows the MS/MS daughter ion spectrum of m/z 100 from heptanes. The only difference between these spectra is that the voltages on the electric sector plates were both reduced by about 10 V. The spectrum in Figure 17 indicates that this causes discrimination against the higher energy parent ions (or reduces discrimination against the lower energy daughter ions possibly in effect under the conditions used to obtain the spectrum in Figure 16) as reflected in the increased relative abundances of the fragment ions. The voltages on the electric sector plates are not observed to significantly affect the positions of the peaks.

Daughter ion MS/MS spectra of the other major hydrocarbon ions observed in the mass spectrum were also acquired to serve as reference spectra. These spectra are included in Appendix I, a collection of reference daughter ion MS/MS spectra for hydrocarbon ions.

2. Benzene

Under mild glow discharge conditions, the only major ion observed in the mass spectrum of benzene is the molecular ion at m/z 78. As the discharge current is increased, fragmentation is observed to give ions predominantly at and near m/z 52. Figure 18 shows the MS/MS spectrum of the molecular ion of benzene. The most abundant daughter ion is observed at m/z 52, which corresponds to loss of ethylene. Less intense daughter ions are observed at m/z 65 and m/z 39.

3. Toluene

The glow discharge mass spectrum of toluene shows the molecular ion at m/z 92 almost exclusively at low discharge currents. At higher discharge currents, the base peak is observed at m/z 91 and fragment ions at m/z 77, m/z 65, and m/z 39 are significant.

Figure 19 shows the daughter ion spectrum of the molecular ion of toluene ($C_7H_8^+$, m/z 92). The fragment ions appear at m/z 77, m/z 65, m/z 51, m/z 39 and m/z 27. Under the conditions of resolution in this experiment other ions may also be present in these peaks. The major point with this spectrum is that it clearly identifies the parent ion as an aromatic hydrocarbon. The daughter ion MS/MS spectra of the ions observed in the mass spectrum at high discharge currents at m/z 91, m/z

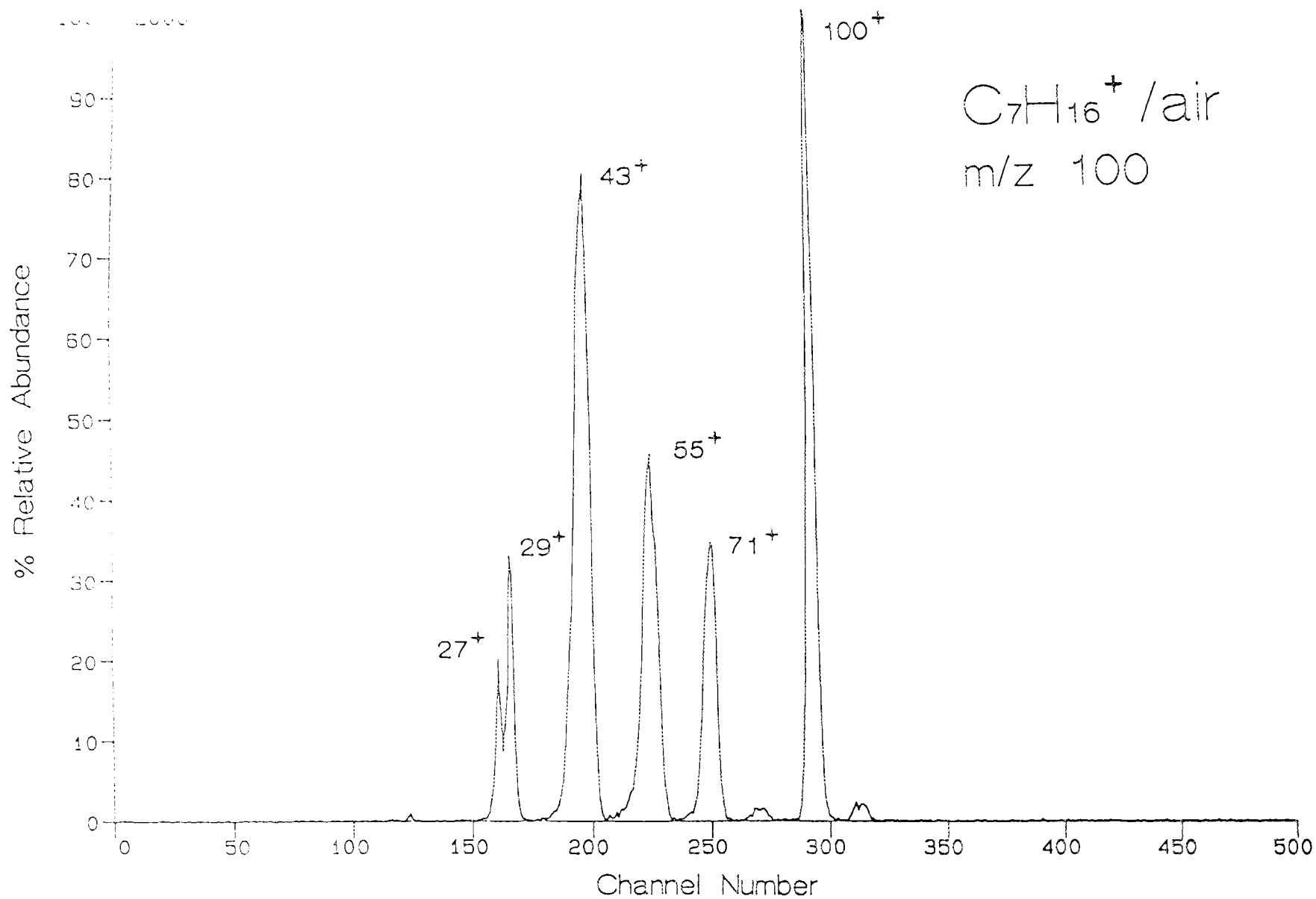


Figure 17. Same spectrum as shown in Figure 16 except that the electric sector plate voltages are reduced by about 10 volts each.

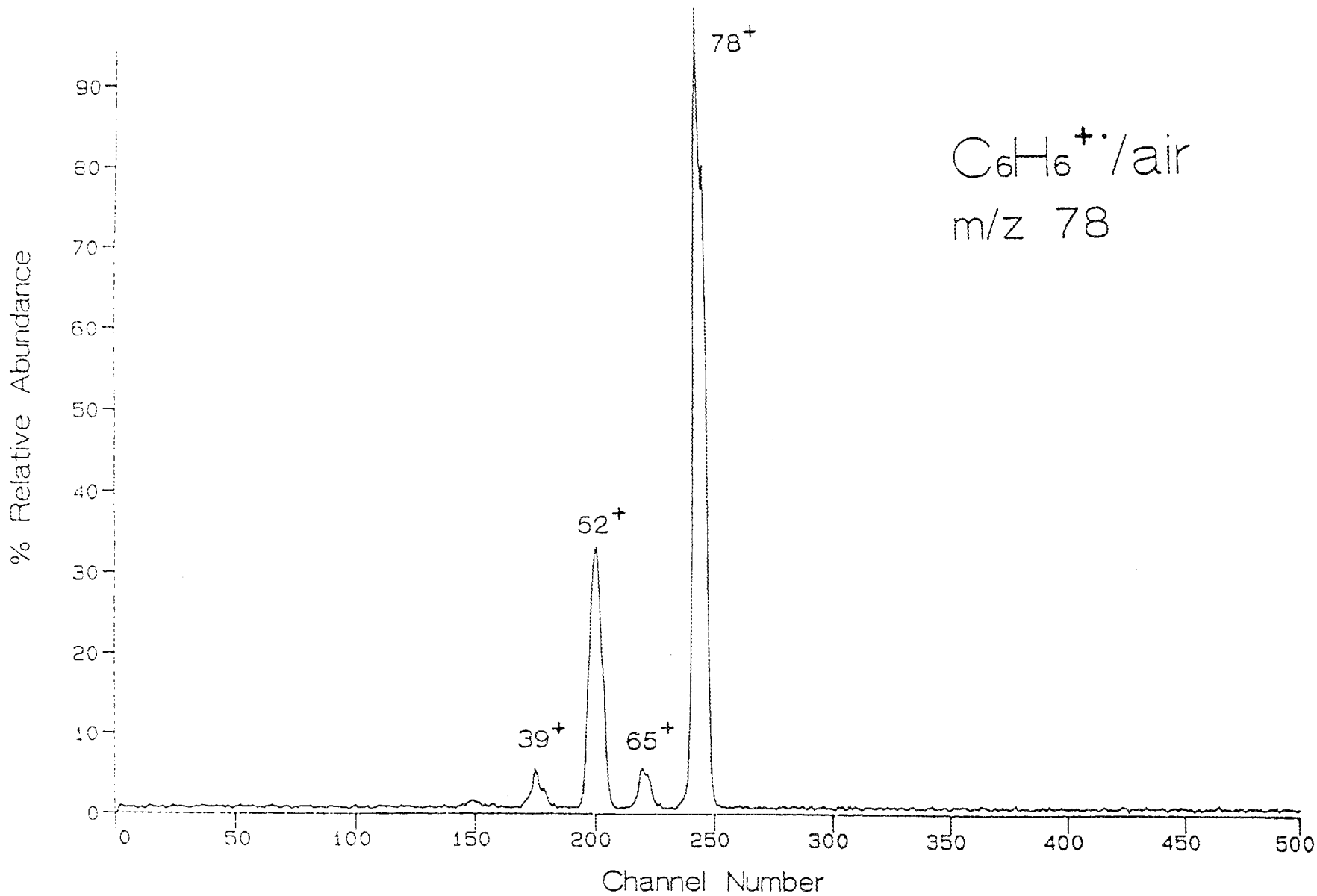


Figure 18. Daughter ion MS/MS spectrum of the benzene molecular ion (m/z 78).

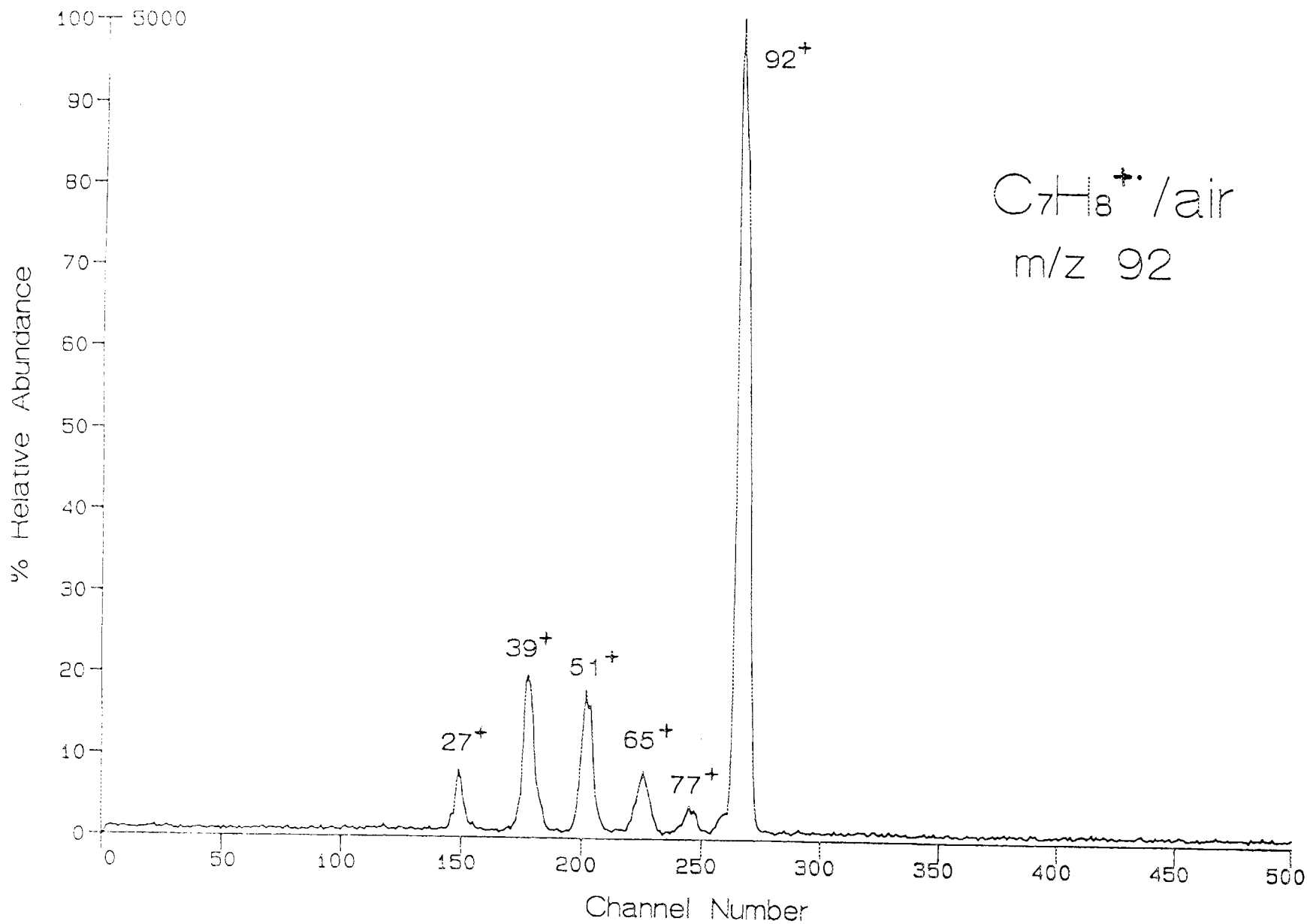


Figure 19. Daughter ion MS/MS spectrum of the toluene molecular ion (m/z 92).

77, and m/z 65 have also been obtained to serve as reference spectra. The daughter ion MS/MS spectrum of $C_7H_7^+$ (m/z 91) is shown in Figure 20. This ion is particularly important in that it is the most abundant ion in the mass spectra of many of the petroleum fuels. The daughter ion MS/MS spectra of $C_6H_5^+$ (m/z 77) and $C_5H_5^+$ (m/z 65) are included in Appendix I.

4. n-Propylbenzene

The glow discharge mass spectrum of n-propylbenzene shows an intense peak for the molecular ion at m/z 120 under mild discharge conditions. At higher discharge currents, the relative intensities of ions at m/z 105, m/z 92, and m/z 91 increase while the signal at m/z 120 essentially disappears. As the discharge current is increased, the ratio of $91^+/92^+$ also increases as is also observed for n-butylbenzene (see Figure 3). Figure 21 shows the daughter ion MS/MS spectrum of the ion at m/z 120. Daughter ions are observed at m/z 105, m/z 91 (and m/z 92), m/z 78, m/z 65, m/z 51, m/z 39, and m/z 27. Most of these ions are common to all of the 70 eV electron impact mass spectra of the C_3 -alkylbenzenes. The relative abundances, however, vary significantly in many cases. For example, most of the C_3 -alkylbenzenes show the base fragment ion peak in the electron impact mass spectrum to be at m/z 105 (methyl loss) rather than at m/z 91. We therefore expect that the m/z 105 daughter ion would appear as the most abundant daughter ion in the MS/MS spectrum of many of the other C_3 -alkylbenzenes.

5. n-Butylbenzene

Figure 3 shows the glow discharge mass spectra of n-butylbenzene acquired at three different discharge conditions. Under mild conditions, the molecular cation is readily observed. Under all conditions, ions at m/z 91 and m/z 92 are observed although at varying relative intensities (see discussion of Section IIA). Figure 22 shows the daughter ion MS/MS spectrum of the molecular cation of n-butylbenzene (m/z 134). By far the most intense daughter ions appear unresolved in the 91-92 m/z region. These ions result from the well-known losses of C_3H_6 and C_3H_7 from ionized n-butylbenzene. Other daughter ions appear at m/z 105, m/z 78, and m/z 65. A small daughter ion signal is observed at m/z 119. The electron impact mass spectra of

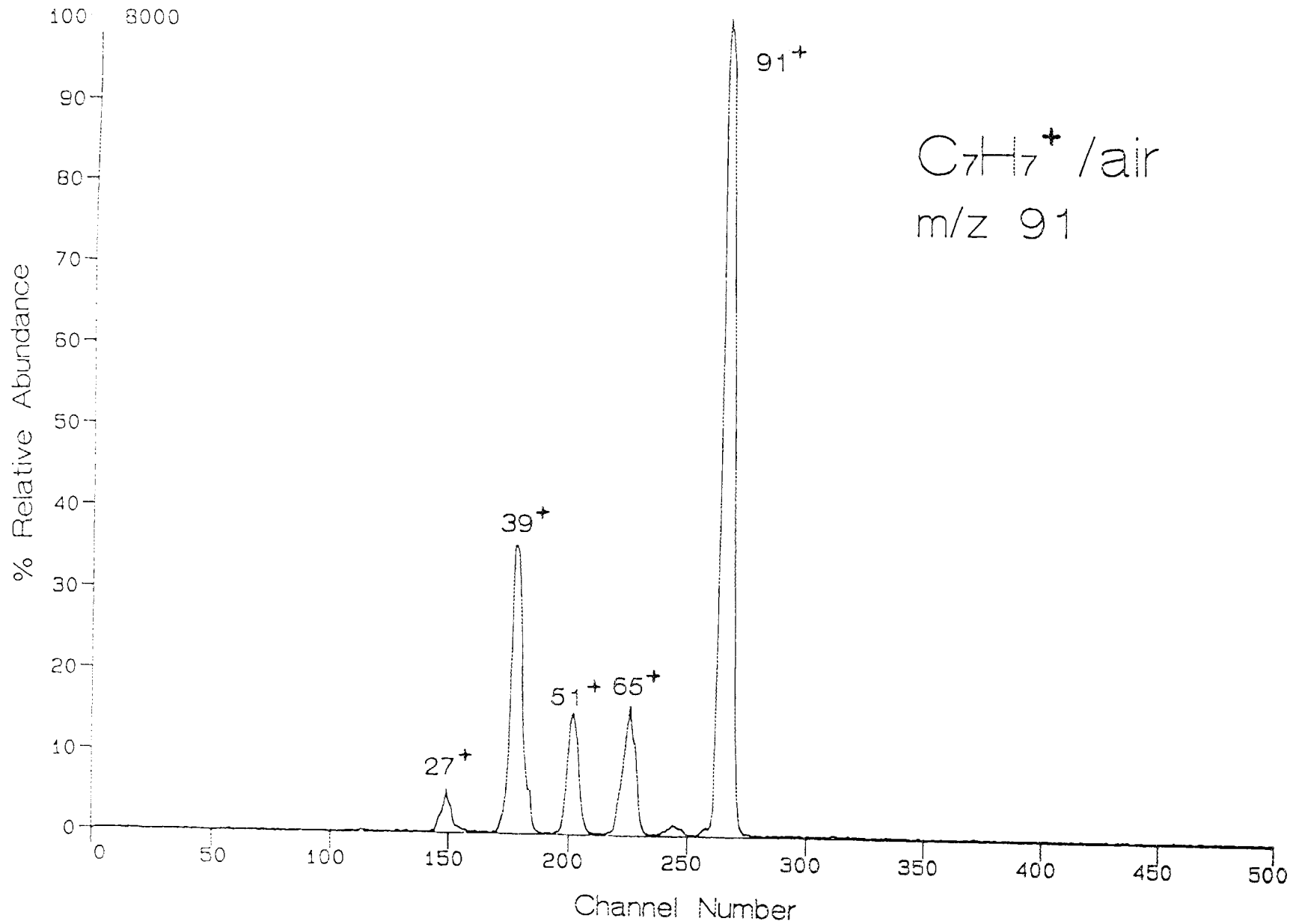


Figure 20. Daughter ion MS/MS spectrum of the m/z 91 ion in the glow discharge mass spectrum of toluene.

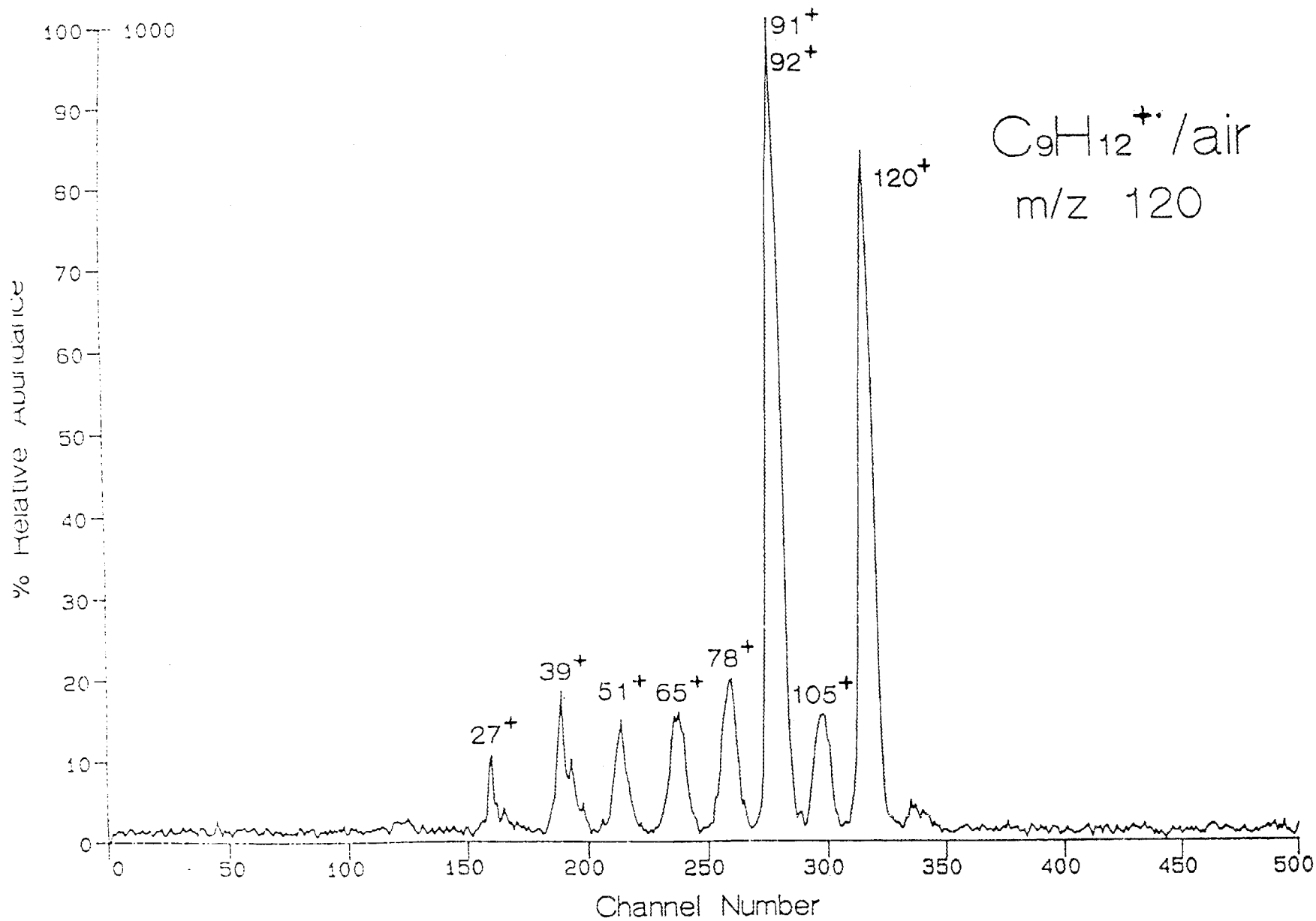


Figure 21. Daughter ion MS/MS spectrum of the n-propylbenzene molecular ion (m/z 120).

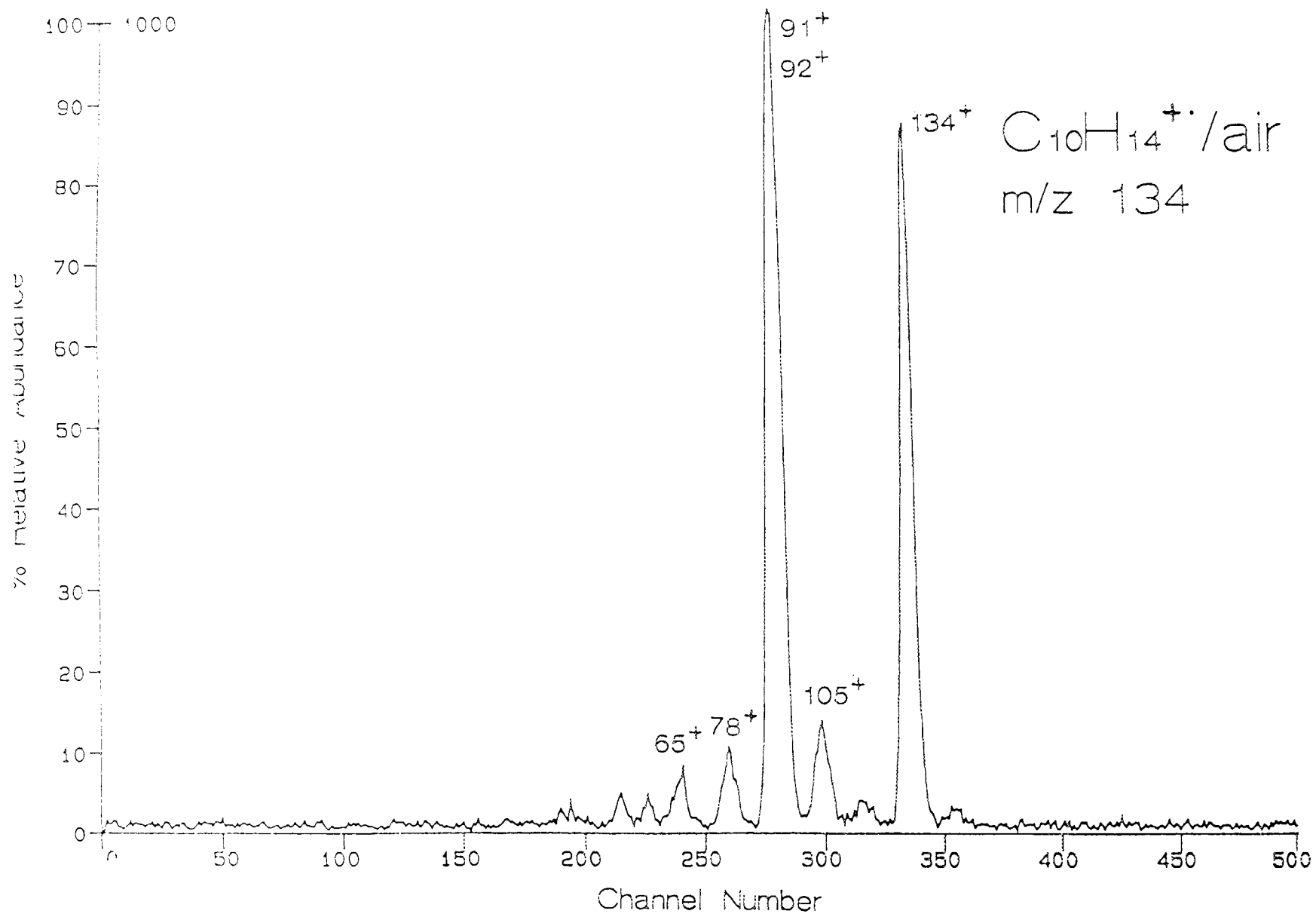


Figure 22. Daughter ion MS/MS spectrum of the n-butylbenzene molecular ion (m/z 134).

many of the C_4 -alkylbenzenes show m/z 119, which results from the loss of a methyl group, as the largest fragment ion peak. We therefore expect that m/z 119 is an intense peak in the MS/MS daughter ion spectra of those C_4 -alkylbenzene isomers that readily lose a methyl group upon electron impact.

6. Methanol

The glow discharge mass spectrum of methanol is strongly dependent upon the discharge current and the concentration of methanol. At low discharge currents, clustering is favored. At high methanol concentrations, such as those obtained with an open bottle near the sampling aperture, proton-bound methanol cluster ions are formed with the general formula $(CH_3OH)_nH^+$ where $n \leq 4$. At lower methanol concentrations, such as those obtained when sampling a closed bottle, proton-bound cluster ions containing methanol and water are formed. Figure 23 shows the glow discharge mass spectrum acquired while sampling a closed bottle of methanol under mild discharge conditions. The major peaks due to ions containing methanol are observed at m/z 33 $(CH_3OH)H^+$, m/z 51 $(CH_3OH)H^+(H_2O)$, m/z 65 $(CH_3OH)_2H^+$, and m/z 69 $(CH_3OH)H^+(H_2O)_2$. Protonated water monomer, dimer, and trimer are observed at m/z 19, m/z 37, and m/z 55, respectively. The daughter ion MS/MS spectrum of protonated methanol shows almost exclusively water loss to give CH_3^+ . Protonated methanol solvated with one water molecule also shows predominantly water loss to give, in this case, $CH_3OH_2^+$. Daughter ions of relatively low abundance ($\approx 10\%$ the intensity of $CH_3OH_2^+$) are observed at m/z 15 (CH_3^+) and m/z 19 (H_3O^+). The proton-bound dimer ion of methanol shows almost exclusively methanol loss to give protonated methanol with a small peak at m/z 15 (CH_3^+). Protonated methanol solvated with two water molecules shows two major peaks in the daughter ion MS/MS spectrum due to the loss of one water molecule to give m/z 51, and the loss of two water molecules to give protonated methanol. The proton-bound dimer of water, H_3O^+ , and CH_3^+ are also observed in low abundance. The daughter ion MS/MS spectra described above are included in Appendix II, a collection of reference daughter ion MS/MS spectra of ions derived from alcohols. Daughter ion MS/MS spectra of ions observed in the glow discharge mass spectrum when

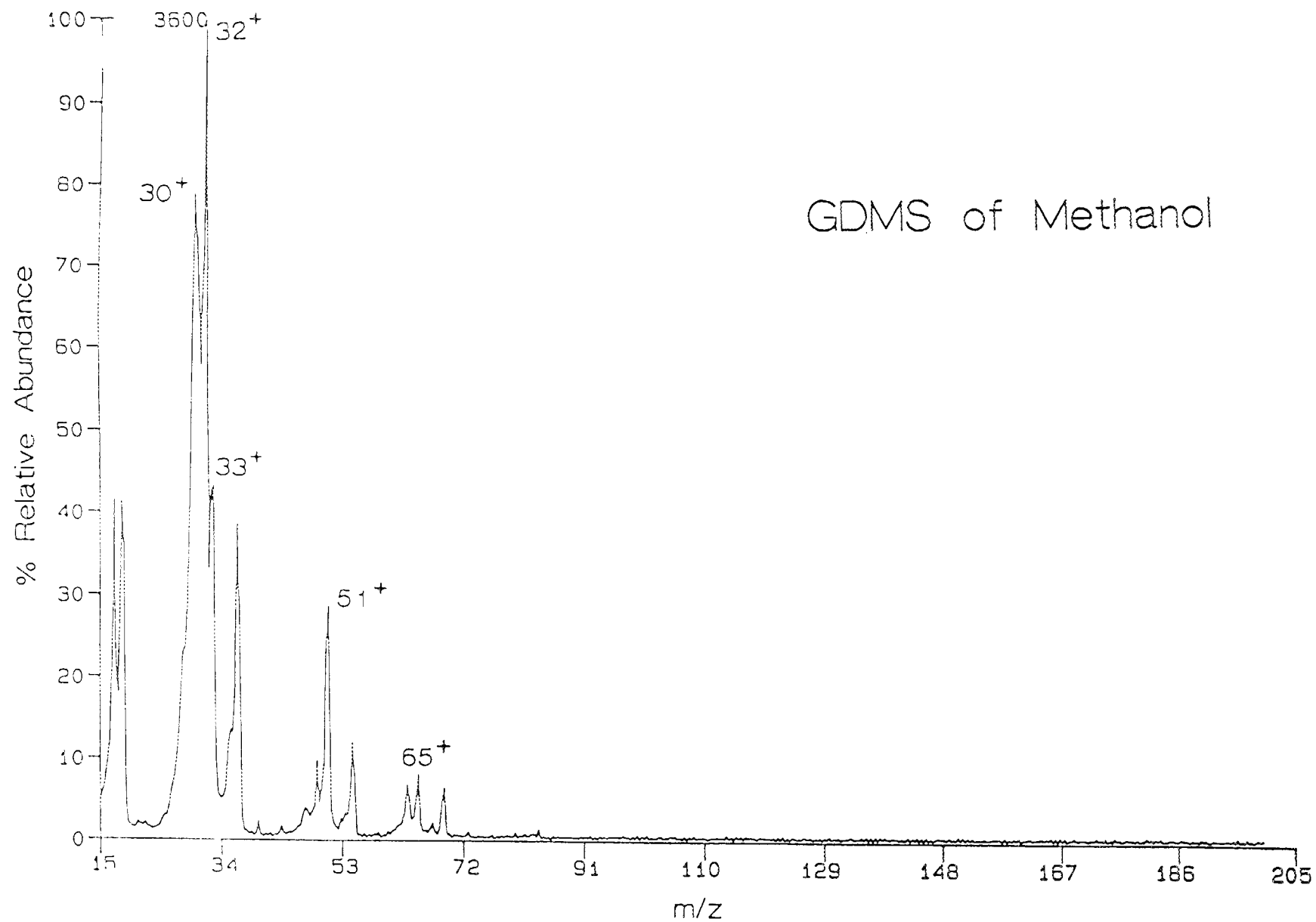


Figure 23. Glow discharge mass spectrum of methanol.

methanol is present in higher concentrations have also been acquired. The parent ions include the trimer ion consisting of two methanol molecules and a water molecule bound by a proton, $(\text{CH}_3\text{OH})_2\text{H}^+(\text{H}_2\text{O})$, the proton-bound trimer of methanol, and the proton-bound tetramer of methanol. The spectra are also included in Appendix II.

7. Ethanol

Like methanol, the glow discharge mass spectrum of ethanol is highly sensitive to the discharge conditions and to the concentration of ethanol. Under mild discharge conditions, the major ions are due to protonated ethanol and proton-bound dimers and trimers consisting of ethanol and water. The proton-bound dimer and trimer of ethanol, however, tend to be the most abundant cluster ions. Clusters containing water are relatively less abundant with ethanol than with methanol. The daughter ion MS/MS spectra of the major ions observed in the glow discharge mass spectra of ethanol have been acquired. The most important parent ions for detection of ethanol in ambient air are likely to be protonated ethanol and the proton-bound dimer of ethanol. The major fragment ions in the daughter ion MS/MS spectrum of protonated ethanol, in order of decreasing abundance, C_2H_5^+ (from water loss), H_3O^+ (from ethylene loss), CH_2OH^+ (from methane loss), and C_2H_3^+ (from H_2 loss from C_2H_5^+). The daughter ion MS/MS spectrum of the ethanol proton-bound dimer shows predominantly loss of ethanol to give protonated ethanol. The daughter ion MS/MS spectra for parent ions derived from ethanol in glow discharge mass spectra are included in Appendix II.

8. i-Propanol

The glow discharge mass spectra of i-propanol are similar to those of the other alcohols in that cluster ions are observed under mild discharge conditions. At low alcohol concentrations and high relative humidity, the cluster ions include one or more water molecules. At high alcohol concentrations, the mass spectrum is dominated by the proton-bound dimer of i-propanol. At high discharge currents, cluster ions are not observed and only a small signal is observed for protonated i-propanol.

The daughter ion MS/MS spectrum of protonated i-propanol shows predominantly water loss to give $C_3H_7^+$ at m/z 43. Smaller peaks at m/z 41 and m/z 39 are probably also present in the shoulder of the signal centered at m/z 43. Small signals are also observed in the m/z 27-31 region and are presumably due to loss of C_2H_6 to give $CH_2=OH^+$ at m/z 31 and further fragmentation of $C_3H_7^+$ to give $C_2H_3^+$ at m/z 27. The proton-bound cluster ions containing both i-propanol and water show the loss of one or more water molecules as the predominant fragmentation(s) in the respective daughter ion MS/MS spectra. The proton-bound dimer of i-propanol shows loss of i-propanol as the major process and further fragmentation to $C_3H_7^+$ to give the second largest daughter ion peak. Small signals are also observed for water loss and for propylene loss at m/z 103 and m/z 79, respectively. The daughter ion MS/MS spectra collected for ions derived from i-propanol are included in Appendix II.

9. Water

Water is obviously not a flammable liquid but it is always present in air at varying concentrations. The effects of water on the glow discharge mass spectra of the flammable liquids were therefore noted and the daughter ion MS/MS spectra of water containing ions observed in the day-to-day background mass spectrum were recorded.

A typical background glow discharge mass spectrum acquired under mild discharge conditions is shown in Figure 24. In addition to the ever-present signals at m/z 30 and m/z 32, intense peaks are also observed for protonated water and its proton-bound cluster ions at m/z 19 (H_3O^+), m/z 37 ($(H_2O)_2H^+$), m/z 55 ($(H_2O)_3H^+$), and m/z 73 ($(H_2O)_4H^+$). Though not evident in the spectrum of Figure 24, the proton-bound pentamer of water ($(H_2O)_5H^+$) is often observed in the background at m/z 91. We have not observed significant intensities of any larger water clusters. The ion at m/z 91 is significant in that one of the most intense ions observed for the petroleum fuel mixtures also appears at m/z 91 ($C_7H_7^+$) so that the protonated pentamer of water could interfere with the detection of, for example, gasoline. The daughter ion MS/MS spectrum of $(H_2O)_5H^+$, shown in Figure 25, however, is distinct from that of $C_7H_7^+$ (compare Figure 20). The proton-bound pentamer of water,

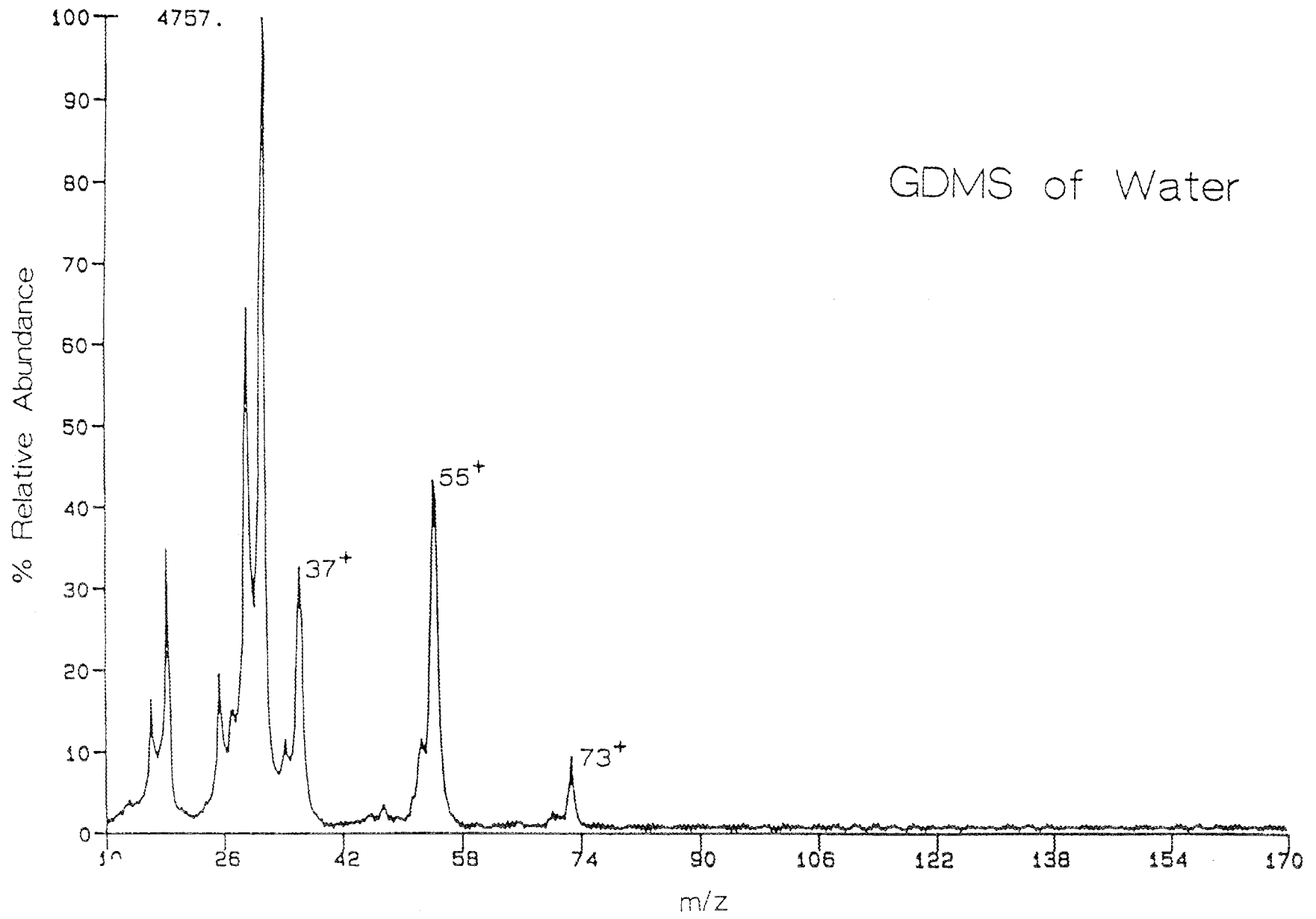


Figure 24. Glow discharge mass spectrum of water.

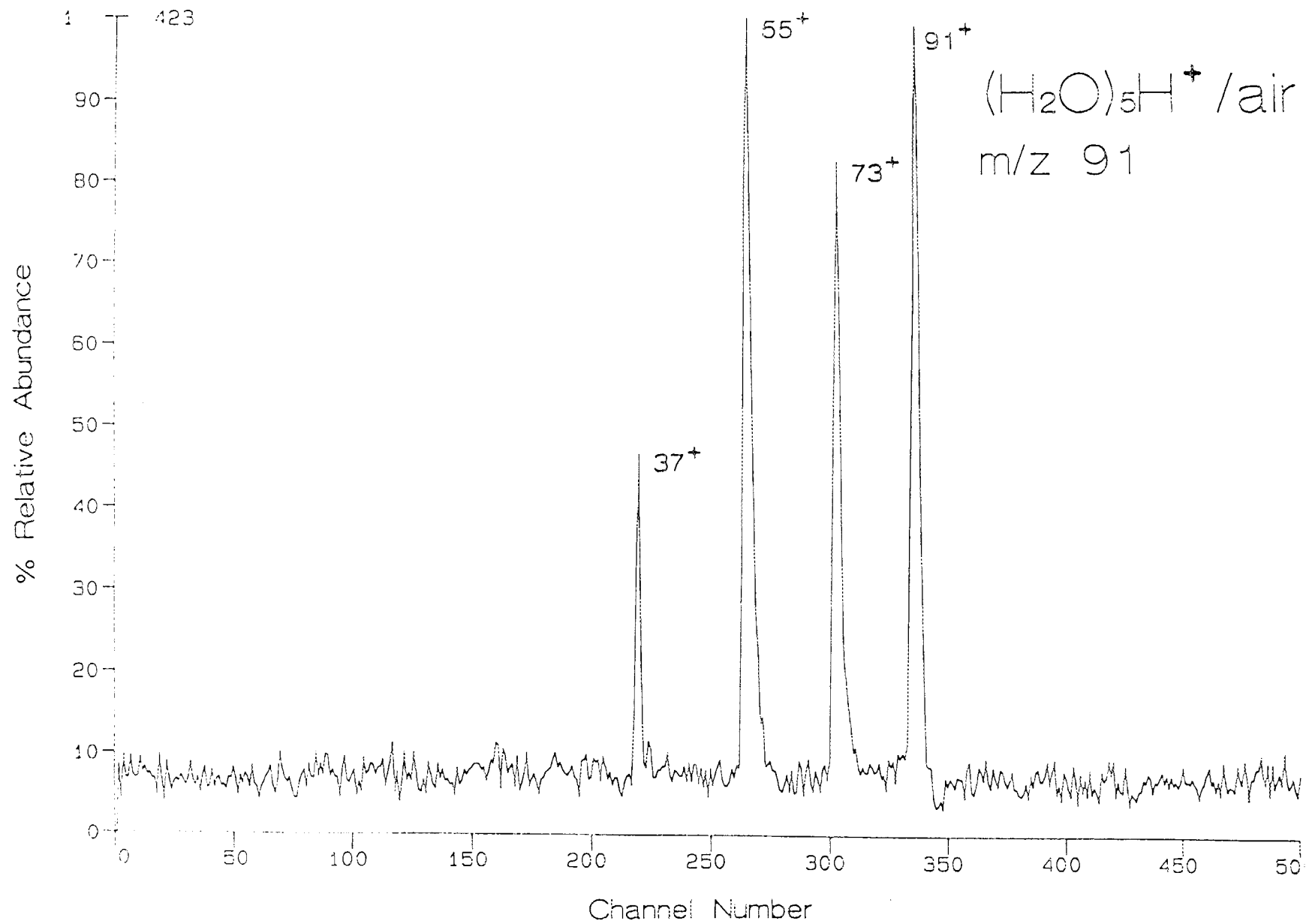


Figure 25. Daughter ion MS/MS spectrum of the m/z 91 ion in the glow discharge mass spectrum of water.

like all of the proton-bound water clusters, fragments exclusively by loss of one or more water molecules. The daughter ion MS/MS spectra of the proton-bound water clusters are included in Appendix III.

Atmospheric water has one obvious effect on the glow discharge mass spectra of all of the flammable liquids we have studied (and, indeed, on all of the compounds we have studied in the positive ion mode), the total ion signal of the mass spectrum tends to increase with water concentration over the range accessible to us. In general, when warm water is intentionally added to the region of air being sampled, the signal for an ion that does not contain water increases by 50-100%. If the ion is a water containing cluster, the signal may increase by over an order of magnitude. The reason for this observation is not clear. It is likely, however, that the rates for the mechanisms of ion formation and destruction are sufficiently altered by the greater concentration of water that a larger steady state ion number density can be accommodated in the discharge.

Clustering is another commonly observed effect of water in the glow discharge mass spectra of some compounds. This is true of the alcohols (see above) and is likely to be true for many organic compounds, particularly heteroatom containing species. The mass spectra of the hydrocarbons, however, show no significant clustering with water even under conditions where clustering is most extensive with the alcohols.

10. Acetone

Acetone is a commonly used solvent in many commercial products and might be encountered in an airport. The behavior of this compound in the glow discharge ionization source was therefore studied and daughter ion MS/MS spectra were obtained for the major ions observed. Figure 26 shows the glow discharge mass spectrum of acetone obtained under mild discharge conditions and with high acetone concentration. Under these conditions clustering is maximized. By far the major ions are observed at m/z 59 and m/z 117 and correspond to protonated acetone and the proton-bound dimer of acetone, respectively. Small peaks are due to clustering with water are observed at m/z 77 and m/z 135 corresponding

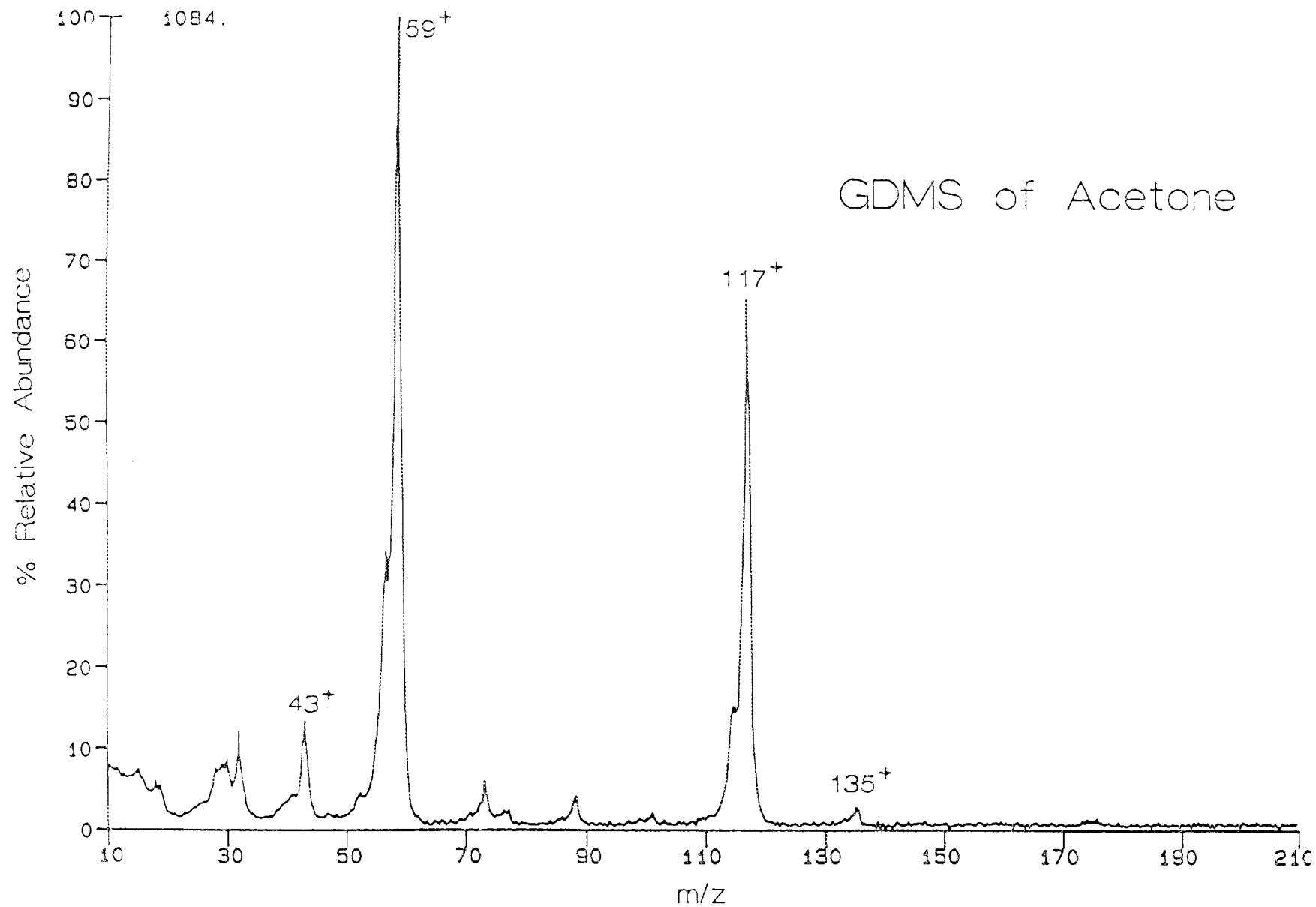


Figure 26. Glow discharge mass spectrum of acetone.

to protonated acetone solvated with a water molecule and the dimer ion solvated with a water molecule, respectively. At lower acetone concentrations, and at higher discharge voltages, the signal for protonated acetone dominates the spectrum.

The daughter ion MS/MS spectrum of protonated acetone shows loss of methane to give CH_3CO^+ as the most important dissociation process. Fragment ions at m/z 41 and m/z 39 are also probably present as a shoulder on the low mass side of the m/z 43 signal. Fragment ions are also observed at m/z 31 (from loss of ethylene), m/z 29, and m/z 27. The daughter ion MS/MS spectrum of the proton-bound dimer of acetone shows predominantly loss of acetone to give protonated acetone. Daughters of low intensity are also observed from further fragmentation of protonated acetone. These and other daughter ion MS/MS spectra of ions derived from acetone in the glow discharge mass spectrum are included in Appendix IV.

B. Mixtures

1. Gasolines

The glow discharge mass spectra of six gasoline samples, obtained from different local vendors, were studied. All of the spectra were very similar when fresh samples were compared. This was expected based on the GC/MS results which showed the gasoline samples to be very similar. When a few of the samples were allowed to partially vaporize, significant changes in the spectra were observed (see below). Since the spectra were very similar, only one spectrum is discussed in the text. Glow discharge mass spectra of other samples are included in Appendix V.

Figure 27a shows the glow discharge mass spectrum of a sample of unleaded regular gasoline that includes the normal background reagent ions and Figure 27b shows the same spectrum over the mass range of 50-200 amu. Several noteworthy observations can be made from the spectrum. The most abundant ion attributable to the gasoline sample is observed at m/z 91. Other significant peaks are observed at or near m/z 77, m/z 105, and m/z 119. Ions that fall at these masses are typical of aromatic compounds, particularly alkylbenzenes. The GC/MS results show that alkylbenzenes are major components of the mixture but

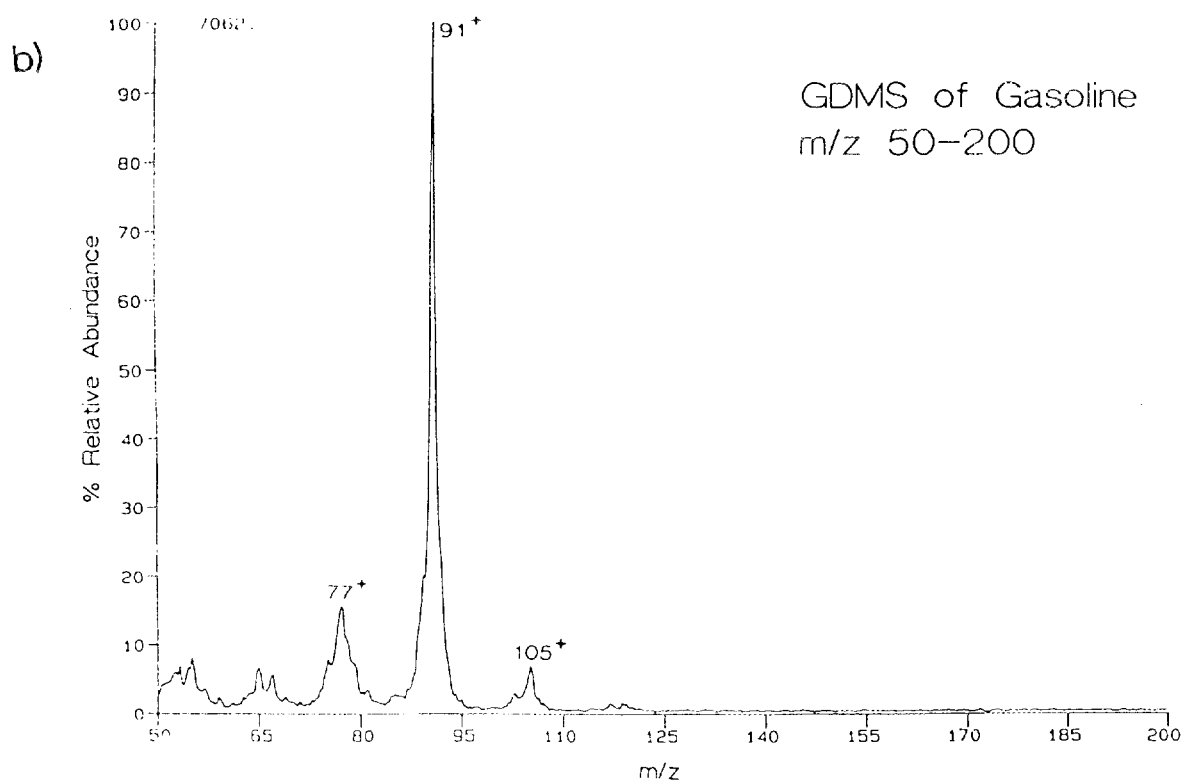
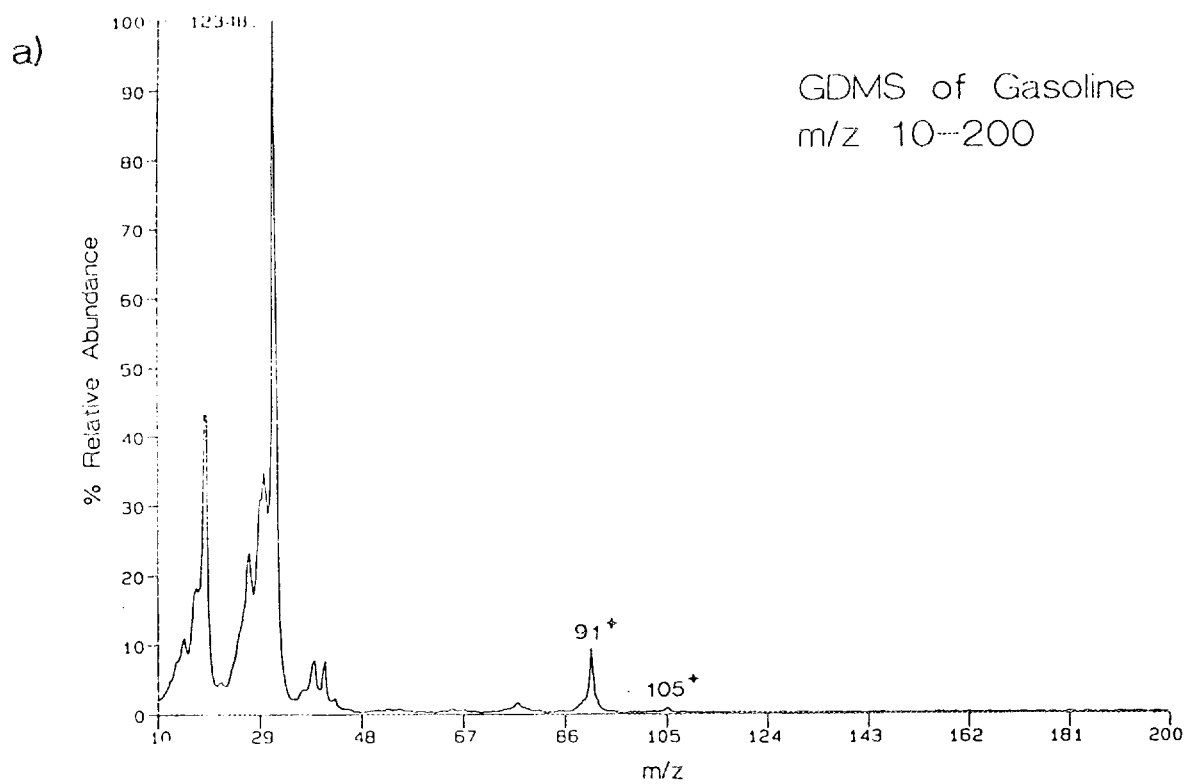


Figure 27. Glow discharge mass spectra of gasoline from a) m/z 10-200 and b) m/z 50-200.

the glow discharge mass spectrum shows that they are preferentially ionized in the glow discharge. The large fraction of aliphatic compounds in the mixture is not reflected in the glow discharge mass spectrum (compare Figure 11). No evidence for clustering with water is present in the spectrum nor is there any evidence for extensive ion/molecule reactions that might give higher mass hydrocarbon ions even when an open bottle of gasoline is sampled. Several samples of gasoline were allowed to partially vaporize until they were noticeably more viscous than fresh sample. The mass spectra of these samples reflected the greater concentration of higher boiling components. Figure 28 shows the most extreme example where ions at or near m/z 105 and m/z 119 are more intense than $C_7H_7^+$. The relatively poor signal/noise ratio of the spectrum reflects the lower absolute number of sample molecules drawn into the ion source and the lower relative abundance of $C_7H_7^+$ probably reflects the lower concentration of toluene remaining in the sample.

The daughter ion MS/MS spectra of the ions at m/z 91 from all of the gasoline samples matched that of the $C_7H_7^+$ ion spectrum obtained from toluene (see Figure 20). The daughter ion spectra for ions at m/z 120 and m/z 134, however, do not match those of the molecular ions of *n*-propylbenzene and *n*-butylbenzene. For example, Figure 29 shows the daughter ion MS/MS spectrum of the ion at m/z 134 from a gasoline sample. This spectrum does not match the daughter ion spectrum of the *n*-butylbenzene cation shown in Figure 22. This might be expected since a mixture of butylbenzene isomers are expected to contribute to the ions at m/z 134 in the gasoline spectrum. Most butylbenzene isomers show methyl loss as the most important fragmentation and a loss of 15 amu gives the base peak in the spectrum of Figure 29. Likewise, the daughter ion MS/MS spectrum of the m/z 119 ion in the gasoline mass spectrum does not match that of the same mass ion from *n*-propylene but rather, appears to reflect a mixture of propylbenzenes. Several daughter ion MS/MS spectra obtained from gasoline samples are included in Appendix V.

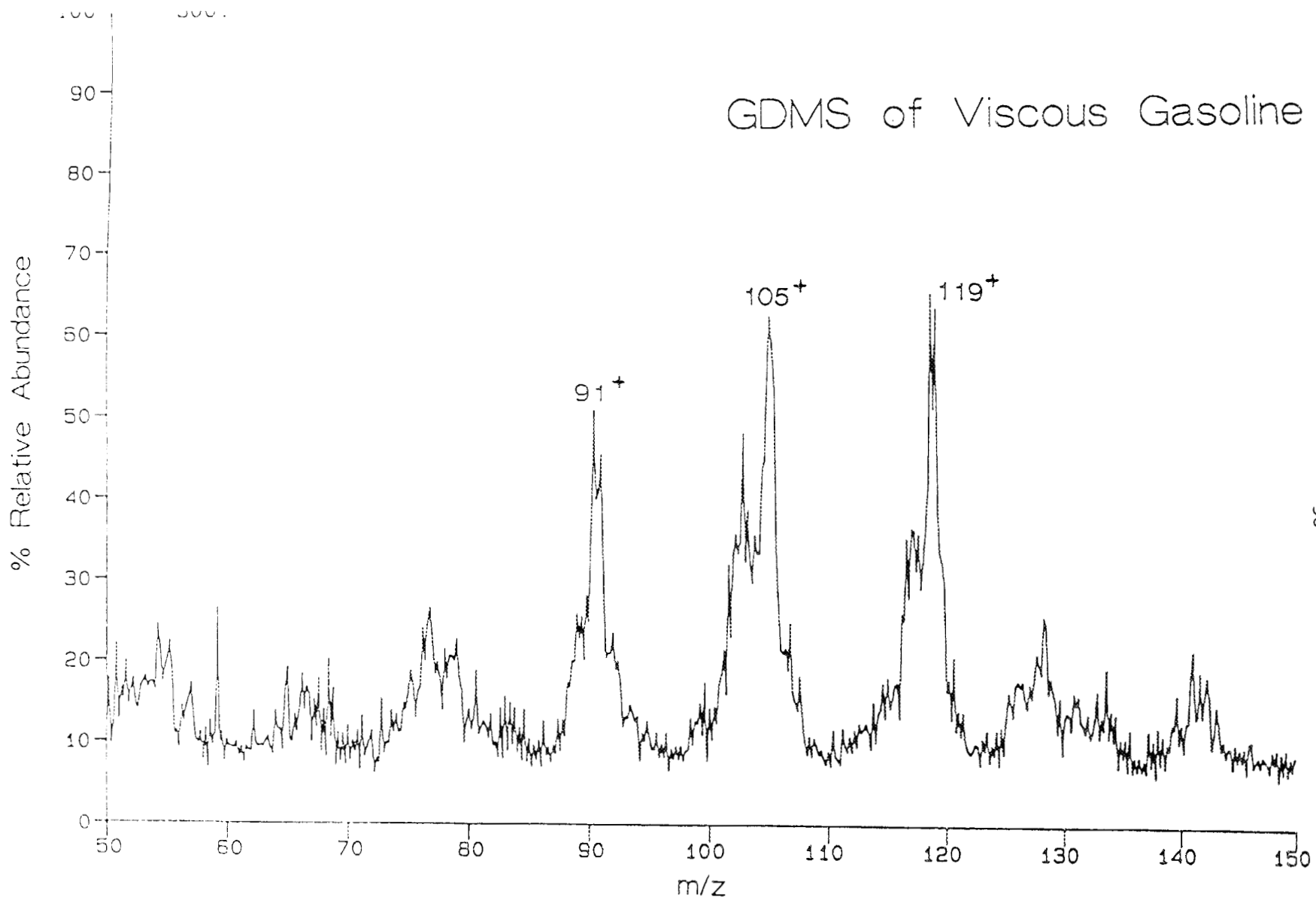


Figure 28. Glow discharge mass spectrum of viscous gasoline sample.

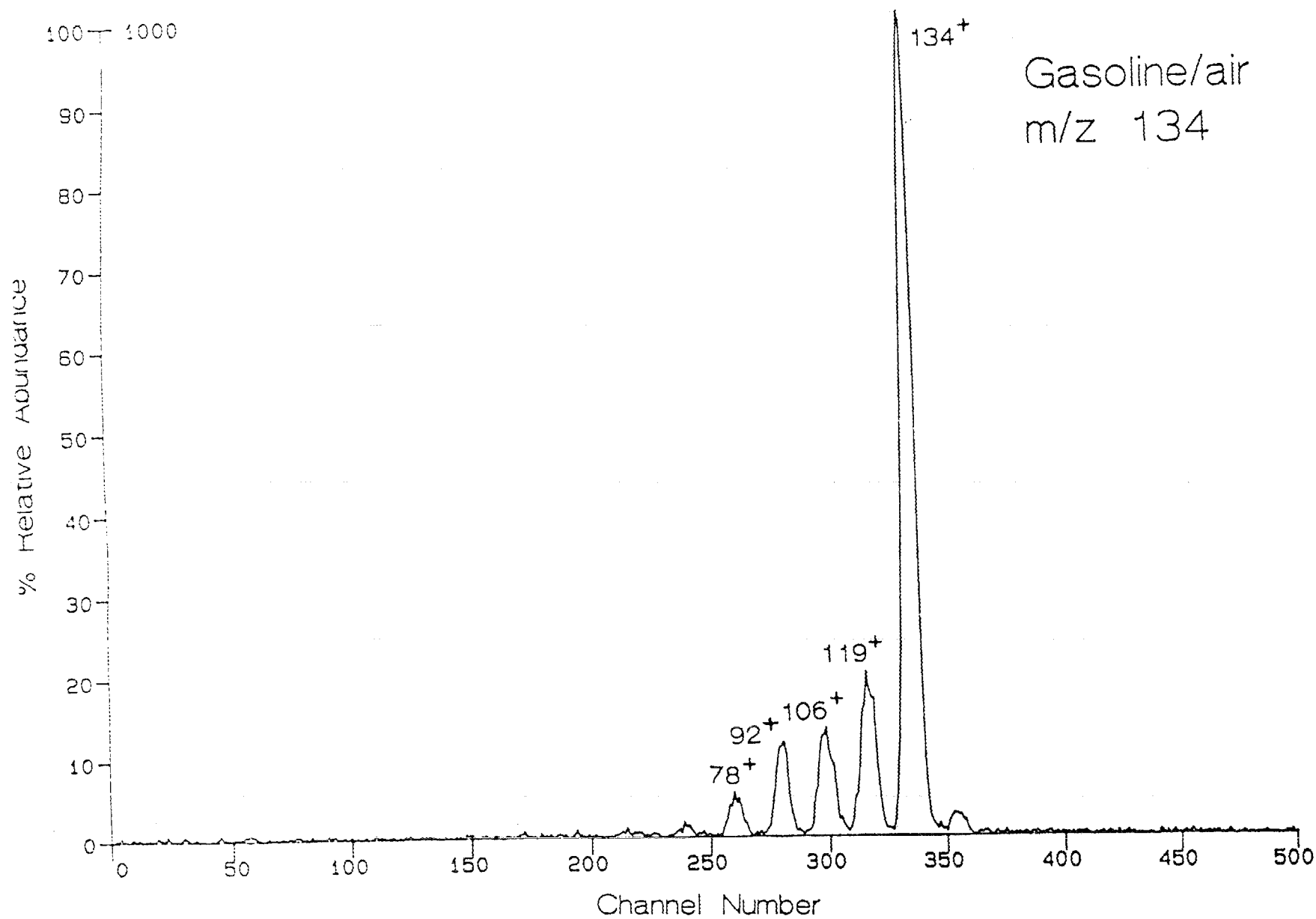


Figure 29. Daughter ion MS/MS spectrum of the m/z 134 ion in the glow discharge mass spectrum of gasoline.

2. Kerosene

Figure 30 shows the glow discharge mass spectrum of the kerosene sample over the mass range of 50-150 amu acquired under the same conditions as those used for the gasoline samples. Two important differences are evident in comparing the mass spectra of kerosene and the gasoline mass spectra. First, the signal intensity is lower with the kerosene. Second, the abundances of the ions at and near m/z 105 and m/z 119 are greater relative to the peak at m/z 91. The former observation is not surprising in light of the GC/MS results which showed that the fraction of alkylbenzenes in the sample mixture is lower for kerosene than it is for gasoline. The latter observation is also consistent with the GC/MS data which showed that longer chain alkylbenzenes are present in the kerosene mixture. The daughter ion MS/MS spectra of the major peaks in the mass spectrum of kerosene are similar to those obtained from the same mass ions in the gasoline mass spectra.

At high discharge currents, a different mass spectrum is observed as shown in Figure 31. Many of the same ions are observed but two groups of higher mass ions are evident and the signal at m/z 55 is increased. The latter observation probably reflects a greater degree of fragmentation for many of the ions at the higher discharge current. The daughter ion MS/MS spectrum of the m/z 55 ion in this spectrum indicates that the peak is composed almost exclusively of $C_4H_7^+$ with no observable contribution from the proton-bound trimer of water. The higher mass ions at and near m/z 128 and m/z 141 arise from the ionization of naphthalene and methylnaphthalene components of the mixture. Figure 32 compares the daughter ion MS/MS spectrum of the ion at m/z 128 in the mass spectrum of Figure 31 with that of the molecular ion of naphthalene. The comparison suggests that most of the ions that make up the signal at m/z 128 in the kerosene mass spectrum are naphthalene molecular ions. This example points out that aromatic hydrocarbons can be detected using the higher discharge conditions whereas the aliphatic hydrocarbons tend to fragment extensively to low

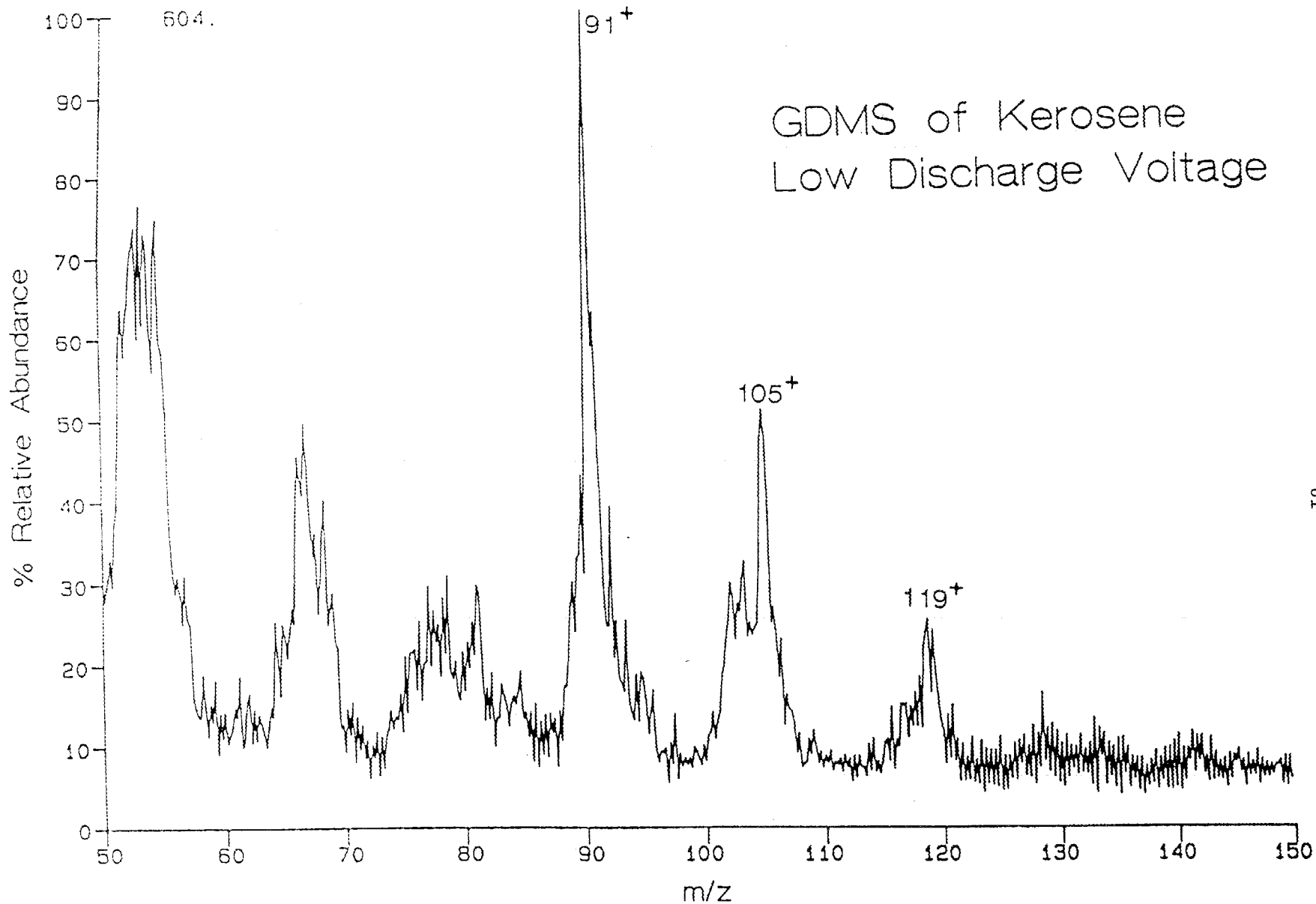


Figure 30. Glow discharge mass spectrum of kerosene-low discharge voltage.

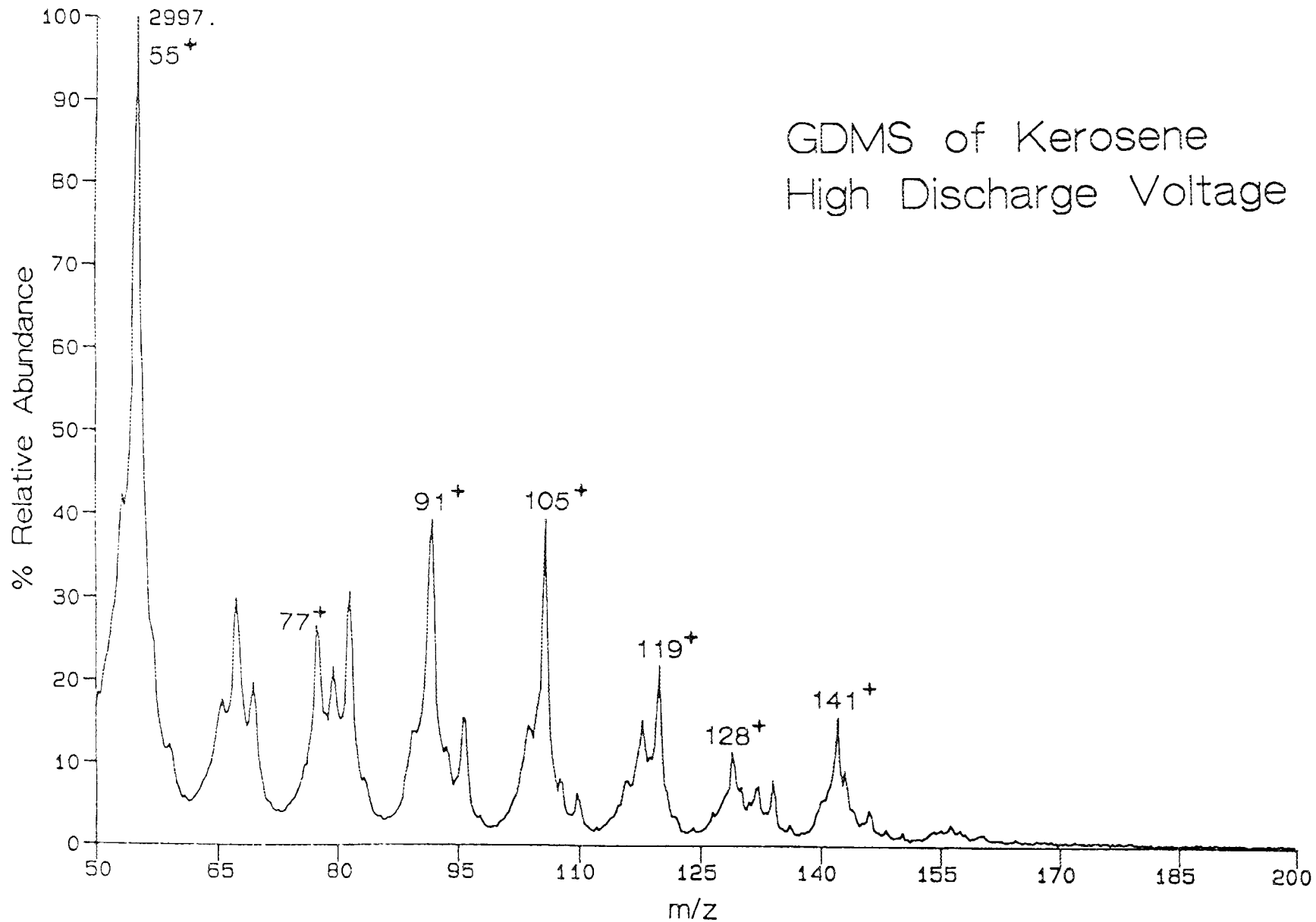


Figure 31. Glow discharge mass spectrum of kerosene- high discharge voltage.

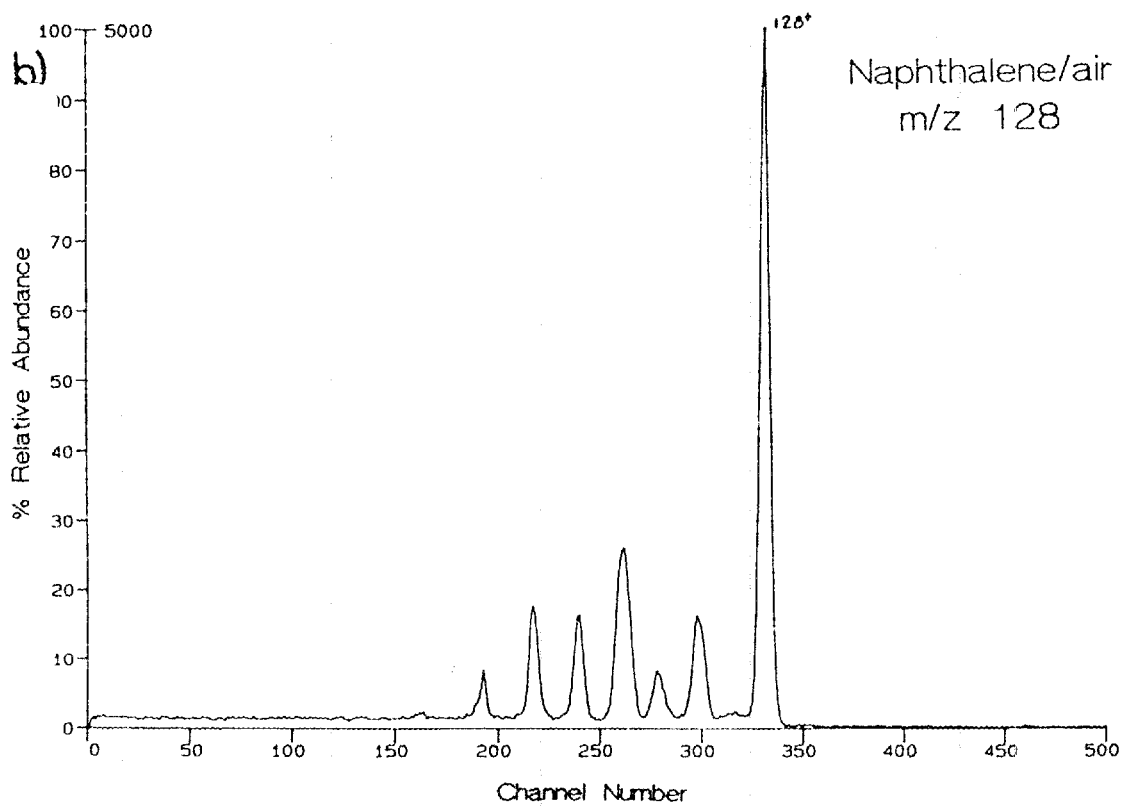
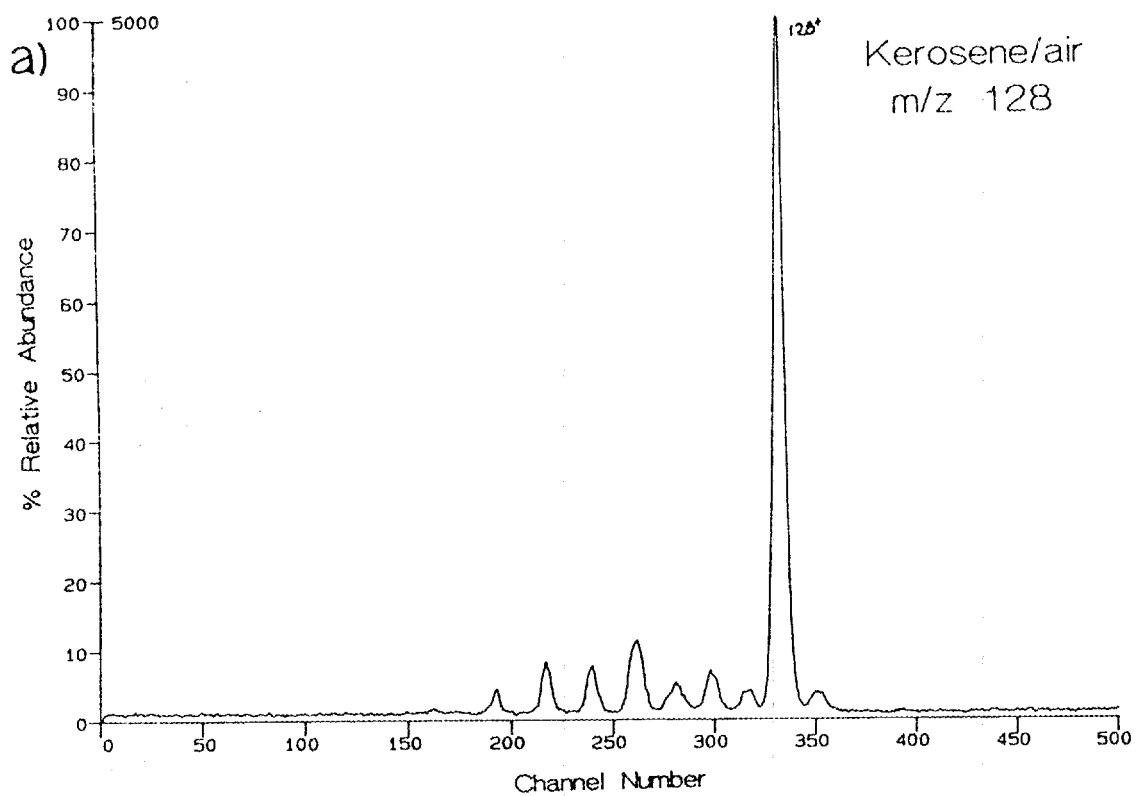


Figure 32. Comparison of MS/MS spectra of m/z 128 from a) kerosene and b) naphthalene.

mass ions that are less structurally diagnostic of the mixture composition. MS/MS spectra derived from kerosene are included in Appendix V.

3. Jet Fuel

The data obtained for jet fuel is very similar to the results obtained for kerosene. This, of course, is expected based on the GC/MS results which showed the two mixtures to be almost identical. Under the same ionization conditions, jet fuel glow discharge mass spectra are very much similar to the corresponding kerosene mass spectra. Likewise, the daughter ion MS/MS spectra are also very similar. Glow discharge mass spectra and MS/MS spectra derived from jet fuel are included in Appendix V.

4. Lighter fluid

The lighter fluid data provides another good illustration of the characteristics of the glow discharge ionization of hydrocarbon mixtures. Figure 33 compares the low discharge current glow discharge mass spectrum with the high discharge mass spectrum. The high discharge current mass spectrum of the lighter fluid is similar to that for gasoline (and jet fuel and kerosene except that the peaks due to naphthalenes are absent in lighter fluid). The ions at m/z 119, m/z 105, and m/z 91 are derived from alkylbenzenes. The daughter ion MS/MS spectra match those obtained for the same mass ions in the derived from the other hydrocarbon mixtures. A large peak is observed at m/z 55 which is demonstrated by MS/MS to be almost exclusively $C_4H_7^+$ ions. The low discharge current mass spectrum, however, shows additional peaks which can mostly be attributable to aliphatic hydrocarbons. For example, the daughter ion MS/MS spectra of ions at m/z 111, m/z 97, m/z 85, m/z 83, m/z 71, and m/z 57 all show these ions to be derived from alkanes (or, in some cases, possibly alkenes). The major ions derived from alkylbenzenes shift from m/z 91, m/z 105, and m/z 119 to molecular ions of toluene, C_2 -alkylbenzenes, and C_3 -alkylbenzenes at m/z 92, m/z 106, and m/z 120, respectively. The low discharge current mass spectrum therefore seems to reflect that less energy is being deposited into the mixture components upon ionization thereby reducing the degree of fragmentation observed at high discharge currents.

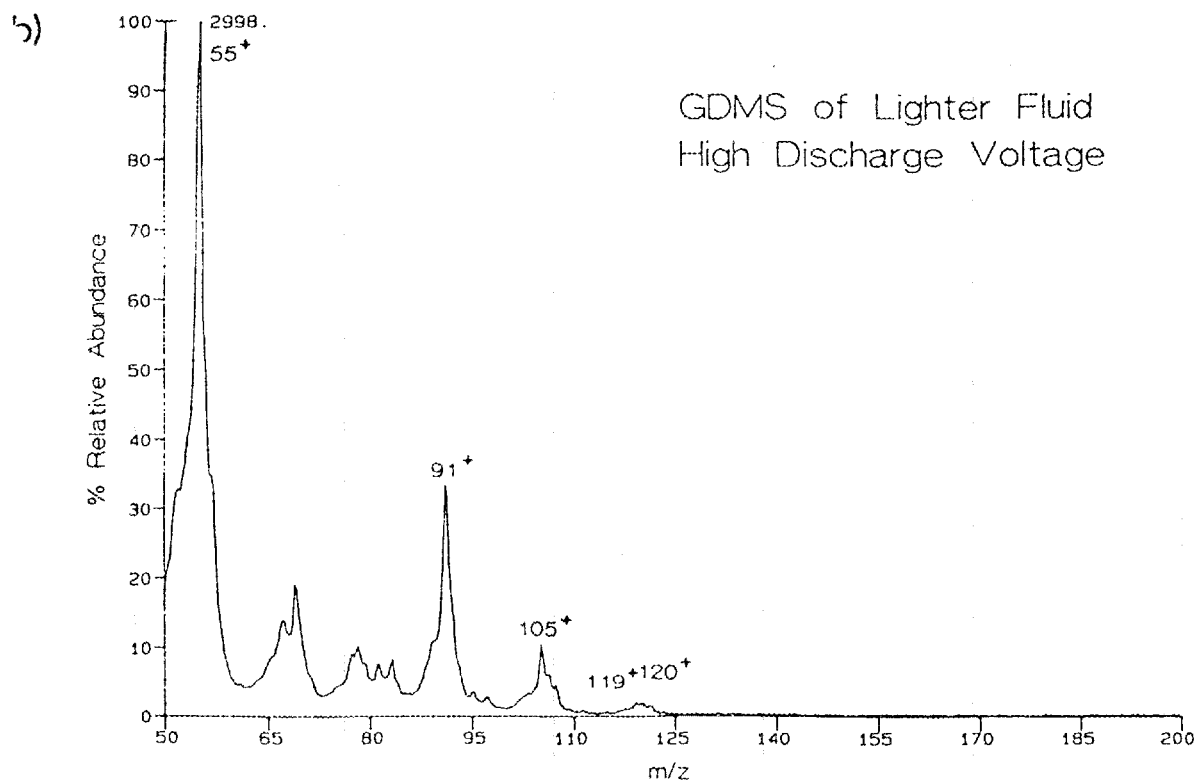
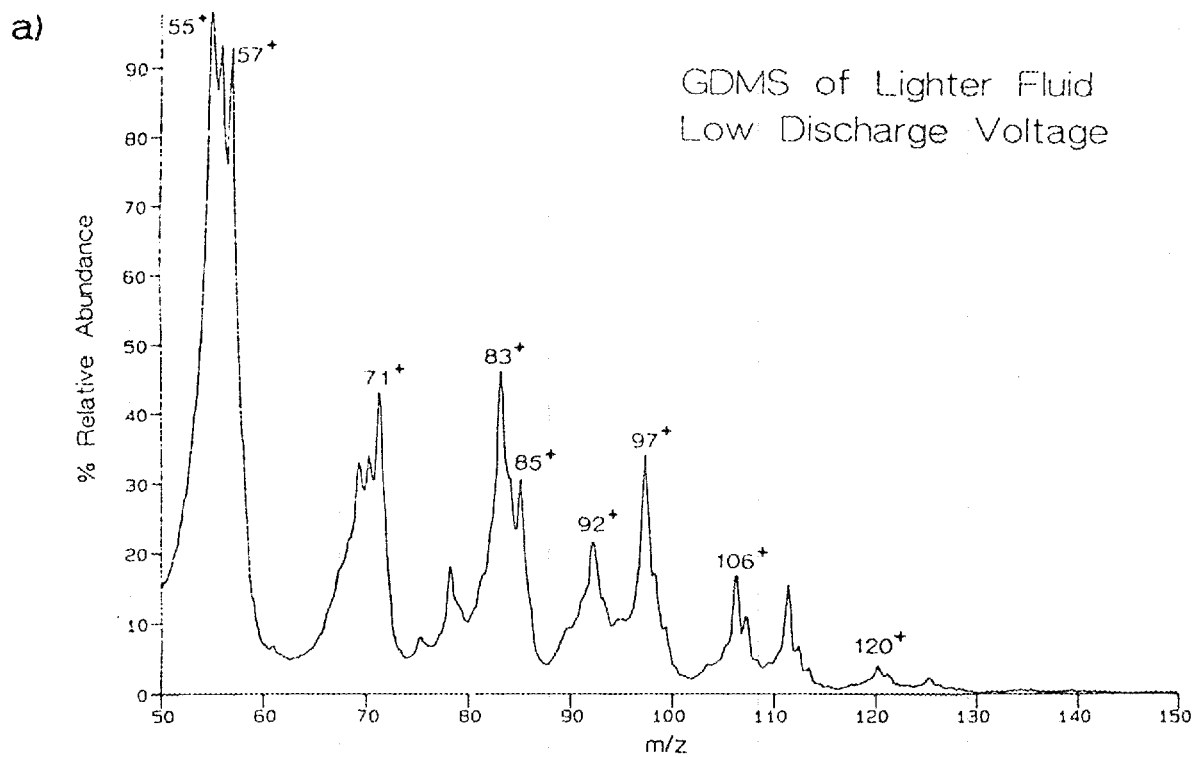


Figure 33. Glow Discharge mass spectra of lighter fluid acquired at a) low and b) high discharge voltages.

The daughter ion MS/MS spectra acquired for the ions in the mass spectra of the lighter fluid are included in Appendix VI.

5. Perfumes and rum

Two different brands of perfume, Madame Rochas and Musk by Alyssa Ashley, and a sample of 80 proof Bacardi rum were tested in the positive ion mode. The mass spectra of the rum and musk perfume both showed predominantly peaks due to ethanol. At high discharge voltages the signal is concentrated almost exclusively in m/z 47, protonated ethanol. At low discharge voltages, cluster ions are also observed, the most abundant being the ethanol proton-bound dimer. In both cases, small peaks are also observed at masses greater than 100 amu but these are about two orders of magnitude less intense than signals due to ethanol. No attempt was made to identify the compounds that give rise to the high mass ions. Similar behavior was noted for the Madame Rochas perfume except that intense signals were also observed at m/z 33 and m/z 65 indicating a significant concentration of methanol in the mixture. The daughter ion MS/MS spectra confirmed that these ions contain methanol.

C. Detection Limits

We are currently not equipped to properly establish the ultimate detection limits for the compounds of interest using this approach, as we will discuss below. We have, however, made measurements that give an overestimate of the detection limit. These measurements are based on diluting the compound of interest in a solvent and injecting a tenth of a microliter of the solution into a tube leading to the intake aperture of the glow discharge source. The total number of counts recorded for the most intense ion derived from the compound of interest in the glow discharge mass spectrum is then recorded at successively greater dilutions.

We have found that the procedure described above is unsatisfactory at very low levels. In order to accurately introduce extremely small amounts of sample material into the ion source, we have diluted the sample in a solvent. All of the solvents we have used, however, give signals at the masses of interest when 0.1 μ l is injected. This may be

due to a dramatic change in the gas-phase ion chemistry in the glow discharge source when a slug of solvent is introduced, or the solvents may be contaminated. The measurement of toluene in carbon disulfide is given here as an example. When 0.1 μl of "pure" CS_2 is injected, the signal at m/z 91 in the glow discharge mass spectrum increases from a background level of a few hundred counts/s to 22,000 counts/s. When 0.1 μl of a solution of 1.7 $\mu\text{g}/\text{ml}$ of toluene in CS_2 is injected, the signal at m/z 91 increases reproducibly to 26,000 counts/s. At this level, we conclude that the toluene added to the CS_2 is detected. In the latter injection, 170 pg or 1.9×10^{-12} mole of toluene is injected. All of the solution vaporizes and is drawn into the ion source in less than one second. The ion source samples 6 ml of atmospheric vapors in one second (or 2.4×10^{-4} mole/s). The concentration in air, therefore, of the toluene added to the CS_2 is, on a mole/mole basis, about 8 parts per billion.

The signal due to the "pure" carbon disulfide could be due to a change in the chemistry of the glow discharge source when it is added in such a large quantity, resulting in an increase in the chemical noise in the mass spectrum. A quantity of 0.1 μl of CS_2 , when vaporized constitutes about 7 parts per thousand on a mole/mole basis of the molecules drawn into the ion source. At this concentration, the reagent ions can change from ions derived from oxygen to ions derived from carbon disulfide. Another possibility for the large signal at m/z 91 when "pure" CS_2 is injected is contamination. In order to give a signal of roughly 20,000 counts/s, the sum of the aromatic hydrocarbon contamination can be as low as 0.2%. The MS/MS spectrum of the ion at m/z 91 in the mass spectrum of the 0.1 μl injection of CS_2 is identical to that for the C_7H_7^+ ion from toluene. This supports, but does not prove, the sample contamination hypothesis.

Despite the problem associated with adding the sample of interest along with an excess of an organic solvent, a detection limit on the order of 8 ppb in air is obtained for toluene. We expect that the ultimate detection limit is likely to be two orders of magnitude lower.

We also anticipate comparable detection limits for the alcohols. Sub-ppb detection limits will only be demonstrated, however, when the sample is not introduced with an excess of organic solvent. One of several approaches can be used to introduce the sample of interest without a solvent. For example, an exponential dilution flask can be incorporated into the system. This device dilutes the sample vapor with air in a quantifiable and reproducible manner. Such a device will need to be constructed in-house since the only commercial vendor of these devices no longer sells them. Another approach, if solvent contamination is not the major cause for background signal, is to incorporate a gas chromatograph with the ion source to separate the sample of interest from the solvent. This approach will also establish whether or not solvent contamination is the major cause for the background signals described above. We presently do not have a gas chromatograph available to interface with the quadrupole/time-of-flight mass spectrometer.

V. Conclusions and Future Work

The work to date indicates that the detection of vapors of flammable liquids in ambient air can be accomplished with high sensitivity, high specificity, and in a matter of seconds using atmospheric sampling glow discharge ionization coupled with MS/MS. The ion source is sensitive to all of the flammable liquids tested and the use of MS/MS makes the possibility for false alarms from compounds other than those being sought very low. The only major possible interference likely to be present that we have identified is the proton-bound pentamer of water at m/z 91. MS/MS analysis, however, clearly distinguishes the ion due to water from $C_7H_7^+$, an ion likely to arise from a hydrocarbon fuel. Among the hydrocarbon fuels tested, gasoline is most readily detected due to higher concentrations of toluene and other alkylaromatics present in the mixture. Jet fuel and kerosene give similar responses both of which are lower than that for gasoline.

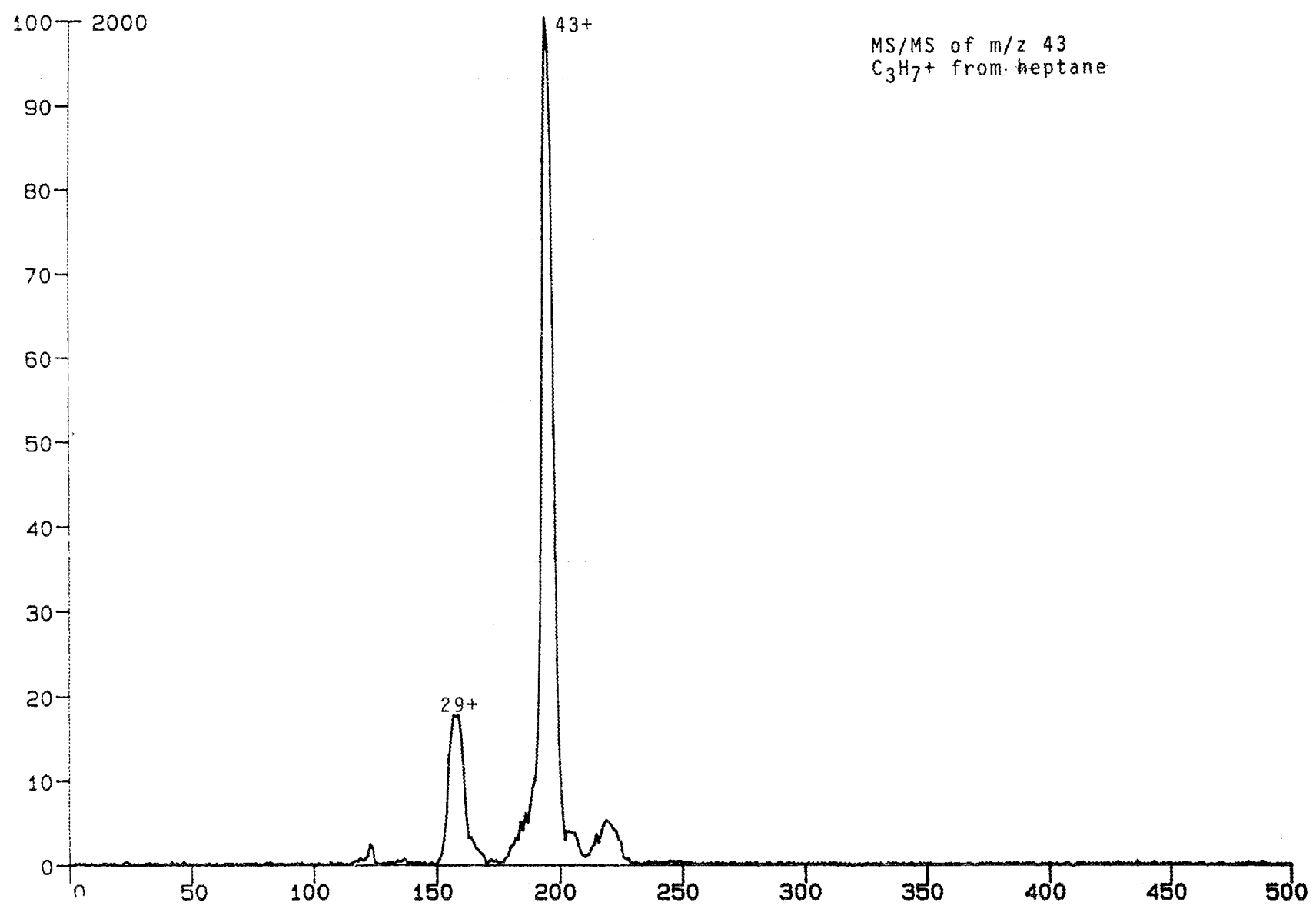
A conservative estimate for the detection limits for the compounds of interest is a few parts per billion. The ultimate detection limits are likely to be much lower. Future work involves the determination of the ultimate detection limits by use of one or both approaches discussed in section IV.C. In the laboratory, the detection limits are low enough to detect flammable liquids in glass vials with plastic caps closed finger tight. The question remains as to what the necessary detection limits are for detecting the vapors of flammable liquids in the atmosphere of an airport. The level of the background hydrocarbons, alcohols, etc. in the air can have a profound influence on any detection system. Establishing the background levels of the compounds of interest will involve testing air samples from an airport and obtaining the concentrations from the calibration data established in the detection limit work. Another question, which cannot be addressed by the detection method, is the potentially large number of "false" alarms from liquids present in baggage and on people intended for personal use only. The alcohols and many hydrocarbons are present in a wide variety of commercial products at high concentrations. The results from the rum and perfumes show that the alcohol in these products is readily detected.

Appendix I

Glow discharge MS/MS data for hydrocarbon ions.

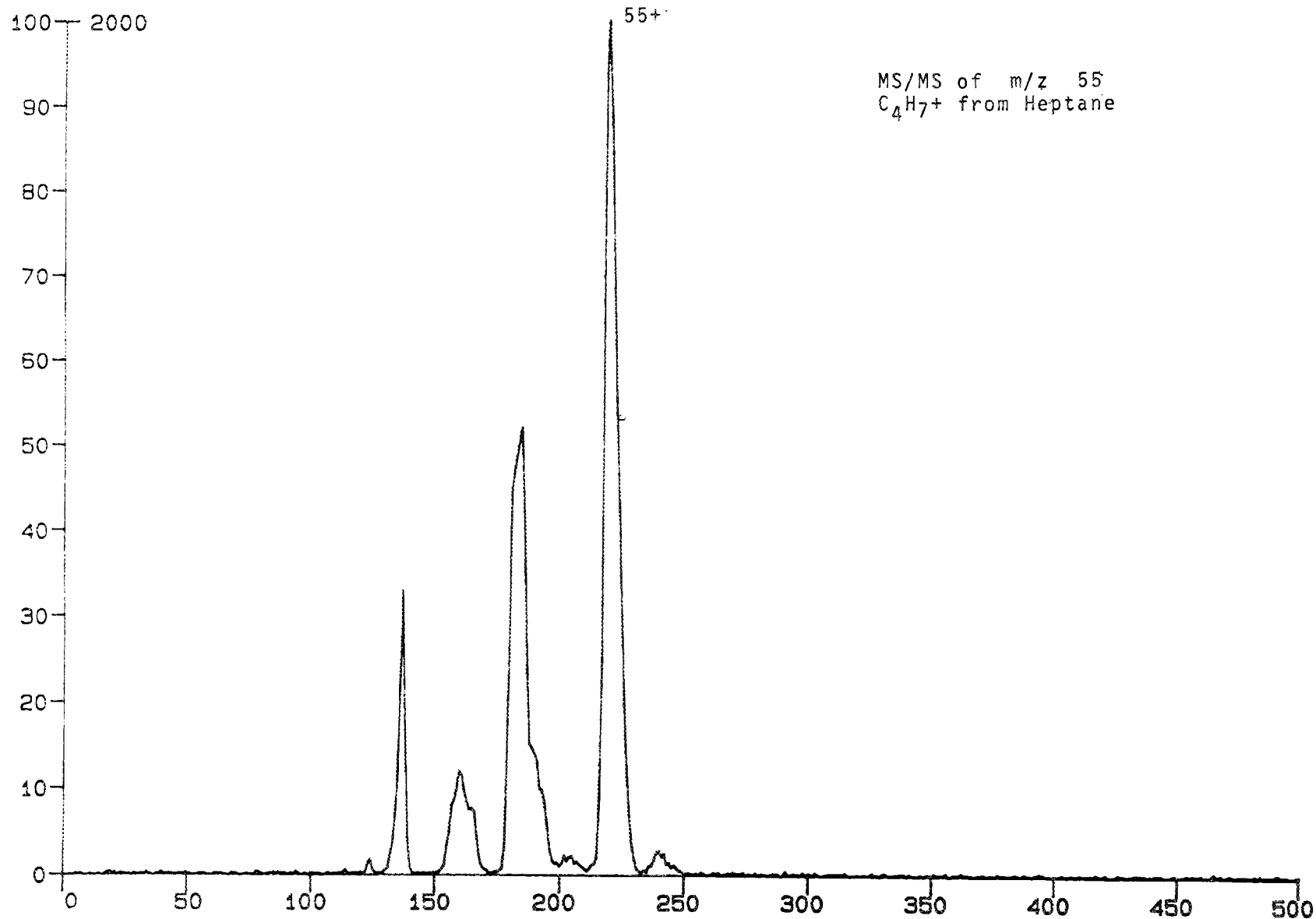
HEPT14.KGA

HEPTANE



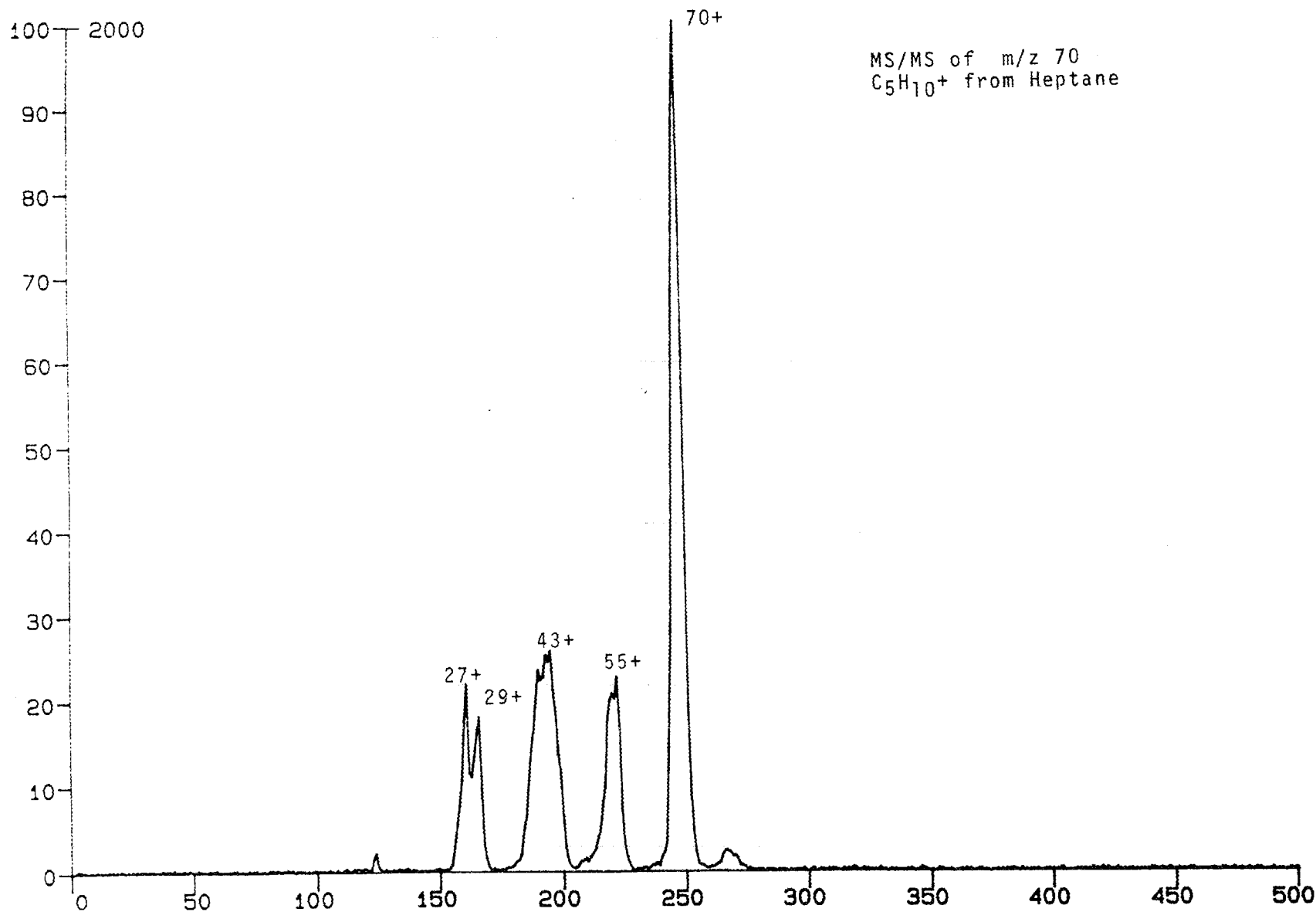
HEPT13.KGA

HEPTANE



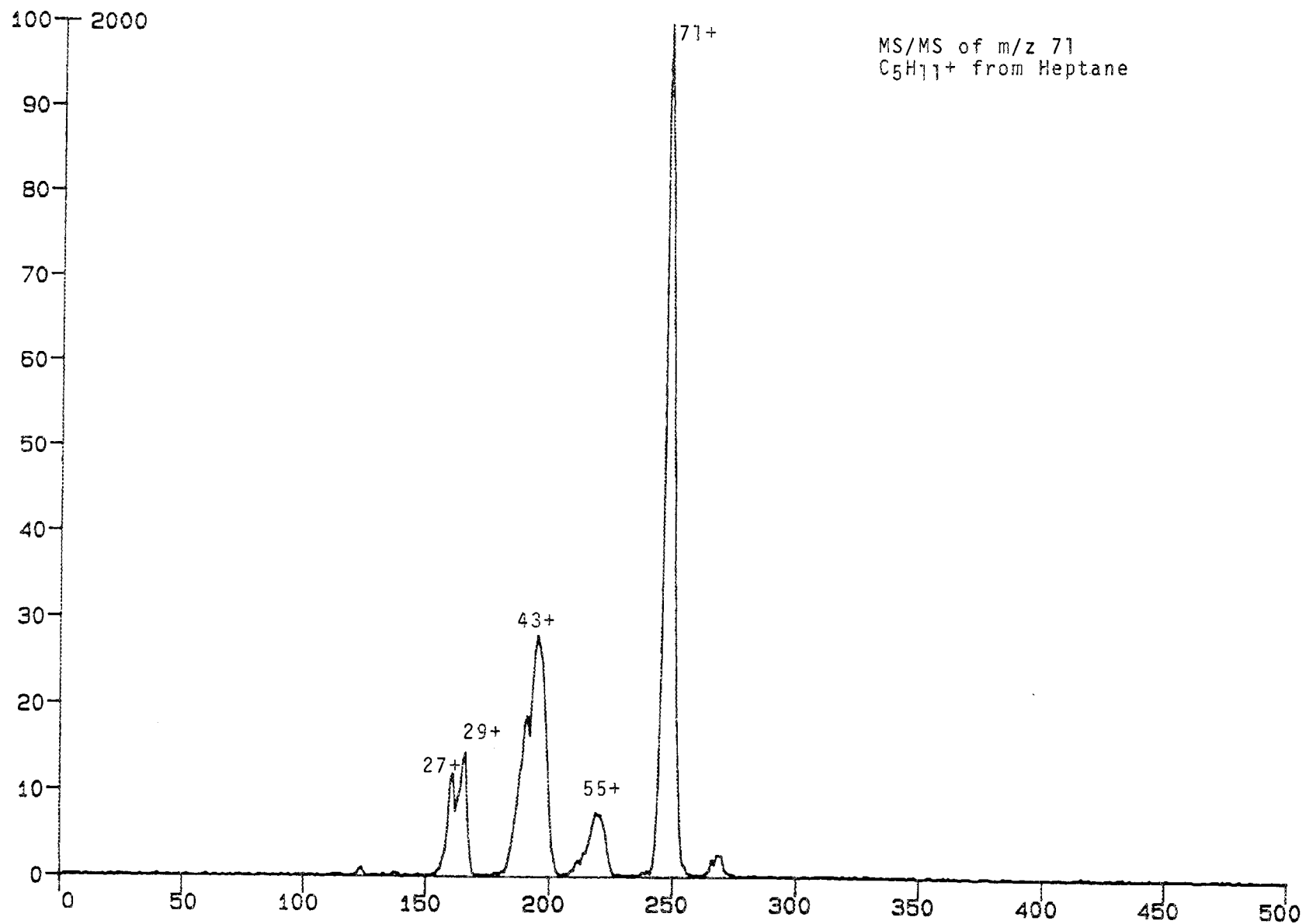
HEPT12.KGA

HEPTANE



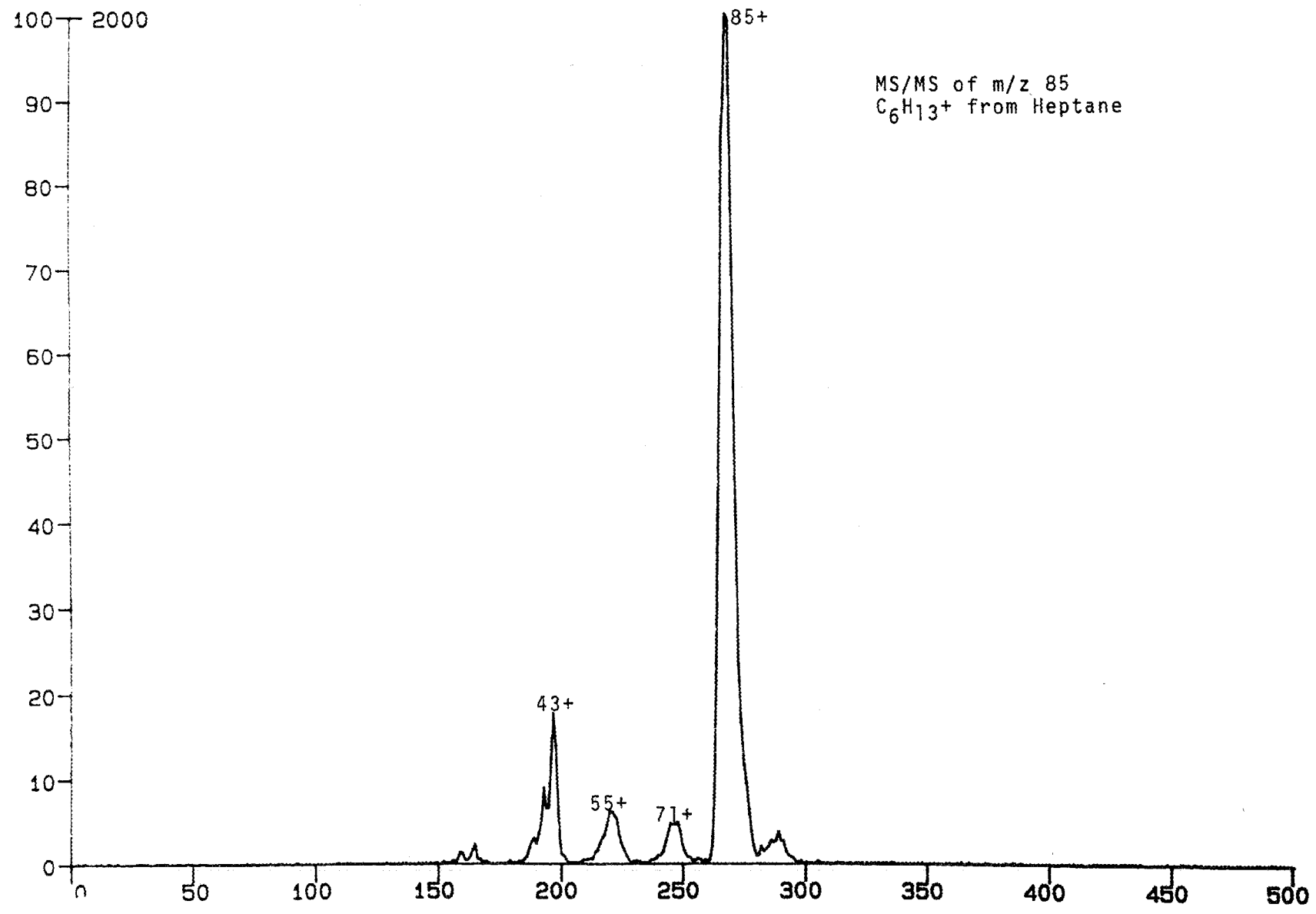
HEPT11.KGA

HEPTANE



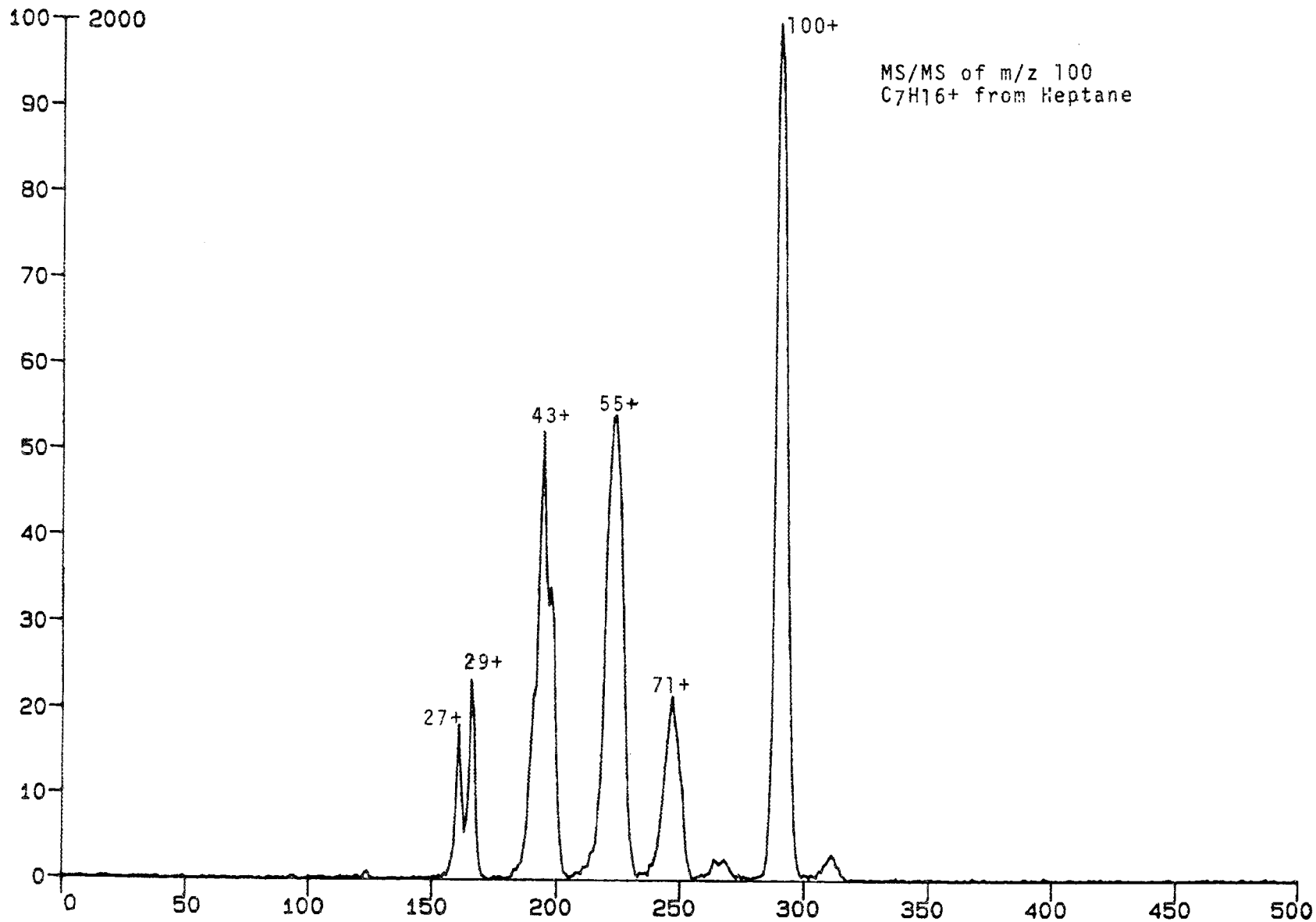
HEPT06.KGA

HEPTANE



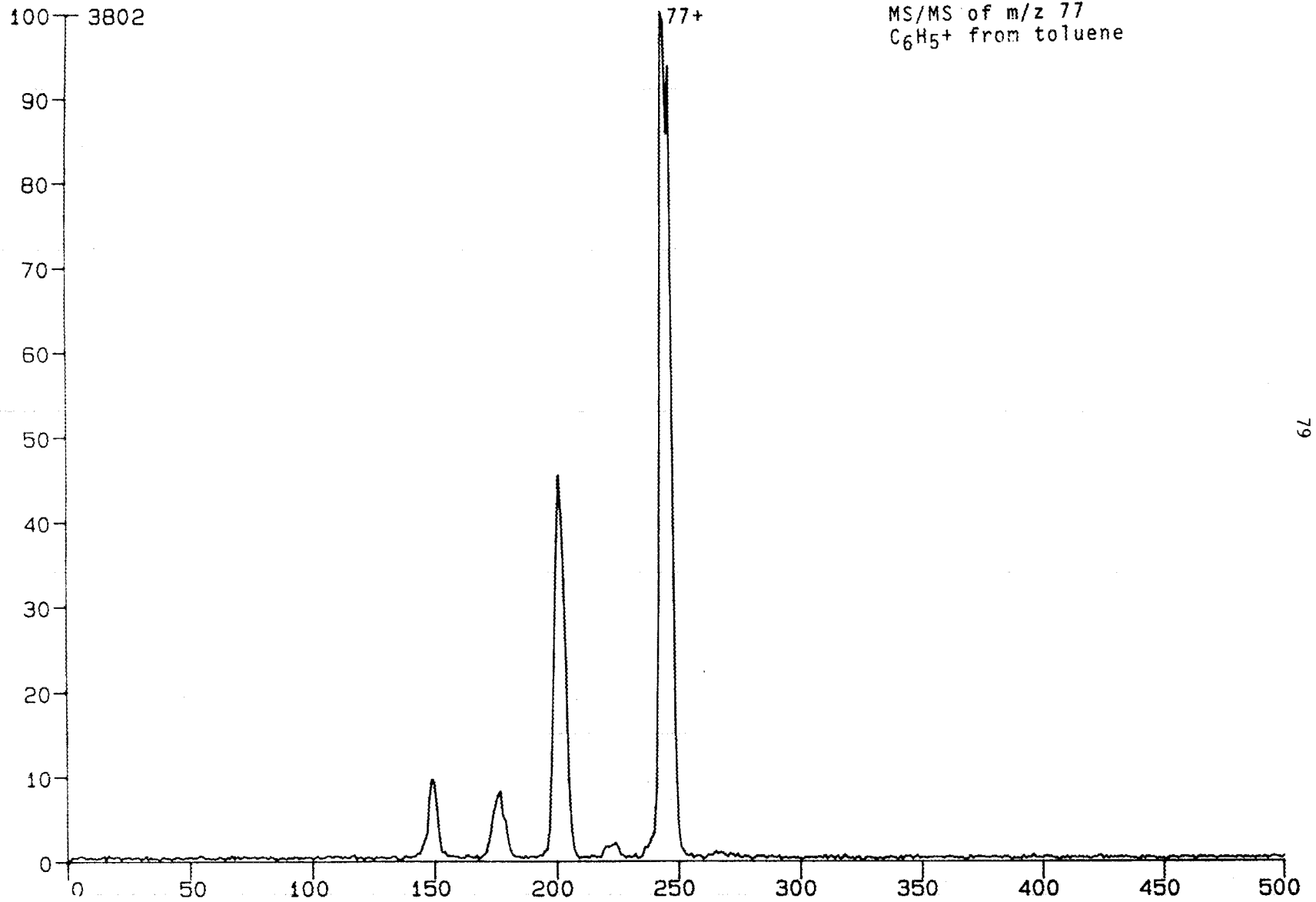
HEPT10.KGA

HEPTANE



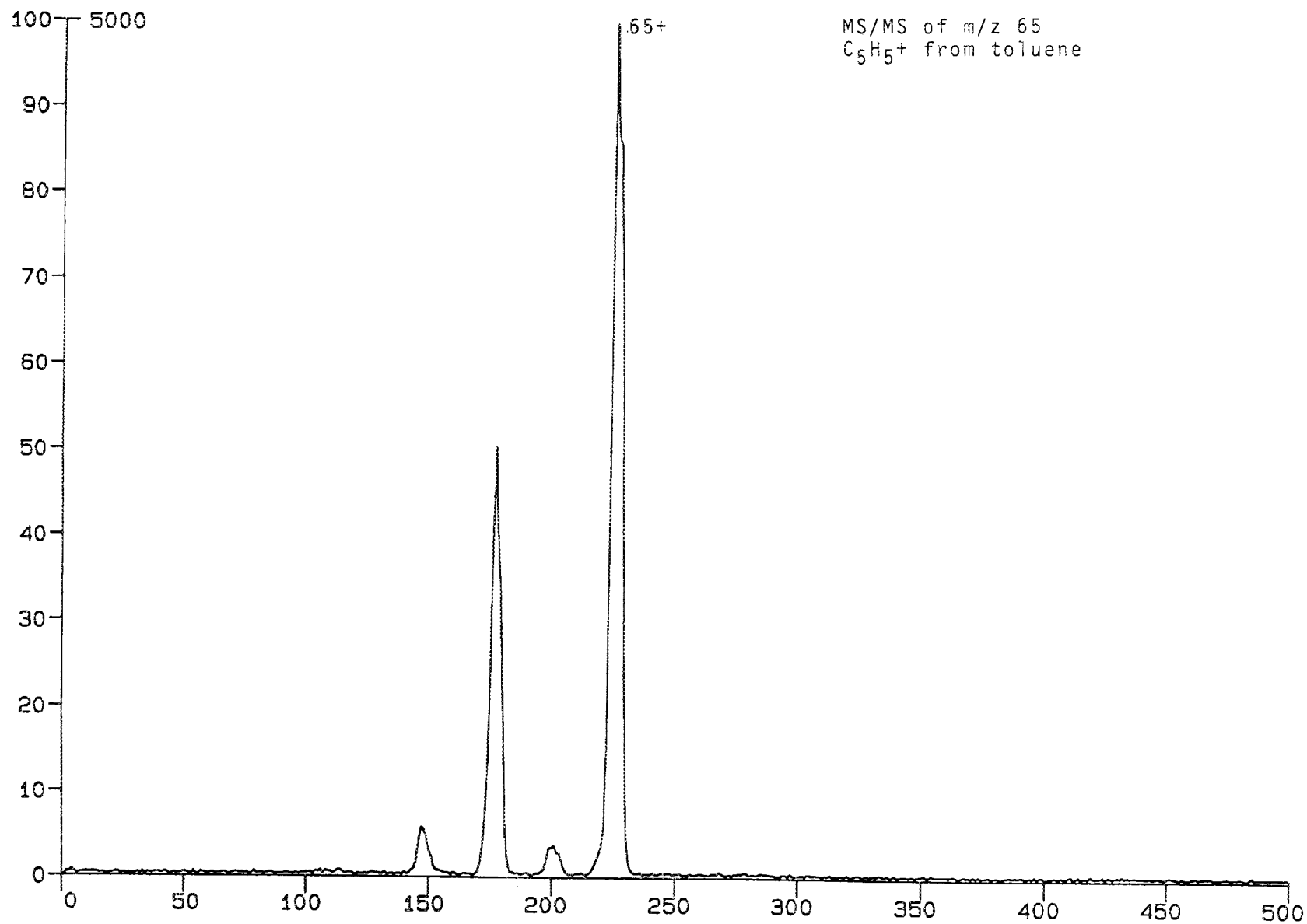
PTOLUE03.SAM

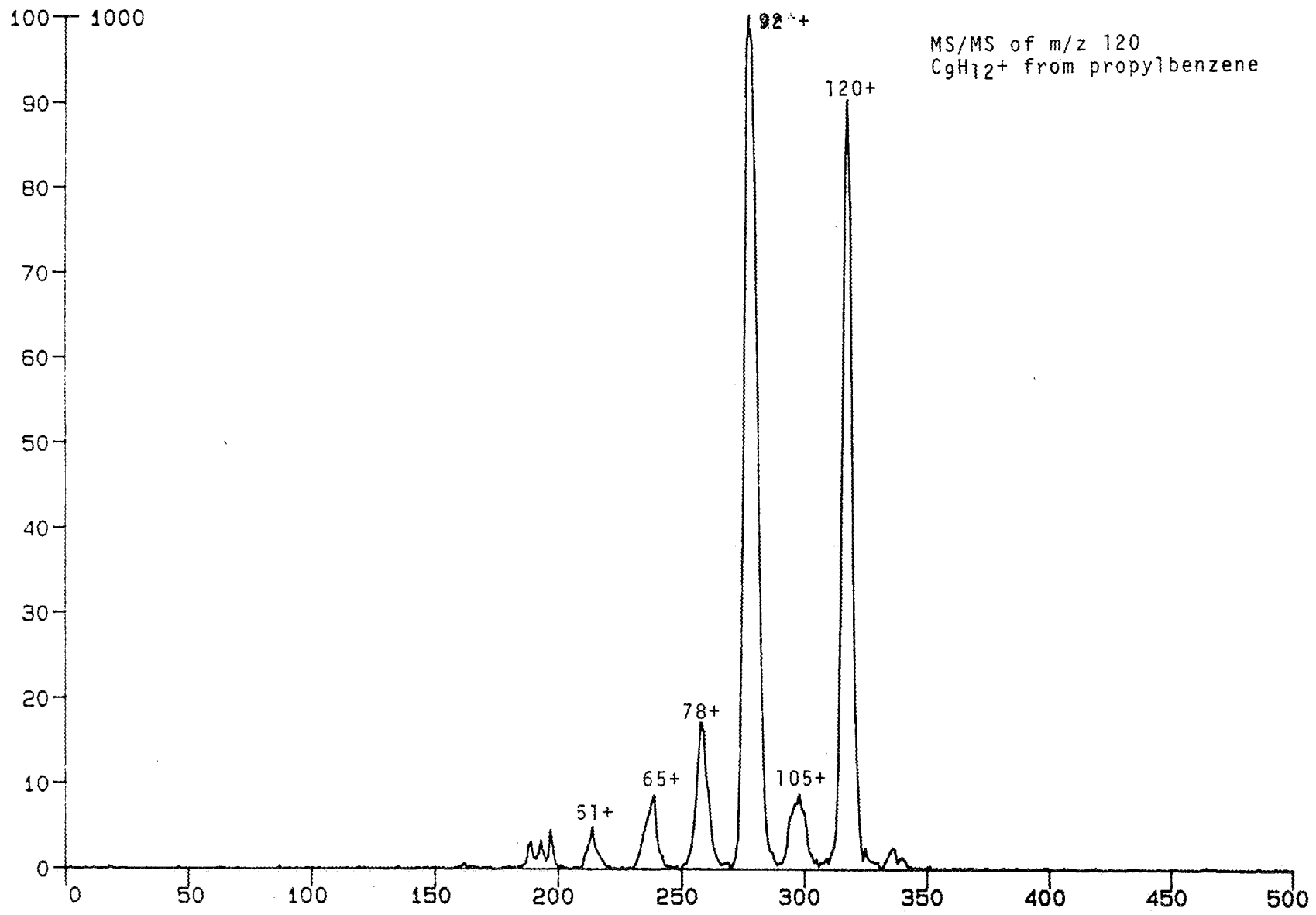
TOLUENE



PTOLUE04.SAM

TOLUENE



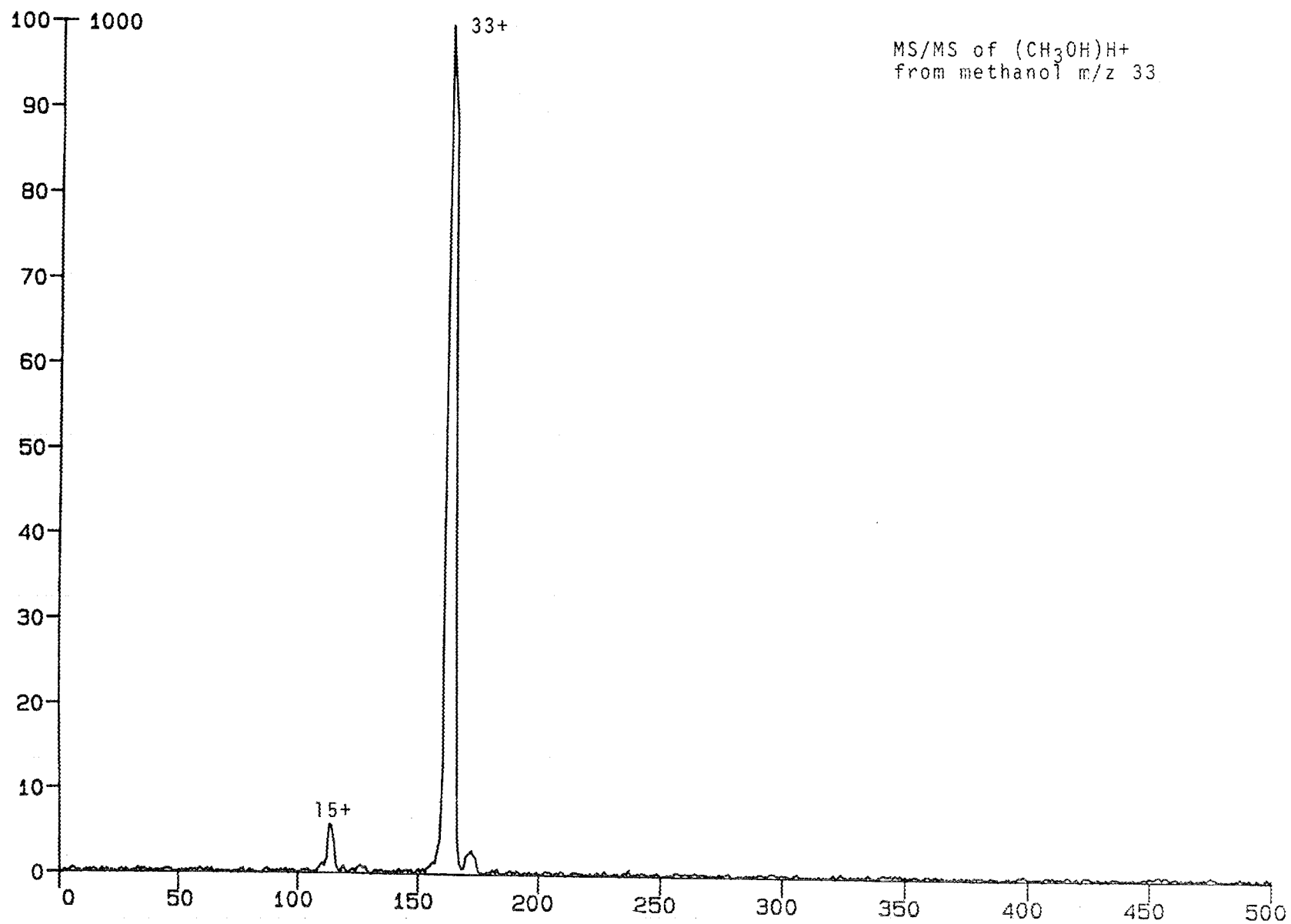


Appendix II

Glow discharge MS/MS data for ions derived from alcohols.

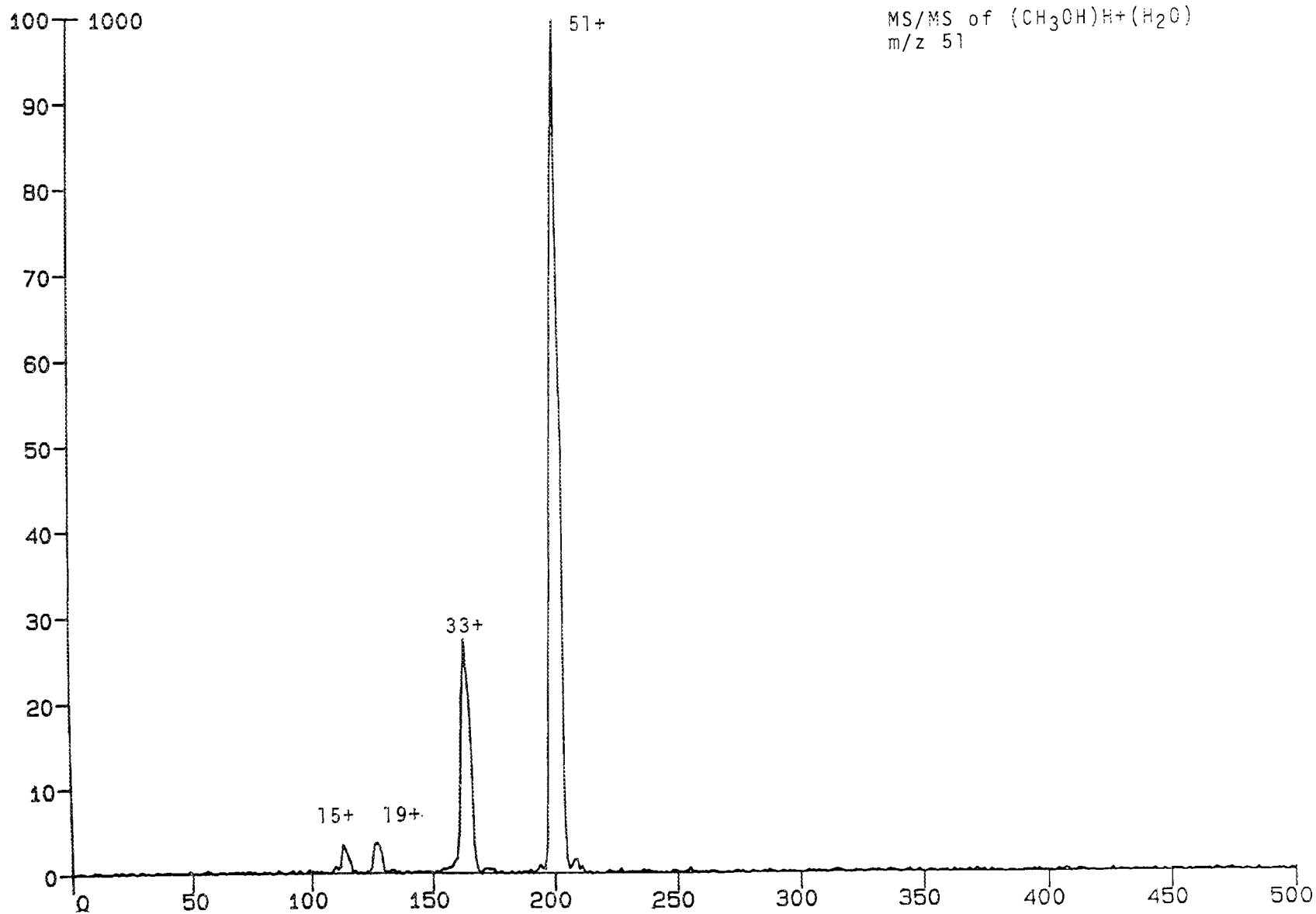
PMEOH01.SAM

METHANOL



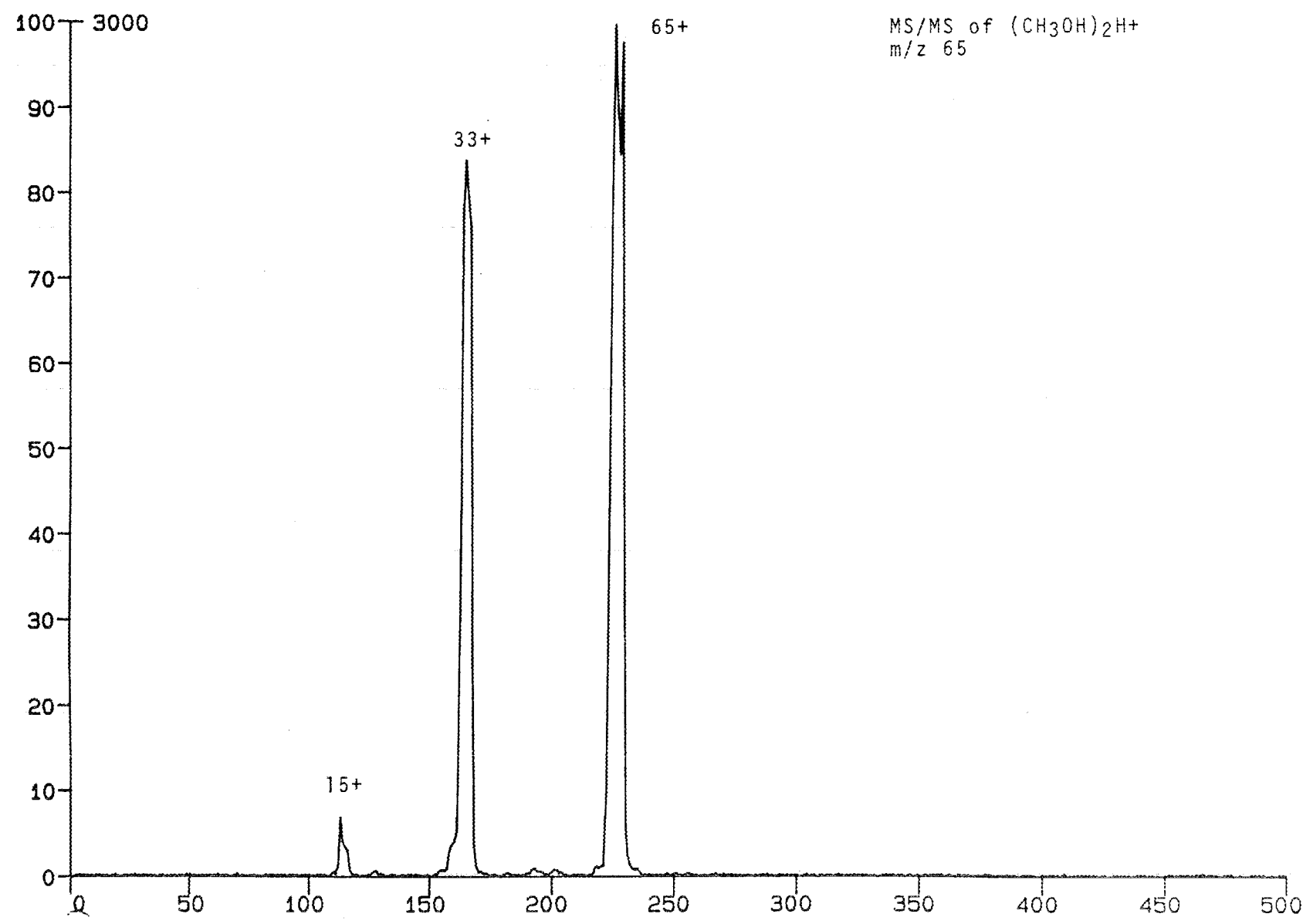
PMEOH02.SAM

METHANOL



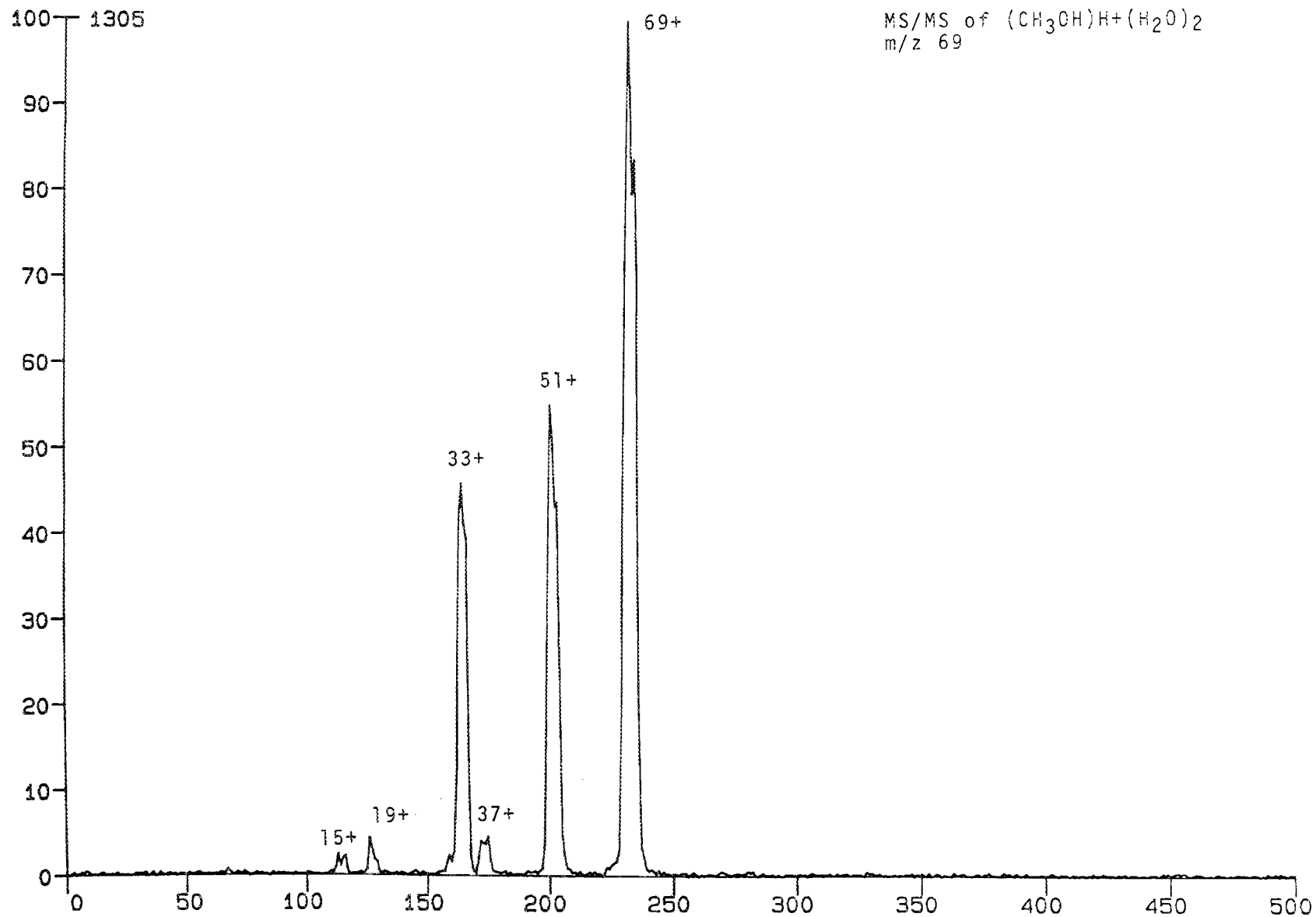
PMEOH04.SAM

METHANOL



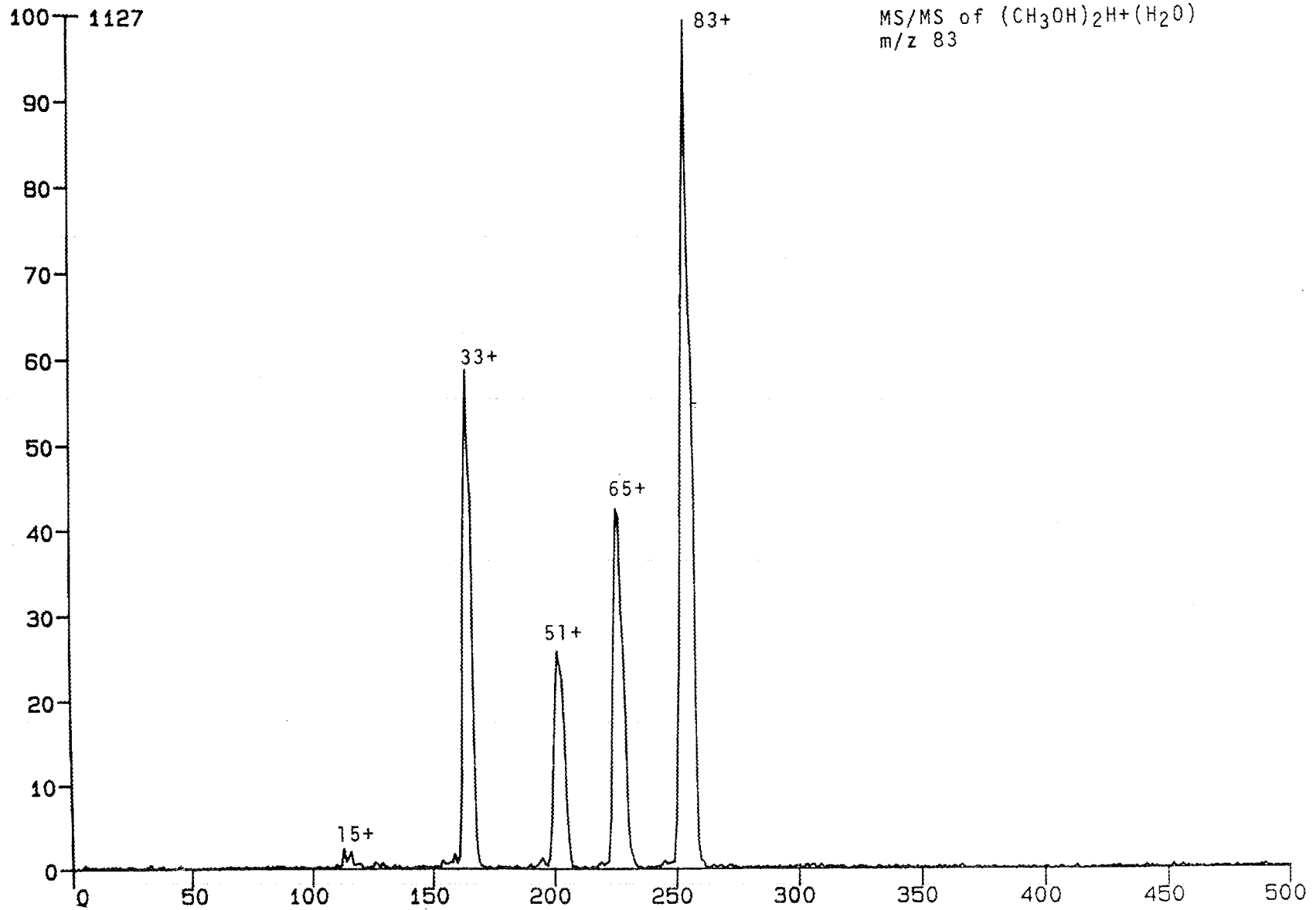
PMEOH05.SAM

METHANOL



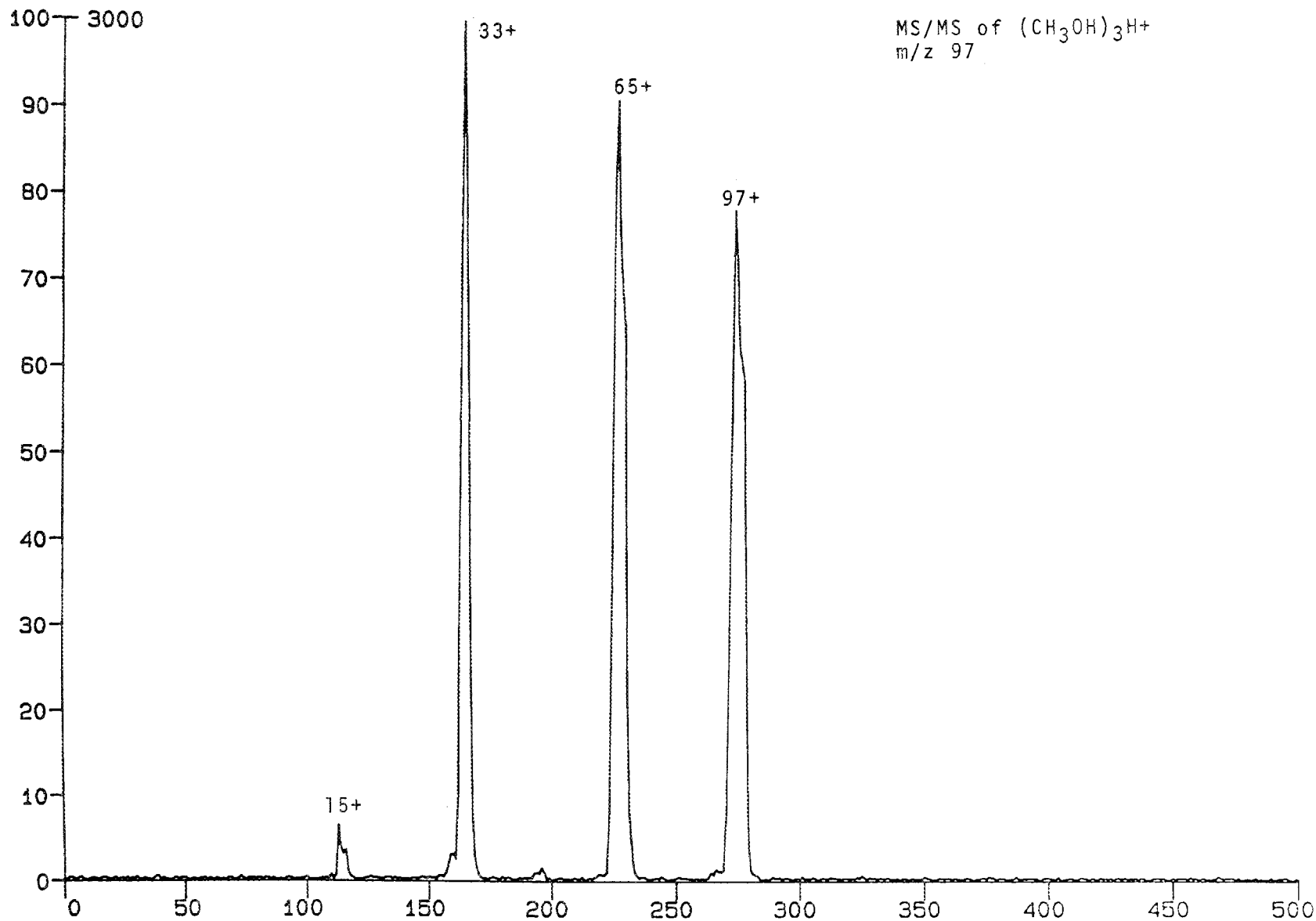
PMEOH07.SAM

METHANOL



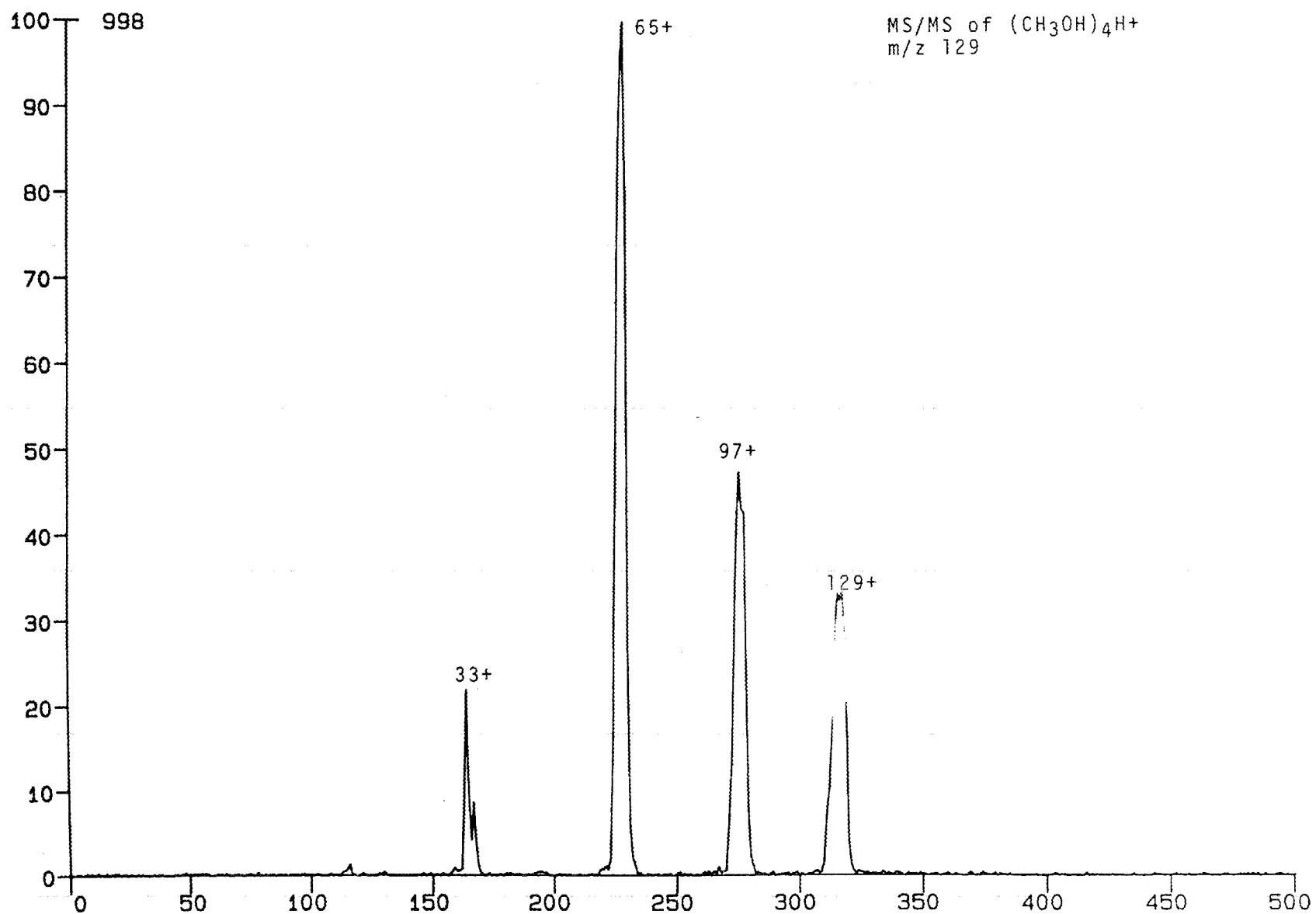
PMEOH09.SAM

METHANOL



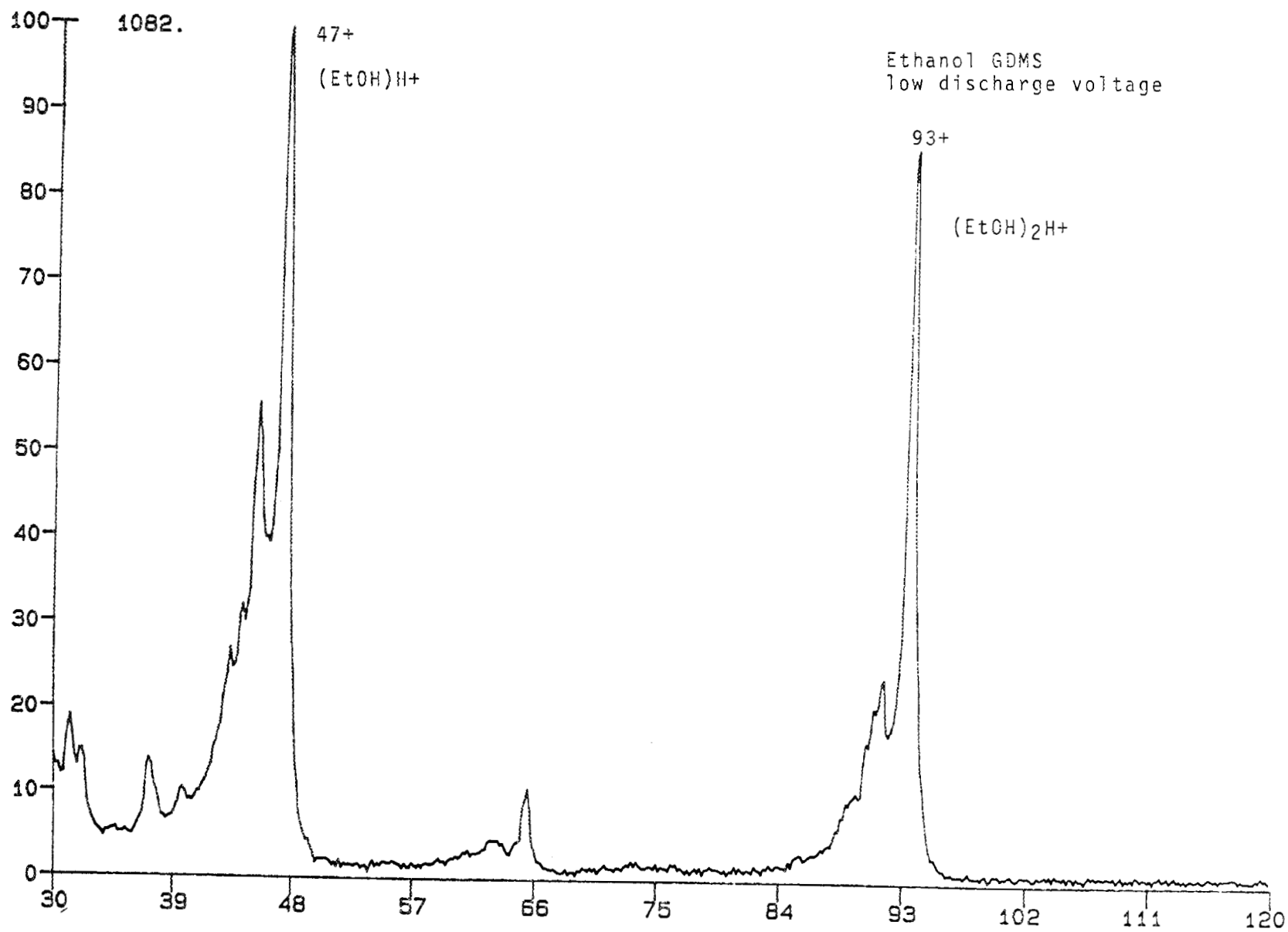
PMEOH10.SAM

METHANOL



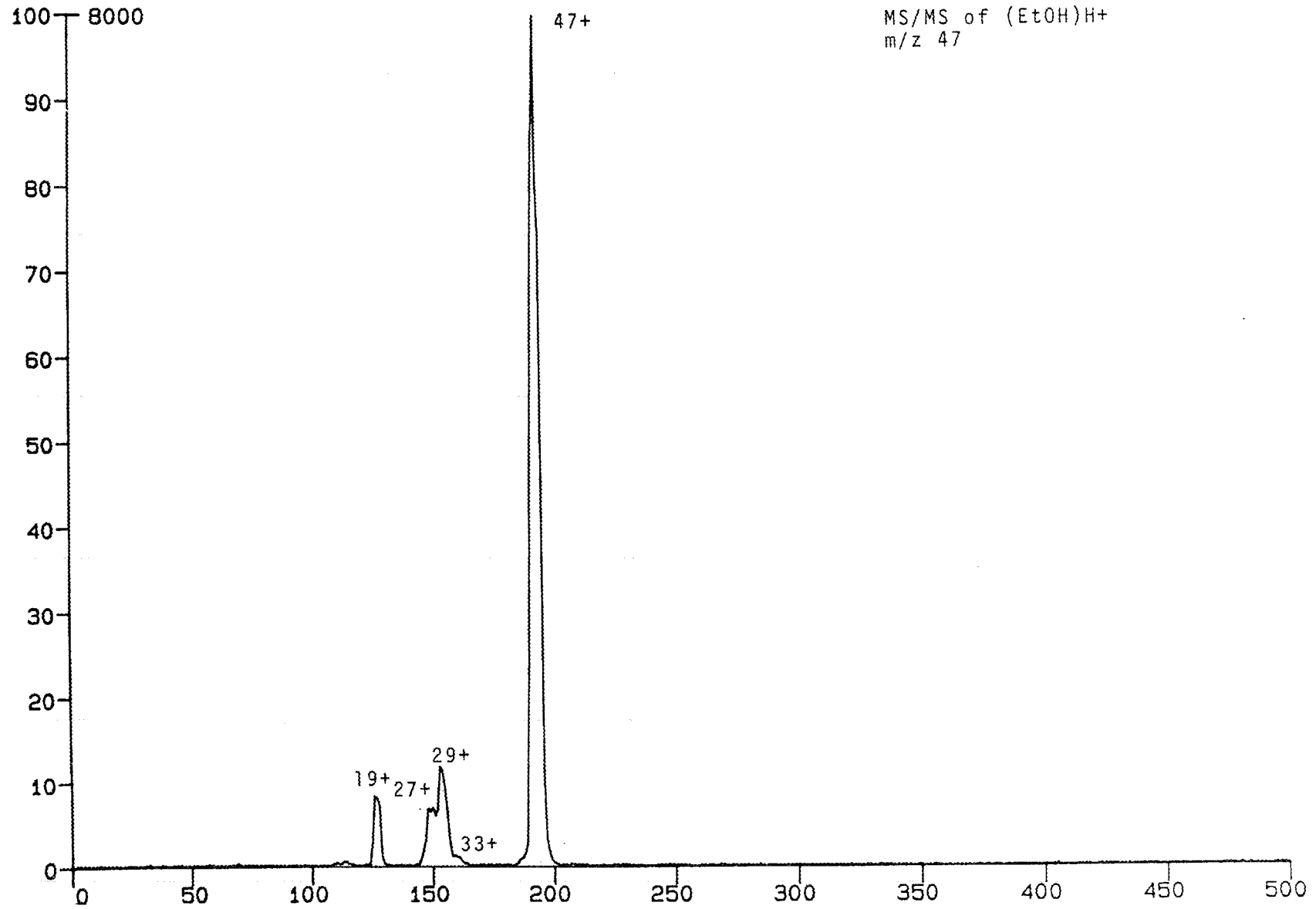
PETH02.QMS

ETHANOL



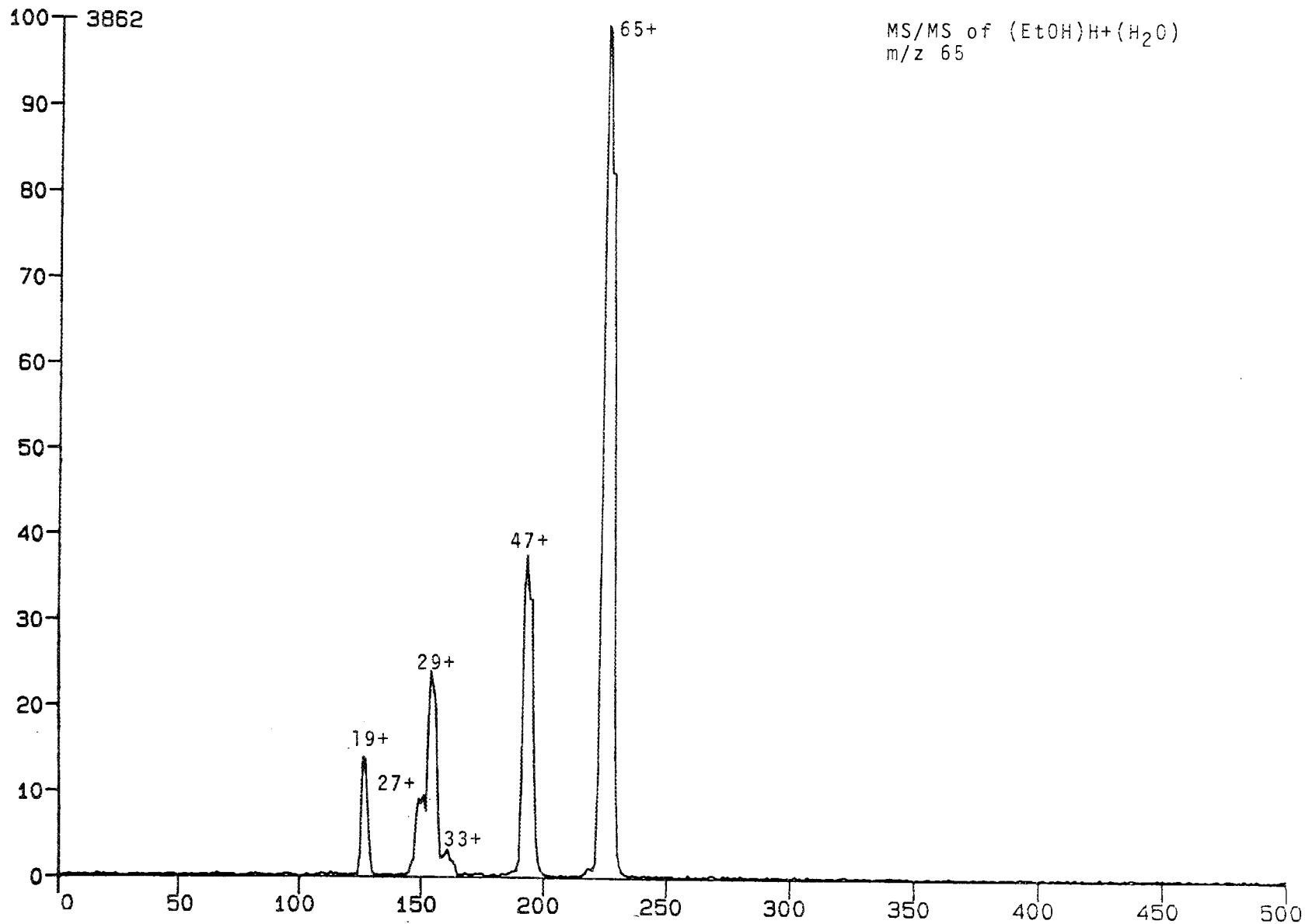
PETOH01.SAM

ETHANOL



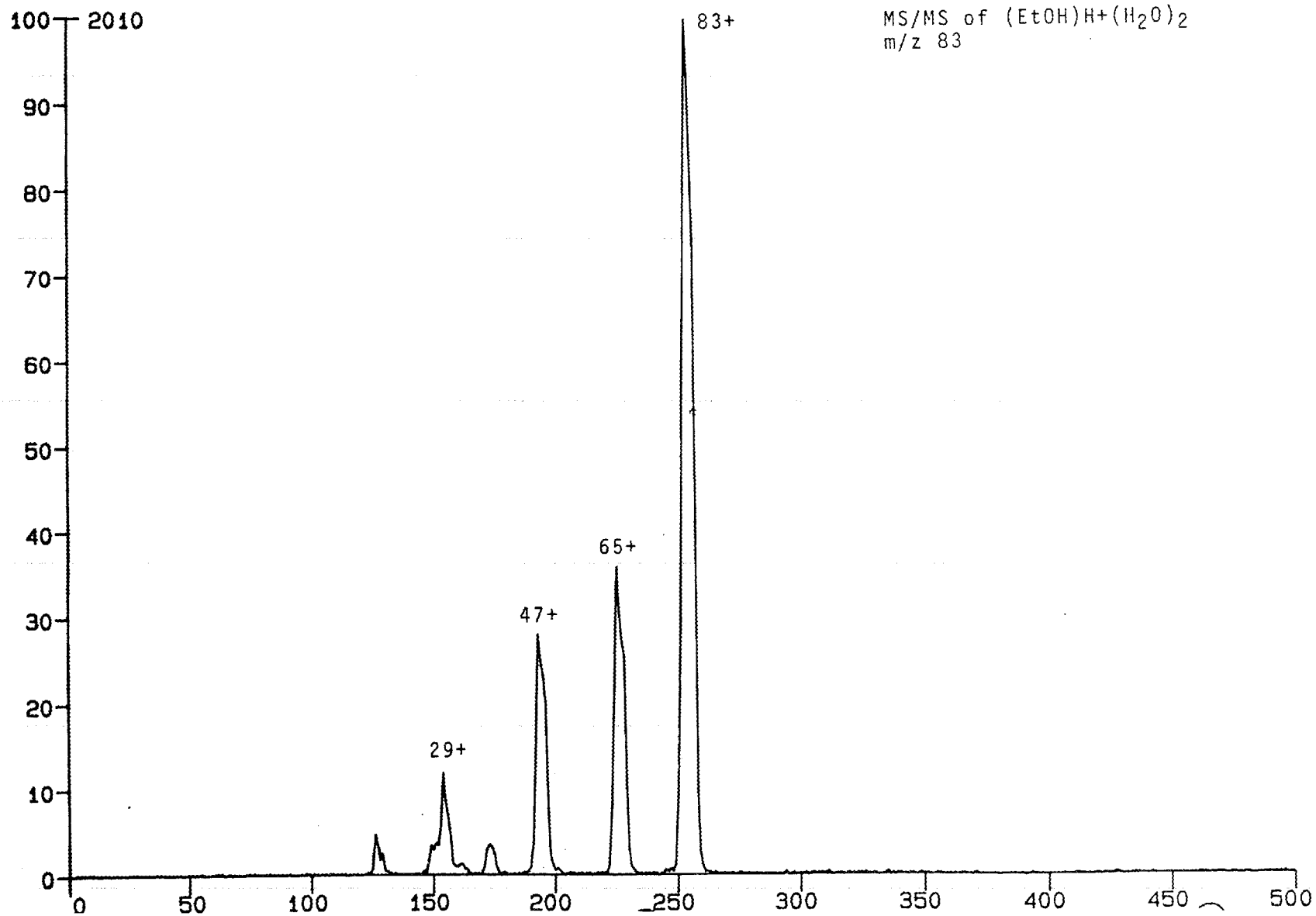
PETOH02.SAM

ETHANOL



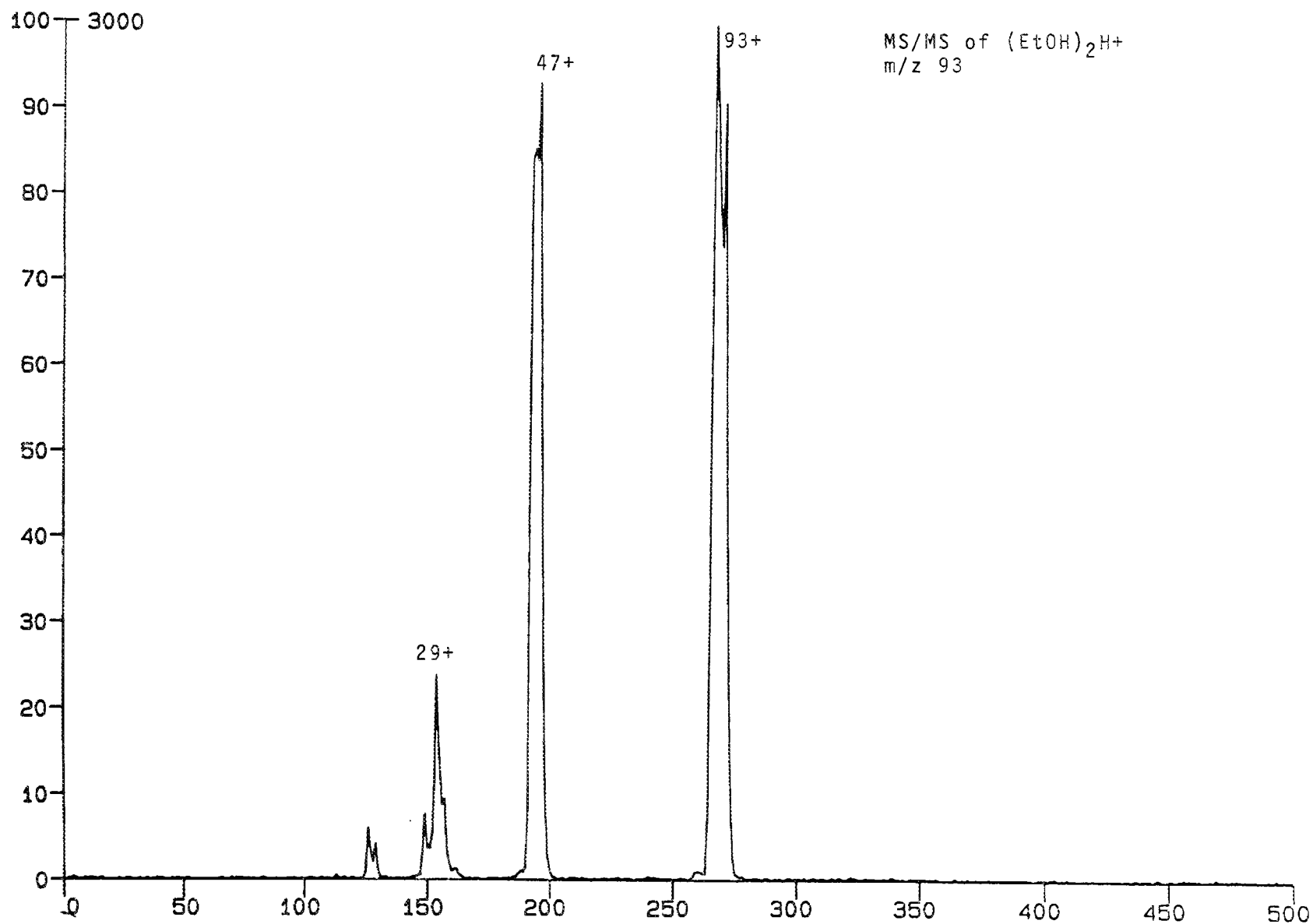
PETOH03.SAM

ETHANOL



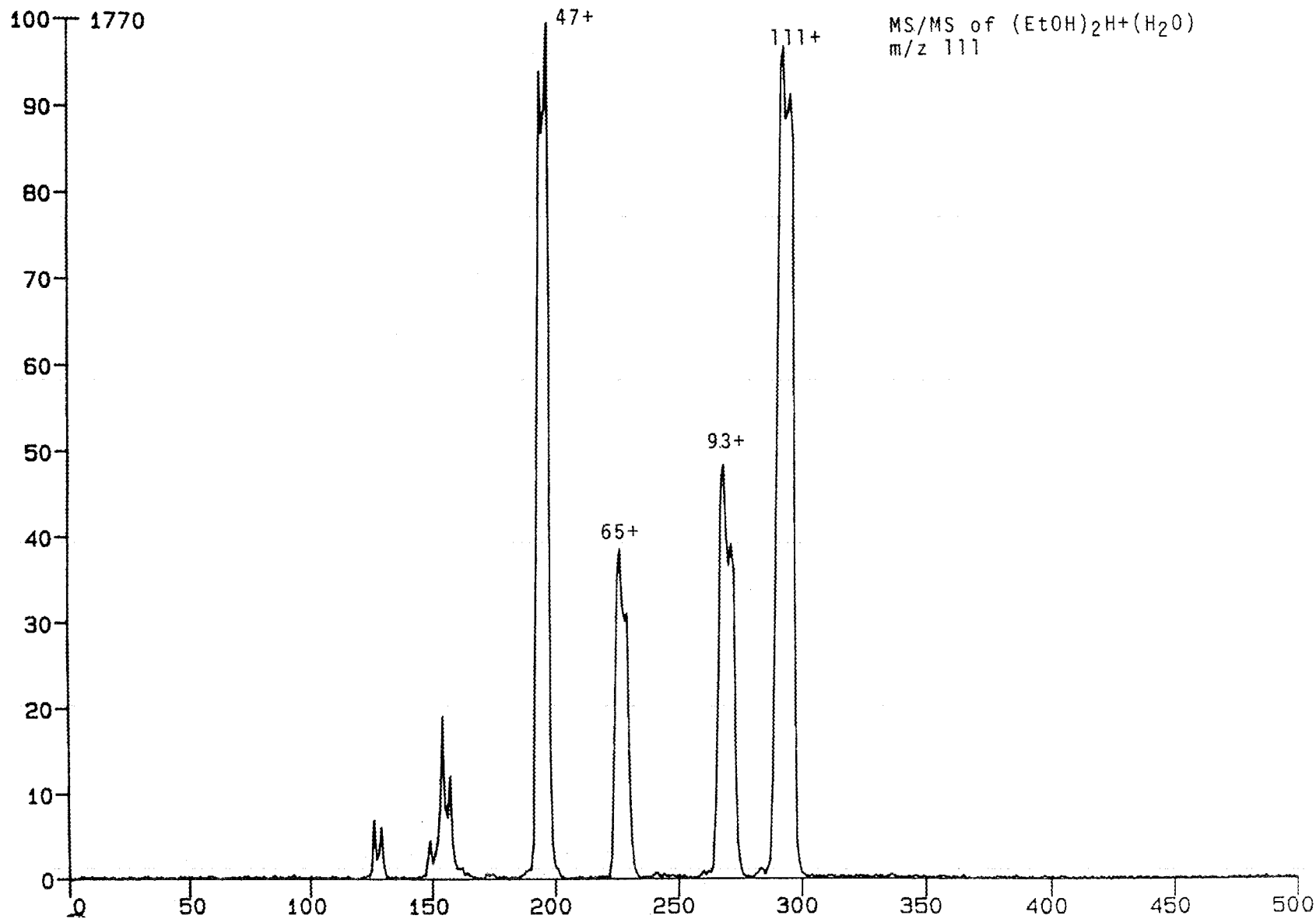
PETOH04.SAM

ETHANOL



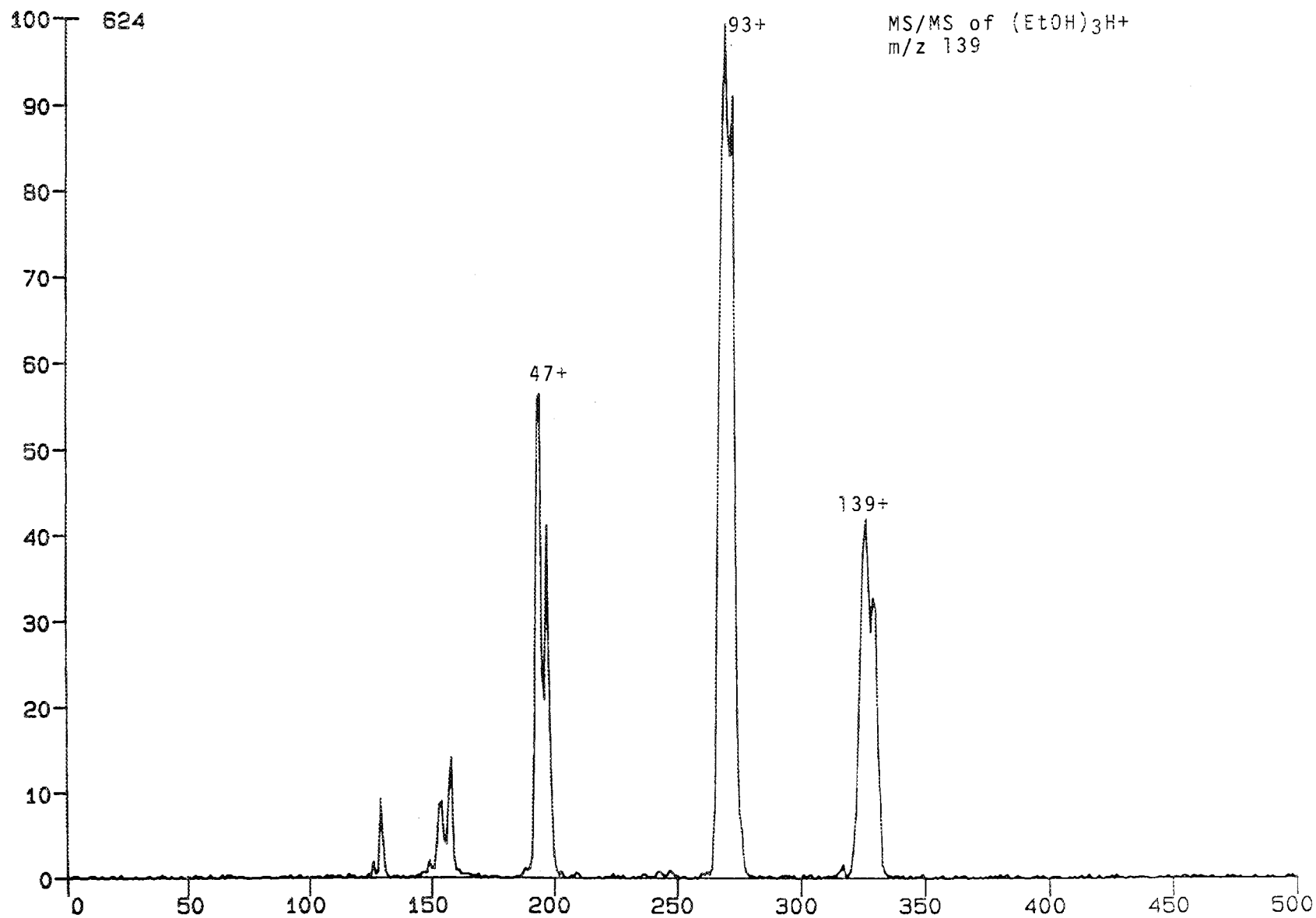
PETOH05.SAM

ETHANOL



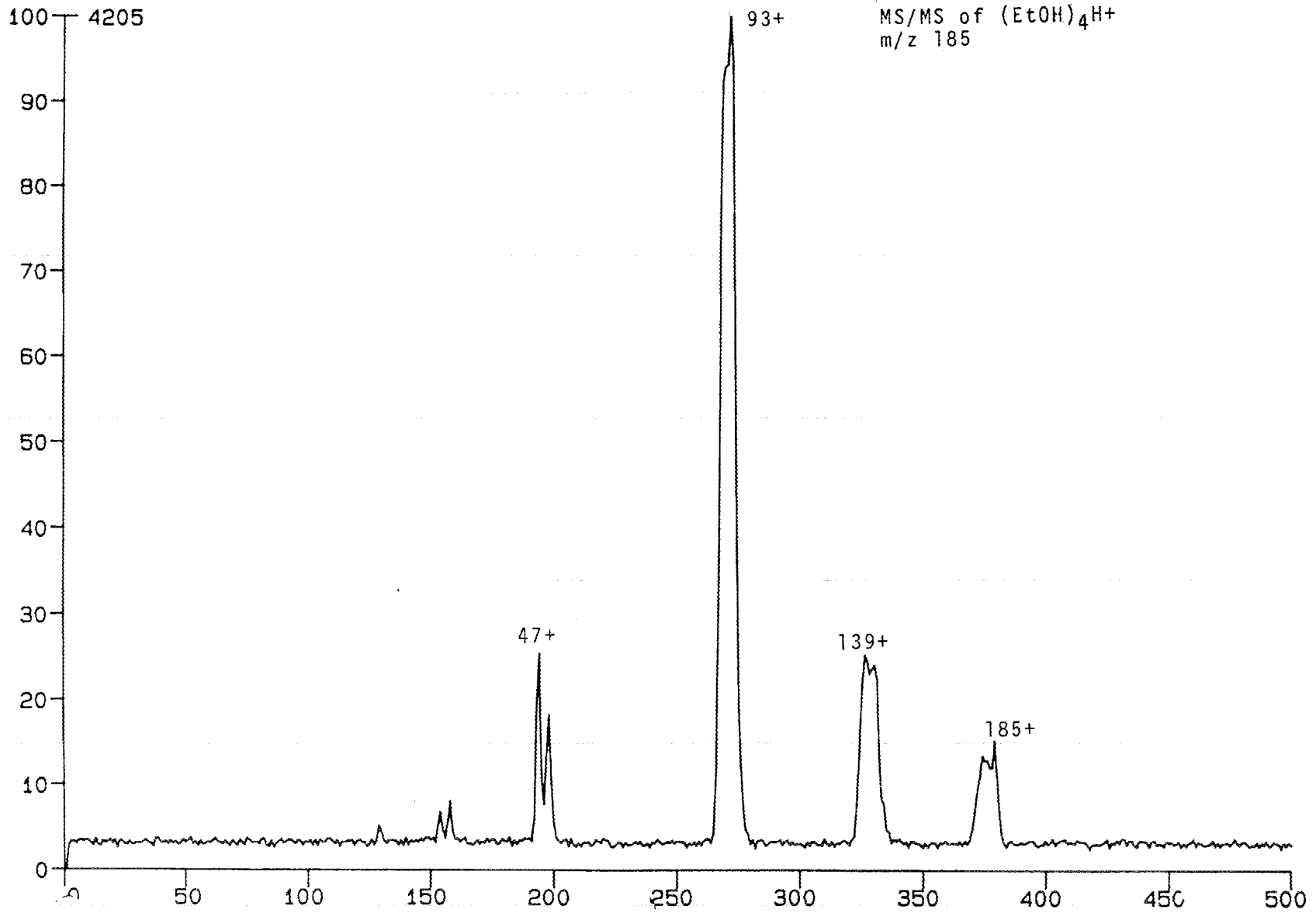
PETOH09.SAM

ETHANOL



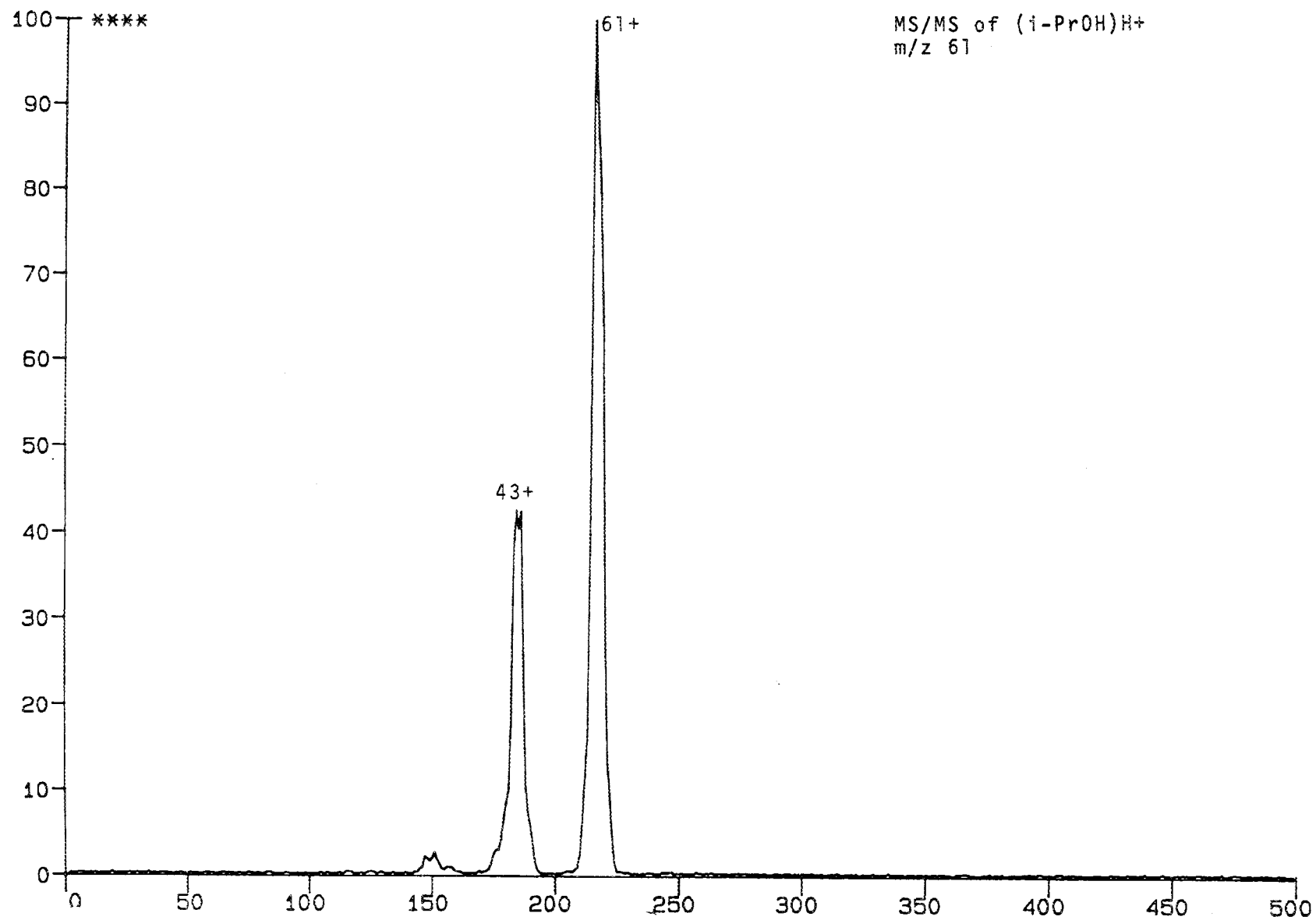
PETOH11.SAM

ETHANOL



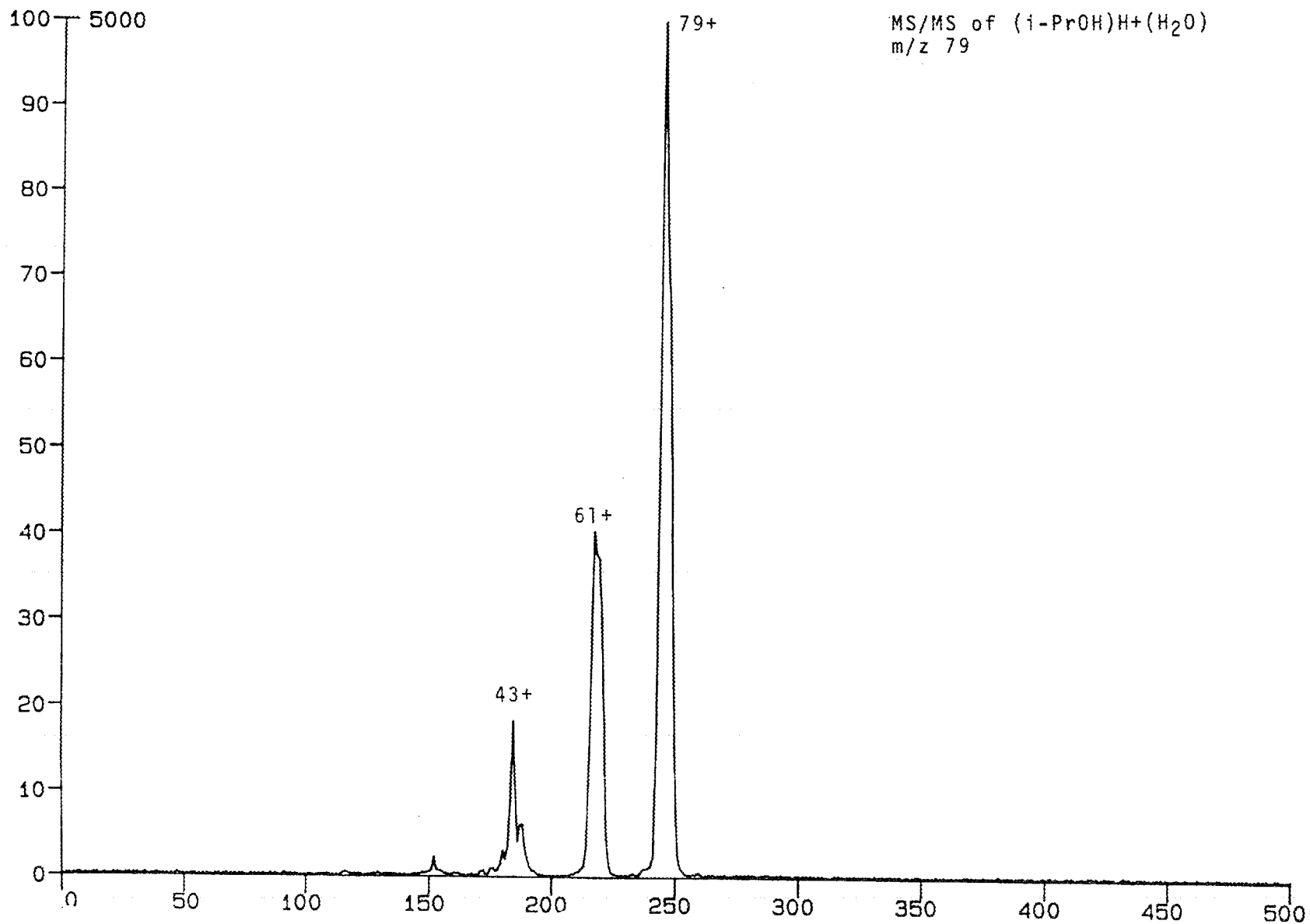
PIPROH01.SAM

isopropanol



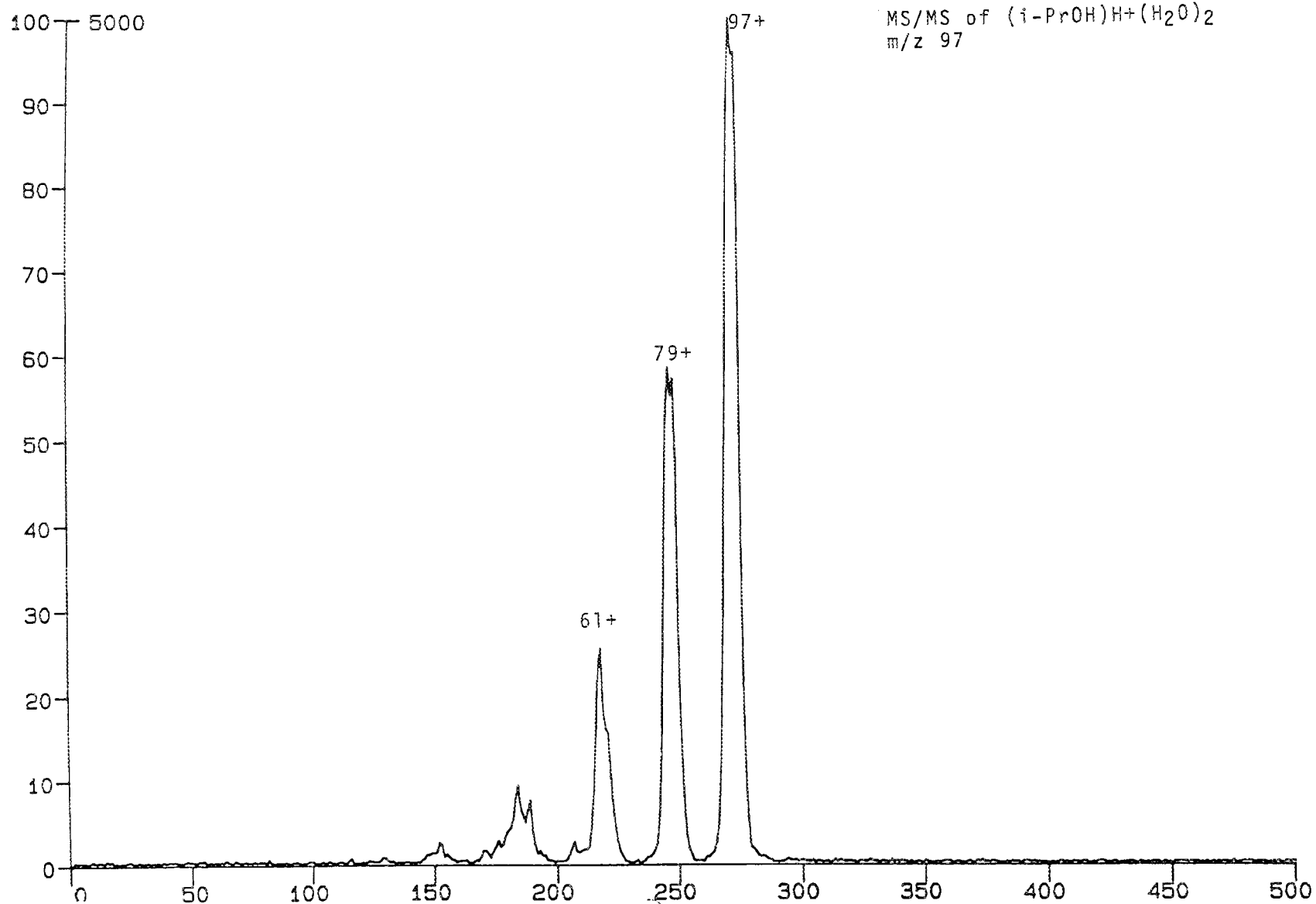
PIPROH04.SAM

isopropanol



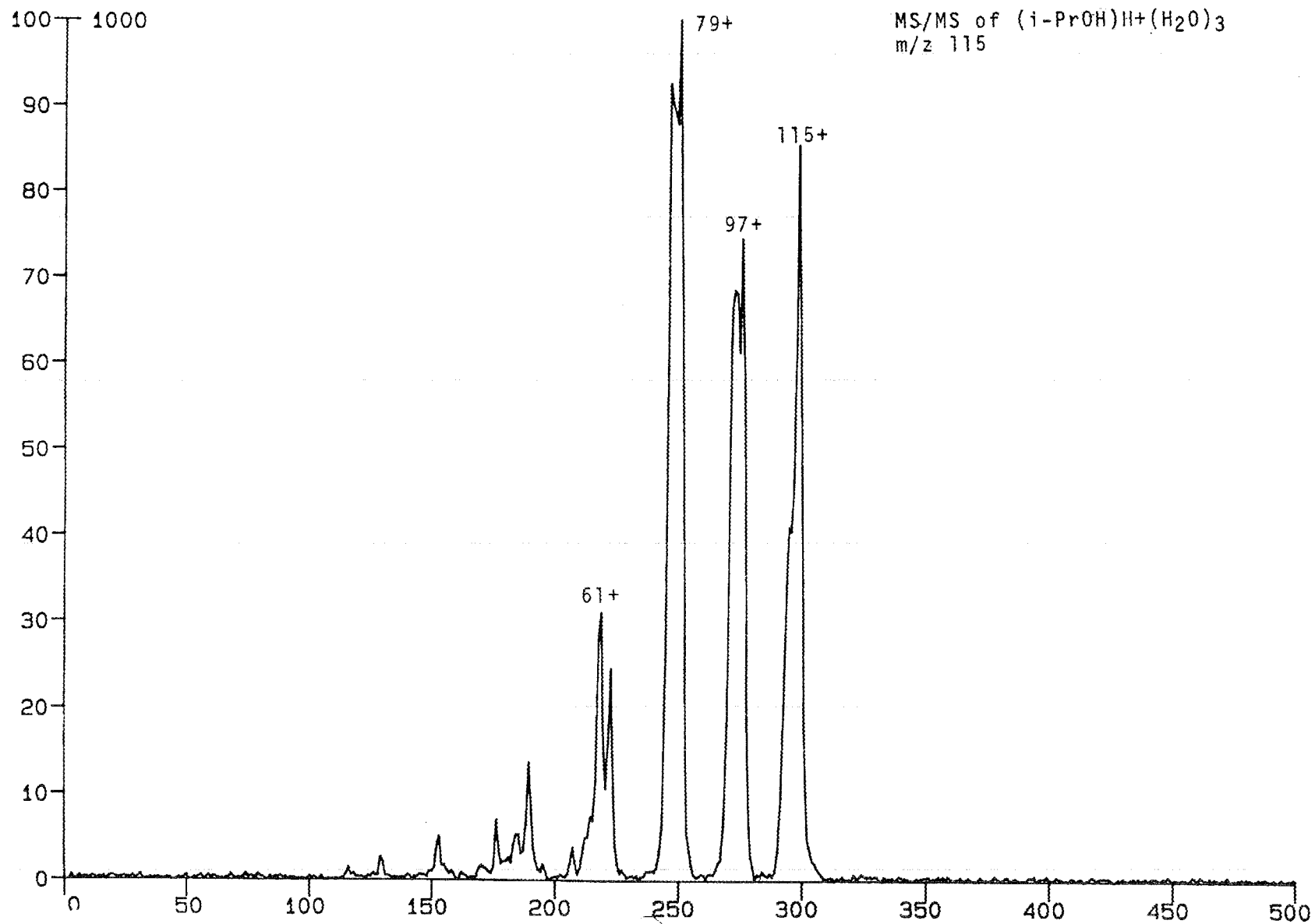
PIPROH05.SAM

isopropanol



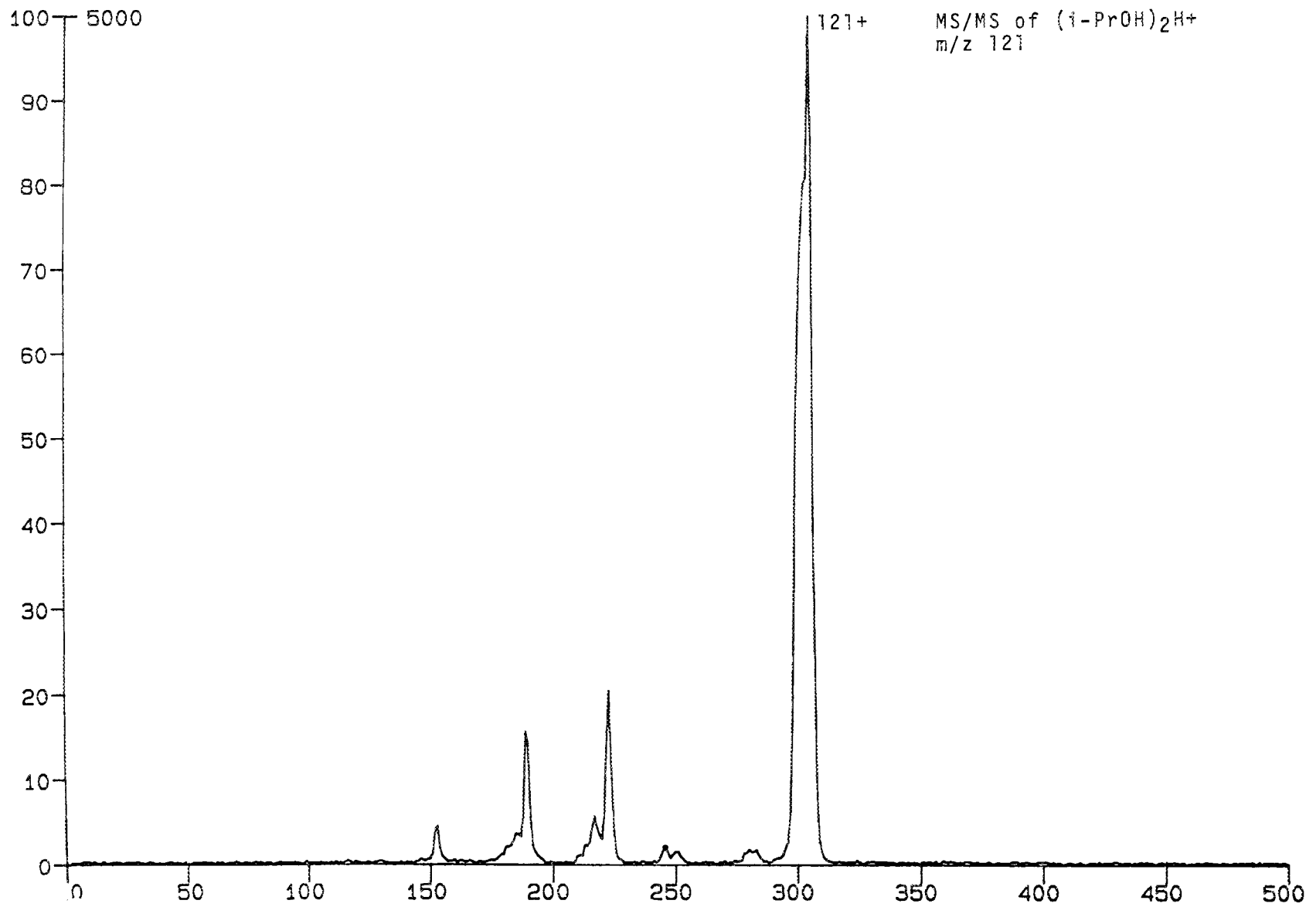
PIPROH06.SAM

isopropanol



PIPROH07.SAM

isopropanol

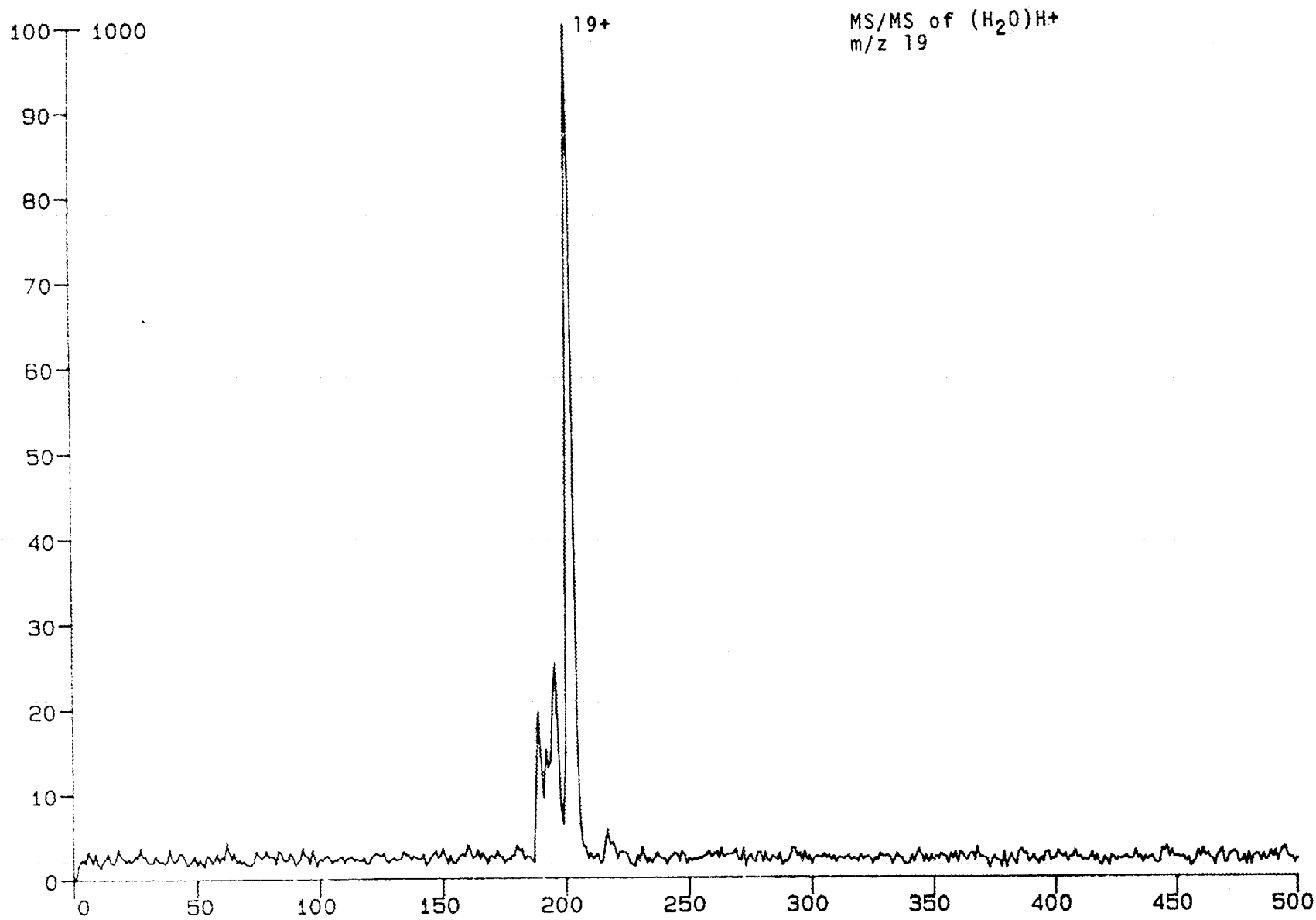


Appendix III

MS/MS spectra of protonated water and water clusters.

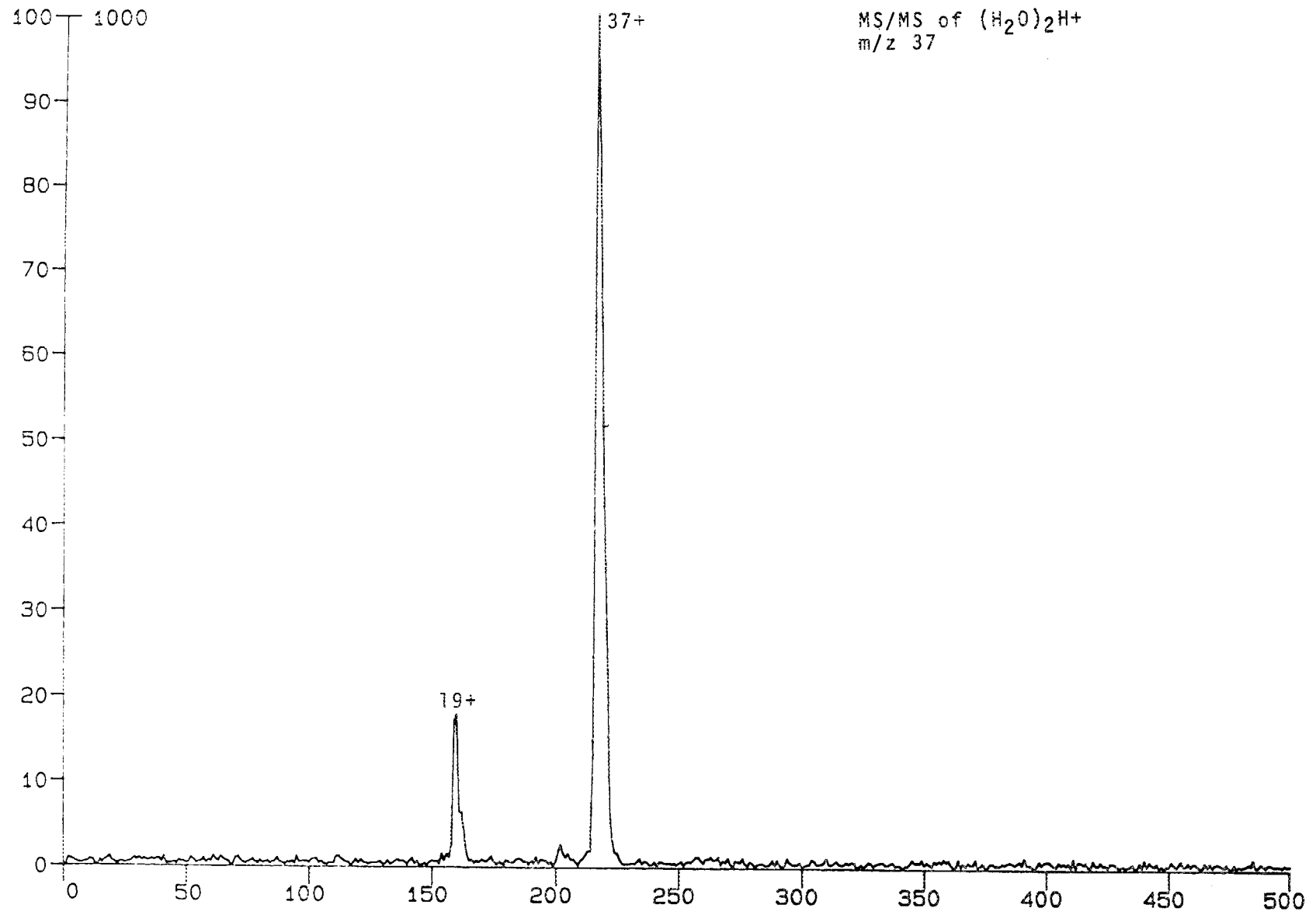
H204HP06.SAM

(H2O) 4H+



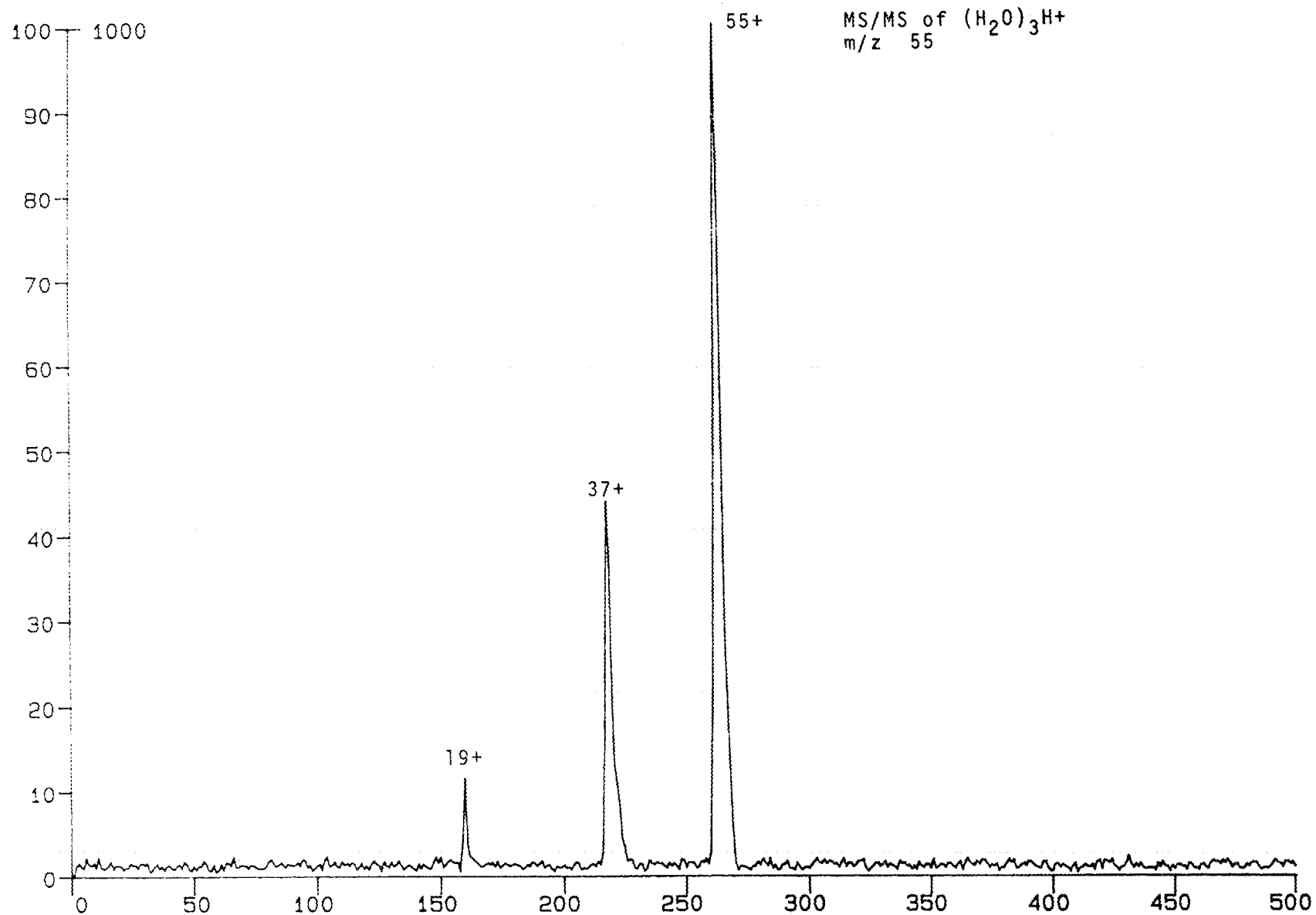
H204HP05.SAM

(H2O) 4H+



H204HP03.SAM

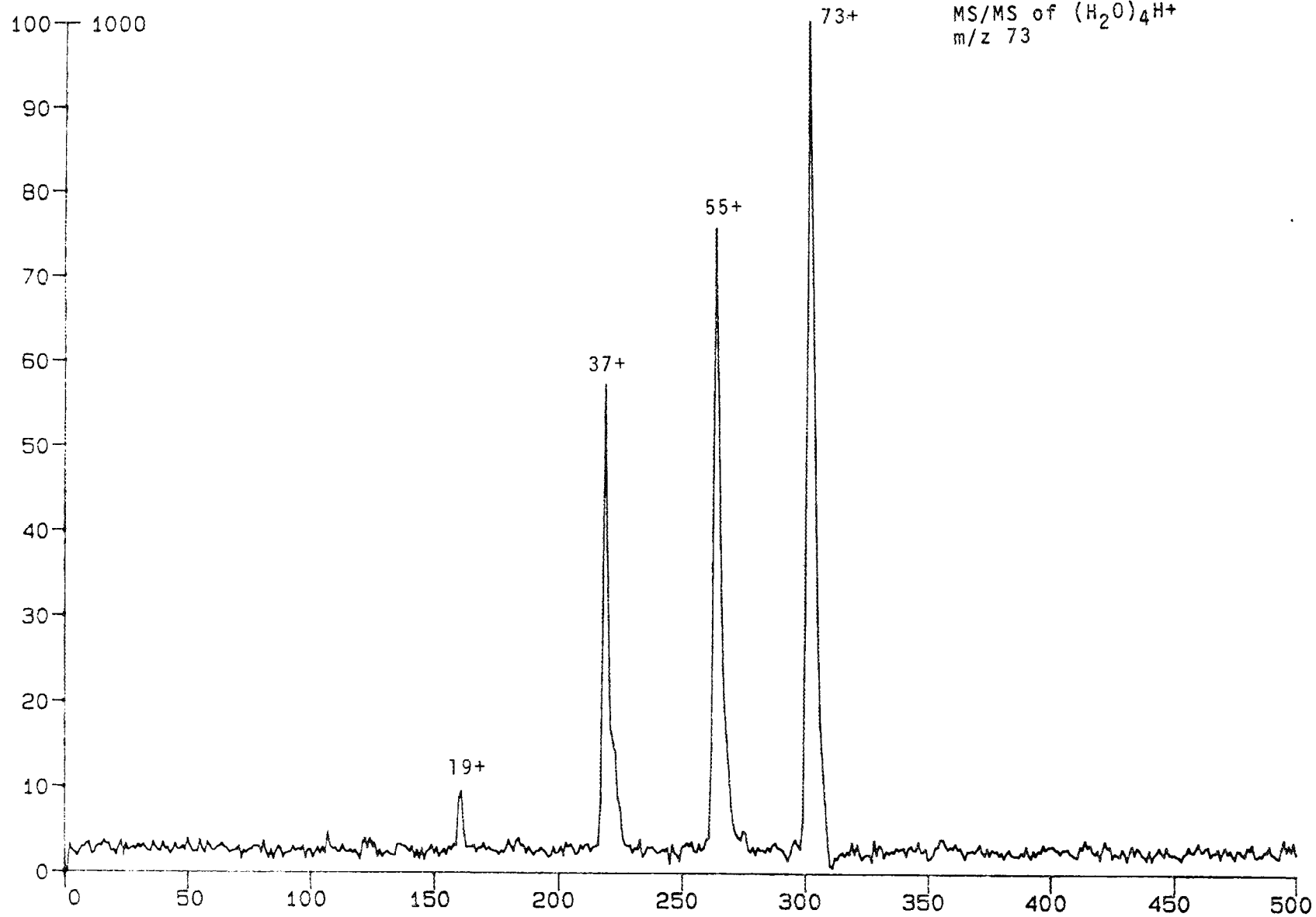
(H2O) 4H+



H2O4HP04.SAM

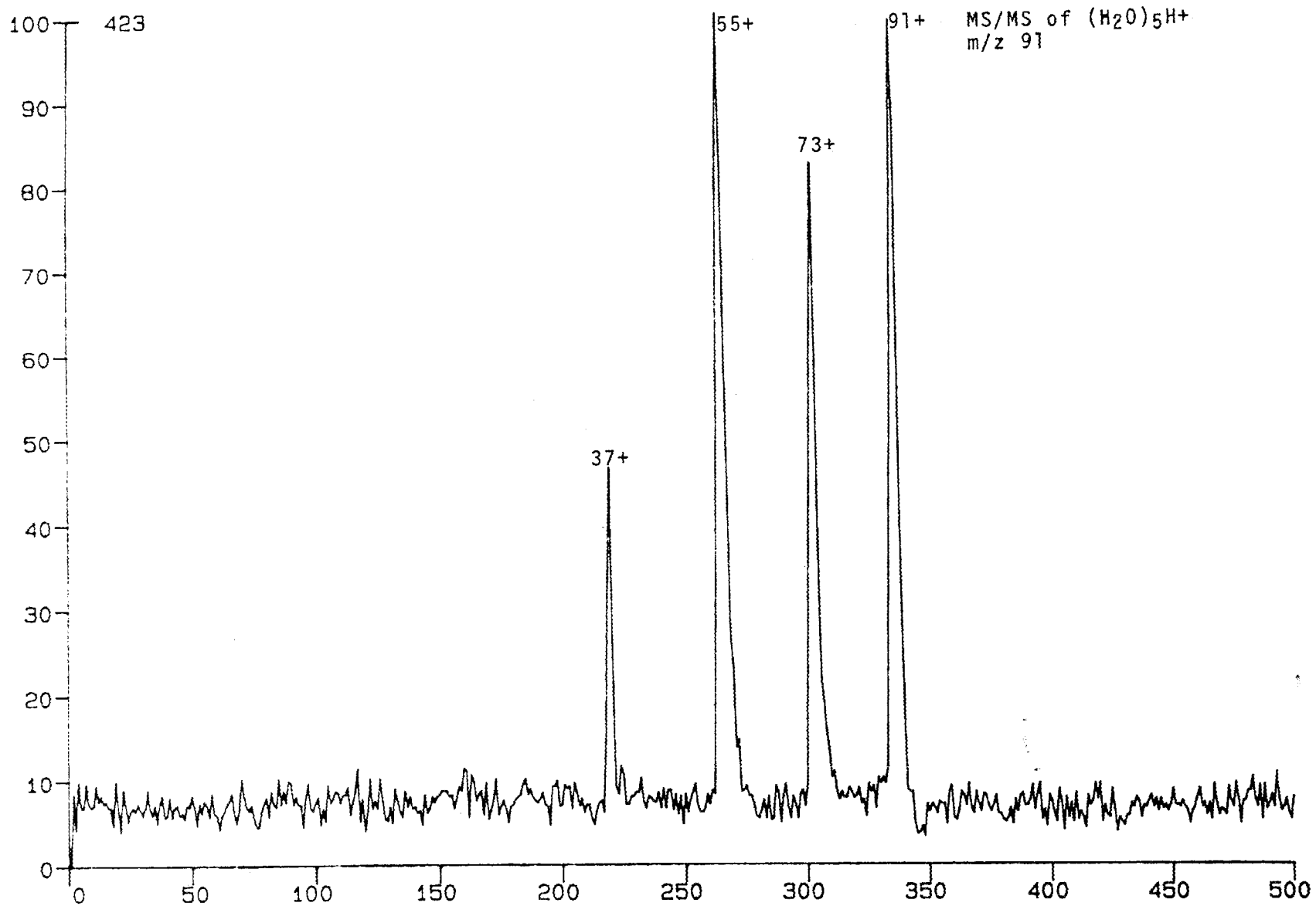
(H2O)4H+

MS/MS of (H₂O)₄H⁺
m/z 73



H204HP02.SAM

(H2O) 4H+

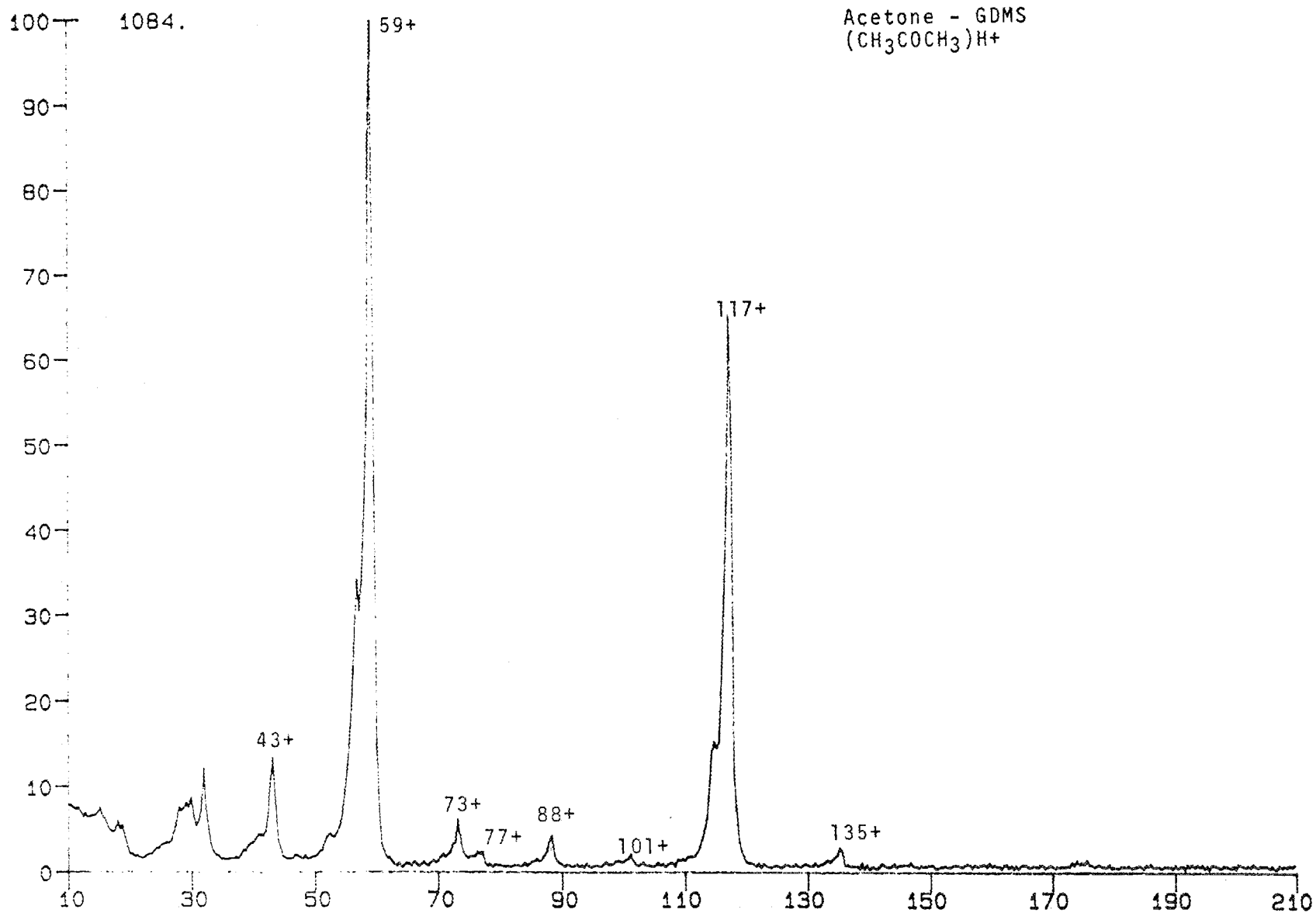


Appendix IV

MS/MS spectra of ions derived from acetone.

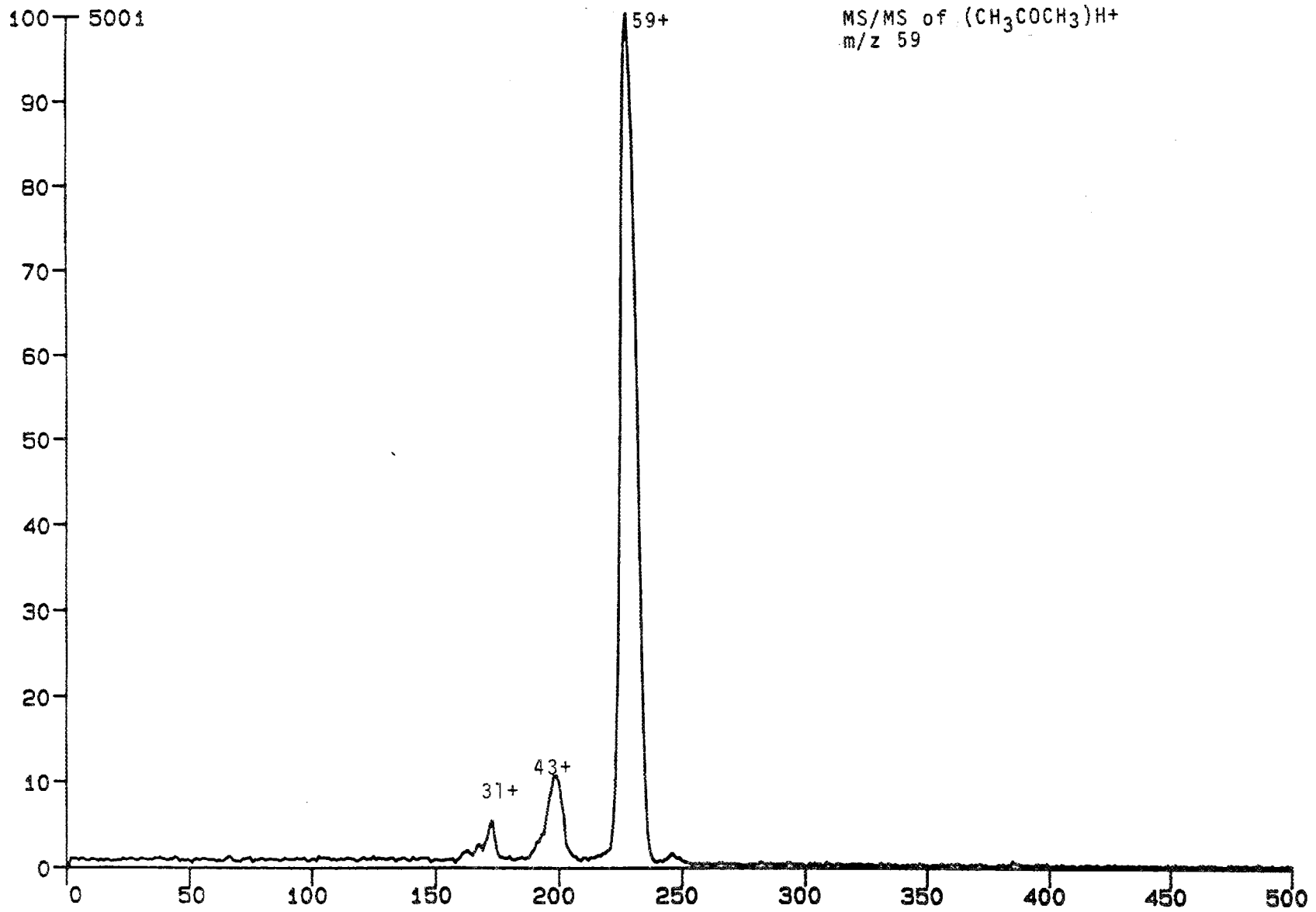
PACE01.QMS

ACETONE



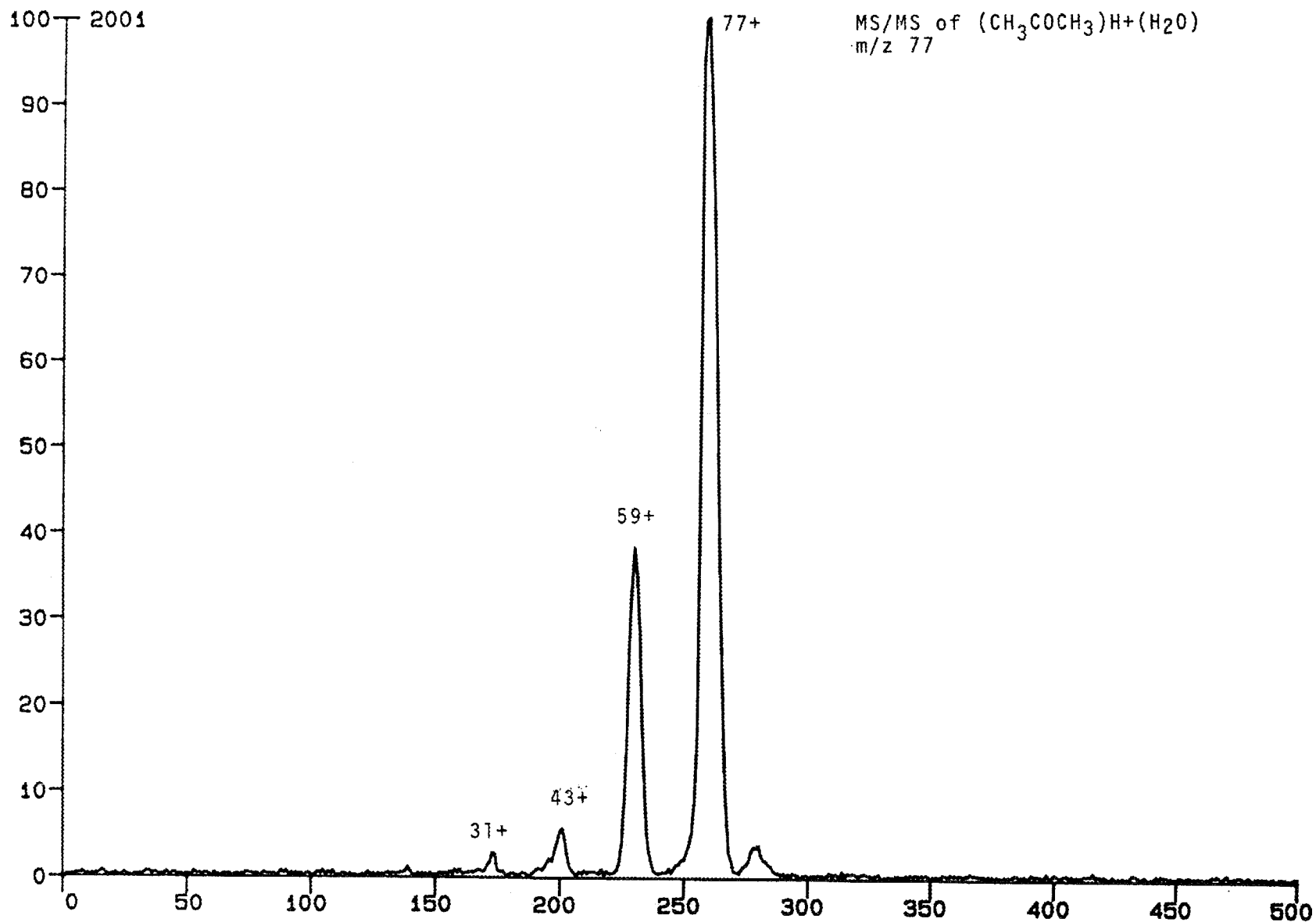
PACE05.KGA

ACETONE



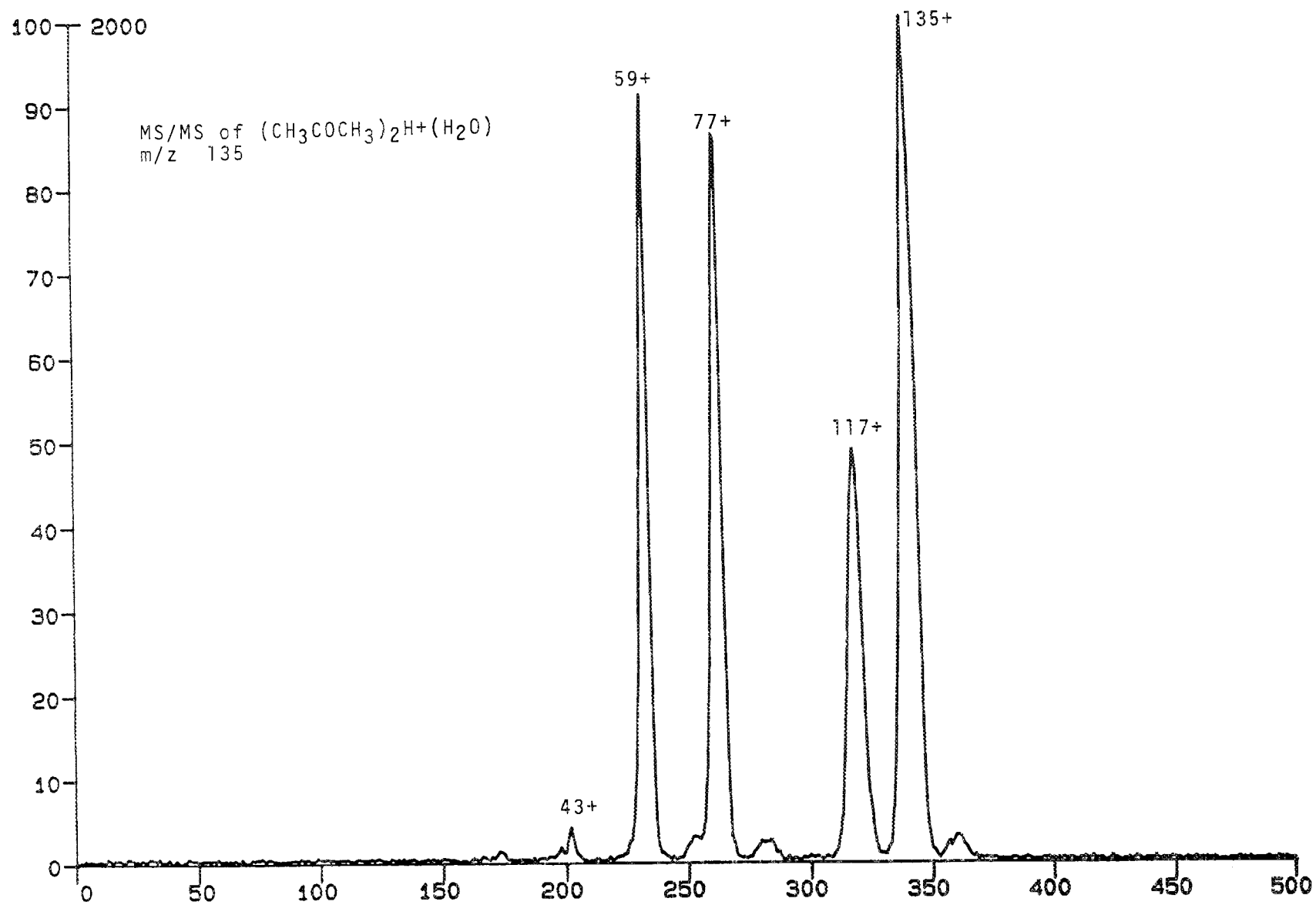
PACE01.KGA

ACETONE



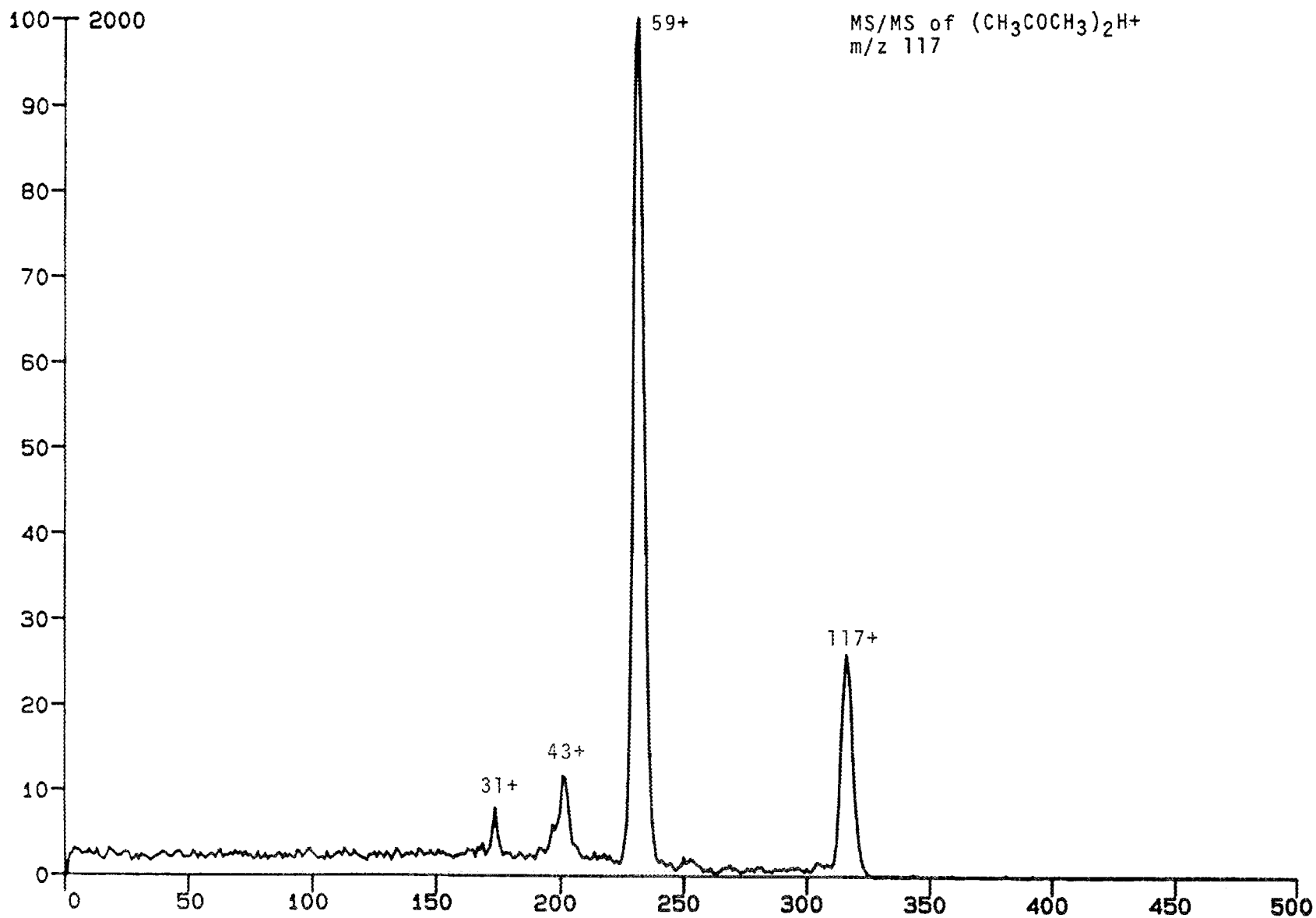
PACE02.KGA

ACETONE



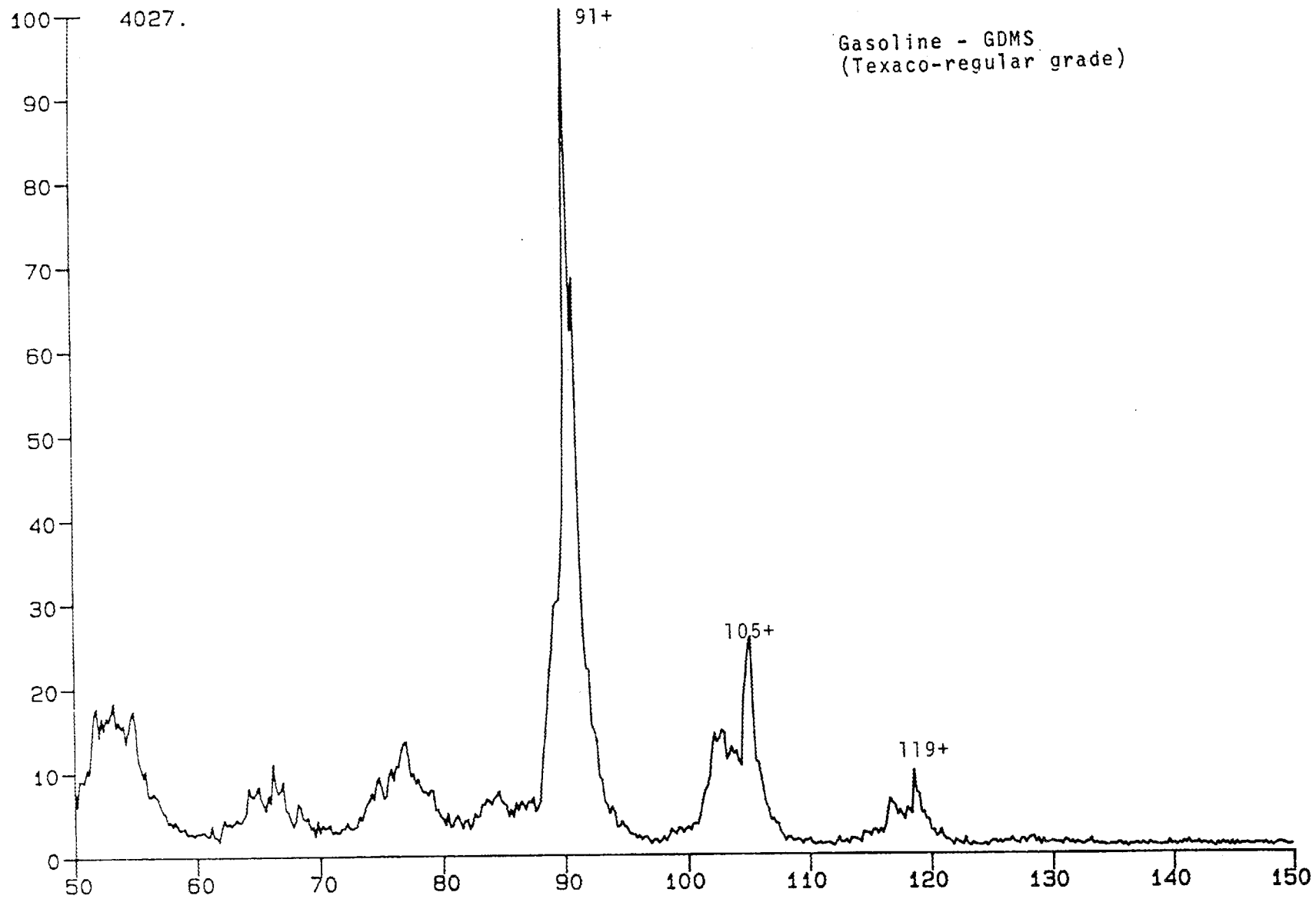
PACE03.KGA

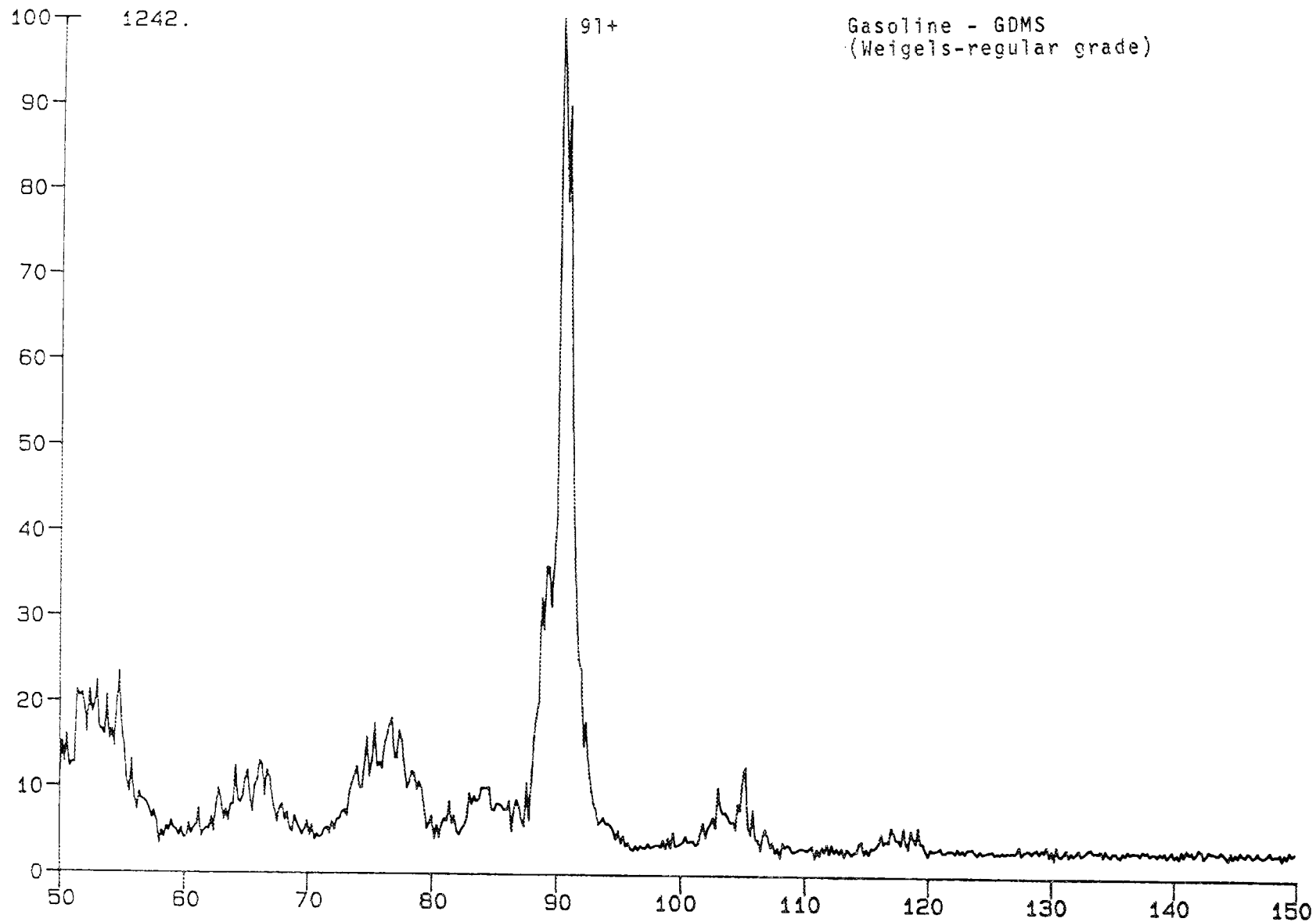
ACETONE

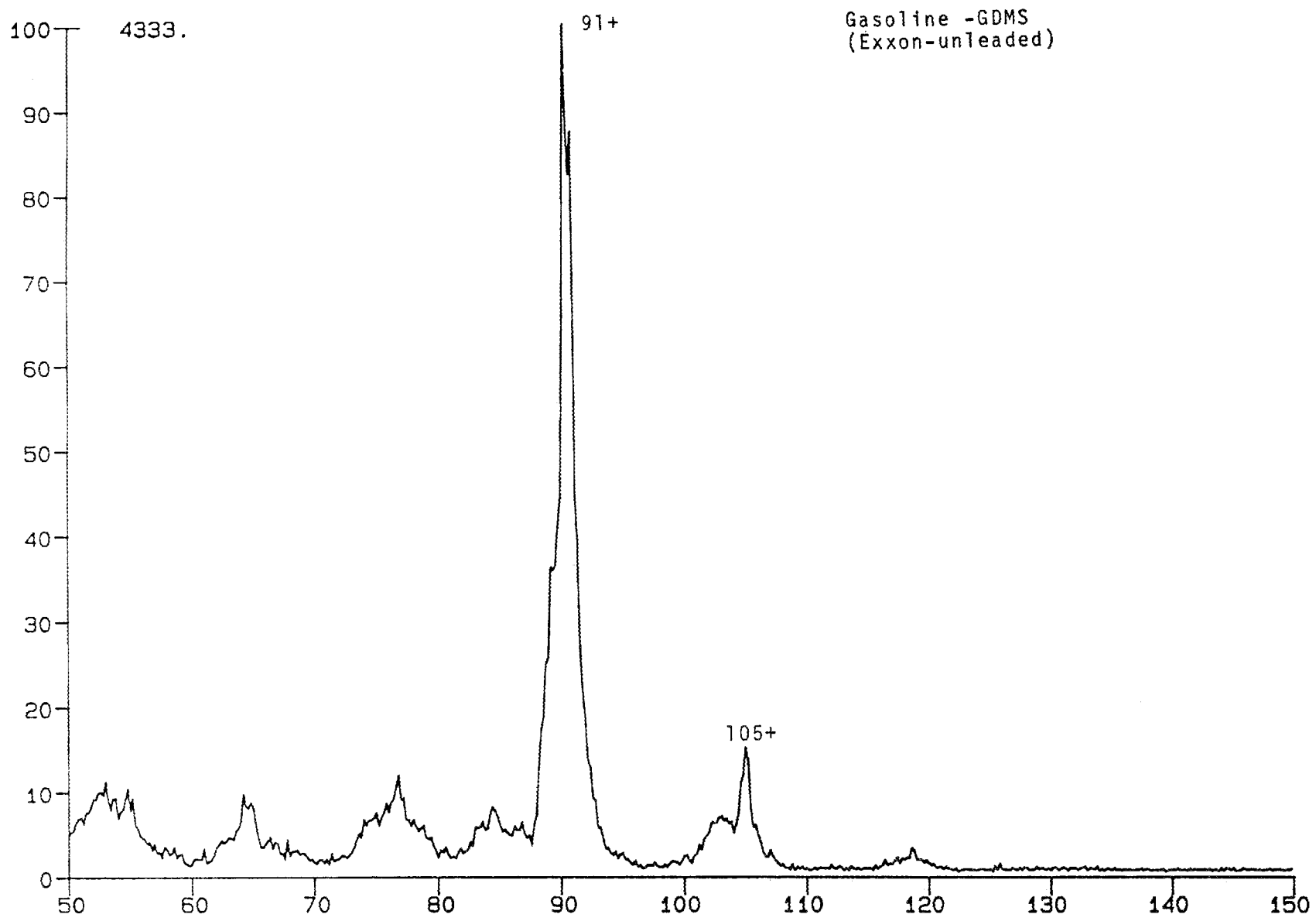


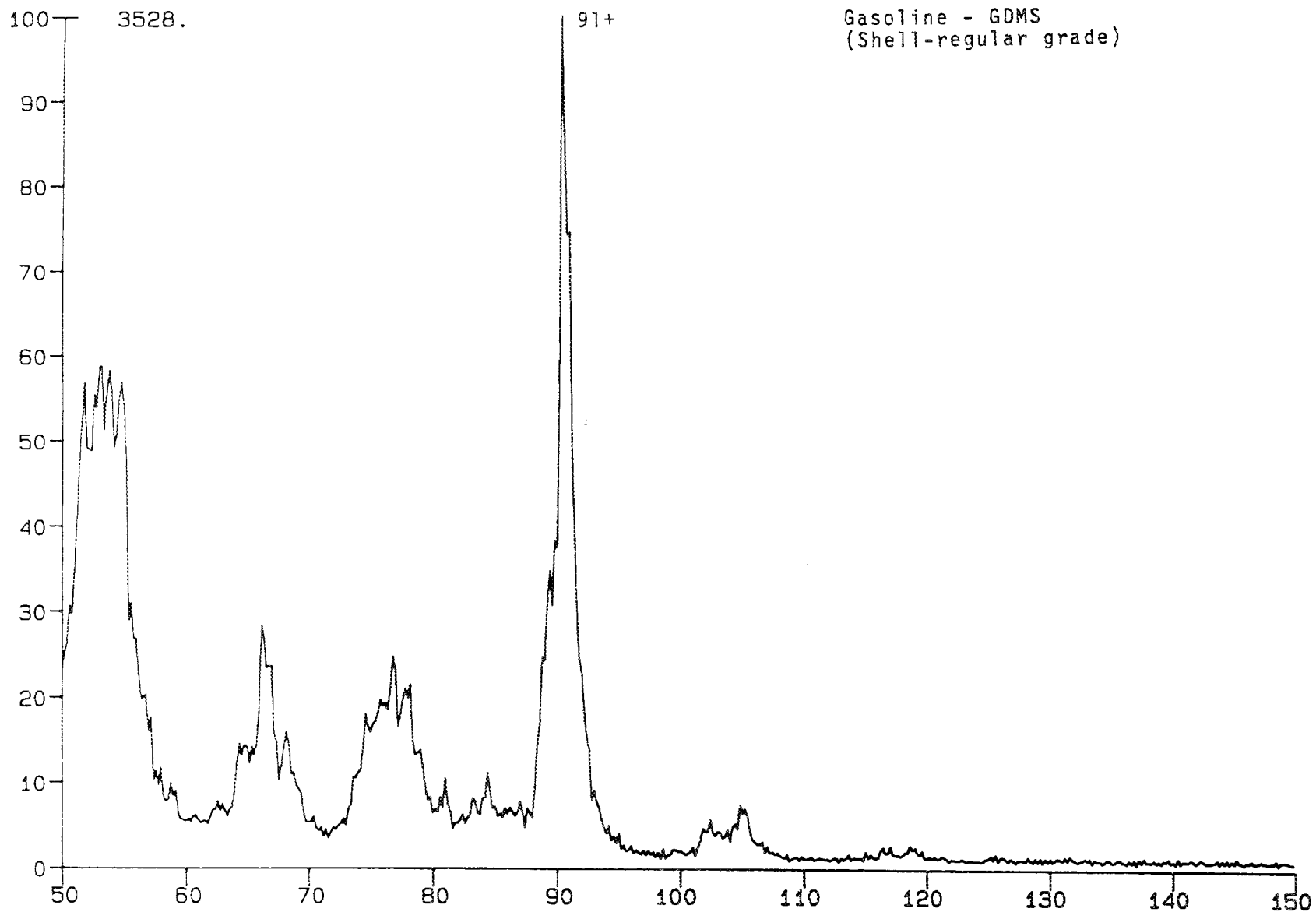
Appendix V

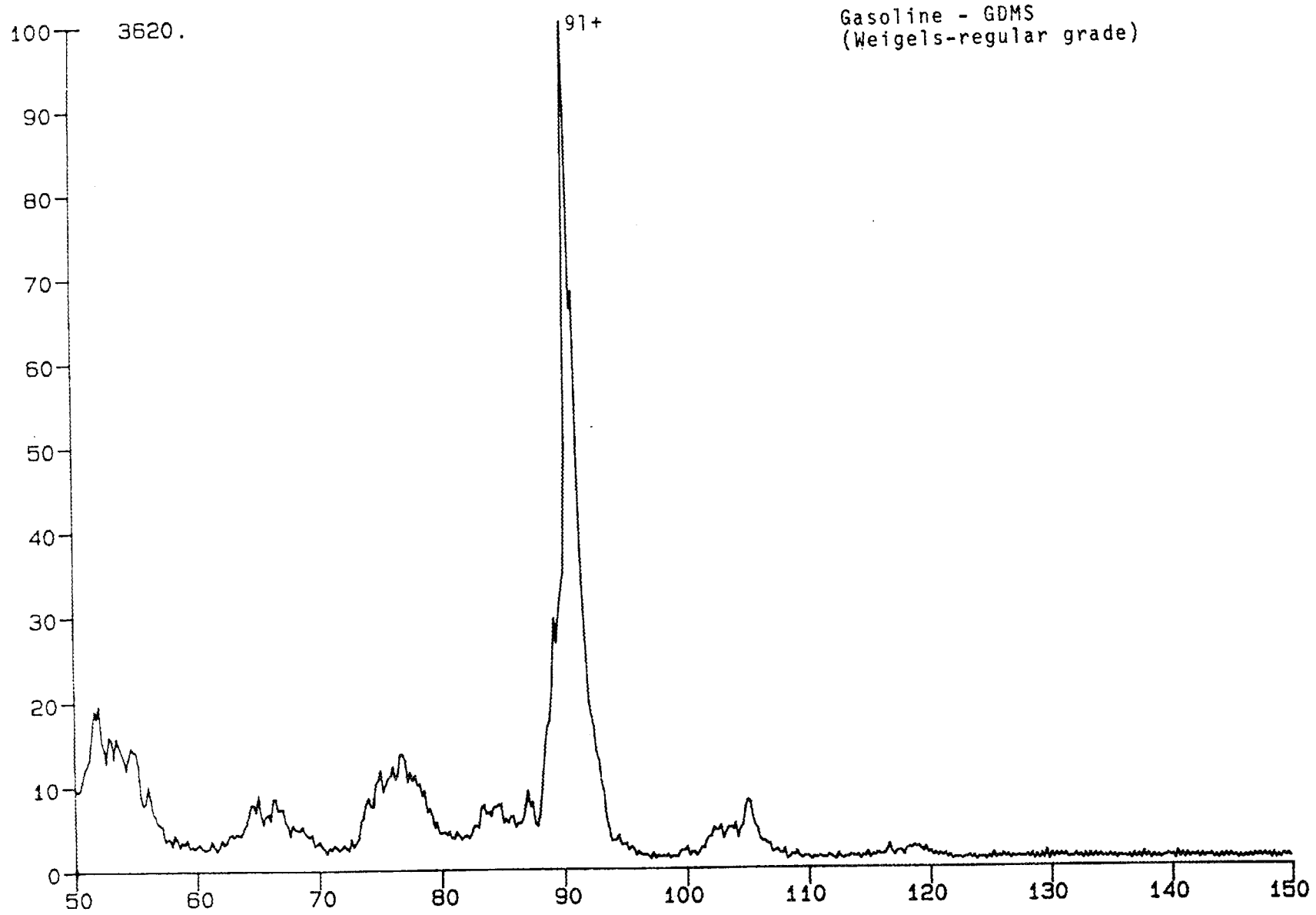
Glow discharge MS and MS/MS data for gasolines,
kerosene, and jet fuel.

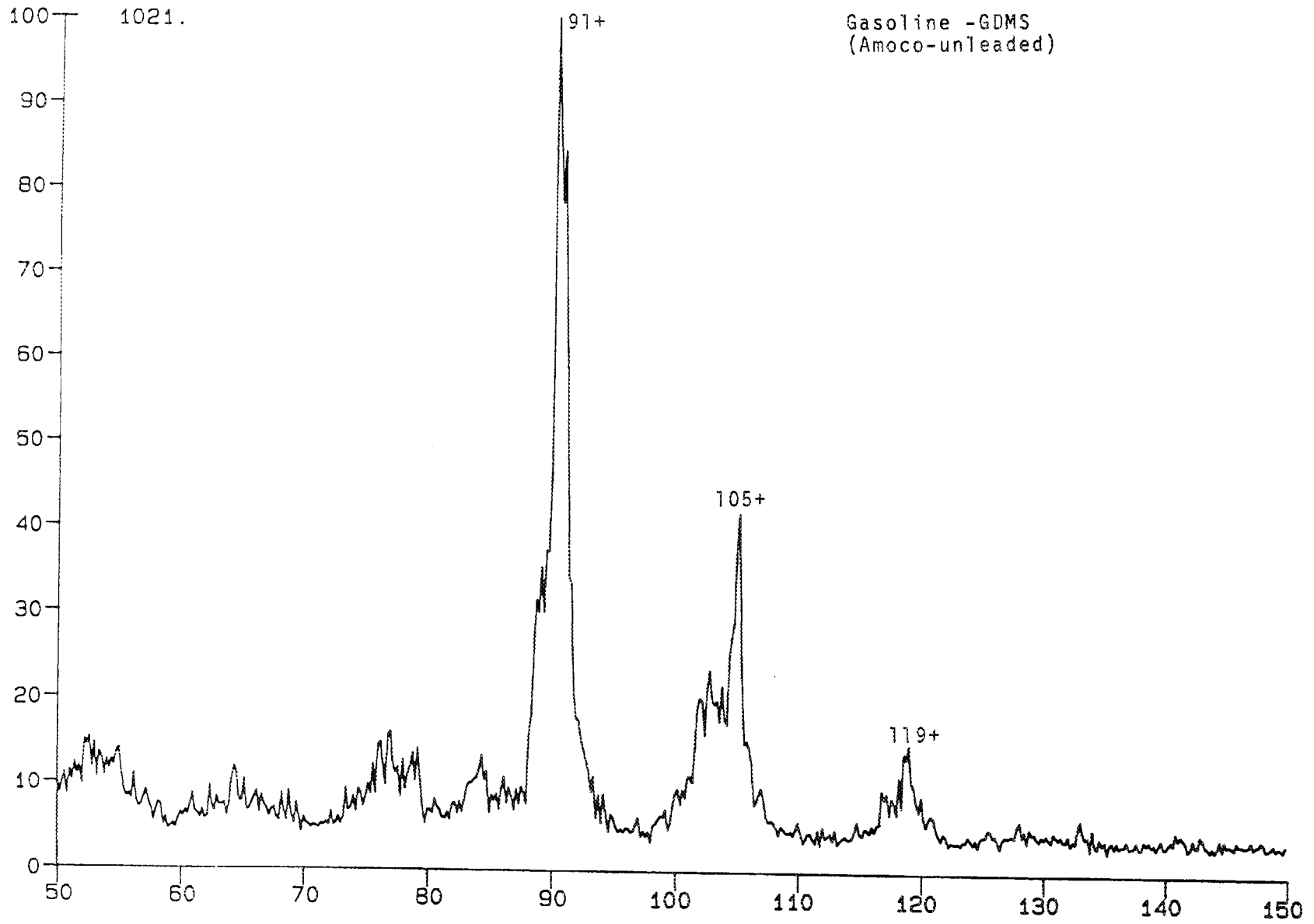


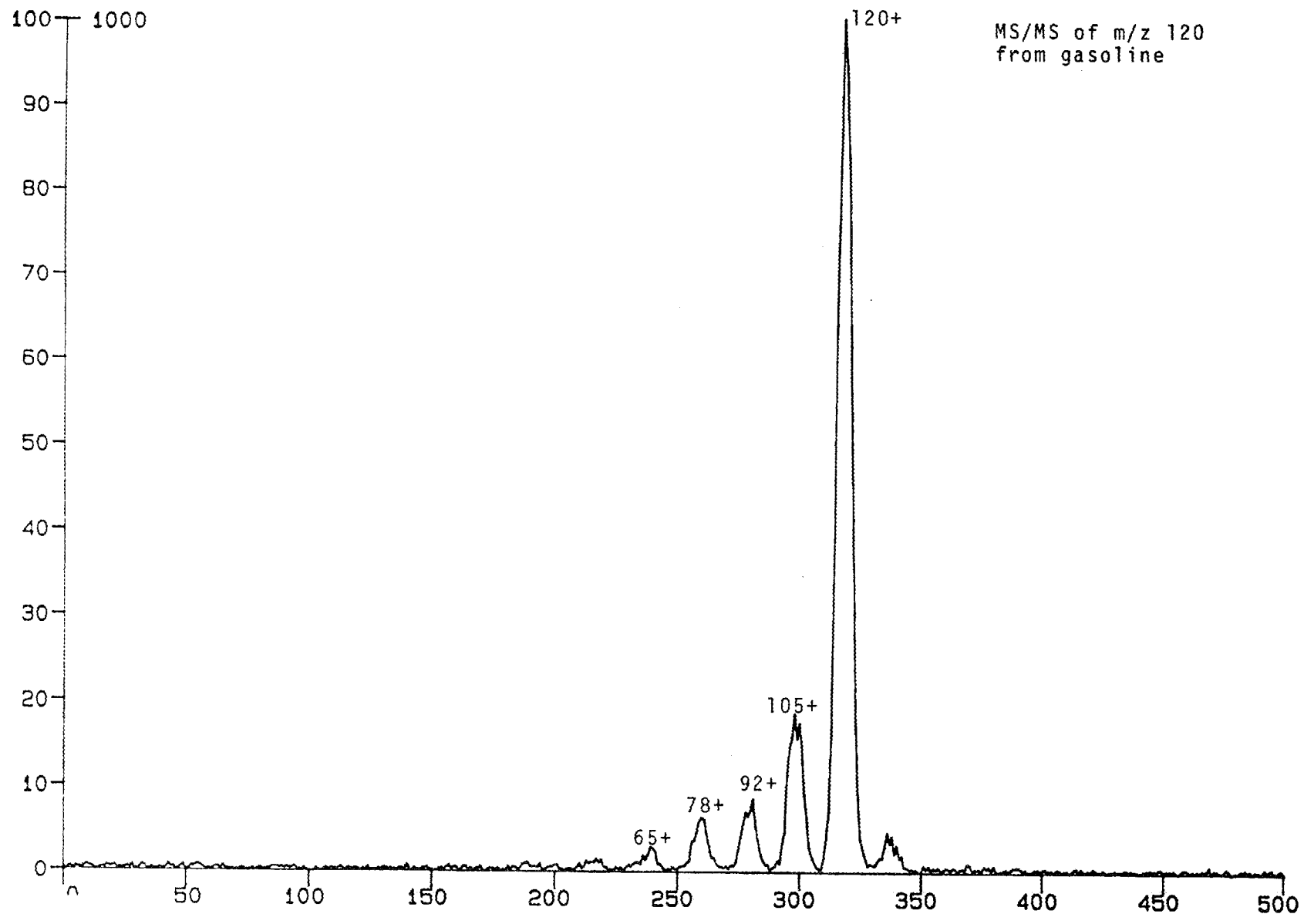


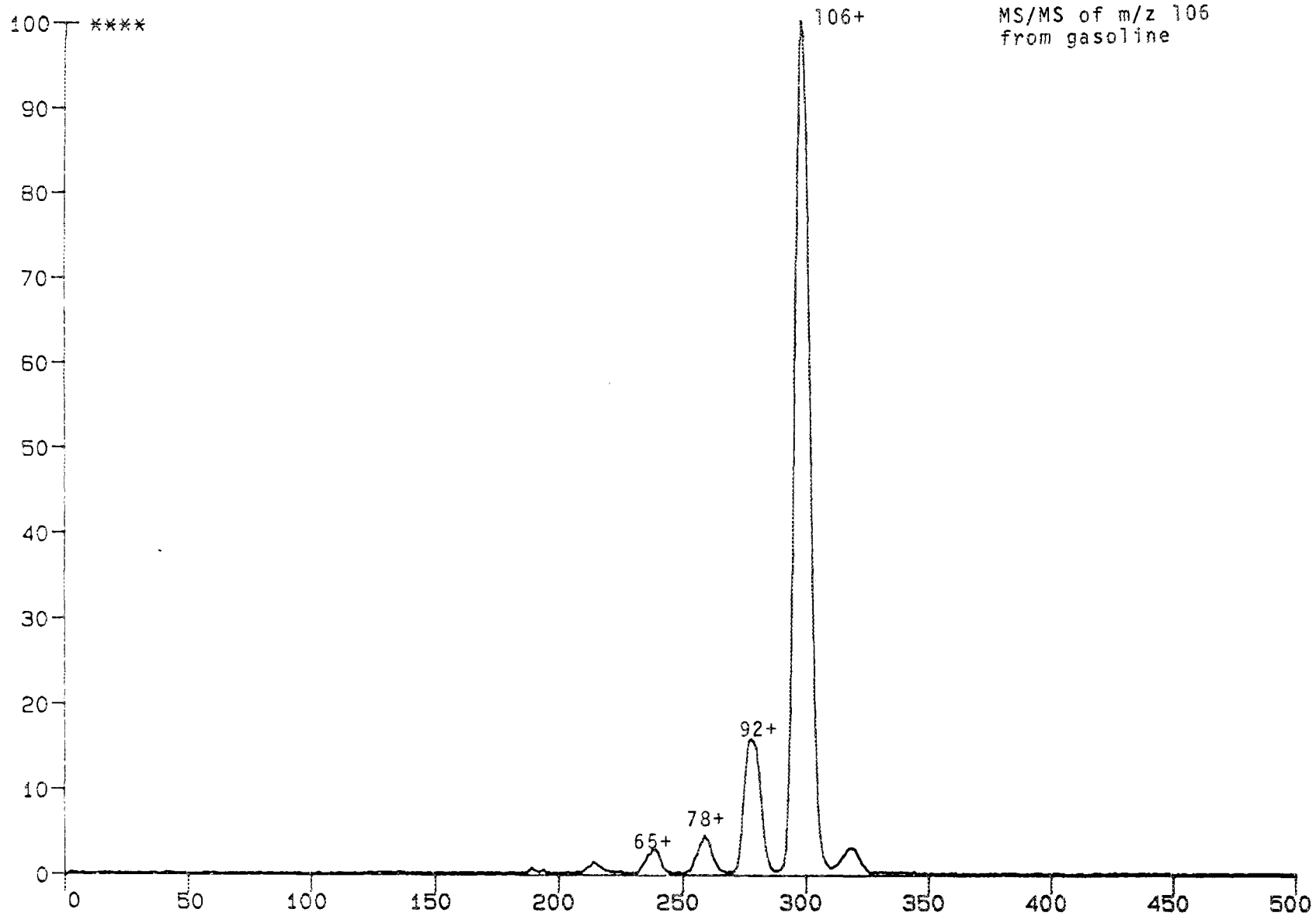


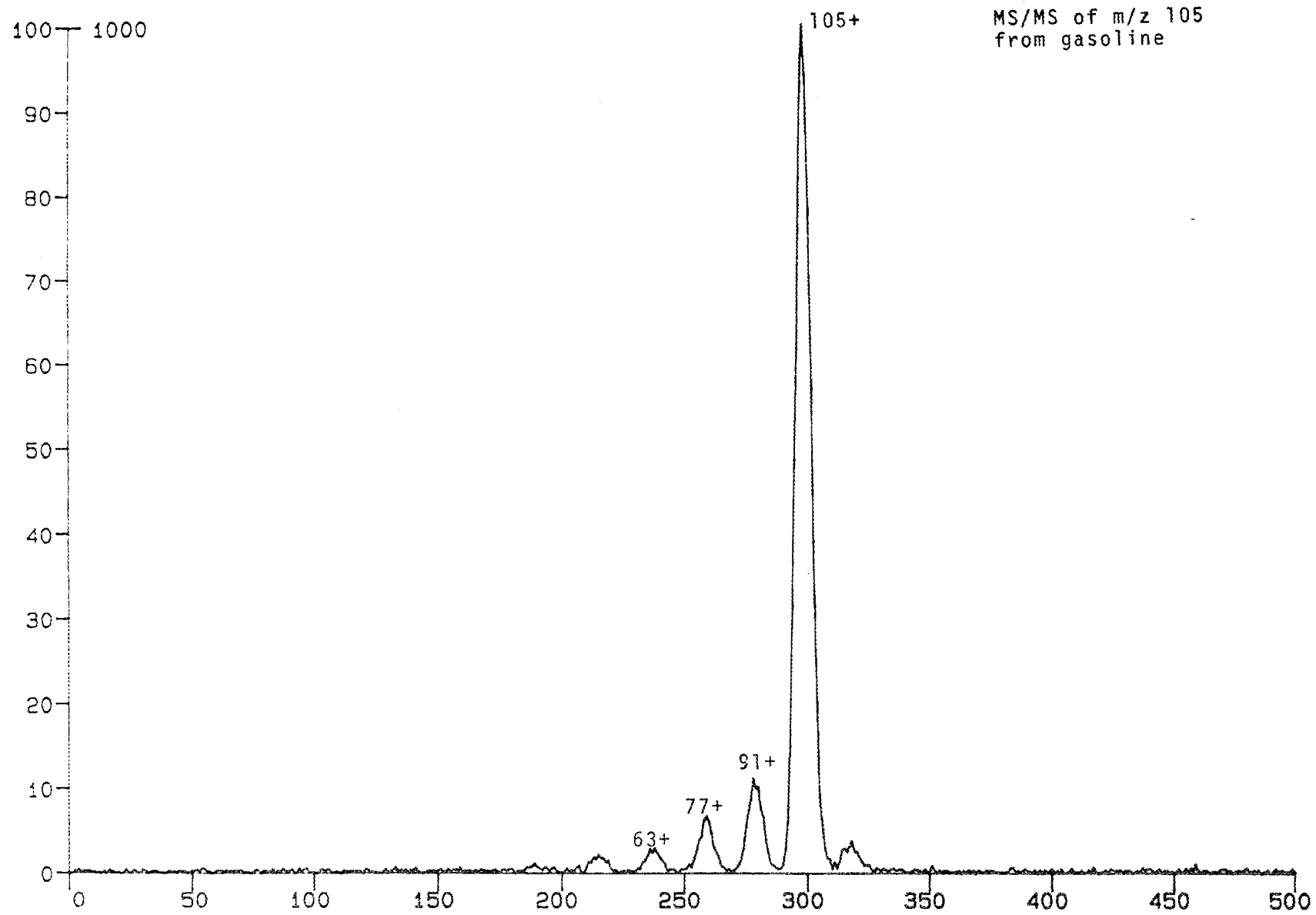


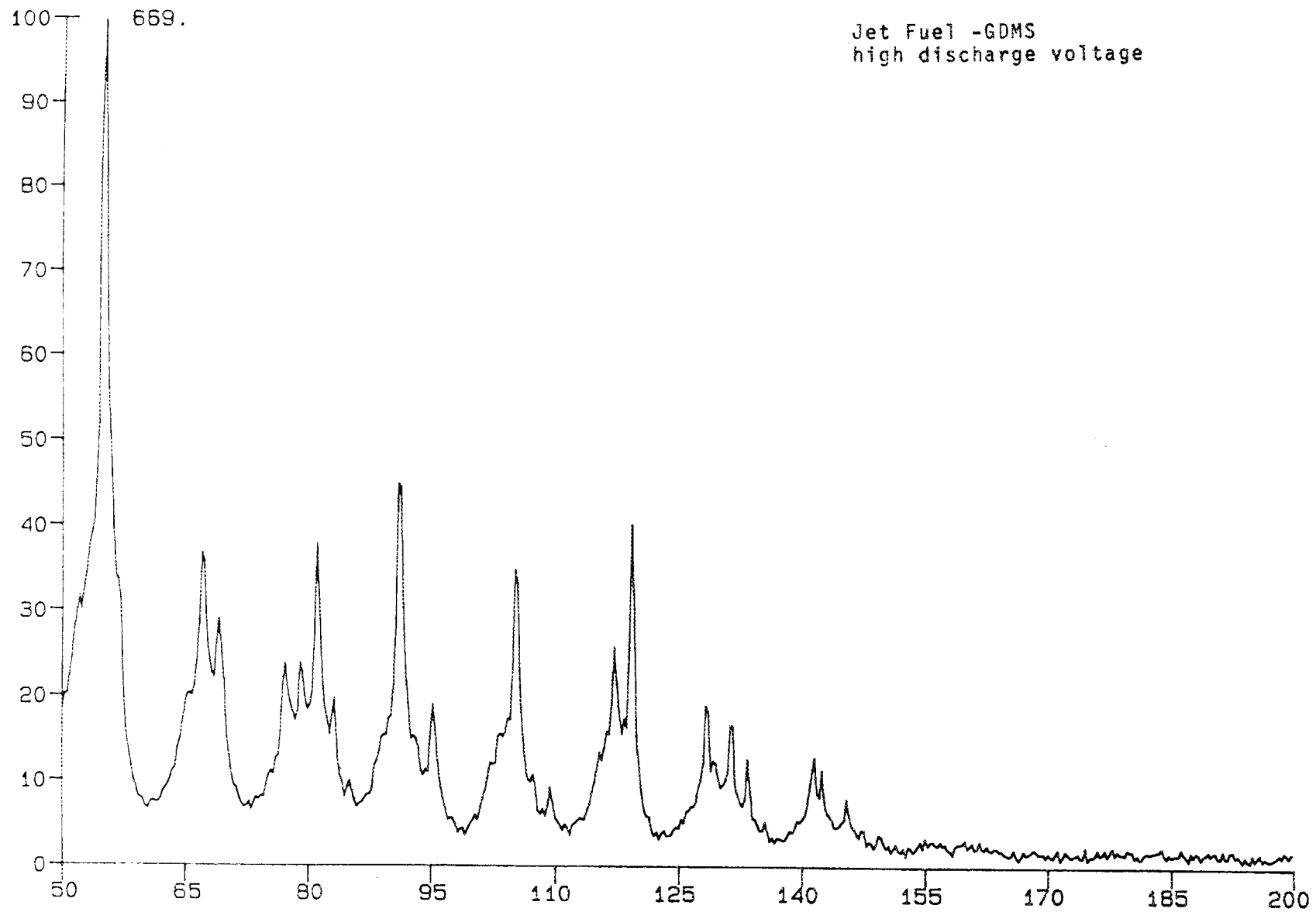






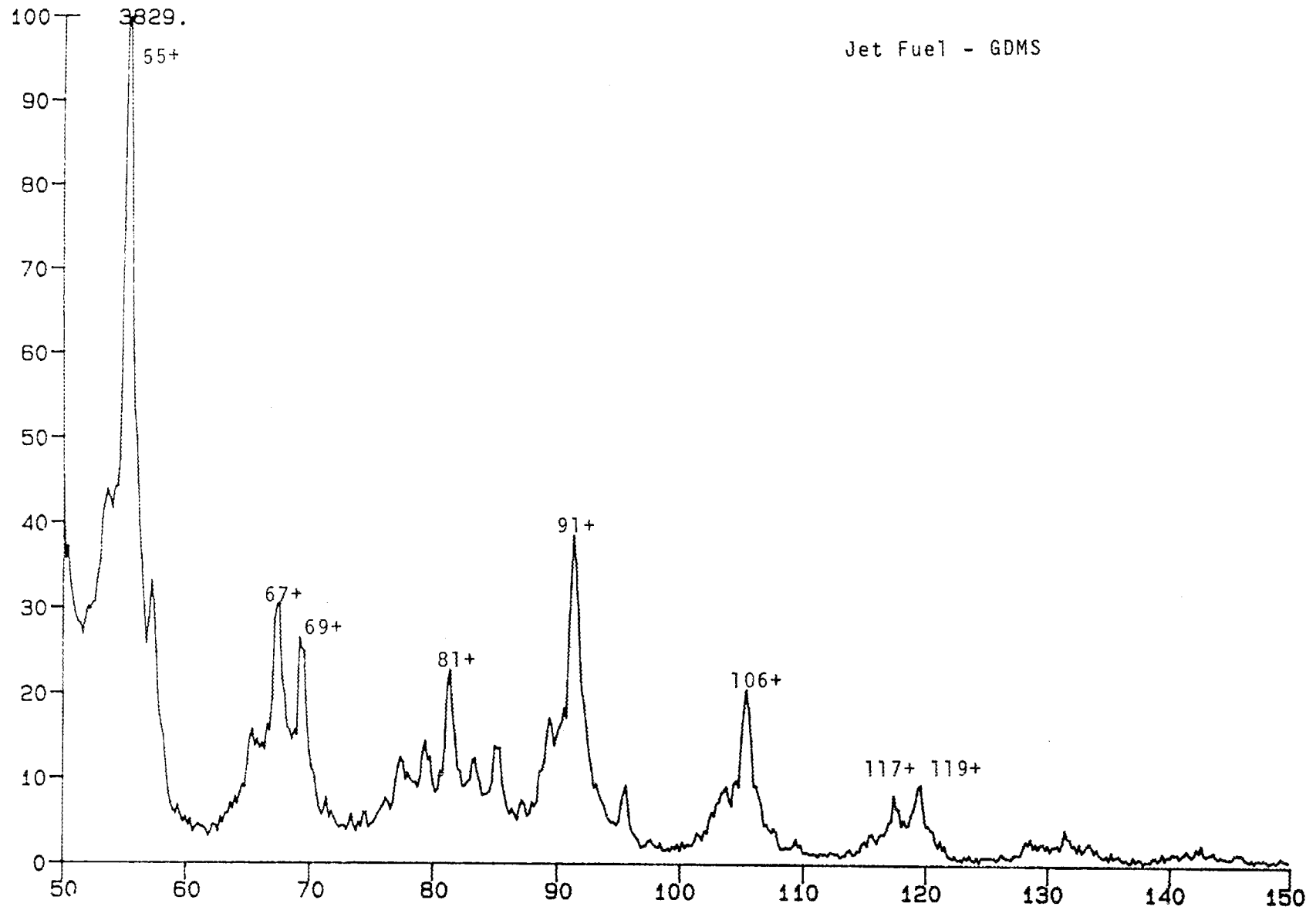


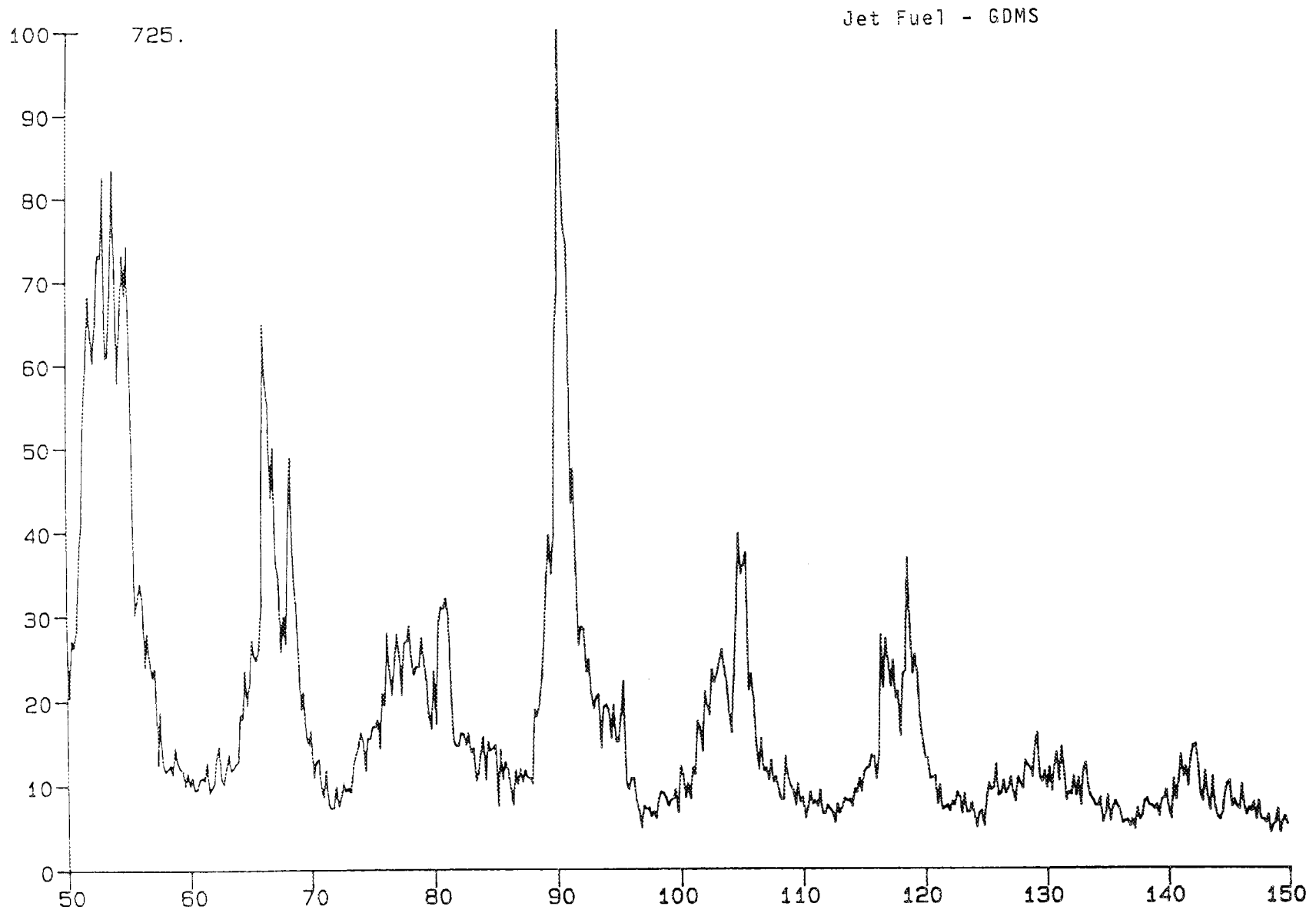




PJET01.QMS

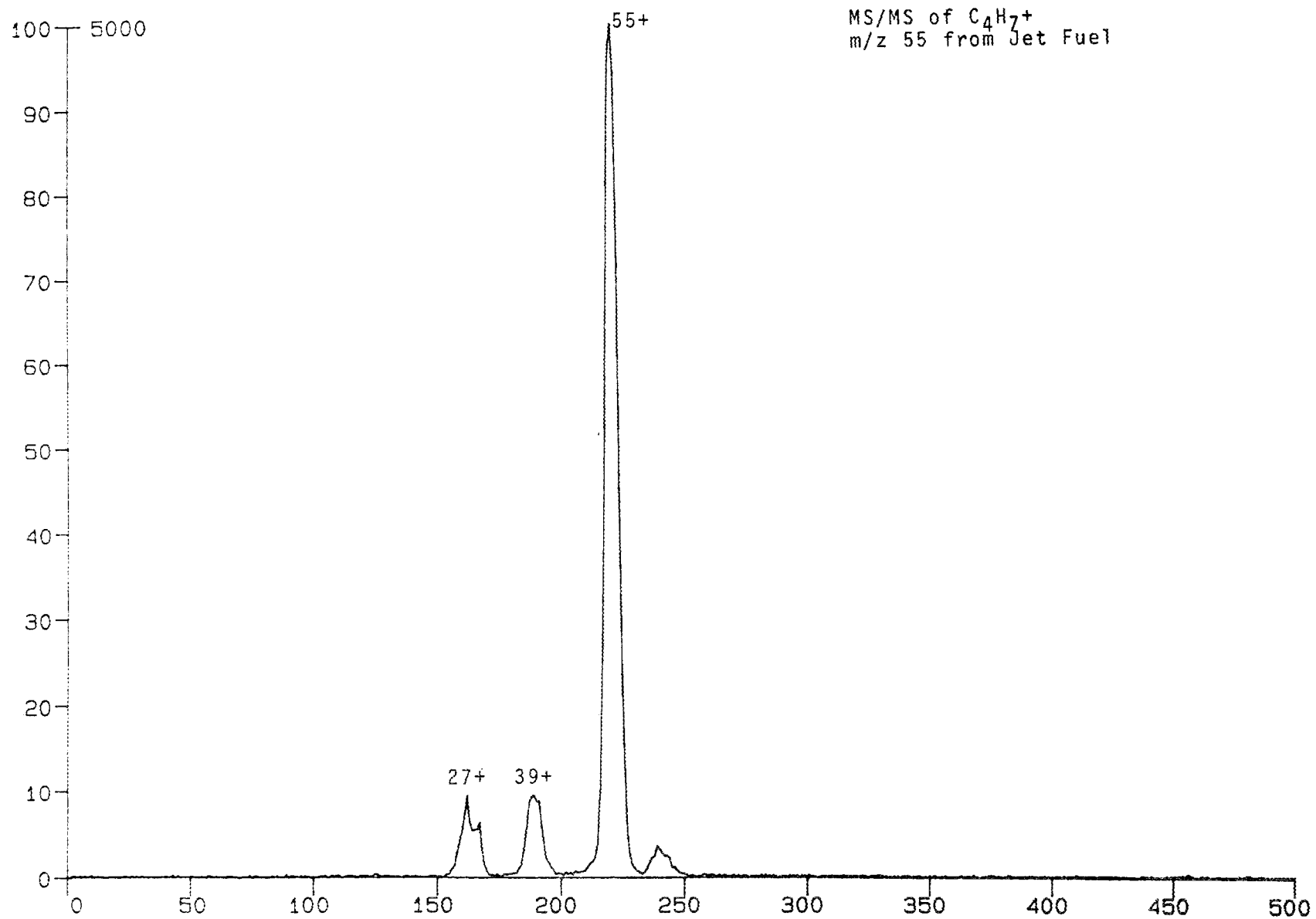
JETFUEL



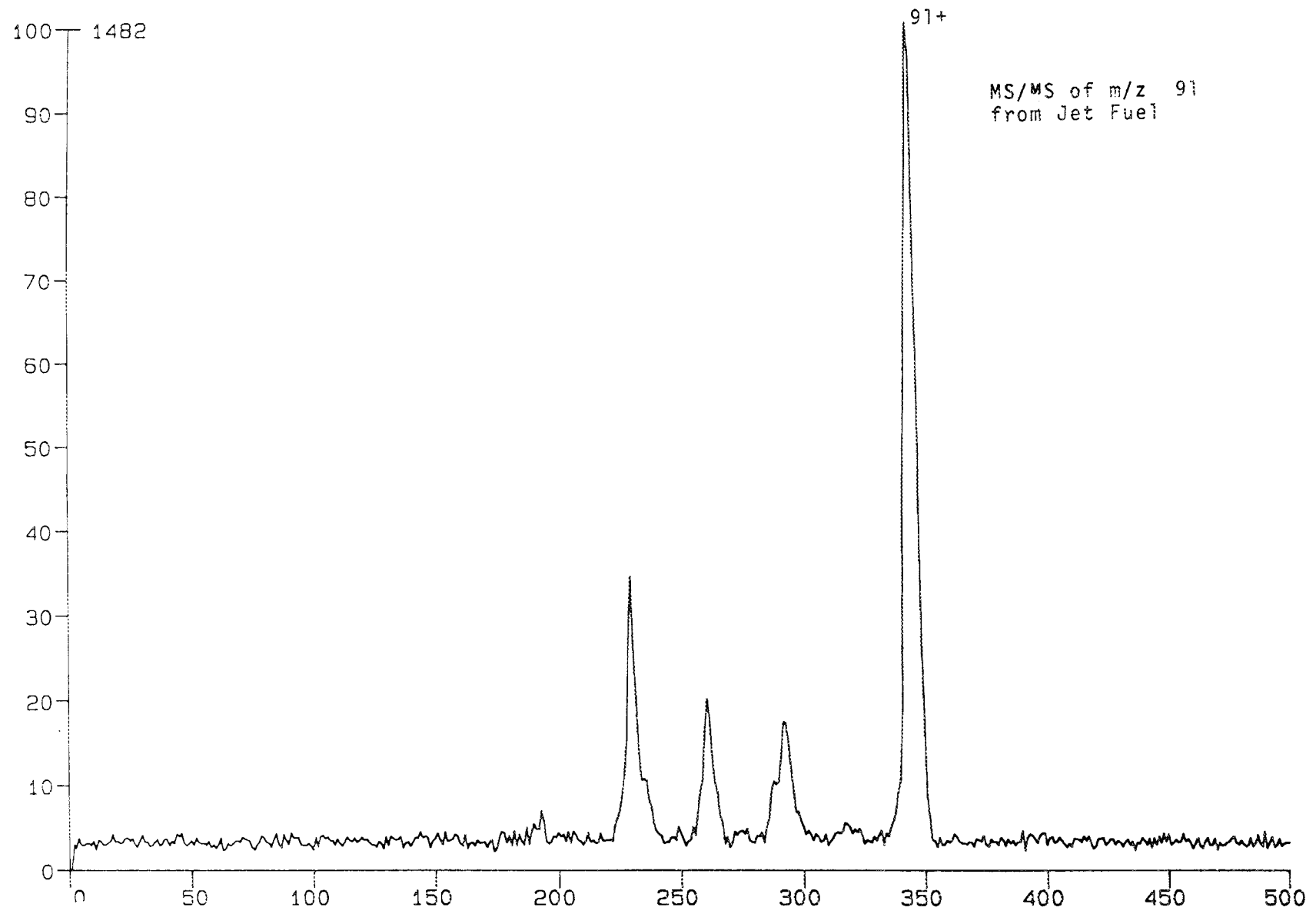


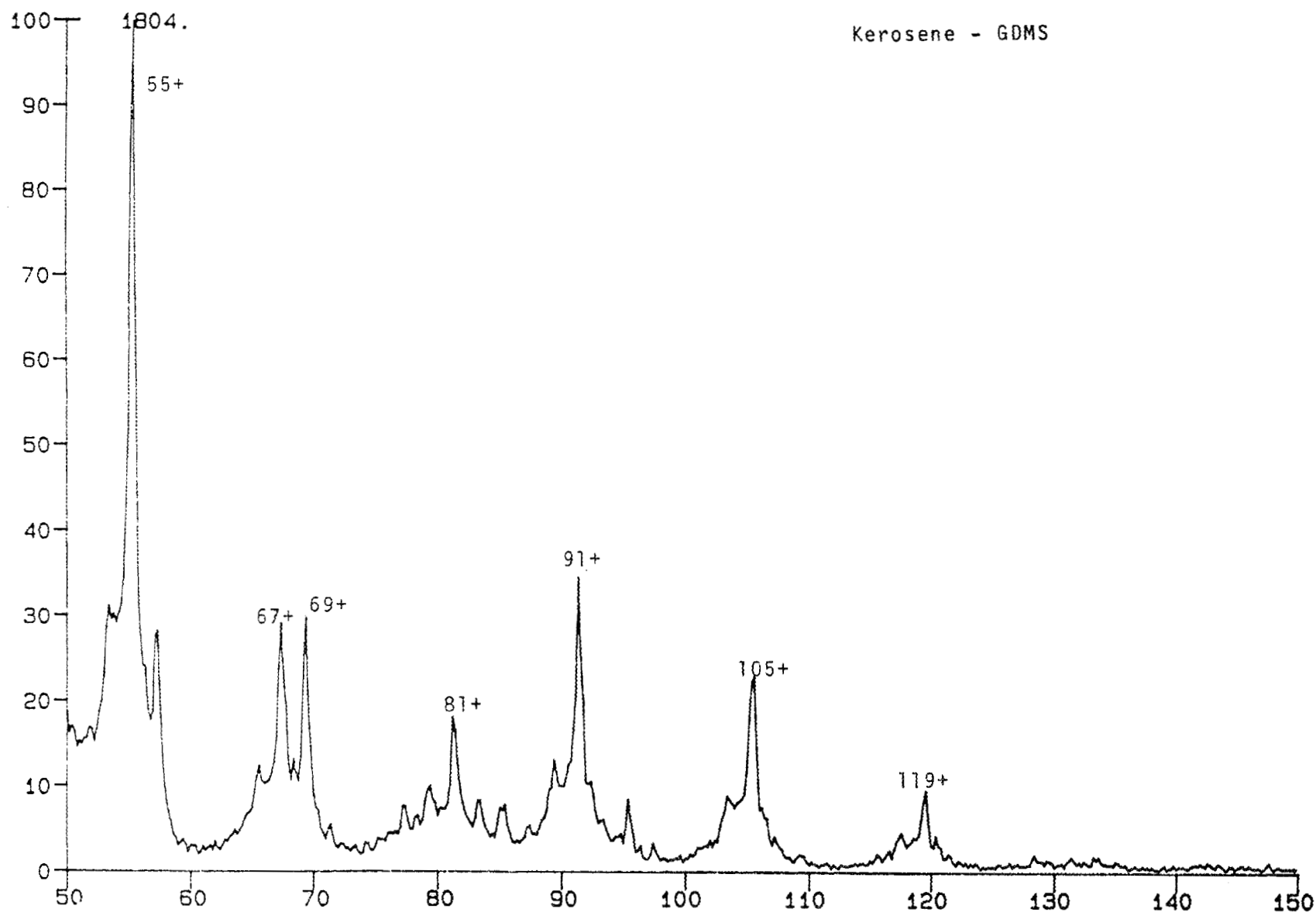
JET01.KGA

JETFUEL



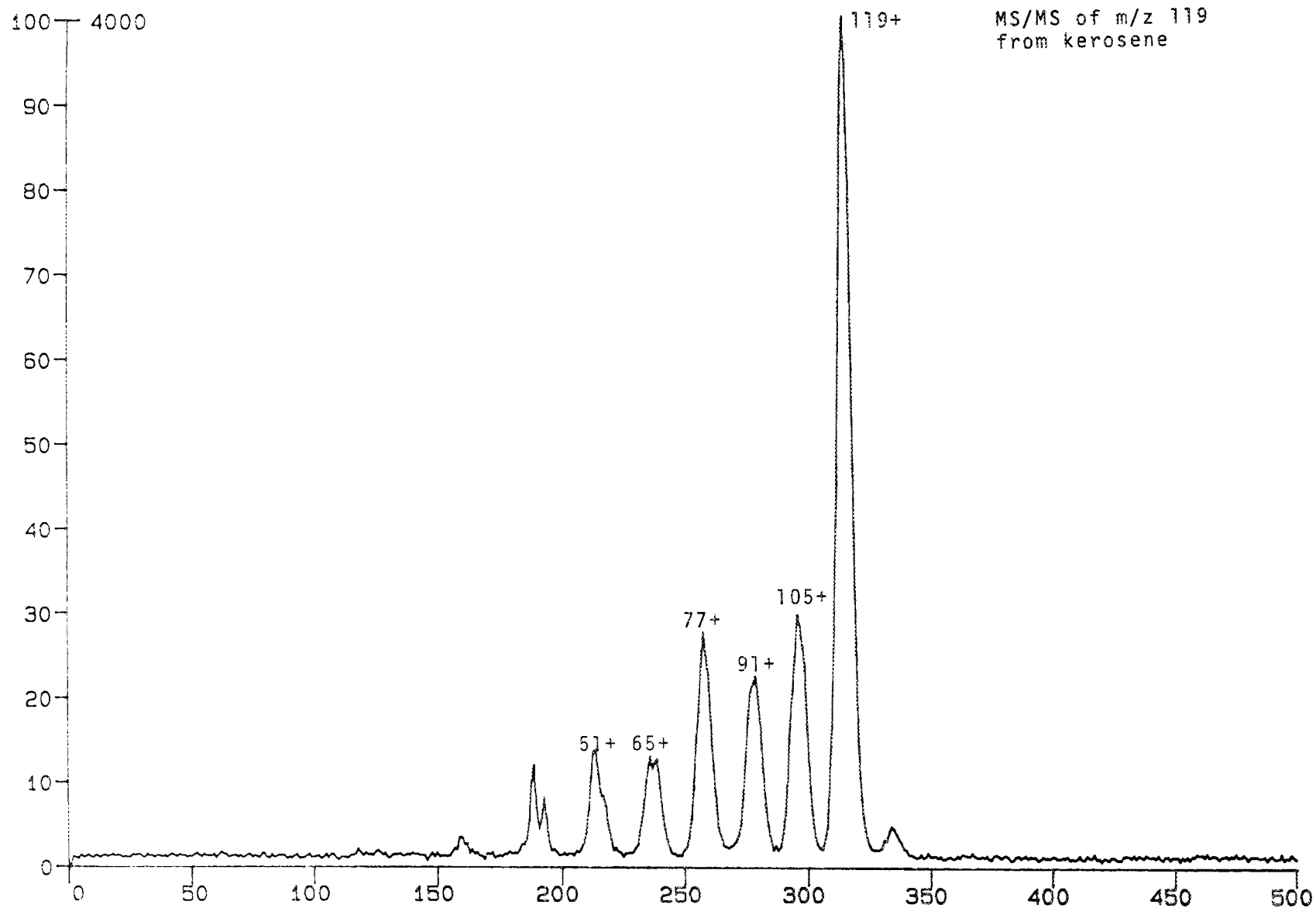
JET FUEL





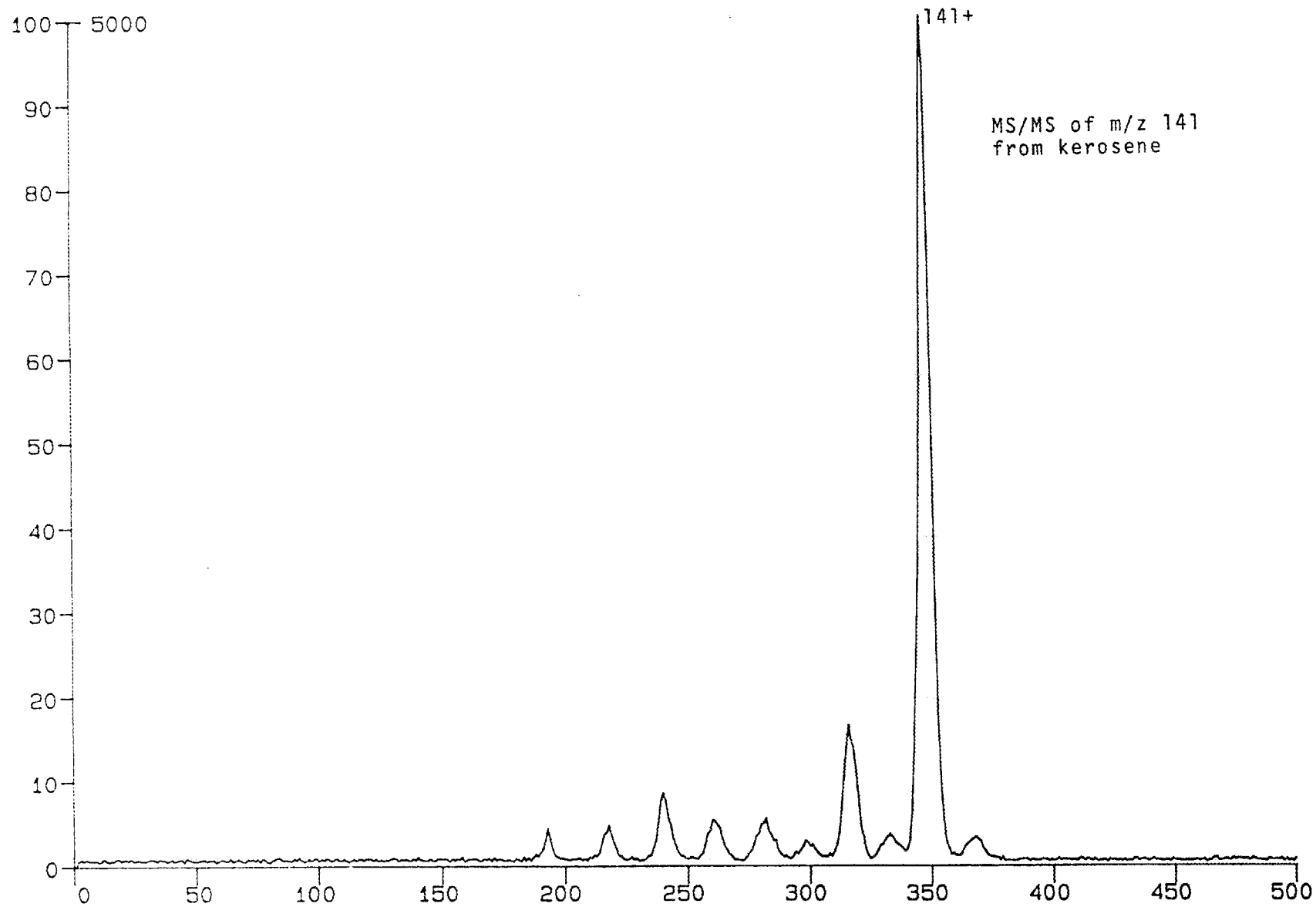
PKER1101.KGA

KEROSE



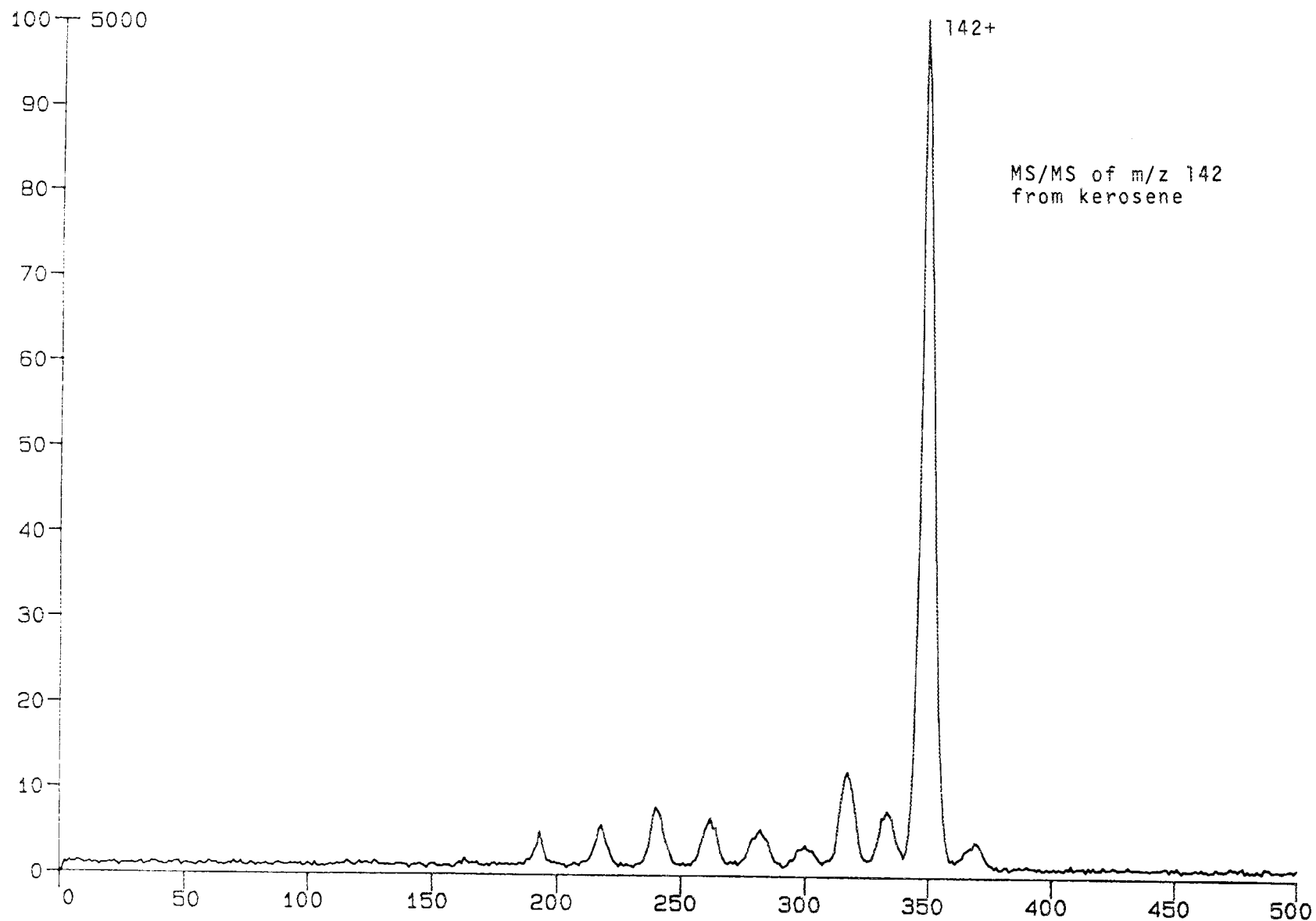
PKER002.KGA

KERO



PKERO03.KGA

KERO



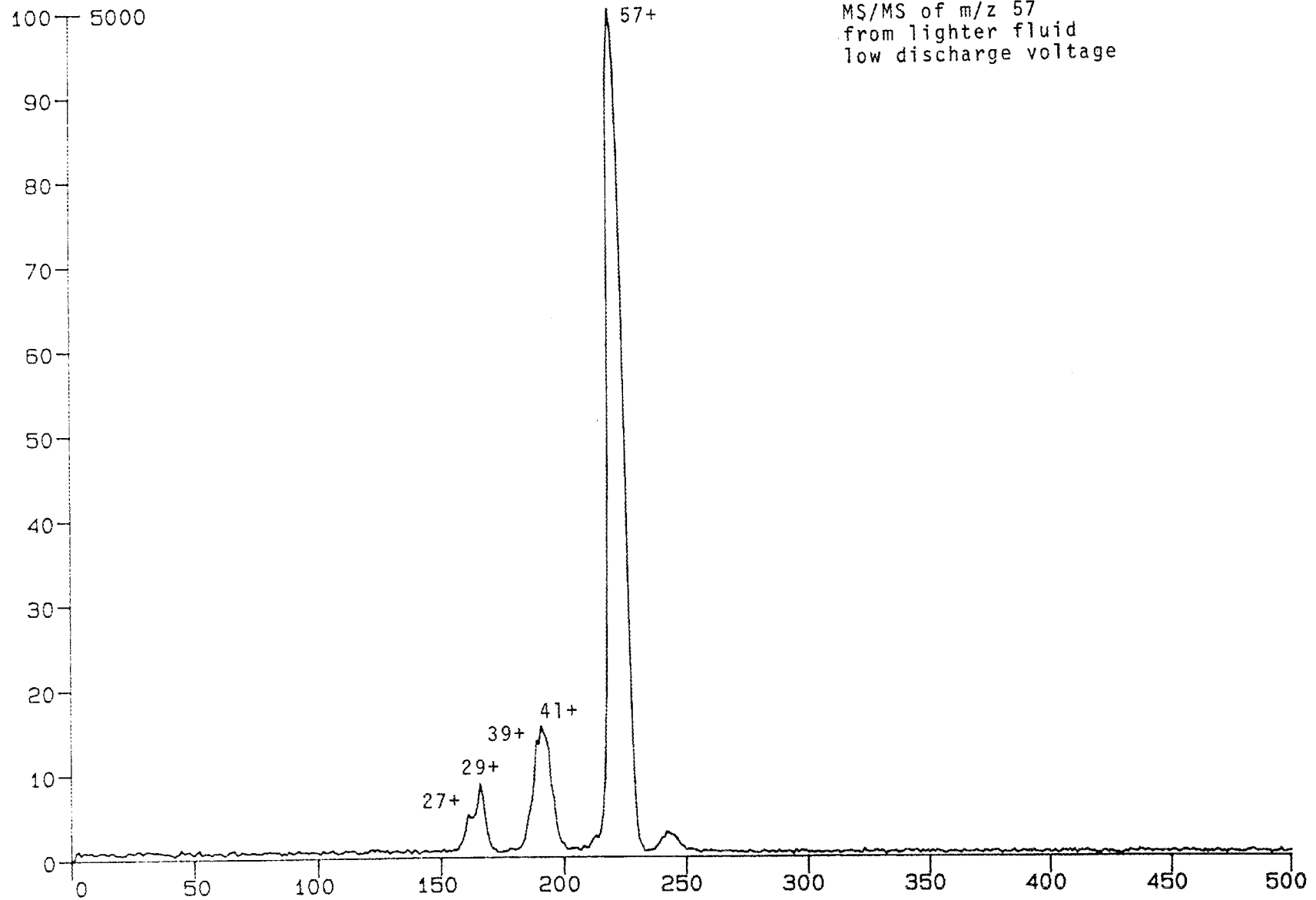
140

Appendix VI

MS/MS spectra of ions derived from lighter fluid.

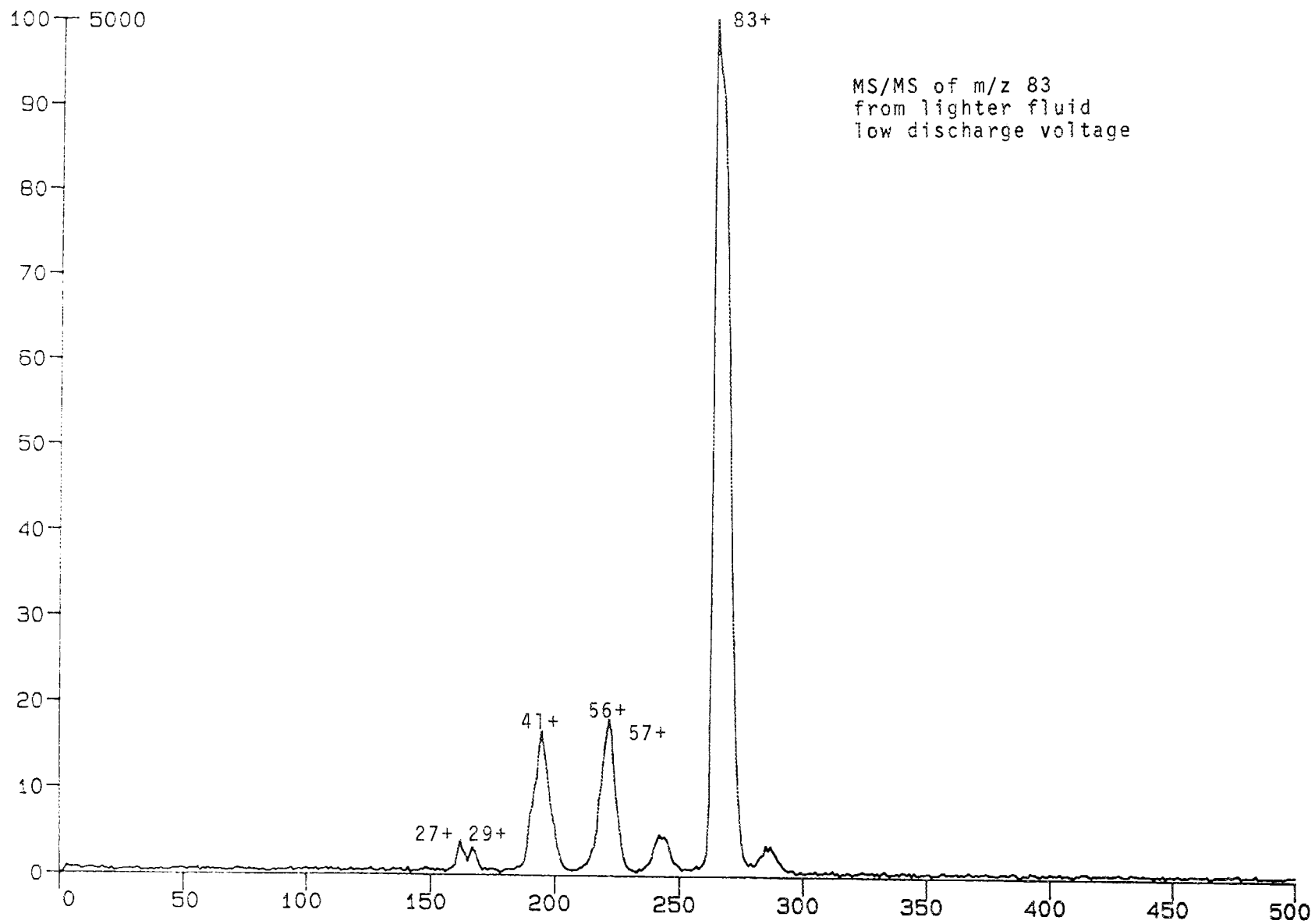
ZIPPO008.KGA

ZIPPO



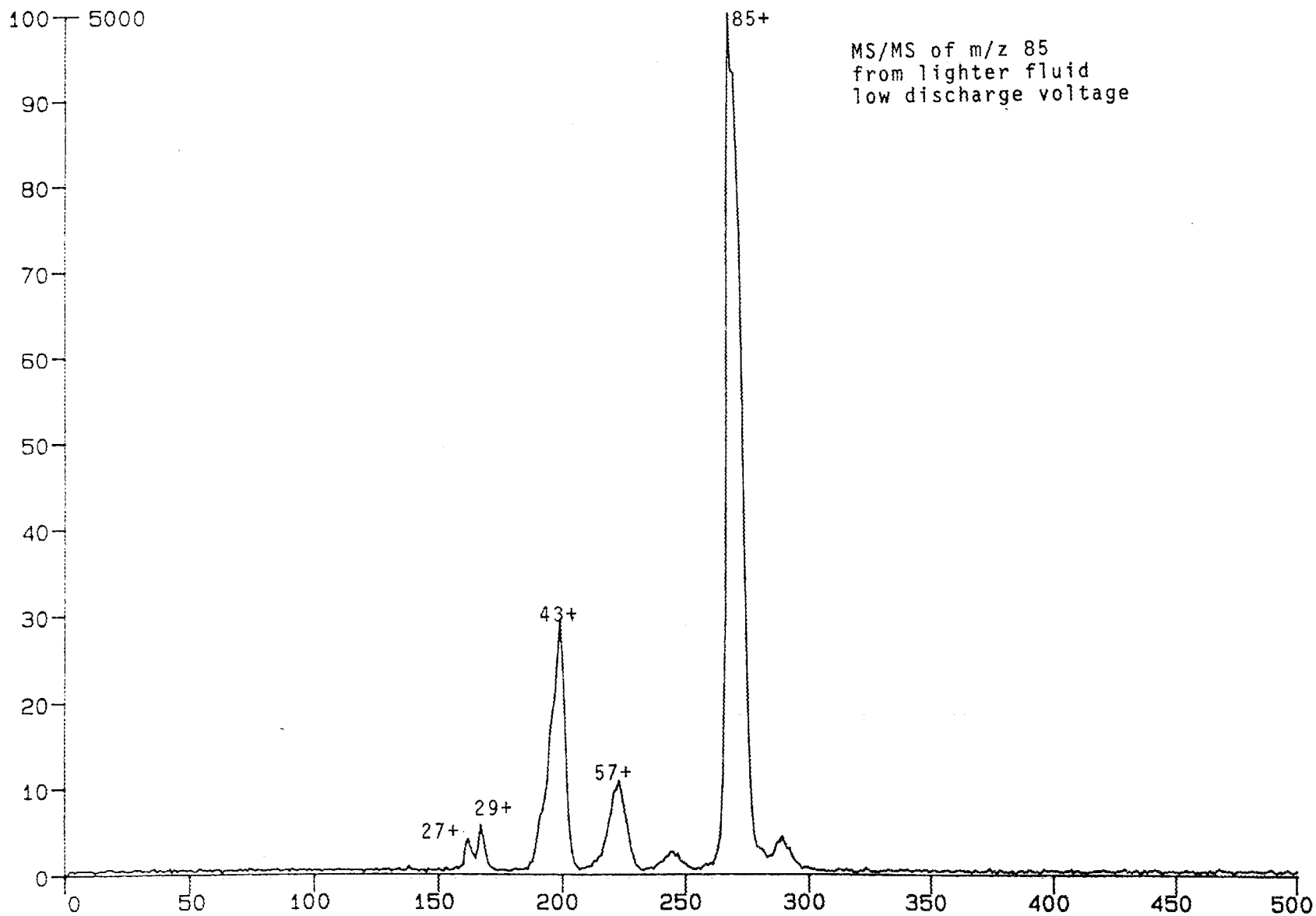
ZIPPO07.KGA

ZIPPO



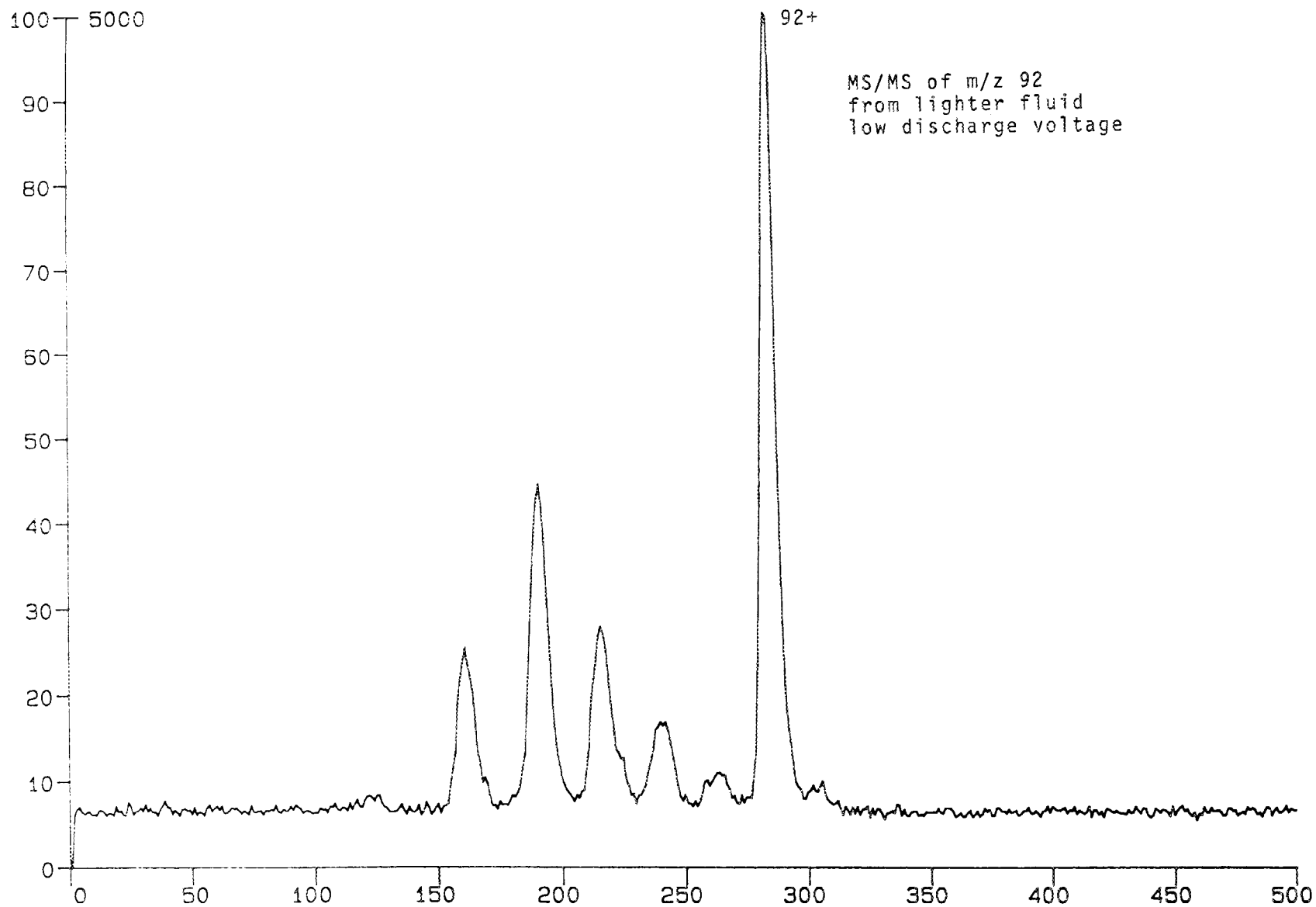
ZIPPO006.KGA

ZIPPO



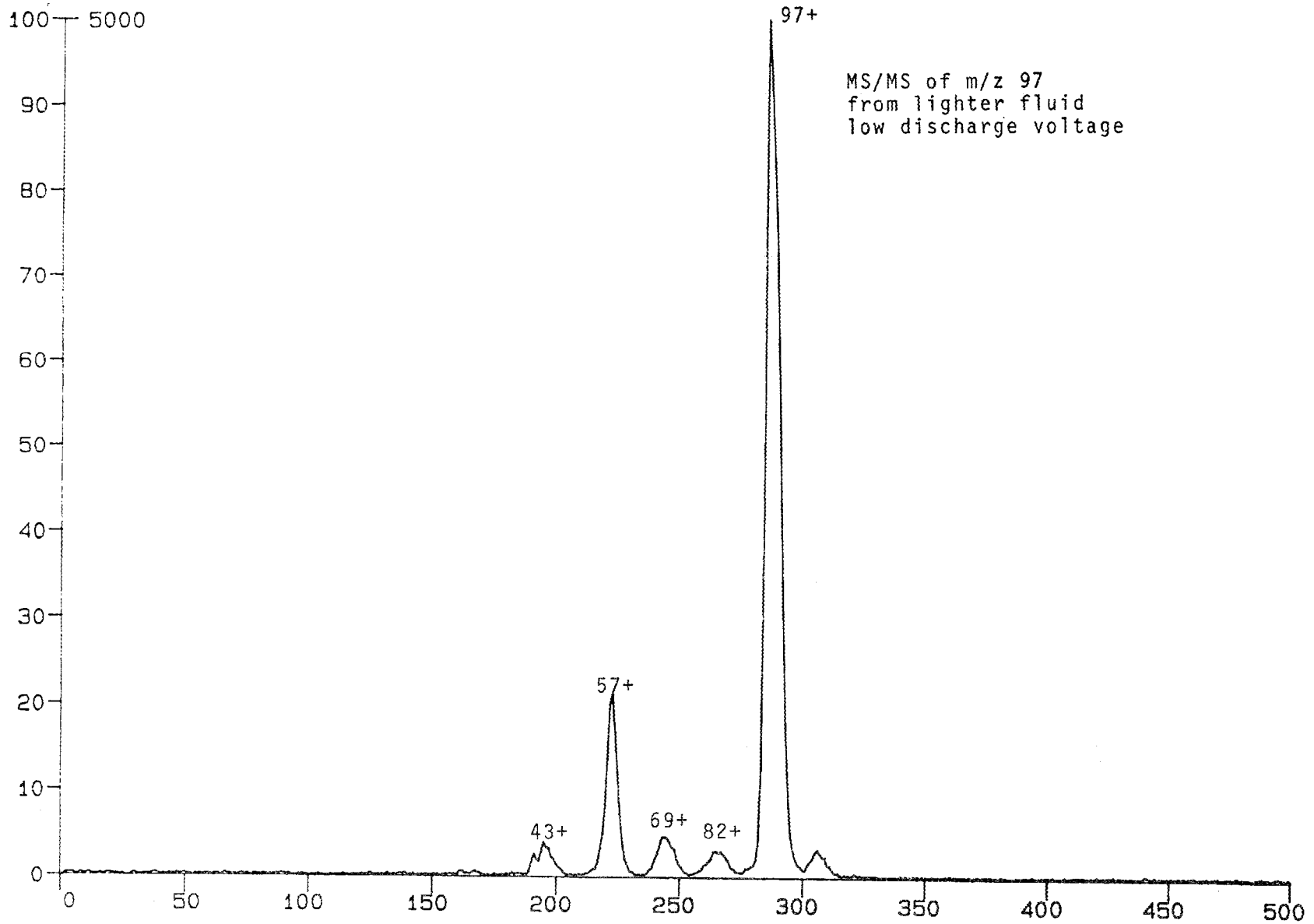
ZIPPO01.KGA

ZIPPO



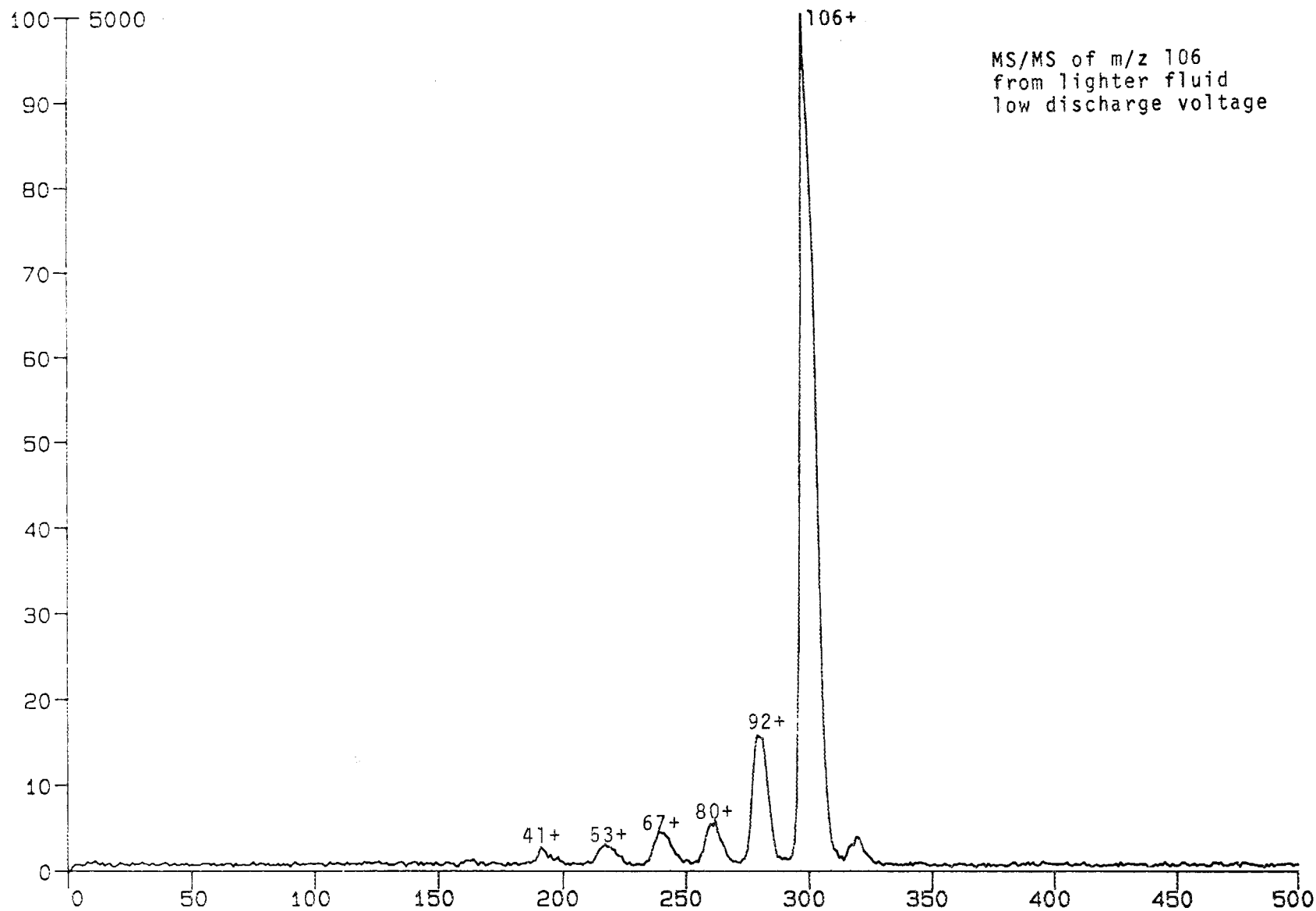
ZIPPO002.KGA

ZIPPO



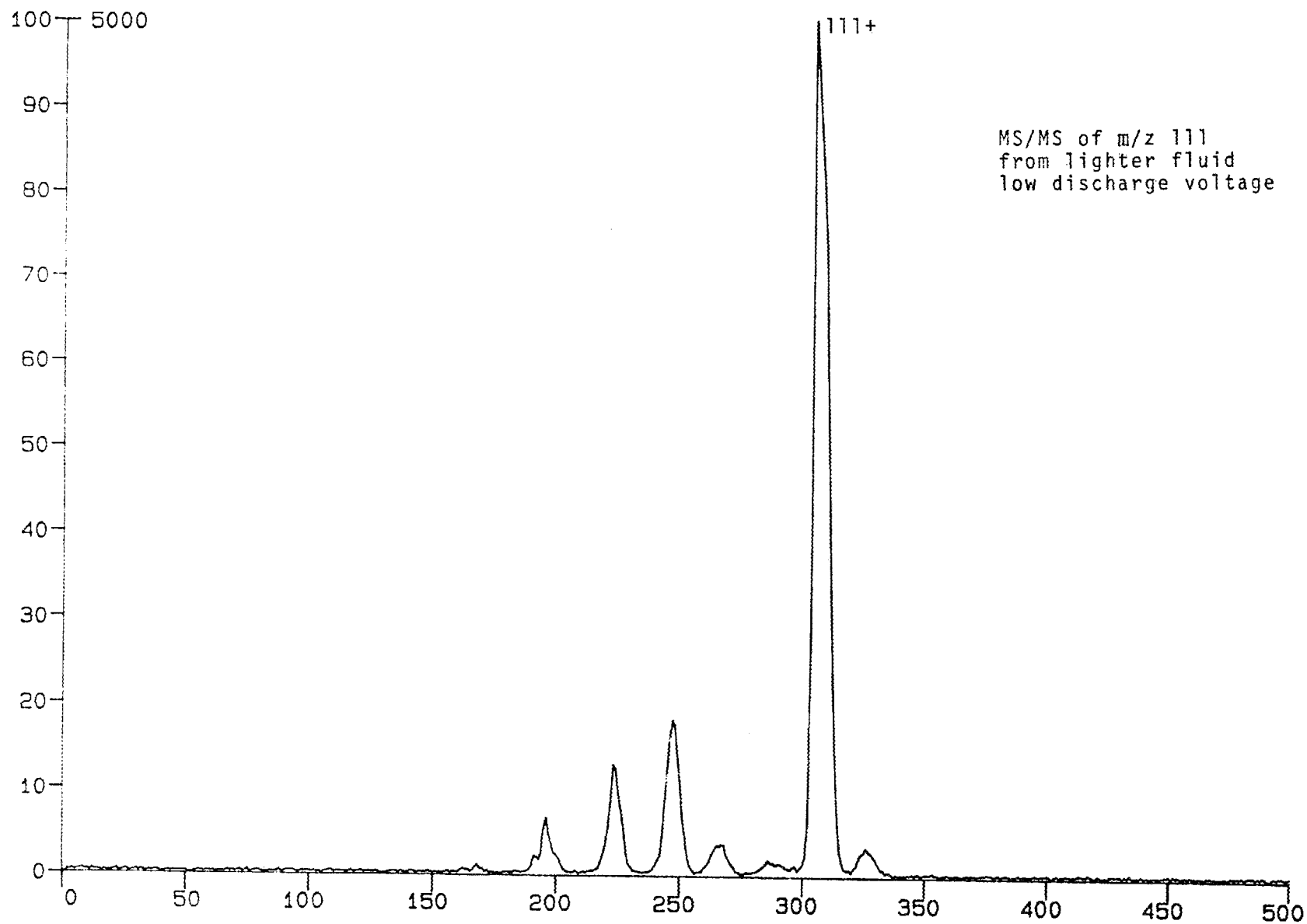
ZIPPO03.KGA

ZIPPO



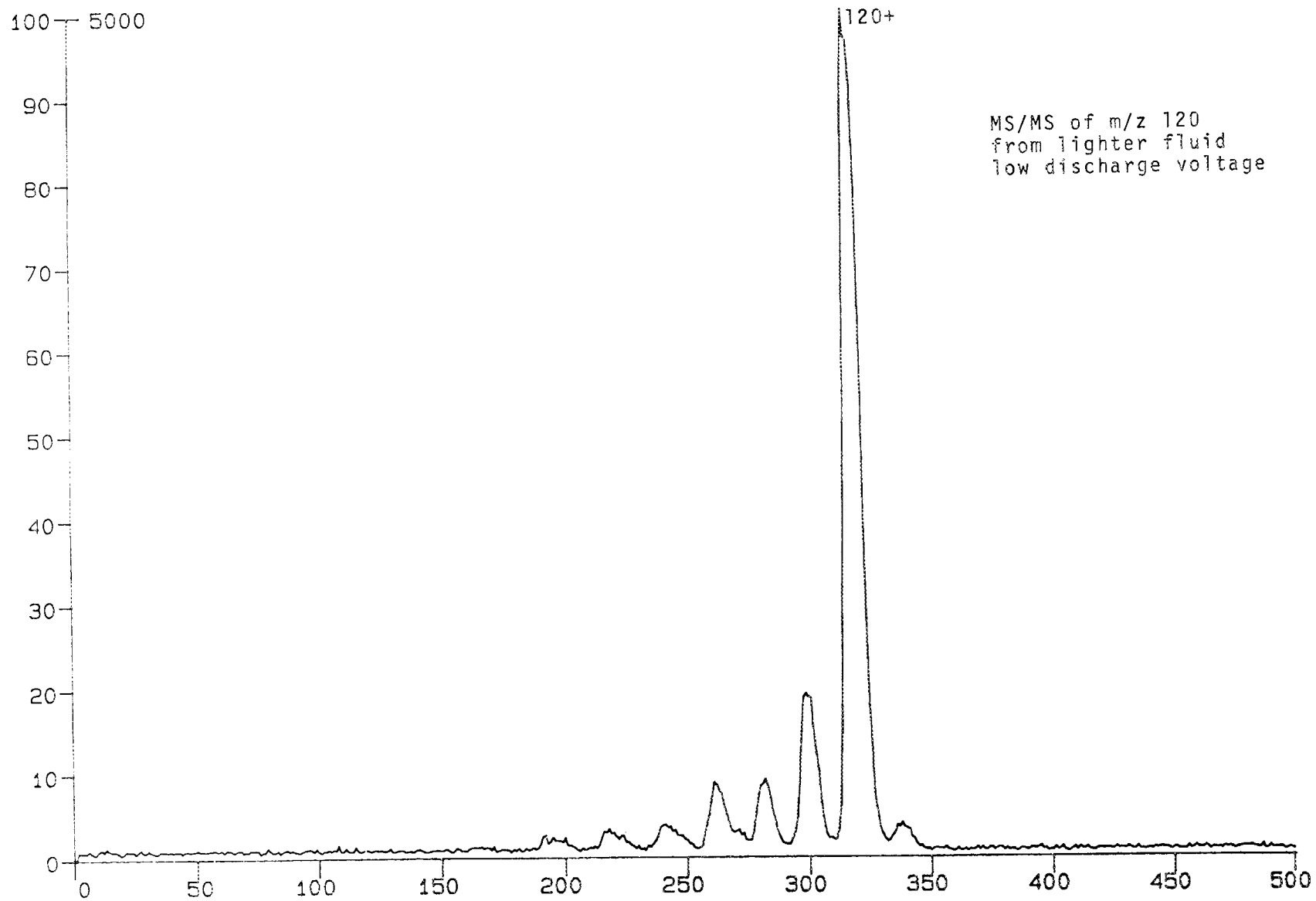
ZIPP005.KGA

ZIPPO



ZIPPO04.KGA

ZIPPO



Internal Distribution

1. T. T. Adams
- 2-6. K. G. Asano
7. M. V. Buchanan
8. C. A. Burtis
- 9-13. J. A. Carter
- 14-18. W. H. Christie
19. E. B. Flanagan
- 20-24. G. L. Glish
25. D. E. Goeringer
26. R. L. Hettich
- 27-31. E. H. McBay
- 32-36. H. S. McKown
- 37-41. S. A. McLuckey
42. R. S. Ramsey
43. E. R. Rogers
44. W. D. Shults
- 45-49. D. H. Smith
50. E. J. Soderstrom
51. P. J. Todd
52. G. J. Van Berkel
- 53-57. R. L. Walker
58. M. B. Wise
59. A. Zucker
60. Central Research Library
61. Document Reference Section
62. ORNL Patent Office
- 63-64. Laboratory Records Department
65. Laboratory Records Department - RC

External Distribution

66. Assistant Manager for Energy Research and Development,
Department of Energy, Oak Ridge Operations Office, Oak Ridge,
TN 37831
- 67-96. Technical Information Center, Oak Ridge, TN 37831

